UNIVERSIDAD COMPLUTENSE DE MADRID

FACULTAD DE CIENCIAS BIOLÓGICAS
DEPARTAMENTO DE BIOQUÍMICA Y BIOLOGÍA MOLECULAR

Diseño y aplicaciones biomédicas de biomateriales funcionalizados basados en poliésteres de origen bacteriano

TESIS DOCTORAL

NINA DINJASKI

Madrid, 2013

UNIVERSIDAD COMPLUTENSE DE MADRID
FACULTAD DE CIENCIAS BIOLÓGICAS
DEPARTAMENTO DE BIOQUÍMICA Y BIOLOGÍA MOLECULAR

Diseño y aplicaciones biomédicas de biomateriales funcionalizados basados en poliésteres de origen bacteriano

TESIS DOCTORAL

NINA DINJASKI

DIRECTORA:

MARÍA AUXILIADORA PRIETO JIMÉNEZ

CONSEJO SUPERIOR DE INVESTIGACIONES CIENTÍFICAS
CENTRO DE INVESTIGACIONES BIOLÓGICAS

Madrid, 2013

Smooth seas do not make skillful sailors.

African proverb

To my mum

To Jorge

ACKNOWLEDGEMENTS

First and foremost, I would like to express my sincere gratitude to my advisor Dr. Mª Auxiliadora Prieto for the continuous support of my Ph.D. study and research. Her guidance helped me during all the time of research and writing of this thesis. I appreciate all her contributions of time, ideas, and funding to make my Ph.D. experience productive and stimulating. It has been an honor to be part of her research team. My sincere thanks also go to Prof. José Luis García for his time, enthusiasm and above all stimulating discussions.

I would also like to acknowledge Prof. Ernesto García, Dr. Eduardo Díaz and Dr. Pedro García, for their encouragement, insightful comments, and hard questions.

Besides, I would like to thank Prof. Julio San Román and Dr. Blanca Vázquez for offering me the opportunity to work in their research group and leading me working on diverse subjects. I am especially grateful to Dr. Mar Fernández-Gutiérrez for unconditional help with *in vitro* tissue culture experiments.

Many thanks to Prof. Andrés García for his willingness to accept me as a part of his research team, amazing interest in the subject, motivation and vast knowledge on *in vivo* animal research he shared.

I am particularly indebted to Prof. Jesús Sanz for his constructive advice on BioF-related doubts.

I appreciated the collaboration of Prof. Iñigo Lasa for construction and supplying luminescent bacterial strains. Methicillin-resistant *Staphylococcus aureus* strains were kindly provided by A. Vindel from Instituto de Salud Carlos III (ISCIII).

The members of Rúben´s group have contributed immensely to my personal and professional time at CIB. The group has been a source of friendships as well as good advice and collaboration. In particular, I am grateful to Dr. Laura de Eugenio and Dr. Beatriz Galán for enlightening me the first glance of research. Work done by Dr. Valle Morales, as well as technical support of Ana Valencia and Fernando de la Peña are greatly appreciated.

Also I would like to acknowledge CIB facilities (Flow Cytometry, Microscopy, Photography), as well as ICTP facilities (SEM Electron Microscopy).

Regarding the production of PHA polymers applied throughout this Ph.D. dissertation, I would like to thank Biópolis S.L. and in particular Dr. Marta Tortajada.

I am indebted with institutions that financially supported this work: Comisión Interministerial de Ciencia y Tecnología and Consejo Superior de Investigaciones

Científicas (CSIC) that supported over JAEPre fellowship the realization of this Ph.D. Thesis in CIB and short stay in Georgia Institute of Technology.

Many thanks to Dr. Dragan Radnovic from University of Novi Sad, for helping me to start this adventure. His scientific and extrascientific support during all the way was greatly appreciated.

Lastly, I would like to thank my family for all their love and encouragement. To my mum, who raised me with a love for science and supported me in all my pursuits.

And above all, to Jorge without whose love and faithful support during all the stages of this Ph.D., this all would have been much harder. Thank you.

INDEX

Table of abbreviations

3HA	[*R*]-3-hydroxyalkanoates
3HDD	[*R*]-3-hydroxydodecanoate
3MB	3-mercaptobutyrate
3MP	3-mercaptopropionate
6-ATH	6-acetylthiohexanoic acid
mcl-OHAs	medium-chain-length oligo(3-hydroxyalkanoates)
mcl-PHA	medium-chain-length polyhydroxyalkanoates
OH-4ATB	3-hydroxy-4-acetylthiobutanoate
OH-6ATH	3-hydroxy-6-acetylthiohexanoate
OHA	oligo(hydroxyalkanoates)
OHB	oligo(3-hydroxybutyrate)
OHB-*co*-4HB	oligo(3-hydroxybutyrate-*co*-4-hydroxybutyrate)
OHB-*co*-HHx	oligo(3-hydroxybutyrate-*co*-3-hydroxyhexanoate)
OH-C6	[*R*]-3-hydroxyhexanoate
OH-C8	[*R*]-3-hydroxyoctanoate
OH-C10	[*R*]-3-hydroxydecanoate
P4HB	poly(4-hydroxybutyrate)
PEG	polyethylene glycol
PGA	poly(glycolic acid)
PHA	polyhydroxyalkanoates
PHACOS	poly(3-hydroxyacilthioalkanoate-*co*-[*R*]-3-hydroxyalkanoate)
PHB	poly([*R*]-3-hydroxybutyrate)
PHB-*co*-HHx	poly([*R*]-3-hydroxybutyrate-*co*-[*R*]-3-hydroxyhexanoate)
PHB-*co*-HV	poly([*R*]-3-hydroxybutyrate-*co*-[*R*]-3-hydroxyvalerate)
PHD	poly([*R*]-3-hydroxydecanoate)
PHO	poly([*R*]-3-hydroxyoctanoate)
PHO-*co*-HHx	poly([*R*]-3-hydroxyoctanoate-*co*-[*R*]-3-hydroxyhexanoate)
PHO-*co*-HU	poly([*R*]-3-hydroxyoctanoate-*co*-[*R*]-3-hydroxyundecenoate)
PLA	poly(lactic acid)
PET	poly(ethylene terephthalate)
scl-PHA	short-chain-length polyhydroxyalkanoates

Resumen

Introducción

Los polihidroxialcanoatos (PHA), conocidos comúnmente como "bioplásticos", son polímeros biodegradables que se acumulan en forma de gránulos en el interior celular de algunas bacterias. Son biopolímeros sintetizados a partir de fuentes renovables, susceptibles a la biodegradación en condiciones controladas, que presentan características mecánicas similares a las de los plásticos derivados de la industria petroquímica (Rehm, 2010). Su carácter biocompatible y nula toxicidad les convierte en materiales con un gran potencial en múltiples aplicaciones, incluyendo su posible uso como biomateriales en el campo de la ingeniería de tejidos. Por tanto, la síntesis de nuevos PHA es de gran interés desde los puntos de vista industrial y biomédico, ya que los nuevos biopolímeros, así como los monómeros que los componen, presentan propiedades físico-químicas y mecánicas diferentes a los PHA convencionales.

Las infecciones asociadas a los implantes y el incremento alarmante de la resistencia a los antibióticos por parte de los microorganismos, justifica la necesidad de generar nuevas superficies antimicrobianas para el desarrollo de biomateriales. En este sentido, una de las propiedades más demandadas para materiales de uso clínico y alimentario, es su capacidad para actuar como polímeros bacteriostáticos o bactericidas, de tal manera que los objetos, envases o dispositivos construidos con estos materiales puedan evitar la proliferación de las bacterias (propiedad bacteriostática) o puedan incluso provocar la muerte de las bacterias en contacto (propiedad bactericida). Los polímeros antimicrobianos representan una clase de biocidas cada vez más importante como una alternativa a los biocidas existentes y en algunos casos incluso a los antibióticos (Siedenbiedel y Tiller, 2012). Debido a sus propiedades biocompatibles y biodegradables, los poliésteres bacterianos, PHA, es una de las clases de biomateriales que se están considerando más seriamente en este tipo de aproximaciones.

En esta Tesis Doctoral se han utilizado dos estrategias para la funcionalización de PHA con alto valor añadido con aplicaciones en los sectores industrial y biomédico. La primera estrategia consiste en la producción bacteriana *in vivo* de nano-partículas funcionalizadas, las cuáles han sido diseñadas para exponer proteínas de fusión en su superficie. Los gránulos de PHA pueden ser utilizados como nano-partículas para inmovilización de proteínas recombinantes mediante el sistema BioF, previamente establecido en el laboratorio. Este sistema se basa en el uso del N-terminal de la fasina PhaF de *Pseudomonas putida* KT2440 como etiqueta de afinidad, lo que permite anclar proteínas recombinantes al gránulo de PHA

(Moldes *et al*., 2004). Uno de los inconvenientes del sistema BioF para purificar e inmovilizar proteínas es el bajo rendimiento, dado que no toda la proteína recombinante se une al gránulo, y que gran parte de la superficie del gránulo está ocupada por las fasinas naturales. Este sistema ha sido mejorado en este trabajo mediante el estudio del proceso de unión de la etiqueta al gránulo de PHA y la identificación de los requerimientos mínimos que permiten la formación y segregación del gránulo de PHA entre las células hijas durante la división celular.

La segunda estrategia desarrollada en esta Tesis Doctoral se basa en el uso de la ingeniería metabólica para diseñar las cepas bacterianas capaces de producir nuevos poliésteres. Se han estudiado las propiedades de los nuevos PHA obtenidos por fermentación, denominados PHACOS, que contienen monómeros con grupos tioéster en la cadena lateral (Escapa *et al*., 2011).

Resultados y discusión

Para optimizar el sistema BioF de inmovilización de proteínas *in vivo* a gránulos de PHA se ha estudiado primeramente la función fisiológica de la fasina PhaF, determinándose que interviene en la segregación de los gránulos durante la división celular y en la localización de los gránulos en el citoplasma. Se han confirmado las dos funciones diferenciadas de los dominios C- y N-terminal de esta proteína. El C-terminal, que contiene repeticiones AAKP-en tándem, se une a ADN de forma inespecífica, lo que está de acuerdo con su similitud con la familia de Histonas tipo H1. El N-terminal es responsable de la unión al gránulo y coincide con la secuencia de la etiqueta de afinidad BioF. Mediante microscopía electrónica de transmisión (TEM), láser confocal y multidimensional *in vivo*, se ha demostrado en células de *P. putida* KT2440 en fase exponencial de crecimiento, que la fasina PhaF dirige los gránulos al centro de la célula generando una distribución característica en forma de aguja en el citoplasma de *P. putida* KT2440. Además, nuestros estudios de citometría de flujo en células mutantes en el gen *phaF* han demostrado la existencia de dos poblaciones diferentes de células (la que contiene PHA y la que no lo contiene). Estudios de complementación han demostrado que, además de su función en la localización celular de los gránulos, PhaF está implicada en segregación de los gránulos entre las células hijas durante la división celular. Los estudios *in vivo* de la proteína de fusión entre la proteína fluorescente verde (GFP) y el C-terminal de PhaF mediante microscopía confocal han demostrado la unión de C-terminal al nucleoide. Por lo tanto, se ha hipotetizado que la función relacionada con la segregación de gránulos se debe a la interacción

del C-terminal con el cromosoma que se está segregando, de forma simultánea a la unión del gránulo de PHA con el N-terminal o dominio BioF.

En esta Tesis doctoral, también se ha estudiado la implicación de la otra fasina de *P. putida* KT2440, la proteína PhaI, en la maquinaria de formación del gránulo de PHA. La fasina PhaI completa y el módulo BioF de la fasina PhaF son similares en su estructura primaria. En este trabajo se demuestra una función coordinada de los módulos de las fasinas (PhaI y N-terminal de PhaF o BioF) para la formación y distribución óptima de los gránulos de PHA. Por una parte, se estudió la producción de las proteínas recombinantes en distintas condiciones de crecimiento, tanto en la estirpe salvaje como en diferentes mutantes en fasinas de *P. putida*. Las construcciones de estos mutantes se llevaron a cabo mediante la técnica de deleción con el plásmido pK18*mobsacB*. Este sistema tiene la ventaja de que provoca deleciones géneticas dirigidas sin incorporar marcadores antibióticos. Por otra parte, se estudió la localización de las fasinas fusionadas a la proteína GFP en presencia y ausencia del gránulo de PHA. Estas construcciones se llevaron a cabo en el plásmido pCNB5 que contiene un mini-transposon, lo que facilita la inserción estable de la construcción genética en monocopia en el cromosoma de *P. putida*. Estos experimentos nos permitieron seleccionar la cepa y las condiciones más idóneas para la producción *in vivo* de nanopartículas de bioplásticos activas. Los estudios realizados mediante microscopía epifluorescente y citometría de flujo de los mutantes en fasinas de *P. putida* que producen la proteína recombinante BioF-GFP han demostrado que la distribución durante la división celular se recupera cuando PhaF, y BioF o PhaI son sintetizados al mismo tiempo, demostrando la posibilidad de intercambio de los módulos de unión a gránulo de las fasinas. Mediante western blot se ha confirmado que concentraciones muy bajas de la fasina natural PhaF son suficientes para asegurar la segregación de los gránulos entre las células hijas durante la división celular, función ligada a su C-terminal. Todos estos estudios han permitido construir y diseñar la cepa huésped óptima derivada de la cepa modelo *P. putida* KT2440 para ser utilizada en el sistema BioF, con las modificaciones genéticas mínimas para producir nanopartículas de bioplásticos activas. La cuantificación de la proteína recombinante se llevo a cabo mediante citometría de flujo y fluorimetría.

La segunda estrategia aplicada en esta Tesis doctoral para diseñar biomateriales funcionalizados consiste en el estudio de las propiedades de los nuevos PHA obtenidos por fermentación bacteriana, denominados PHACOS, que contienen monómeros con grupos tioéster en la cadena lateral. Se conoce muy poco sobre si los monómeros derivados de los PHA convencionales pueden poseer actividad antibacteriana. Así por ejemplo, se ha descrito que algunos hidroxiácidos monoméricos derivados de PHA tienen actividad sobre

Staphylococcus aureus (Ruth *et al*., 2007). Sin embargo, la potencia antibacteriana de estos compuestos es baja presentando MICs (Concentración Mínima Inhibitoria) del orden de 1-5 mM.

Para investigar la posible actividad antibacteriana de PHACOS, se produjo el poliéster siguiendo el protocolo de fermentación bacteriana previamente descrito (Escapa *et al*., 2011). La actividad antibacteriana de PHACOS y el PHA control no funcionalizado (PHO) frente a diferentes cepas bacterianas se determinó según la norma ISO 22196:2011 (Medida de la actividad antibacteriana en superficies de plástico). El resultado obtenido indicó que PHACOS inhibe el crecimiento de las cepas de *S. aureus* incluyendo tres aislados clínicos MRSA, de forma que sólo sobreviven un 10% de las células cuando se comparan con el control.

Además, se estudió la capacidad de PHACOS para inhibir la formación de biopelículas bacterianas en su superficie en comparación con otros materiales. Con este fin se utilizaron como modelo las bacterias *S. aureus* CECT 86 y *P. aeruginosa* CECT 4122 mediante dos procedimientos: (i) la tinción de la biopelícula con el colorante cristal violeta; y (ii) el contaje de las unidades formadoras de colonia (UFC) de bacterias adheridas a los discos. Los resultados obtenidos demostraron que la presencia de PHACOS provoca una disminución de dos veces en la formación de biopelículas de *S. aureus* y no de *P. aeruginosa*, comparado con el polímero control. Además, se estudió la capacidad de PHACOS para matar las bacterias adheridas a su superficie en comparación con otros materiales. El número y la viabilidad de las bacterias adheridas a la superficie de los biopolímeros se determinaron por microscopía de fluorescencia utilizando el *kit* de viabilidad bacteriana BacLightTM LIVE/DEAD (Invitrogen L13152). Los resultados demostraron que el 80% de las células de *S. aureus* no fueron viables, es decir, mueren tras entrar en contacto con PHACOS. Sin embargo, tan solo un 17% de las células no son viables tras entrar en contacto con polímero control. El número total de bacterias (viables y no viables) adheridas a discos recubiertos de PHACOS comparadas con las bacterias presentes en los discos controles recubiertos con PHO fue similar, lo que demuestra que la adhesión bacteriana no está disminuida, pero sí que se afecta la supervivencia de las bacterias.

Por otro lado, se estudió la biocompatibilidad y actividad antimicrobiana de PHO y PHACOS *in vivo* en ratones BALB c mediante el uso de una sonda fluorescente (H-ICG). Se demostró tanto la biocompatibilidad de PHO y PHACOS como la actividad antimicrobiana de PHACOS *in vivo*. Por lo tanto, se concluyó que PHACOS es un material con capacidad

antibacteriana intrínseca, tal cual se obtiene de la fermentación bacteriana, sin tener que someterlo a modificaciones químicas posteriores a su síntesis.

En general, se pueden distinguir tres tipos de polímeros antimicrobianos: biocidas poliméricos, polímeros biocidas y polímeros liberadores de biocidas. Los biocidas poliméricos son polímeros que constan de unidades de repetición bioactivas, es decir, los polímeros son múltiples biocidas interconectados, que actúan de manera similar a los monómeros. No siempre, la polimerización de monómeros biocidas conduce a polímeros antimicrobianos activos, ya sea debido a que los polímeros son insolubles en agua o a que las funciones biocidas no llegan a su destino. Los polímeros biocidas son usualmente macromoléculas cargadas positivamente que interactúan con las células microbianas que, generalmente, presentan una carga negativa neta en la superficie debido a sus proteínas de membrana, a los ácidos teicoicos en las bacterias Gram-positivas, o a los fosfolípidos cargados negativamente en la membrana externa de las bacterias Gram-negativas. Los últimos experimentos que forman parte de esta Tesis doctoral demuestran la actividad microbiana de los monómeros que componen el polímero PHACOS, por lo que se propone que PHACOS es un biocida polimérico.

Summary

INTRODUCTION

Polyhydroxyalkanoates (PHA), commonly known as “bioplastic", are biodegradable polymers accumulated by certain bacteria in the form of intracellular inclusions. These biopolymers are synthesized from renewable sources, can be biodegraded under controlled conditions and have similar physico-chemical characteristics to plastic materials derived from the petrochemical industry (Rehm, 2010). Considering the fact that they are biodegradable, biocompatible and non toxic, these compounds have great potential for multiple applications, such as biomaterials. Synthesis of new PHA is of great interest from both the industrial and biomedical standpoint, as the novel biopolymers and monomers that constitute them present physico-chemical and mechanical properties that differ from conventional PHA.

Implant-associated infections and the alarming rise in antibiotic resistance highlight the need to generate new antimicrobial surfaces to develop biomaterials and tissue-engineered products. Bacterial polyesters, PHA, have become one of the leading biomaterials under investigation due to their biocompatible and absorbable features. Among other properties, one of the characteristics required for clinical or alimentary use is their capacity to act as bacteriostatic or bactericidal polymers, so designed packaging materials or devices stop bacterial proliferation (bacteriostatic property) or even cause bacterial death (bactericidal property). Antimicrobial polymers represent a class of biocides of increasing importance as an alternative to existing biocides, and in some cases even antibiotics (Siedenbiedel and Tiller, 2012).

Bearing all this in mind, in this PhD Thesis two different polymer functionalization strategies were followed to obtain added-value PHA for industrial and biomedical applications. The first strategy involved *in vivo* bacterial production of tailor-made functionalized nano-beads, where proteins attached to the natural PHA granule were engineered to display fusion proteins of interest. Such PHA granules can be utilized as nano-beads to immobilize recombinant proteins using the BioF system previously designed in our laboratory. This system is based on the use of the N-terminal domain

of *Pseudomonas putida* KT2440 PhaF phasin as affinity tag, which enables the recombinant protein to anchor to the PHA granule (Moldes *et al*., 2004). One of the drawbacks of the BioF system is its low yield, which is due to the fact that not all fusion proteins are attached to the granule and that an important part of the granule surface is occupied by natural phasins. This system has been improved by studying the process of tag binding to the PHA granule and identifying the minimal necessary factors that drive PHA granule formation and segregation between daughter cells during cell division. The second approach is based on the use of metabolic engineering to design bacterial strains able to produce new non-natural polyesters (Escapa *et al*., 2011). We studied the properties of the new PHA family obtained, named PHACOS (poly(3-hydroxyacilthioalkanoate-*co*-[*R*]-3-hydroxyalkanoate)), carrying functionalized groups in the side chain.

Results and discussion

To optimize the BioF system for *in vivo* immobilization of proteins to PHA granules, we studied physiological function of PhaF phasin, determining the factors that influence the granule segregation process during cell division, as well as granule intracellular localization. We identified two different functions of the C- and N-terminal domain of this protein. It was demonstrated that C-terminal contains AAKP-like tandem repeats, characteristic of the histone H1-family, and binds DNA in a non-specific manner, whereas N-terminal domain is responsible for granule binding and shares high sequence similarity with PhaI phasin. Transmission electronic microscopy (TEM), confocal microscopy and multidimensional microscopy revealed that, in the cells producing granules at early growth stage, PhaF directs the PHA granules to the center of the *P. putida* KT2440 cells, forming a characteristic needle array. Moreover, by means of flow cytometry studies, we demonstrated the presence of two markedly different cell populations in the strain lacking the PhaF protein, *i.e.,* cells with and without PHA. Complementation studies definitively demonstrated a key role of PhaF in

granule segregation during cell division, ensuring the equal distribution of granules between daughter cells. Confocal microscopy *in vivo* monitoring of green fluorescent protein (GFP) and C-terminal domain of PhaF fusion protein showed that C-terminal binds nucleoid. All these findings suggested PhaF plays a major role in the PHA apparatus through interactions with the segregating chromosome.

In this PhD Thesis, we have also studied the involvement of the other *P. putida* KT2440 phasin, PhaI protein, in the PHA machinery, as PhaI phasin and BioF domain of PhaF share a similar primary structure. We demonstrated the cooperative work of phasin domains (PhaI and N-terminal of PhaF) to obtain optimal PHA granule formation and distribution. On the one hand, we studied the production of recombinant protein under different growth conditions, both in *P. putida* wild type and phasin mutant strains. The said mutant strains were constructed by gene deletion using the pK18*mobsacB* plasmid. This system represents an environmentally friendly approach as directed genetic deletions are produced without incorporating antibiotic markers. On the other hand, we studied the localization of phasin proteins fused with GFP in the presence and absence of PHA granules. These constructions were performed using the pCNB5 plasmid, which carries a mini-transposon facilitating stable insertion of genetic construction, such as monocopy in the *P. putida* chromosome. These experiments enabled us to determine the optimal conditions and host strain for *in vivo* production of bioactive nano-beads. Studies of phasin-mutant *P. putida* strains producing BioF-GFP recombinant protein performed by epifluorescent microscopy and flow cytometry demonstrated that balanced distribution after cell division is recovered when PhaF, and BioF or PhaI are produced concurrently, thereby showing the swappable nature of phasin domains. By means of Western blot analysis, we confirmed that low concentrations of natural PhaF phasin are sufficient for proper granule segregation between daughter cells during cell division. All these findings enabled the construction and design of an optimal host strain for BioF system expression, derived from the model *P. putida* KT2440 strain with minimal genetic modifications, making it ideal for bioactive nano-bead production. Quantification of the recombinant protein was performed by fluorimetry and flow cytometry. Taken

together, this system provides a useful tool for *in vivo* immobilization of active proteins to a biodegradable support, with many potential applications.

Applying a second strategy, previously described by Escapa *et al*., (2011), functionalized biomaterials called PHACOS were synthesized. In this PhD Thesis, we focused on studying the new properties of this non-natural polyester carrying functionalized groups at the side chain. There have been no previous reports of the antibacterial activity of PHA polymers that have not been modified or mixed with other compounds for that purpose. However, it is known that PHA-derived monomers, [*R*]-3-hydroxyalkanoates (3HA), show antibacterial activity against *Stapylococcus aureus* (Ruth *et al*., 2007) with antibacterial efficiency of 3HA showing very high MIC values (Minimal Inhibitory Concentration), 1-5 mM.

The antibacterial activity of PHACOS and non-functionalized control polymer PHO against several Gram-positive and Gram-negative bacterial strains was determined following ISO 22196:2011 “Measurement of Antibacterial Activity on Plastics Surfaces” standard protocol, with certain modifications. The results demonstrated that PHACOS inhibit growth of *S. aureus,* including three methicilline resistant (MRSA) clinical isolates, showing less than 10% bacterial cell survival when compared to the control.

Moreover, we studied the ability of PHACOS to prevent bacterial biofilm formation on its surface in comparison to other materials. To that end, *S. aureus*^{T} and *Pseudomonas aeruginosa* CECT 4122 were used as model strains able to form biofilm on different materials. The ability of bacteria to form biofilm *in vitro* on polymer surfaces was examined by: (i) environmental scanning electron microscopy (ESEM); (ii) crystal violet assay and (iii) colony forming unit (CFU) counting. Results show that biofilm formation of *S. aureus* decreased 2-fold in the presence of PHACOS as compared to biofilm formation on the control polymer; however, this was not the case for *P. aeruginosa*. Furthermore, we studied the ability of PHACOS to kill bacteria adhered to its surface, in comparison with other materials. The number of viable bacterial cells adhering to the surface of biopolymers was determined by fluorescence microscopy using the Bacterial Viability test LIVE/DEAD BacLightTM (Invitrogen L13152). Interestingly, results demonstrated that the number of viable *S. aureus* cells

incubated on PHACOS was much lower (80%) in comparison to those on PHO. However, just 17% of cells incubated on the control polymer were non viable. The total number of bacterial cells (viable and non viable) adhering to disks coated with PHACOS and the total number of bacteria adhering to disks coated with control polymer were similar. This demonstrated that there was no decrease in bacterial adhesion but that bacterial survival was affected.

Moreover, biocompatibility and antibacterial activity of PHO and PHACOS were studied and demonstrated *in vivo* using BALB/c male mice and fluorescent dye (H-ICG). Therefore, we concluded that PHACOS have intrinsic antibacterial activity, as they are obtained from bacterial fermentation, and do not require chemical modification.

In general, three types of antimicrobial polymers are known: biocidal polymers, polymeric biocides and biocide-releasing polymers. Biocidal polymers are usually positively charged macromolecules that interact with microbial cells, which generally carry a negative net charge at the surface due to their membrane proteins, teichoic acids of Gram-positive bacteria, and negatively charged phospholipids on the outer membrane of Gram-negative bacteria. Polymeric biocides consist of bioactive repeating units, *i.e.*, the polymers are just multiple interconnected biocides, which act similarly to monomers. Often, polymerization of biocidal monomers does not lead to active antimicrobial polymers, either, because the polymers are water-insoluble or the biocidal functions do not reach their target. The last experiments that form part of this PhD Thesis demonstrated the antibacterial activity of PHACOS-derived dimers/trimers and therefore we propose that PHACOS act as a polymeric biocide.

I. Introduction

1. Polyhydroxyalkanoates (PHA) historical overview

Bacterial polyhydroxyalkanoates (PHA) constitute a family of biopolyesters composed of a range of different polymers, mainly discovered during the past 20 years (Steinbüchel, 1991). The exception is the simplest member of the class, poly([*R*]-3-hydroxybutyrate) (PHB), which was first identified in 1926 in *Bacillus megaterium* (Lemoigne, 1926) and is the most well-known PHA polymer.

During the 1980s, many companies tried to produce various PHA at pilot or industrial scale. The British company Imperial Chemical Industries (ICI) developed a commercial process to produce PHB, and the copolymer poly([*R*]-3-hydroxybutyrate-*co*-[*R*]-3-hydroxyvalerate) (PHB-*co*-HV) (Chen, 2009). Over the past years, PHA-based polymeric materials have been designed for biomedical applications, such as drug-delivery carriers, nutritional supplements, drugs, fine chemicals and others (Chen and Wu, 2005). More recent interest has arisen in their medical application as implants, primarily in response to the emerging requirements of the tissue-engineering field. In fact, in the past two years, PHA has become one of the leading types of biomaterials under investigation for the development of tissue-engineered cardiovascular products, due to inherent properties that are unavailable in existing synthetic absorbable polymers. Although most products containing these materials have yet to be approved for *in vivo* medical use, some companies are currently engaged in developing diverse tissue-engineered products based on PHA polymers (*e.g*. Tepha, Inc., USA). PHA have drawn particular interest since they were shown to be biodegradable and biocompatible (Brandl *et al*., 1995; Brandl *et al*., 1990). The best approach to achieve those properties is by producing them in bacteria, thus, guaranteeing complete stereospecificity (all chiral carbon atoms in the back-bone are in the *R* configuration), which is essential for their biodegradability and biocompatibility. Both, bacterial type and growth conditions determine the chemical composition of PHA as well as molecular weight, which typically ranges from 2×10^2 to 3×10^3 kDa (Byrom, 1987; Lee, 1996).

Apart from immense potential for medical applications, due to their biodegradable properties and natural origin, PHA are also considered as bioplastics, an alternative to petrochemical-derived plastic materials. Since bacteria utilize renewable sources for PHA production, dependency on fossil resources can be reduced (Chen, 2009; Chen and Patel, 2012). At present, production costs of bioplastic synthesis are 5 to 10 times higher than the cost of petrochemical-derived plastic synthesis, which is currently a major hindrance to their successful commercialization (Rehm, 2010).

This work will focus on design and application of added value PHA using different approaches for polymer functionalization. The strategy is founded on seizing the advantages of intrinsic polymer features and adding modifications that confer new properties to the biomaterial for medical applications. The work is based on the processes developed in bacterial model strain *Pseudomonas putida* KT2440 and therefore in many aspects will be centered on PHA produced by this strain.

2. Occurrence of PHA

PHA are synthesized by many bacteria as carbon and energy storage in response to an excess carbon source, when growth is limited due to the starvation of other nutrients, such as nitrogen and phosphorus (Madison and Huisman, 1999; Prieto *et al*., 2007; Escapa *et al*., 2012). PHA are accumulated as intracellular inclusions with an amorphous, hydrophobic PHA core, mainly enveloped by proteins involved in PHA metabolism (see section 3; Potter and Steinbüchel, 2005) (Figure 1).

This accumulation is subject to extensive regulation: (i) at enzymatic level, by cofactor inhibition and availability of metabolites (Escapa *et al*., 2012); (ii) at transcriptional level by specific and global transcriptional regulatory factors (see Annex 3; De Eugenio *et al*., 2010b) and (iii) at translational level, driven by global post-transcriptional regulators (Ryan *et al*., 2013; De Eugenio PhD-thesis, 2009). Moreover, new investigations of PHB granules have revealed that granules isolated in native form can perform their function autonomously of the rest of the cell content since they

harbor all the proteins required for PHA metabolism (Jendrossek, 2009). Therefore, they are considered as subcellular organelles, named carbonosomes, performing at least three functions (PHA synthesis, storage and mobilization).

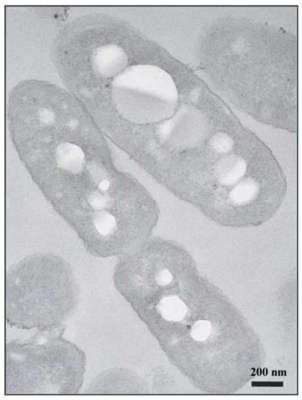

Figure 1. Transmission electron microscopy (TEM) image of PHA producing *P. putida* KT2442 cells. PHA reserve granules are located intracellularly. The number and size of granules is species dependent ranging from 100-500 nm and 2-8 granules per cell.

PHA have been classified according to various criteria: (i) their monomer size as short-chain-length PHA (scl-PHA), with C4-C5 monomers and medium-chain-length PHA (mcl-PHA) with C6-C14 monomers (Anderson *et al*., 1990); (ii) their functional substituents found in the radical chain (such as double bonds or aromatic groups); or (iii) the structure of the polymer (formed by homogenous, random or block copolymers) (Tortajada *et al*., 2013) (Figure 2).

Scl-PHA, such as PHB, and copolymers PHB-*co*-HV are being produced on a commercial scale, and they have been extensively applied to packaging, molding, fibers and other commodities (Chen, 2009). Mcl-PHA mainly produced by bacteria belonging to genera *Pseudomonas,* are currently considered promising candidates for bioplastic applications owing the properties derived from their longer side-chains and altered crystalline structure, such as elasticity, hydrophobicity, low oxygen permeability, water resistance and biodegradability. They can be molded and processed into compostable packaging and resorbable materials for medical applications and have also been used as food coatings, pressure-sensitive adhesives, paint binders and biodegradable rubbers (Zinn *et al*., 2001; Elbahloul and Steinbüchel, 2009).

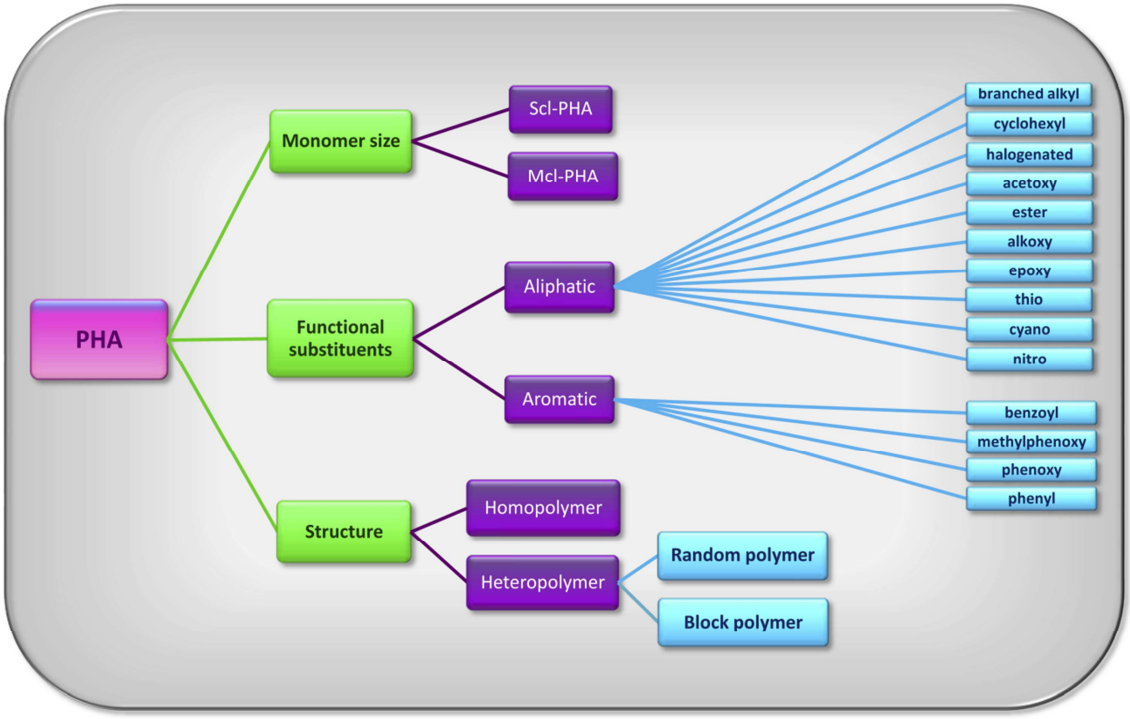

Figure 2. Classification of PHA according to different criteria.

Furthermore, unconventional mcl-PHA bearing different functional moieties in their side chains can be produced through different biotechnological strategies, which will be revised in detail in the following section. These reactive groups allow fine tuning of physical and chemical properties of the polymer, and represent potential targets for post-biosynthetic modifications (Escapa *et al*., 2011).

3. Granule-associated proteins (GAPs): PhaF Phasin

As previously mentioned, PHA constrain the hydrophobic core of intracellular inclusions surrounded by proteins involved in PHA metabolism (Potter and Steinbüchel, 2005). These granule-associated proteins (GAPs), have been designated to the following classes, namely, PHA synthases, depolymerases, regulatory proteins, acyl-CoA synthetase (ACS1) and phasins (Figure 3). *Pseudomonas* genes encoding GAP

proteins are organized in the *pha* cluster (Prieto *et al*., 1999). The organization of the *pha* gene cluster for mcl-PHA synthesis was partially reported in 1991 in the strain *Pseudomonas putida* GPo1 (Huisman *et al*., 1991) and completed in 1999 with the discovery of the genes encoding phasins (Prieto *et al*., 1999) (Figure 4).

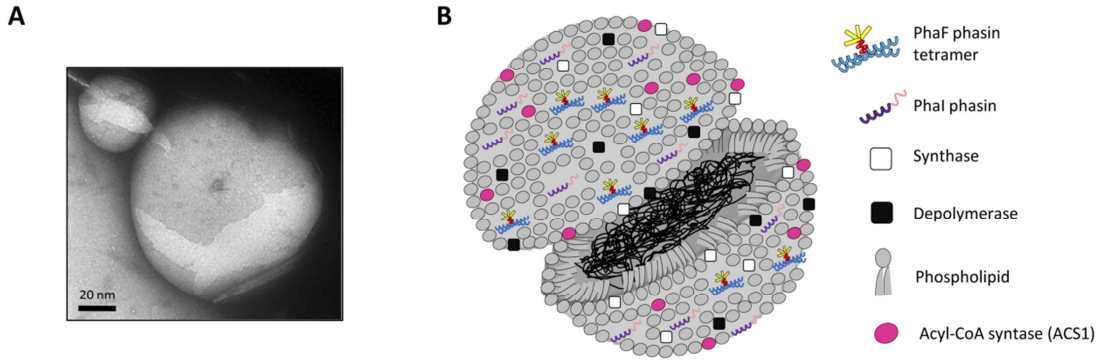

Figure 3. TEM image of PHA granule (A) and a model of PHA granule structure (B). A, TEM image of *P. putida* KT2442 mcl-PHA granule; B, The PHA granule is composed of a PHA core coated with phospholipid monolayer where granule-associated proteins GAPs (phasins, synthases, depolymerase, ACS1) are embedded or attached. Among GAPs phasins are the most abundant proteins.

Phasins, the major GAPs, were described as amphiphilic proteins which generate an interphase between the cytoplasm and the hydrophobic core of PHA granules (Steinbüchel *et al*., 1995). They also play a role in controlling granule size and number per cell (Pieper-Furst *et al*., 1995; Wieczorek *et al*., 1995; Grage *et al*., 2009). Other functions proposed for phasins are prevention of protein misfolding on the granule surface (Steinbüchel *et al*., 1995) and storage of nitrogen source (McCool and Cannon, 1999).

Phasins are widespread among bacteria, sharing similar functions but differing in their primary structures (Grage *et al*., 2009). It is generally accepted that they are composed of a hydrophobic domain associated to the PHA granule surface and a hydrophilic domain exposed to the cytoplasm. The amphiphilic layer stabilizes the PHA granules and prevents them from coalescing (Wieczorek *et al*., 1995).

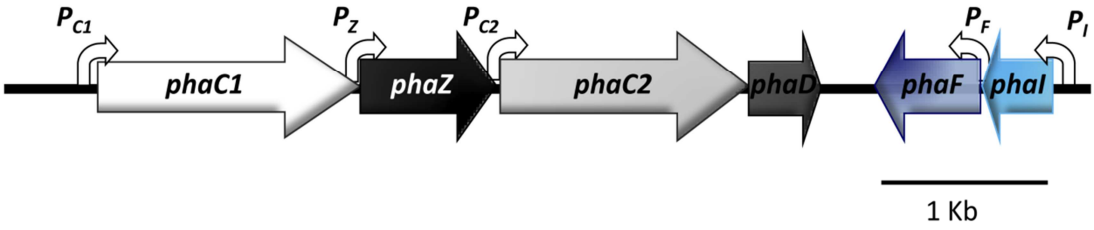

Figure 4. Genetic organization of *pha* cluster in *P. putida* KT2442. Straight arrows indicate different genes involved in PHA metabolism, their relative size and transcriptional direction. Promoter regions are indicated as curved white arrows. The *pha* is composed of two synthase coding genes, *phaC1* (white) and *phaC2* (light grey), interspersed by depolymerase coding gene *phaZ* (black), *phaD* gene coding for transcriptional regulator not classified as GAP (grey) and two genes coding for the phasins, *phaF* (dark blue) and *phaI* (light blue) transcribed divergently to the other *pha* genes.

P. putida strains contain two phasins PhaI (15 kDa) and PhaF (26 kDa) (Prieto *et al*., 1999). PhaF is a nucleoid-associated protein involved in the transcriptional regulation of genes linked to PHA metabolism (Prieto *et al*., 1999; Galan *et al*., 2011). According to the structural three-dimensional model prediction, PhaF is an elongated protein, composed of long, amphipathic N-terminal helix with PHA binding capacity, followed by a short leucine zipper proposed as protein oligomerization linker, and a superhelical C-terminal domain wrapped around the chromosomal DNA (Maestro *et al*., 2013) (Figure 5). The C-terminal half contains AAKP-like tandem repeats characteristic of the histone H1-family (Prieto *et al*., 1999).

There is evidence for the structural and functional independence of the domains. First, the PhaI phasin, which shares considerable sequence similarity with the N-terminal region of PhaF (57% similarity, 38% identity) (Prieto *et al*., 1999) is capable of acquiring a folded, stable and functional structure by itself (Moldes *et al*., 2004). Also, the N-terminal domain is conserved in other PHA-binding phasins with a different C-terminal part (Moldes *et al*., 2004; Maestro *et al*., 2013). Moreover, highly diverse fusion proteins containing the N-terminal moiety of PhaF (the BioF affinity tag, see below) can be adsorbed on PHA granules without compromising their function (Moldes *et al*., 2004; Moldes *et al*., 2006).

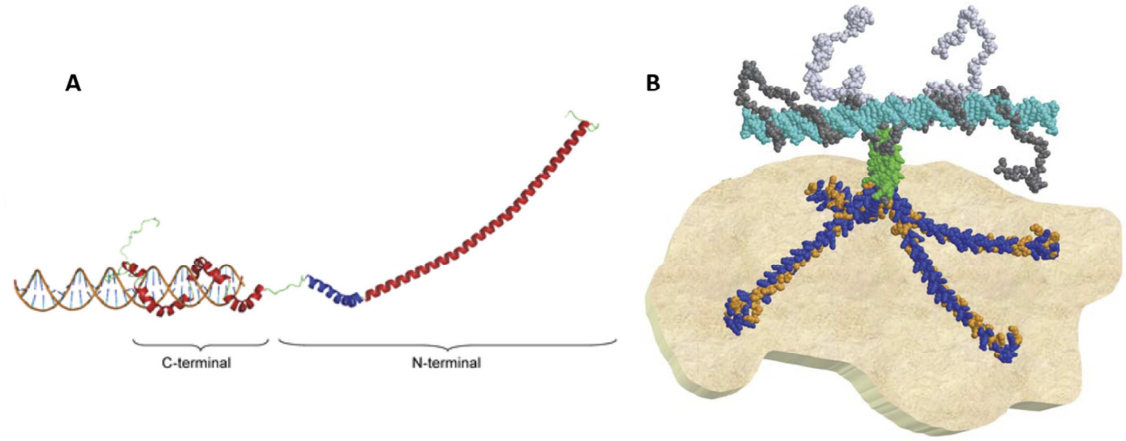

Figure 5. A structural model of PhaF phasin and a model of the interaction between PHA granules, phasins and chromosomal DNA in *P. putida* KT2440. A, Joint model structure of monomeric PhaF complex with DNA. The leucine zipper is shown in blue; B, PhaF tetramer is depicted interacting with the PHA granule while also attached to a fragment of nucleoid DNA. The hydrophobic residues in the N-terminal domain are shown in orange, while the polar ones are colored blue. The leucine zipper is colored green and the DNA in cyan (Maestro *et al*., 2013).

4. Peptide functionalized PHA using GAPs

PHA granules are becoming increasingly recognized as potential functionalized beads for biotechnological and medical applications. Recently, granules formed inside recombinant bacterial cells were used as tailor-made functionalized micro- or nano-beads, in which specific proteins attached to the PHA core have been engineered to display various functions. The performance of engineered PHA beads has been demonstrated in high-affinity bioseparation (Lewis and Rehm, 2009), enzyme immobilization (Moldes *et al*., 2004; Peters and Rehm, 2006), protein delivery to natural environments (Moldes *et al*., 2006), diagnostics (Bäckström *et al*., 2007) and as an antigen delivery system (Parlane *et al*., 2009) has been demonstrated. To do so, different strategies were employed using GAP proteins located on the surface of PHA granules, such as synthase, depolymerase and phasins (see below).

Moreover, the approach using GAPs can be applied *in vitro* or *in vivo*. Namely, for *in vitro* technology, PHA extraction is followed by *in vitro* bead production and, using the advantage of strong GAP-bead hydrophobic interaction, fusion proteins are *in vitro* purified/immobilized (Yao *et al*., 2008). The *in vivo* approach consists of GAP fusion immobilization onto the PHA granule surface while the granules are being formed inside the PHA-producing cell (Moldes *et al*., 2004).

Among GAPs, PHA granule-binding proteins, phasins, are highly attractive due to their diversity compared to the other GAPs. Thus, phasins have been utilized as affinity tags to design recombinant protein purification system based on an *in vitro* approach. This method provides low cost production and purification of high-value-added proteins in a continuous way (Wang *et al*., 2008a). Significant improvements in bio-separation technology were made by upgrading the system interconnecting phasins and target proteins via self-cleaving intein (Banki *et al*., 2005). This approach enabled *in vivo* immobilization onto the granule and the release of purified recombinant proteins once the native PHB particles were recovered, which in turn pushed bio-separation technology several steps forward towards convenience and cheapness. A receptor-mediated drug delivery system has been developed based on PhaP phasin. The system consists of *in vitro* synthesized PHA nanoparticles, PhaP and polypeptide or protein ligands (*e.g.* mannosylated human α1-acid glycoprotein (hAGP) and human epidermal growth factor (hEGF)) (Yao *et al*., 2008). Moreover, *in vivo* immobilized correctly folded eukaryotic proteins on the surface of PHA granules via phasin protein have been used for fluorescence activated cell sorting (FACS) based diagnostics which is a powerful technique for the qualitative and quantitative detection of biomolecules used widely, in both basic research and clinical diagnostic applications. Beads displaying a specific antigen are used to bind antibodies which are then fluorescently labeled using secondary antibodies (Backstrom *et al*., 2007).

Similarly, applying the *in vitro* approach the substrate binding domain of PHA depolymerase has been used to anchor fusion proteins to PHA microbeads (Lee *et al*., 2005). Another example of successful GAP application is for enzyme immobilization on the *in vivo* PHA granule surface using N-terminus of PHA synthase from *Pseudomonas aeruginosa* as a tag (Peters and Rehm, 2006).

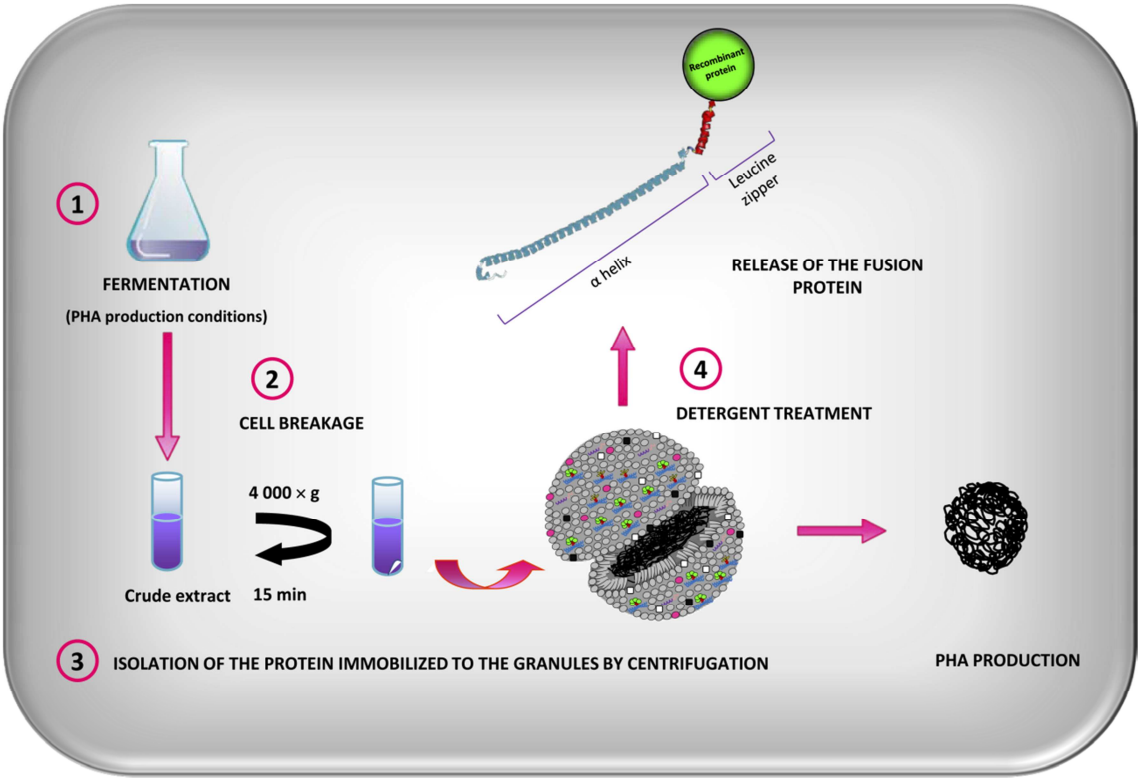

Figure 6. *In vivo* immobilization of fusion proteins to bioplastics by BioF tag. The procedure consists of: 1, the fermentation in *P. putida* under optimal PHA production conditions; 2, 3, isolation of the granules carrying the BioF-proteins fusions from the crude cell lysate by a simple centrifugation step; 4, release of fusion proteins via detergent treatment (modified from Moldes *et al*., 2004).

In vitro technology is highly convenient for medical applications, such as drug targeting, where the use of endotoxin-free PHA is preferable for GAP-fusion coating (see below). However, other applications such as protein delivery to natural environments do not necessary acquire extremely pure PHA and can benefit from an *in vivo* approach. Thus, a protein immobilization/purification system was designed, based on the use of PHA granules and the N-terminal domain of the protein PhaF (BioF tag) (Moldes *et al*., 2004). The BioF system constitutes a specific biotechnological tool for producing mcl-PHA beads (Figure 6). Once fermentation under optimal mcl-PHA production conditions is accomplished in *P. putida*, the granules carrying the BioF-protein fusions can be isolated from the crude cell lysate by a simple centrifugation process, and directly used for further applications. This approach was used for *in vivo*

immobilization of Cry1Ab derived insect-specific toxin protein in mcl-PHA granules. Generating BioF insect-specific toxin immobilized to bioplastics, suggested that the BioF tag could be exploited as a new tool for spreading active polypeptides to the environment (Moldes *et al*., 2006) (Figure 6).

5. PHA metabolic network and polyester functionalization

In most bacteria, such as the paradigmatic *Cupriavidus necator* H16 (formerly *Ralstonia eutropha* H16), PHB is synthesized in a three-step reaction starting with acetyl-CoA (Peoples and Sinskey, 1989) (Figure 7). In the first step two acetyl-CoA molecules are condensed in a reaction catalysed by a 3-ketothiolase. Then, generated acetoacetyl-CoA is stereoselectively reduced to [*R*]-3-hydroxybutyryl-CoA by a NADPH-dependent acetoacetyl-CoA reductase. Finally, the [*R*]-3-hydroxybutyryl-CoA monomers are polymerized by a PHB synthase, releasing PHB and free CoA as end products.

Pseudomonas species rely on β-oxidation pathway and *de novo* fatty acid synthesis to convert fatty acid or carbohydrate intermediates, respectively, into different [*R*]-3-hydroxyacyl-CoAs. These metabolites are used as substrates by PHA synthases which catalyze the committed step of mcl-PHA biosynthesis and finally end up as PHA polymer (Prieto *et al*., 2007).

The β-oxidation pathway involves the participation of a transport system coupled to an acyl-CoA synthetase (FadD), which catalyses the activation of n-alkanoic acid to its acyl-CoA derivates. Later, an acyl-CoA dehydrogenase (FadF), requiring the participation of an electron-transferring protein (FadE), catalyses the formation of a double bond in the β-position. Finally, a protein complex (FadBA) with five enzymatic activities (enol-CoA-hydratase, 3-OH-acyl-CoA dehydrogenase, cis-Δ^3-*trans*-Δ^2-enoyl-CoA isomerase, 3-OH-acyl-CoA epimerase and 3-ketoacyl-CoA thiolase) catalyses the removal of two carbon units of the acyl-chain being processed (Olivera *et al*., 2001a) (Figure 7). Concerning the fatty acid β-oxidation protein complex (FadAB), two set of

fadAB genes have been described in the *P. putida* KT2442 strain, *fadB* and *fadA* (PP_2136 and PP_2137) and *fadBx* and *fadAx* (PP_2214 and PP_2215). Apparently, the first set plays the most important role in fatty acid degradation, since *fadB* and *fadA* deletion mutants did not show completely blocked β-oxidation, but the production of PHA with a higher content of longer chain monomers, possibly due to their defective β-oxidation pathway (Escapa *et al*., 2011; Ouyang *et al*., 2007; Chung *et al*, 2009).

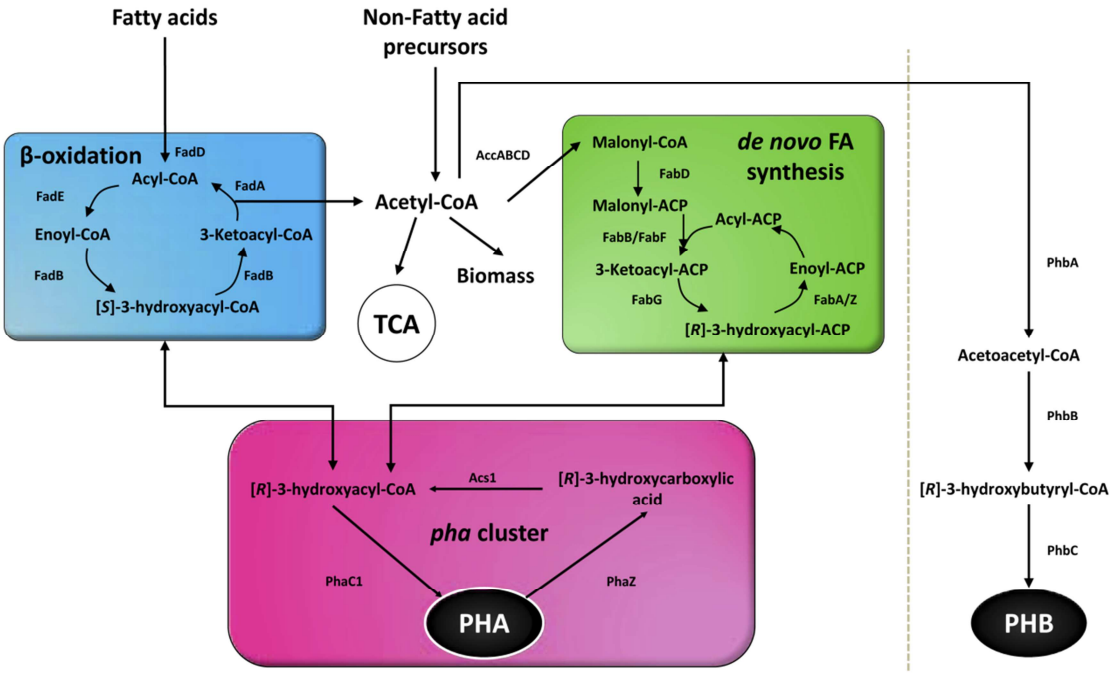

Figure 7. Metabolic pathways involved in PHA biosynthesis. Intermediates for PHA synthesis are derived from pathways connected with central carbon metabolism. Acetyl-CoA is the key intermediate in PHA synthesis, as the connection between catabolic and anabolic pathways involved in this system. The PHA cycle is a continuous process of synthesis (PhaC1) and degradation (PhaZ) of the polymer, in which acyl-CoA synthetase (ACS1) transforms the depolymerization products. Resulting products of ACS1 activity, [*R*]-3-hydroxyacyl-CoA, are potential substrates for polymerase or enzymes of fatty acid metabolism. PHB is synthesized from acetyl-CoA in three successive steps, involving the activity of β-ketoacyl-CoA thiolase (PhbA), acetoacetyl-CoA dehydrogenase (PhbB) and PHB polymerase (PhbC) (Escapa *et al*., 2012).

Non-fatty acid precursors can be oxidized to acetyl-CoA and channeled into PHA by *de novo* synthesis pathway, via [*R*]-3-hydroxyacyl-acyl carrier protein (ACP) intermediates. In this process, malonyl-CoA and its precursor, acetyl-CoA, are activated by transacylation to acyl-carrier protein (ACP). Malonyl and acyl-ACP derivatives are condensed by ketoacyl-ACP synthetase, reduced on losing a ketone group, dehydrated and saturated to the corresponding [*R*]-3-hydroxyacyl-ACP chain, which may be further elongated into two-carbon growing chains. Acyl-ACP intermediates can then be re-transformed into [*R*]-3-hydroxyacyl-CoAs by a specific transacylase, PhaG, present in most Pseudomonads (Fiedler *et al*., 2000) (Figure 7). Interestingly, unsaturated monomers such as 3-hydroxy-5-dodecenoate and 3-hydroxy-7-tetradecenoate are also generated by fatty acid *de novo* synthesis (Huijberts *et al*., 1992; Escapa *et al*., 2013).

Due to the broad substrate specificity of PHA synthase (PhaC), many organic molecules containing a carboxyl and a hydroxyl group in position 3, can be converted to the respective CoA thioester and can, in principle, be incorporated into a high-molecular-mass PHA. The biosynthetic pathways of the activated PHA precursor, [*R*]-3-hydroxyacyl-CoA, have been extensively studied and exploited through metabolic engineering, leading to the production of modified PHA, which, is a range of heteropolymers and homopolymers containing [*R*]-3-hydroxy fatty acids (Rehm and Steinbüchel, 1999).

5.1. Functionalized PHA through metabolic engineering strategies

Over the past decade, we have gained a better understanding of the molecular mechanisms and regulatory processes underlying biopolymer synthesis. Genome sequencing, functional genomics and systems biology, cloning and characterization of biosynthesis genes have all had a substantial impact on our understanding of biosynthetic pathways in organisms producing commercially relevant polymers, and have also led to the discovery of new biopolymer-producing bacteria (Pohlmann *et al*., 2006; Kalia *et al*., 2003; Escapa *et al*., 2012; Follonier *et al*., 2013; Poblete-Castro *et al*., 2012a; Poblete-Castro *et al*., 2012b; Poblete-Castro *et al*., 2013). This knowledge has provided a powerful tool for engineering bacteria capable not only of efficient

biopolymer production, but also of producing modified or even unnatural polymers with unique material properties for specific high-value applications. Since the discovery that some bacteria can incorporate [*R*]-3-hydroxyalkanoates (3HA) bearing functional groups from related substrates (Lenz *et al*., 1992), research has led to structural diversification of PHA by biosynthesis and post-biosynthetic chemical modifications (Hazer and Steinbüchel, 2007; Scholz, 2010). Structural and functional diversity is readily addressed in bacterial polyesters, as they are produced by modulated fermentation processes.

This concept has been exploited to produce a plethora of tailor-designed mcl-PHA, with highly diverse structures that include acetylthioester, acetoxy, alkoxy, amino, cyano, cyclohexyl, epoxy, halogenated, hydroxy or propylthiol groups (Table 1) (Kim *et al*., 2007; Scholz, 2010). A larger variety of PHA compositions with varying molar amounts of functional groups can be generated in most cases, by altering the ratio of co-substrates. Functional groups prone to chemical modifications have been introduced, mainly in *P. oleovorans* and *P. putida*, such as thiol, bromine, chlorine and fluorine radicals, cyano and epoxy groups. The introduction of such groups also modifies the thermal properties, and thus the processing requirements of the resulting polymers, enabling higher melting and lower glass-transition temperatures, or modified biological activities (see below).

Recently, our research team has produced poly(3-hydroxyacylthioalkanoate-*co*-3-[*R*]-hydroxyalkanoate) (PHACOS) (Figure 8), a new second-generation family of polymers containing thioester groups in the side chain. PHACOS are composed of 3-hydroxy-6-acetylthiohexanoate (OH-6ATH) and and the shorter derivative 3-hydroxy-4-acetylthiobutanoate (OH-6ATH). Previous studies described the biosynthesis of PHA containing sulfur groups in side chains, comprising either thiophenoxy functional groups (Takagi *et al*., 1999) or thioether groups (Ewering *et al*., 2002). Moreover, biopolymers with thioester bonds in the polymer backbone were isolated from the PHA-accumulating bacterium *R. eutropha*, containing 3-mercaptopropionate (3MP) or 3-mercaptobutyrate (3MB) as constituents (Lütke-Eversloh *et al*., 2002; Lütke-Eversloh and Steinbüchel, 2004).

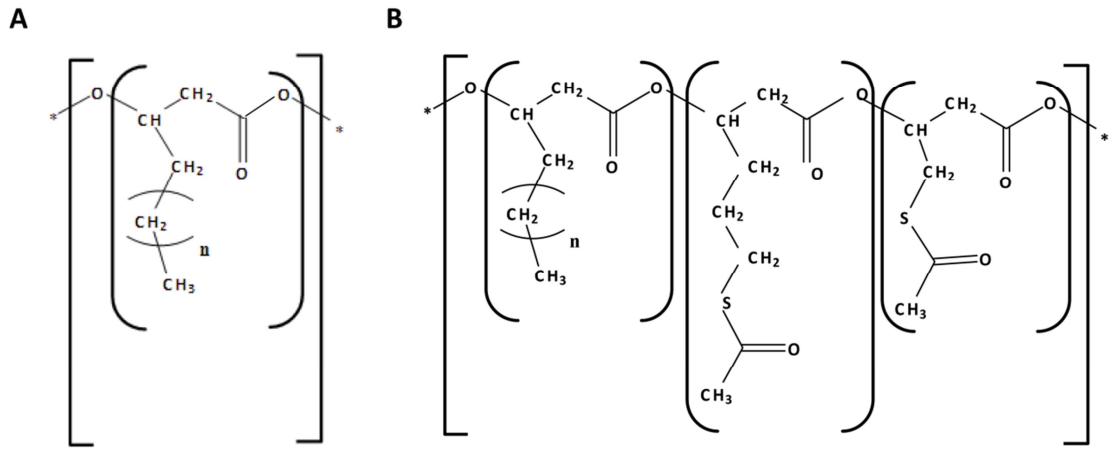

Figure 8. Schematic representation of mcl-PHA chemical structures. A, PHO-*co*-HHx composed of non-functionalized monomers 3HA (3-[*R*]-hydroxyoctanoate (OH-C8) and 3-[*R*]-hydroxyhexanoate (OH-C6)); B, PHACOS composed of functionalized monomers (3-hydroxy-6-acetylthiohexanoate (OH-6ATH) and 3-hydroxy-4-acetylthiobutanoate (OH-4ATB)) and of non-functionalized monomers OH-Alk (OH-C8, 3-[*R*]-hydroxydecanoate (OH-C10), and OH-C6 traces).

To obtain PHACOS, 6-acetylthiohexanoic acid (6-ATH) was used as precursor in a co-feeding strategy with decanoic acid as co-substrate. *P. putida* KT2442 and its *fadB* mutant (mutated *fadB* gene from the β-oxidation pathway, KT42FadB) were used for PHACOS synthesis. The need to add mcl-fatty acids to the medium in order to promote PHA synthesis in the presence of 6-ATH was clearly demonstrated. Decanoic acid was confirmed to be a good PHA precursor in cultures containing 6-ATH. However, results showed that PHACOS cannot be efficiently produced in a mutant strain under conventional one-step culture process due to the inability of strain KT42FadB to use 6-ATH and incorporate thioester groups in the side chain of polymer. A two-step culture process proved optimal for efficient production of PHACOS in both strains. The procedure comprised two consecutive cultivation steps. In the first step, cells were grown in Lysogeny broth (LB) medium for biomass production. In the second step, cells were incubated in minimal medium in the presence of 6-ATH as precursor in a co-feeding strategy with decanoic acid as co-substrate. When the derived strain KT42FadB is used, the polymer is overproduced and contains mainly OH-6ATH units (Escapa *et al*., 2011).

Table 1. Precursors used in the literature to produce functionalized mcl-PHA (branched alkyl, cyclohexyl, halogenated, acetoxy, ester, alkoxy, epoxy, thio, cyano, nitro, aromatics) (modified from Tortajada *et al*., 2013)

Precursor	%Mol functional Groups	Strain	Reference
Branched alkyl			
Citronellol	>99.0	*P. citronellolis* ATCC 13674	Choi *et al*., (1994)
Alkylhydroxyoctanoates	5.0	*P. oleovorans* ATCC 29347	Scholz *et al*.,(1994a)
Methyloctanoates	3.0-96.4	*P. oleovorans* ATCC 29347	Fritzsche *et al*., (1990c), Lenz *et al*., (1992)
Cyclohexyl			
Cyclohexylbutyric acid	>99.0	*P. cichorii* YN2	Honma *et al*., (2004)
Cyclohexylvaleric/ butytic acid	13.2-100.0	*P. oleovorans* ATCC 29347	Andújar *et al*., (1997), Kim *et al*., (2001)
Unsaturated alkenes (C7-C9)	45.0-55.0	*P. oleovorans* ATCC 29347	Lageveen *et al*., (1988)
Undecenoic acid	27.1-100.0	*P. putida* KCTC 2407	Kim *et al*., (2000)
Undecenoic acid	5.0-99.0	*P. oleovorans* ATCC 29347	Kim *et al*., (1995b), Park *et al*., (1998), Sparks *et al*., (2008)
Hydroxyoctenoic acids	63.5-81.6	*P. oleovorans* ATCC 29347	Fritzsche *et al*., (1990b)
Dicarboxylic acids (C4-C10)	4.7-11.7	*P. citronellolis* ATCC 13674	Choi *et al*., (1994)
Undecynoic acid	32.0-100.0	*P. oleovorans* ATCC 29347	Kim *et al*., (1998)
Undecynoic acid	22.0-100.0	*P. putida* KCTC 2407	Kim *et al*., (1998)
Halogens			
Bromoalkanoic acids(C6-C11)	3.7-38.0	*P. oleovorans* ATCC 29347	Kim *et al*., (1992), Lenz *et al*., (1992)
Chlorooctane	69.0	*P. oleovorans* ATCC 29347	Doi *et al*., (1990)

Precursor	%Mol functional Groups	Strain	Reference
Halogens			
Fluorohexanoic/ nonanoic acids	1.9-8.8	*P. oleovorans* ATCC 29347	Kim *et al*., (1996a)
Fluorohexanoic/ nonanoic acids	1.0-17.3	*P. putida* KT2440	Kim *et al*., (1996a)
Fluorophenoxyundecanoic acid	>99.0	*P. putida* 27N01	Takagi *et al*., (2004)
Acetoxy			
Octanone, octylacetate	3.3-10.3	*P. oleovorans* ATCC 29347	Jung *et al*., (2000)
Ester, Alkoxy, Epoxy			
Alkylheptanoate	2.5-60.0	*P. oleovorans* ATCC 29347	Scholz *et al*.,(1994b)
Alkxyhexanoic/octanoic/ undecanoic acids	31-100.0	*P. oleovorans* ATCC 29347	Kim *et al*., (2003)
10-epoxyundecanoic acid	25.0-75.0	*P. oleovorans* ATCC 29347	Bear *et al*., (1997)
C7-C12 alkenes	4.2-20.0	*P. cichorii* YN2	Imamura *et al*., (2001)
Soybean oil	63.0	*P. stutzeri* 1317	He *et al*., (1998)
Thio, sulfanyl			
Acetylthiohexanoic acid	16.5-78.5	*P. putida* KT2442, KT24FadB	Escapa *et al*., (2011)
Propylthiohexanoic acid	14.5-17.5	*R. eutropha* DSM541	Ewering *et al*., (2002)
Propylthioundecanoic acid	6.02	*P. putida* KT2440	Ewering *et al*., (2002)
Methylsulfanylphenoxyvaleric acid	12.2-35.6	*P. cichorii* H45, YN2	Kenmoku *et al*., (2002)
Methylsulfanylphenoxyvaleric acid	18.4	*P. jessenii* P161	Kenmoku *et al*., (2002)
Thiophenoxyundecanoic acid	>99.0	*P. putida* 27N01	Takagi *et al*., (1999)

Precursor	%Mol functional Groups	Strain	Reference
Cyano, nitro			
Cyanoundecanoic acid	17.0-32.0	*P. oleovorans* ATCC 29347	Lenz *et al*., (1992)
Cyanophenoxyhexanoi acid	0.0-2.2	*P. oleovorans* ATCC 29347	Kim *et al*., (1996a)
Cyanophenoxyhexanoi acid	0.0-34.0	*P. putida* KT2440	Gross *et al*., (1996), Kim *et al*., (1995a)
Nitrophenoxyhexanoc acid	4.2-5.1	*P. oleovorans* ATCC 29347	Kim *et al*., (1996a)
Nitrophenoxyhexanoic acid	1.0-4.8	*P. putida* KT2440	Kim *et al*., (1996a)
Dinitrophenylvaleric acid	1.2-6.9	*P. oleovorans* ATCC 29347	Aróstegui *et al*., (1999)
Aromatics (benzoyl, methylphenoxy, phenoxy, phenyl)			
Benzoylalkanoic acids (C4-C8)	8.3-79.8	*P. cichorii* YN2	Honma *et al*., (2004)
Methylphenoxyalkanoic acids (C6, C8)	40.0-65.0	*P. putida* KCTC 2407	Kim *et al*., (2000)
Methylphenoxyalkanoic acids (C6, C8) (PVA, NA)	68.0-100.0	*P. oleovorans* ATCC 29347	Kim *et al*., (1999)
Methylphenoxyalkanoic acids (C6, C8)	24.0-100.0	*P. putida* KCTC 2407	Kim *et al*., (1999)
Phenoxyundecanoic acid	>99.0	*P. oleovorans* ATCC 29347	Ritter *et al*., (1994)
Phenoxyalkanoic acids (C6,C8,C11)	100.0	*P. oleovorans* ATCC 29347	Kim *et al*., (1996b)
Phenoxyundecanoic acid	12.0-100.0	*P. putida* BM01	Song *et al*., (1996)
Phenylvaleric acid	13.7-19.5	*P. putida* BM01	Song *et al*., (2001)
Phenylvaleric acid	>99.0	*P. oleovorans* ATCC 29347	Curley *et al*.,(1996b)
Phenyl, tolylvaleric/ octanoic acids	3.0-64.0	*P. oleovorans* ATCC 29347	Curley *et al*., (1996a)

Precursor	%Mol functional Groups	Strain	Reference
Aromatics (benzoyl, methylphenoxy, phenoxy, phenyl)			
Phenylalkanoic acids (C4-C8)	>95.0	*P. jessenii* C8	Tobin *et al*., (2005)
Phenylalkanoic acids (C4-C8)	>95.0	*P. putida* S12, CA-1, H4, F6, D5	Tobin *et al*., (2005)
Phenylalkanoic acids (C6-C11)	>99.0	*P. putida* U fadA-, ΔFadBA-PhaZ	Abraham *et al*., (2001), García *et al*., (1999), Olivera *et al*., (2001b)
Phenylvaleric acid	>99.0	*P. oleovorans* ATCC 29347	Fritzsche *et al*., (1990a)
Phenylvaleric acid	12.6-40.6	*P. oleovorans* ATCC 29347	Kim *et al*., (1991)

Although most functionalized mcl-PHA intermediates are obtained through β-oxidation of fatty-acids, non-related carbon sources such as acetate, ethanol, fructose, glucose, gluconate or glycerol are channeled to PHA by the *de novo* fatty acid pathway, yielding a fraction of unsaturated monomers (3-hydroxy-5-dodecenoate and 3-hydroxy-7-tetradecenoate, see above and Figure 7). The molar fraction of unsaturated monomers usually ranges from 5 to 10 mol% depending on the strain (Sanchez *et al*., 2003; Silva-Queiroz *et al*., 2009) and can be increased by decreasing the culture temperature (Huijberts *et al*., 1992). The use of carbohydrate-related sources is advantageous in terms of substrate cost and diversity of monomer composition. However, PHA yields are generally lower in comparison to yields obtained when using fatty acids as substrates. Besides carbohydrates, glycerol has also been considered as an attractive raw material for PHA production due to its availability as a by-product of the biodiesel industry (Gómez *et al*., 2012). In *Pseudomonas* strains, glycerol is converted to glycerol-3-phosphate and then to dihydroxyacetone phosphate, which is further catabolized by a branch of the Entner–Doudoroff (ED) pathway (Schweizer *et al*., 1997; Cuskey *et al*., 1985). A prolonged lag phase hinders the use of glycerol, caused by the transcriptional repressor GlpR; however, GlpR knock-out mutants resulted in faster glycerol consumption, together with improved PHA accumulation,

possibly as a consequence of the larger availability of intermediates generated by *de novo* fatty acid synthesis (Escapa *et al*., 2013).

5.2. Properties of PHA carrying functionalized groups

The physical and mechanical properties of PHA are significantly influenced by their monomer composition and chemical structure (Chen, 2009). On the one hand, scl-PHA may be too rigid and brittle and lack the finer mechanical properties required for biomedical and packaging film applications. Poly([*R*]-3-hydroxybutyrate-*co*-[*R*]-3-hydroxyhexanoate) (PHB-*co*-HHx) copolymers with low 3-hydroxyhexanoate (OH-C6) fraction are the most commonly used PHA because their mechanical properties are more appropriate for use as flexible films than those of PHB (Noda, 1996). On the other hand, mcl-PHA may be elastomeric but are also characterized by very low mechanical strength. Therefore, the physical and mechanical properties of microbial polyesters need to be diversified and improved for application to packaging materials, tissue engineering and other specific applications (Hazer *et al*., 2012). To date, more than 100 different monomers, including linear, branched, saturated, unsaturated and aromatic (Huijberts *et al*., 1992; Olivera *et al*., 2001b; Scholz, 2010; Scholz *et al*., 1994) have been reported as PHA constituents (Steinbüchel and Valentin, 1995). Polymer properties are considerably influenced by the length of the side chain and its functional group. Of special interest are functionalized groups in the side chain that allow further chemical modification, *e.g*. halogens, carboxyl, hydroxyl, epoxy, phenoxy, cyanophenoxy, nitro phenoxy, thiophenoxy, and methylester groups (Kim and Lenz, 2001).

The family of PHA carrying thioester group in the side chain, PHACOS, generally show amorphous behavior due to the inability of the polymer backbone to fold tightly enough and organize to form crystals. This property is due to the presence of bulky side chains and functional groups that lead to stiffer and less mobile chains. Moreover, PHACOS show good thermal stability up to 200 °C, likely implying good processing properties for these materials and potentially interesting mechanical properties too. The molecular weights (M_n and M_w) of PHACOS are within the typical range observed

for mcl-PHA (Witholt and Kessler, 1999); furthermore, during production, neither culture procedure nor bacterial strain (mutant or wild-type) has a significant influence on molecular weight. However, PHACOS have tunable thermal properties as a result of different glass transition temperatures (T_g) derived from the numerous possible monomer compositions. The *fadB* mutant strain produces PHACOS with a lower content of thioester-based monomers, but monomers have longer side chains (Table 2) resulting in polymers with much lower T_g. This amorphous mcl-PHA with low glass transition (T_g) values are expected to display relatively high smoothness and marked elasticity, which are very interesting properties for biomedical applications (Escapa *et al*., 2011).

Table 2. PHA monomer composition (%mol) of PHACOS polymers obtained from *P. putida* KT2442 and *P. putida* KT42FadB 24 h cultures (Escapa *et al*., 2011)

Carbon source	**Strain**	**Culture procedure**	**Monomer composition (mol%)**						
			OH-C6	OH-C8	OH-C10	Σ 3HA	OH-4ATB	OH-6ATH	Σ Thio.
15 mM SO	KT2442	One-stage	8.5	91.5	-	100	-	-	-
12 mM DA	KT2442	One-stage	2.0	36.6	61.4	100	-	-	-
2.4 mM DA + 12 mM 6ATH	KT2442	One-stage	1.5	11.2	6.6	19.3	26.5	51.0	77.0
2.4 mM DA + 12 mM 6ATH	KT42FadB	One-stage	0.9	19.6	60.9	81.4	2.5	14.0	16.5
2.4 mM DA + 12 mM 6ATH	KT2442	Two-stage	2.1	13.6	7.1	22.8	31.5	47.0	78.5
2.4 mM DA + 12 mM 6ATH	KT42FadB	Two-stage	0.6	15.5	19.1	35.2	7.5	58.0	65.0

SO, Sodium octanoate; DA, Decanoic acid.

Concerning mcl-PHA obtained from non-fatty acid precursors, it is observed that the higher the molar fraction of unsaturated constituents in the monomers, the lower the resulting melting and T_g, very likely due to crystallization inhibition by unsaturated side chains (Ashby and Foglia, 1998). Double bonds are also easily attacked in chemical

reactions, allowing even higher diversification of the polymer properties (Lageveen *et al*., 1988; Hazer and Steinbüchel, 2007). A number of treatments have been described for crosslinking of unsaturated PHA, namely electron-beam irradiation, UV-irradiation or even autoxidation (De Koning *et al*., 1994; Bassas *et al*., 2008a; Bassas *et al*., 2008b; Silva-Queiroz *et al*., 2009) and in some cases those PHA can be transformed into rubbers (De Koning *et al*., 1994). Moreover, chemical epoxidation of the pendant vinyl groups has been applied to decrease melting temperature and increase glass transition temperature (Park *et al*., 1998). In addition, new plastic properties can also be achieved by blending PHA with other polymers.

6. PHA as scaffold biomaterial in tissue engineering

Biomaterials are defined as any material, natural or man-made, biodegradable and biocompatible, comprising whole or part of a living structure or biomedical device which performs, augments, or replaces a function lost through disease or injury. They have played an important role role in treating disease and improving health care (Langer and Tirrell, 2004). Among them, PHA polymers are promising materials for biomedical applications because they are natural, renewable, biodegradable and biocompatible thermoplastics (Hazer and Steinbüchel, 2007).

Elastomeric mcl-PHA and its copolymers offer extensive design potential with a large range of properties, paving the way for novel polymer applications and subsequently facilitating research in the past few years (Chen, 2009). However, the lack of availability of these polymers in large quantities still limits investigation. Hence, most of the current research focuses on poly([*R*]-3-hydroxyoctanoate) (PHO) and PHB-*co*-HHx copolymer due to their large production quantities and improved mechanical and elastomeric properties compared to scl-PHA (Williams and Martin, 2000; Chen *et al*., 2001).

Many successful studies using various animal models have clearly demonstrated that PHA, represented by PHB, poly(4-hydroxybutyrate) (P4HB), PHO and PHB-*co*-HV and PHB-*co*-HHx copolymers possess the necessary traits (biodegradability, biocompatibility and thermoprocessibility) not only for implant applications but also for controlled drug release (Chen and Wu, 2005). The performance of the aforementioned PHA has been studied in different biomedical devices (*e.g.,* sutures, repair devices, repair patches, slings, cardiovascular patches, orthopedic pins, adhesion barriers, stents, guided tissue repair/regeneration devices, articular cartilage repair devices, nerve guides, tendon repair devices, bone-marrow scaffolds, artificial esophagus and wound dressings) (revised in Chen and Wu, 2005) (Table 3). Among them, P4HB has been approved by the FDA (The Food and Drug Administration agency of the United States Department of Health and Human Services) for suture application under the trade name TephaFLEX, marketed by Tepha Inc., of Cambridge, Mass., USA. Tepha specializes in manufacturing pericardial patches, artery augments, cardiological stents, vascular grafts, heart valves, implants and tablets, sutures, dressings, dusting powders and prodrugs (Figure 9). With successful approval of P4HB as an implant biomaterial, more PHA-based biomaterials are expected to go under clinical trials soon. Given the diversity of PHA materials, they are expected to become a family of bioimplant materials with rich applications (Chen, 2009). Herein the most outstanding potential applications of PHA in the biomedical field will be revised.

There has been intensive research into the potential use of PHA in the construction of devices for cardiovascular application. One of the most advanced applications of PHB is the development of regenerative pericardial patches (Bowald and Johansson-Rudel, 1997) used to close the pericardium after surgery and thereby avoiding heart-sternum adhesion. Following an *in vivo* study in animal models, clinical testing on human patients has also been successful (Duvernoy *et al*., 1995). In addition, PHB was successfully used for arterial septal defect repair (Malm *et al*, 1992) and construction of cardiovascular stents (Behrend *et al*., 1998). Furthermore, PHA polymers have been tested in vascular grafting studies for repair or replacement of malfunctioning blood vessels in the arterial or venous systems due to damage or disease.

Table 3. PHA used in the biomedical field

Modified/unmodified PHA	Medical application	Reference
PHB	Subcutanous patches	Baptist, (1965)
PHB	Peripheral nerve guide	Hazari *et al*., (1999), Moshahebi *et al*., (2002)
PHB	Regenerative pericardial patch	Bowald *et al*., (1997), Duvernoy *et al*., (1995)
PHB	Pulmonary artery regeneration	Malm *et al*., (1994)
PHB	Arterial septal defect repair	Malm *et al*., (1992)
PHB	Cardiovascular stents	Behrend *et al*., (1998)
PHB	Stomach wall patch	Löbler *et al*., (2002)
PHB	Drug delivery, chemoembolization	Kassab *et al*., (1999)
PHB	Spinal cord injury	Navikov *et al*., (2002)
PHB-*co*-HV	Guided tissue regeneration	Leenstra *et al*., (1995)
PHB-*co*-HV	Bone regeneration	Cool *et al*., (2008)
Tricalcium phosphate reinforced PHB, PHB-*co*-HV	Internal bone fixation	Jones *et al*., (2000)
PHB-*co*-HV	Urethral reconstruction	Bowald *et al*., (1990)
PHB-*co*-HV	Subcutanous patches	Gogolewski *et al*., (1993)
PHB-*co*-HV	Myocardial patch	Kenar *et al*., (2010)
PHB-*co*-HV	Bone regeneration	Cool *et al*., (2008)

Modified/unmodified PHA	Medical application	Reference
PHB-*co*-HV	Auricular implant for drug delivery	Jones *et al*., (1994)
PHB-*co*-HV	Rods, drug delivery	Hasirci *et al*., (1998), Korkusuz *et al*., (2001)
PHB-*co*-HV	Cartilage proliferation	Köse *et al*., (2005)
PHB/PHB-*co*-HV	Suture	Shishatskaya *et al*., (2004)
PHB-*co*-HHx	Vessel stent	Qu *et al*., (2006)
PHB-*co*-HHx	Nerve conduit	Bian *et al*., (2009)
PHB-*co*-HHx	Bone regeneration	Wang *et al*., (2004a)
PHB-*co*-HHx	Cartilage proliferation	Wang *et al*., (2005)
PHB/PHB-*co*-HHx	Cartilage proliferation	Ye *et al*., (2009)
PHB-*co*-HV,PHB-4HB	Drug delivery	Türesin *et al*., (2001)
PHB-*co*-HV-PLGA	Nerve guide	Yücel *et al*., (2010)
HA reinforced PHB	Bone regeneration	Shishatskaya *et al*., (2006)
HA reinforced PHB/VA	Bone regeneration	Luklinska *et al*., (2003)
PHO	Pulmonary valve	Stock *et al*., (2000)

Modified/unmodified PHA	Medical application	Reference
PHO	Pulmonary heart valve	Sodian *et al*., (2000a), Sodian *et al*., (2000b), Sodian *et al*., (2000c) , Sodian *et al*., (2000d)
PHO-*co*-HHx-PGA	Abdominal aorta scaffold	Shum-Tim *et al*., (1999), Stock *et al*., (2000)
PHO-Sy	Subcutaneous patches	Hazer *et al*., (2009)
PHOU-Au	Subcutaneous patches	Hazer *et al*., (2011)
PHA monomers (*R*3HB)	Therapeutic effects on Alzheimer's and Parkinson's diseases, osteoporosis, memory improvement	Massieu *et al*., (2003), Zou *et al*., (2009), Kashiwaya *et al*., (2000)
PHA monomers and oligomers	Nutritional and energy supplements Ca^{2+} stimulation effect	Qu *et al*., (2006), Cheng *et al*., (2005), Cheng *et al*., (2006)

The elastomeric polymer PHO-*co*-HHx has been evaluated as a two-component scaffold for abdominal aorta tissue engineering in a lamb model (Shum-Tim *et al*., 1999; Stock *et al*., 2000). Perhaps the most remarkable results with PHA polymers have been obtained in the development of cell-seeded tissue-engineered heart valves. P4HB and PHO heart valve scaffolds were constructed and tested *in vivo* (see below; Sodian *et al.*, 2000a) (Figure 9).

In the dental and maxillofacial fields, PHB-*co*-HV has been utilized for guided tissue regeneration, where polymer barrier membranes were constructed to encourage regeneration of a new periodontal ligament by creating a space that excludes gingival tissue from the healing wound. Performance *in vivo* was found to be satisfying

(Leenstra *et al*., 1995). Moreover, PHB-*co*-HV has been used for guided bone regeneration (Cool *et al*., 2008). When used in orthopedics for internal bone fixation, PHB and PHB-*co*-HV polymers were reinforced with hydroxyapatite (HA), glass or tricalcium phosphate (Jones *et al*., 2000). Results showed favorable overall tissue responses, as well as some indication of osteogenic activity; therefore, it was concluded that they can serve as an alternative to corticocancellous bone grafts.

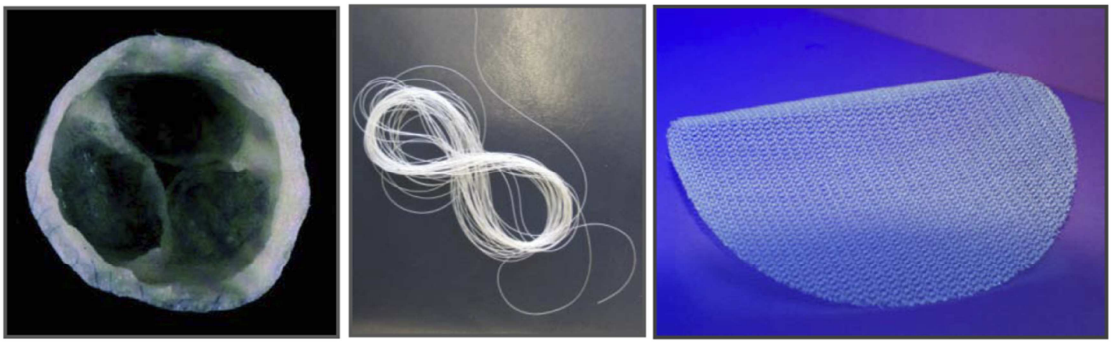

Figure 9. Examples of PHA applications of in the biomedical field. From left to right PHO heart valve scaffolds, PHB-*co*-HV suture and TephaFLEX® surgical mesh (used for soft tissue reinforcement in plastic and reconstructive surgery, for temporary wound support, reinforcement of soft tissues and hernia repair).

Another possible application of PHB-*co*-HV copolymer was reported in urology for urethral reconstruction, in which the polymer scaffold supports regeneration of fully functional urethra tissue (Bowald and Johansson, 1990). Moreover, wound management is one of the well studied areas in which PHA have many applications. In another study, PHB and PHB-*co*-HV sutures were proven to possess the necessary strength for the healing muscle-fascial wounds, without causing any acute vascular reaction at the implantation site or any adverse events (Shishatskaya *et al*., 2004) (Figure 9). Finally, PHB has been shown to have good polymer characteristics for soft tissue defect repair, especially for the closure of lesions in the gastrointestinal tract (Löbler *et al*., 2002).

The use of PHB and PHB-*co*-HV for drug delivery has been evaluated in numerous studies, including investigation into their performance as subcutaneous implants (Jones *et al*., 1994), compressed tablets for oral administration (Hasirci *et al*., 1998; Korkusuz *et al*., 2001) and microparticles for intravenous use (Kassab *et al*., 1999). The therapeutic potential of P4HB was investigated and was found to have possible beneficial effects in narcolepsy treatment among others (Williams and Martin, 2001).

Oligomeric forms of ketone body hydroxybutyrate (HB) have been evaluated as an alternative to the sodium salt of the monomer to provide controlled release systems for monomers, thus overcoming problems associated with administering large amounts of sodium ion *in vivo*. This system could be applied to seizure control, reduction of protein catabolism, appetite suppression, metabolic disease control, treatment of diabetes and insulin resistant states, among others (Martin *et al*., 2000).

Due to the elastomeric behavior and biodegradability of mcl-PHA they can be used as promising base polymers to develop biodegradable pressure synthetic adhesives (PSA). Such PSA can find applications in wound coverings and closures, surgical drapes, electrocardiograph electrode mounts and transdermal drug delivery (Babu *et al*., 1993). In the development of PSA, PHO, poly([*R*]-3-hydroxydecanoate) (PHD) and mixtures of poly([*R*]-3-hydroxyoctanoate-*co*-[*R*]-3-hydroxyundecenoate) (PHO-*co*-HU) were used (Babu *et al*., 1993). Moreover, mcl-PHA like PHO and copolymers such as PHB-*co*-HHx have been used as biopolymer scaffolds for the regeneration of nerve axons (Bian *et al*., 2009). Many other applications of PHA have been addressed, showing them to have great clinical potential (Table 3).

7. Factors affecting PHA application

7.1. Pyrogen removal

For medical use as attractive biopolyesters, most PHA have been sterilized using ethylene oxide, without significantly affecting the physicochemical properties of the polymers. However, inappropriate extraction of PHA from bacterial biomass results in contamination with lipopolysaccharides (LPS), which form an integral part of the gram-negative bacteria outer membrane (Petsch and Anspach, 2000). Due to their high heat stability and insensitivity to pH changes, they cannot be eliminated by a simple sterilization step. These cell-associated compounds, named endotoxins, are pyrogenic and cause fever and pathology when injected into animals. Special attention has been paid to minimize the endotoxin contamination of PHA as a number of contaminants were reported in industrial samples of PHB-*co*-HV (Rouxhet *et al*., 1998; Garrido, 1999).

Endotoxin levels are measured in endotoxin units (EU) because their molecular weight may vary a great deal (10 to 1 000 kDa). One EU is equivalent to approximately 100 pg of *Escherichia coli* lipopolysaccharide, the amount present in around 10^5 bacteria. Humans can develop symptoms when exposed to as little as 5 EU/kg body weight. These symptoms include, but are not limited to fever, low blood pressure, increased heart rate, low urine output. Even smaller doses of endotoxin in the blood stream are often fatal.

A conventional industrial sample of PHB was found to contain more than 120 EU/g (Williams *et al*., 1999). Several methods have been reported for endotoxin removal, such as depyrogenation based on the use of peroxide (Williams *et al*., 1999) and sodium hydroxide (Lee *et al*., 1999). The FDA permits concentrations of less than 20 EU/g of PHA or per medical device. This can be successfully achieved by heat-driven PHA extraction with a solvent, followed by non solvent precipitation. Another method is temperature-controlled recovery of PHO-*co*-HHx from *P. putida* GPo1. In contrast to other methods, precipitation of PHO was triggered by cooling the hot solution to a

particular temperature. Applying this method, a minimal endotoxicity of 2 EU/g PHO can be achieved and a purity of close to 100% (w/w) (Furrera *et al*., 2007).

7.2. Biocompatibility

There have been many attempts to define biocompatibility related to the behavior of biomaterials in various contexts. The term refers to the ability of a material to perform its desired function generating an appropriate host response in a specific situation (Black, 2006). The ambiguity of the term reflects the ongoing development of insights into how biomaterials interact with the human body and how those interactions eventually determine the clinical success of a medical device. Indeed, the main objective when using biomaterials is to generate the most appropriate beneficial cellular or tissue response without eliciting any undesirable local or systemic effects in the recipient of the therapy. However, since the immune response and repair functions in the body are so complicated, the biocompatibility of a material should not be described in relation to a single cell type or tissue. Nevertheless, it is essential to consider *in vitro* cellular behavior for further comprehensive biocompatibility evaluation of implanted polymers.

High biocompatibility is essential for the acceptance of any object implanted in humans and other mammals. Several factors are shown to influence implant biocompatibility such as shape, surface porosity, surface hydrophilicity, surface energy, chemistry of the material, the environment (tissue) of the implant, and its degradation products (Zinn *et al*., 2001). In this respect, PHA have the potential to become an important compound for medical applications as tests have shown PHB biocompatibility. This is not surprising if one considers that [*R*]-3-hydroxybutyric acid is a normal constituent of blood, at concentrations between 0.3 and 1.3 mM (Wiggam *et al*., 1997), and it is also found in the cell envelope of eukaryotes (Reusch, 2000).

7.2.1. *In vitro* effect of PHA on mammalian cells

In vitro investigations have proven suitable to elucidate several aspects of cell interactions with biomaterials. They preclude the numerous events that might occur after implantation of a foreign material in an animal model and provide a simple environment to study cellular responses. As upon implantation of polymers, local tissue reacts with an inflammatory response, which initiates tissue repair and regeneration processes. Many different mammalian cell lines have been used in *in vitro* studies, the most common being fibroblasts, macrophages, polymorphonuclear leukocytes (PMNs) and endothelial cells (Saad *et al*., 1999).

Cytotoxicity and inflammation studies of PHA have mainly focused on characterizing cell responses to polymer extracts, whereas few studies have attempted to analyze cell response in direct contact with the polymer (Chaput *et al*., 1995). However, results varied with the medium, surface-to-volume ratio, time and temperature.

Tissue response has been characterized by seeding cells on the polymer surface and evaluating their initial attachment, growth and morphology. Thus, the effect of surface morphology of PHA, as one of the factors influencing biocompatibility, was studied *in vitro* on mouse fibroblast (Kai *et al*., 2002). The study demonstrated that films with a fairly regular and smooth surface, such as PHB-*co*-HHx/PHB blends with low crystallization, facilitate cell attachment and growth of the seeded mouse cell line L929, thereby increasing biocompatibility (Kai *et al*., 2002). Moreover, good endothelial cell and myofibroblast attachment to PHO-*co*-HHx was reported (Sodian *et al*., 1999). Interactions have been studied between PHA, such as PHB-*co*-HV, and human keratinocytes (Ji *et al*., 2008), allogeneic chondrocytes (Wang *et al*., 2008b), glial cells (Xiao *et al*., 2007), fibroblast and osteoblast (Wang *et al*., 2005) and results proved the ability of abovementioned cell lines to adhere and proliferate properly.

In tissue engineering, apart from reactions to material itself, it is very important to evaluate how cellular behavior is affected by the degradation products, and especially in the case of PHA, considered to be biodegradable. To analyze the effect of PHA degradation products, oligo-hydroxyalkanoates (OHAs), studies were carried out on

macrophages, Kupffer cells, fibroblasts, osteoblasts and others (Sun *et al*., 2007; Saad *et al*., 1996a; Saad *et al*., 1996b; Saad *et al*., 1996c). Results demonstrated that OHAs in low concentrations (10-20 mg/L) do not significantly affect cell viability, whereas higher concentrations (>40 mg/L) reduce cell viability, with increased cell apoptosis, more cell death, delayed cell cycle and reduced cell proliferation. Moreover, OHA cytotoxicity decreased with increasing OHA side chain length, indicating that medium chain length OHA and mcl-PHA are more biocompatible then scl-PHA (Sun *et al*., 2007).

Attempts to increase polymer scaffold biocompatibility have been made using different approaches. Current strategies to improve implant biocompatibility may be grouped into two areas: (i) passive coatings and (ii) active release. Passive strategies rely on modification of the implant surface through chemical and physical means. Alternatively, active release is based on the release of molecules that may modify the host´s foreign-body response, direct the wound healing process and favor tissue integration of the implant (Bridges and Garcia, 2008).

Because surface chemistry at the tissue-implant interface largely influences immune system activation, the outer surface of the implant is of great importance. One of passive strategies includes increasing polymer hydrophilicity to enable better cell adherence to the scaffolds. To that end, graft co-polymerization of acrylamide onto PHO films was carried out, and was found to improve ovary cells attachment (Kim *et al*., 2002). Coating the surface of the polymer with a biocompatible compound is another approach adopted to increase polymer biocompatibility. With that aim, the surfaces of PHB-*co*-HHx matrices were coated with a biocompatible silk fibroin protein (Mei *et al*., 2006), PHA granule binding protein PhaP fused with cell adhesion motif Arg-Gly-Asp, RGD (Dong *et al*., 2010) and others. Moreover, approaches such as cell deposition can increase biocompatibility (Sodian *et al*., 2000d).

In another initiative, active strategies have been designed for different implant coatings that deliver active molecules (*e.g.* anti-inflammatory agents) and offer more interactive and direct approaches to modulate cell behavior (Bridges and Garcia, 2008). Immunomodulatory agents can be immobilized onto the surface or delivered in soluble form. Possible strategies for the controlled release of agents include passive

diffusion, bioerodible/degradable coatings, hydrolysable or enzyme-degradable linkages and many others.

7.2.2. *In vivo* tissue response

Despite the fact that investigation of *in vivo* response to PHA implants began back in the mid 1960s (Baptis and Ziegler, 1965), it is still a controversial subject as multiple factors and the wide range of PHA with different monomer composition have a particular influence and produce distinctive tissue and inflammatory responses. For example, inflammatory cells have been reported in the vicinity of some PHA implants (Gogolewski *et al*., 1993). However, care should be taken when interpreting these data, since some of the studies were based on industrial and commercially available PHA rather than medical-grade PHA polymers (Williams *et al*., 1999). Moreover, inflammation and other undesirable reactions of tested biomaterials may be related to polymer chemical composition, a particular implantation site, the shape of the implant, the degree of chemical purity of the material among other factors. The biocompatibility of implants is evaluated by applying various criteria. The histological approach is based on determining the degree of fibrotic reaction surrounding the samples and the presence of inflammatory or malign cells. Biochemical assays are used to reveal cellular and extracellular matrix formation (*e.g.,* presence of collagen by 4-hydroxyproline assay). Immunocytochemical analysis is based on the use of antibodies for inflammatory cell detection. Many other assays can be performed depending on the specificity of scaffold function (*e.g.* thrombus formation, echocardiography to check proper functioning of 3-leaflet heart valves, scaffold vascularization, etc.).

Hosts react upon the implantation of a foreign body (biomaterial). This host reaction includes: (i) blood-material interactions; (ii) acute inflammation; (iii) chronic inflammation; (iv) granulation tissue development; (v) fibrosis/fibrous capsule development and (vi) resolution (Figure 10). In the very early stages of implantation, proteins and other biomolecules present in the blood plasma and biological fluids rapidly adsorb onto the surface of the biomaterial, completing the first step of the process, blood-material interactions. Adsorbed molecules (fibrinogen, IgG and

complement fragments) mediate leukocyte-biomaterial interactions and subsequent inflammatory reactions. During the acute phase, neutrophils are stimulated and recruited to the implantation site. The biological role of the acute inflammatory response is to phagocytose foreign material. The attempt made by inflammatory cells to engulf and degrade the implant leads to reduced analyte diffusion. Subsequently, neutrophils are replaced by macrophages and chronic inflammation begins. Additionally, consumption of oxygen and glucose produces reactive oxygen species (ROS), chemically reactive molecules containing oxygen (superoxide and peroxide). Moreover, local pH may drop due to this oxidative process, resulting in enzyme degradation. Differentiated macrophages secrete a variety of inflammatory mediators and often fuse to form multinucleated foreign body giant cells (FBGC), which are the hallmark of chronic response. The FBGC further enhance degradation of the underlying implant surface. The extent of the chronic inflammatory response is dependent not only on the physical and chemical properties of the implant but also on mechanical stresses (*i.e.,* movement) at the implant site. Granulation tissue is formed following resolution of the chronic inflammatory response due to the persistence of macrophages and infiltration of fibroblasts at the wound site. During the final step in the immune sequence, fibroblasts infiltrate the site and generate a fibrous capsule around the implant (Bridges and Garcia, 2008) (Figure 10). The final steady-state is called resolution. There are three possible outcomes for the implant: (i) resorption; (ii) integration and (iii) encapsulation (fibrosis). The severity and extent of the biological response to an implanted biomaterial or device influence the probability of its successful integration into the surrounding tissue, as well as overall device performance. Initial phases of foreign-body reaction are dictated largely by the extent of injury and surgical technique, implantation site, implant shape, size and local and systemic health of the recipient (Anderson, 2001). Significant research efforts have focused on modifying material properties to generate more biocompatible implants.

A small amount of information on PHO, PHO-*co*-HHX and P4HB is available, whereas most current information relates to PHB and PHB-*co*-HB (reviewed in Chen *et al*., 2001) as previously discussed. One of the earliest *in vivo* studies on mcl-PHA was carried out on the copolymer PHO-*co*-HHx through subcutaneous polymer

implantation in mice (Williams *et al*., 1999). No evidence of macrophages was found in the implant sites and the tissue response continued to be very mild even 40 weeks post-implantation. Histological analysis revealed that the implants were encapsulated with a thin layer of fibroblasts surrounded by collagen and the polymer proved to be particularly inert, and could be readily removed with little tissue adhering to the implants (Williams *et al*., 1999).

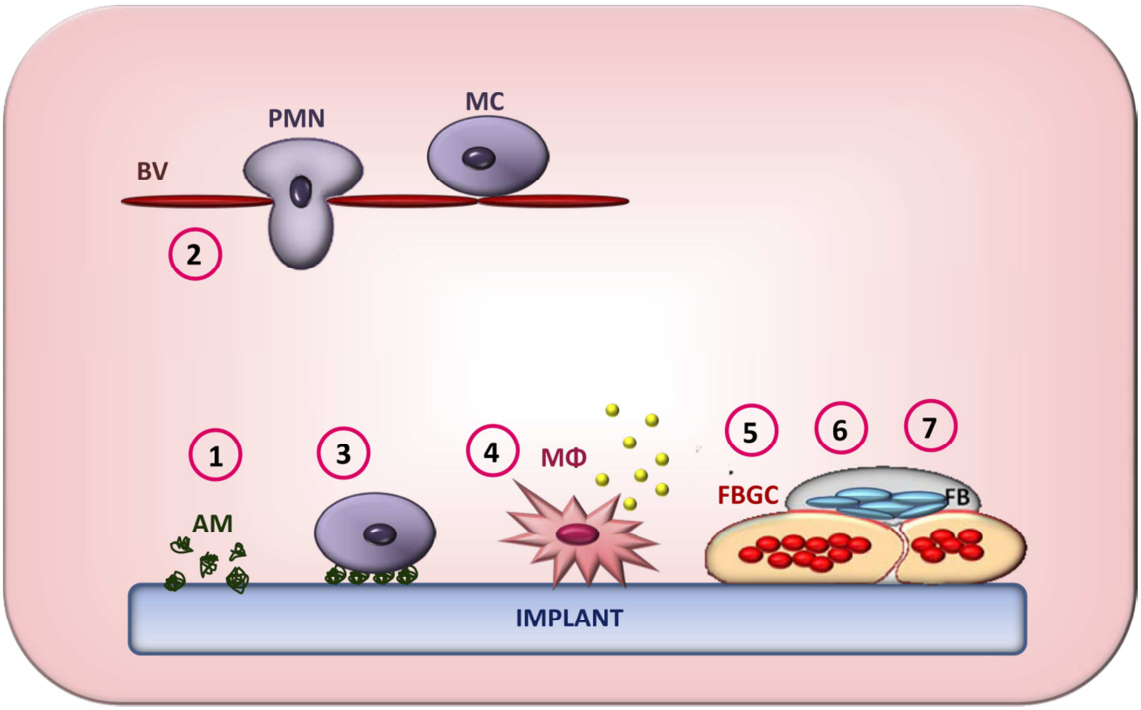

Figure 10. Host foreign body response events to implanted materials. 1-3, Polymorphonuclear leukocytes (PMF) and monocytes (MC), recruited by stimulatory cues, emigrate from blood vessels (BV) and adhere to the layer of adsorbed molecules (AM) on the implant; 4-6, Differentiated macrophages (MΦ) become activated, secreting a variety of inflammatory mediators, and often fuse into a foreign body giant cell (FBGC); 7, Fibroblasts (FB) infiltrate the site and generate a collagen fibrous capsule around the implant (modified from Bridges and Garcia, 2008).

One of the strategies to improve biocompatibility and implant integration is by their *in vitro* seeding with autologous cells. Thus, a PHO trileaflet heart valve scaffold was seeded with vascular cells harvested from vascular arteries (Sodian *et al*., 2000d), after its proper functioning (synchronous opening and closing) was confirmed in

pulsatile bioreactor (Sodian *et al*., 2002. This study demonstrated that tissue-engineered PHO heart valve scaffolds can be used for implantation in the pulmonary position with an appropriate function for 120 days in lambs (Sodian *et al*., 2000d). In another study the feasibility of creating PHO trileaflet pulmonary conducts seeded with autologous cells was evaluated (Stock *et al*., 2000). Based on these results, it was concluded that an engineered scaffold can work properly in pulmonary circulation.

7.3. *In vitro* and *in vivo* PHA biodegradation

The interest in studying PHA hydrolysis lies not only in their potential use as bioplastics or biomaterials, but also in the production of intermediates (3HA), as they can be used as chiral starting materials in the pharmaceutical and medical industries (Luengo *et al*., 2003; Ren *et al*., 2005). In addition, PHA polymers have numerous applications in medicine and surgery. These materials are designed to degrade *in vivo* in a controlled way over a predetermined implantation period, so that degradation helps to achieve a particular function.

PHA polymers are biodegradable, and their degradation can be triggered by different mechanisms. The best studied process is enzymatic hydrolysis by microbial depolymerases. Many microorganisms can catabolize PHA through extracellular or intracellular degradation under aerobic or anaerobic conditions (Jendrossek and Handrick, 2002). To date, both extracellular scl-PHA (Jendrossek and Handrick, 2002) and intracellular mcl-PHA depolymerases have been characterized (De Eugenio *et al*., 2007). However, PHA depolymerases are even abundant in the environment, their PHA degradation activity is linked to soil and there is no evidence of their presence in animal tissue (Williams and Martin, 2002). Nevertheless, characterization of PHA depolymerases has shed light on the properties that other α/β hydrolases from animal tissue might harbor (Winkler *et al*., 1990; Jendrossek *et al*., 1996).

Studies on PHA polymers enzymatic hydrolysis in animal tissue are primarily based on *in vitro* investigation. Thus it was demonstrated that macrophages are able to phagocytize PHB *in vitro* (Saad *et al*., 1999) and free radicals, acidic products or enzymes produced by these cells may also accelerate degradation (Tracy *et al*., 1999). Moreover, when a biodegradable polymer is implanted *in vivo*, macrophages and FBGC phagocytize and resorb the polymer (Marios *et al*., 1999a; Shishatskaya *et al*., 2008). In studies carried out *in vivo* in a murine model, it was found that the molecular weight of PHO-*co*-HHx subcutaneous implants decreased two-fold over 40 weeks. Another proposed mechanism of PHA degradation is based on non-enzymatic chemical hydrolysis (Marios *et al*., 1999b). Also, two different degradation mechanisms: enzymatic and non-enzymatic catalysis, have been proposed to coexist (Qu *et al*., 2006). Nevertheless, the exact mechanism and enzymes involved in the degradation process *in vivo* have not been identified, as they are shown to differ depending of the PHA polymer.

The rates of PHA polymer degradation *in vitro* and *in vivo* vary considerably and depend primarily upon chemical composition. It was demonstrated that PHA biodegradation is influenced by the presence of functional groups in the polymer chain, as well as by the hydrophilicity/hydrophobicity balance (Mochizuki and Hirami, 1997; Tokiwa and Calabia, 2004). Moreover, stereoregularity, molecular mass, morphological properties and crystallinity affect PHA biodegradability (Mochizuki and Hirami, 1997; Tokiwa and Calabia, 2004). Other factors influencing *in vivo* degradation such as location, surface area, physical shape and form can be very important. Thus, *in vitro* studies are not always good indicators of *in vivo* polymer behavior as the specific material requirements will differ according to the nature of the application.

Different approaches have been taken to increase PHA degradability, such as increasing hydrophilicity, polymer surface modification, crystallinity reduction and others. Studies have been carried out to increase polymer hydrophilicity, either by incorporating more hydrophilic groups in the polymer chain or by grafting more hydrophilic molecules onto the polymer chain. Such modifications enable improved water uptake and swelling of the polymer matrix, thus leading to increased polymer degradation. In one such study, efficient improvement of degradation was achieved by

PLA and polyethylene glycol (PEG) grafting onto a backbone of PHO-*co*-HU (Babinot *et al*., 2010). Moreover, PHO-*co*-HHx was blended with gelatin and degradation was accelerated (Wang *et al*., 2004b) as blending created a more porous polymer surface and subsequently a greater surface area of the polymer was exposed for hydrolysis attack (Wang *et al*., 2004b).

II. Objectives

As previously mentioned functionalization of PHA confers new properties to the polymer and subsequently opens a wide range of possibilities for industrial and biomedical application. Nevertheless, polymer modification processes need to be refined and studied in detail for each specific application. Hence, one of the goals of this PhD Thesis was to address the key factors that drive phasin tag immobilization to the granule. In addition, the study aimed to investigate the new properties of functionalized PHA obtained applying metabolic engineering. Thus, this PhD Thesis was organized under the following objectives:

- Design of natural PHA nano-beads, engineered to display fusion proteins of interest.
- Test new properties of second generation bacterial polyesters (PHACOS) carrying a chemically modifiable functionalized side chain that confers new properties to the polymer.
- *In vivo* investigation of PHACOS antibacterial properties and biocompatibility.
- Development of a non-invasive method for *in vivo* real-time monitoring of mcl-PHA implant-associated infection and inflammation.

III. Materials and methods

1. Bacterial strains, plasmids, media and growth conditions

The bacterial strains used throughout this study are listed in Table 4. Unless otherwise stated *Escherichia coli* and *Pseudomonas putida* strains were grown in Lysogeny broth (LB) medium (Sambrook and Russell, 2001) with aeration at 37 °C and 30 °C respectively. The appropriate selection antibiotics, kanamycin (50 μg/mL), gentamycin (5 μg/mL), rifampicin (50 μg/mL) or ampicillin (100 μg/mL) were added when needed. The *P. putida* strain KT2442, a derivative strain of the parental strain KT2440 whose complete nucleotide sequence of the genome is accessible in the data bank (Nelson *et al.*, 2002), was used throughout this study. *E. coli* DH10B (Invitrogen™), *E. coli* CC18λ*pir* and *E. coli* SM10λ*pir* were used as hosts for gene cloning.

Table 4. Bacterial strains, plasmids and oligonucleotide primers

Bacterial strains		
Escherichia coli		
CC118λ*pir*	Host for pVLT35 plasmids	Herrero *et al*., (1990)
DH10B	Host for *E. coli* plasmids	Invitrogen™
HB101	Host for pRK600 plasmid	Sambrook and Russell (2001)
SM10λ*pir*	Host for pPF61 plasmids	Prieto *et al.*, (1999)
SM10λ*pir* (pKNGFdel)	Host for pKNGFdel plasmids	Galan *et al.*, (2011)
Pseudomonas putida		
KT2442	KT2440 derivative strain	Nelson *et al*., (2002)
KT42-BG	KT2442 derivative strain containing *bioF-gfp*	This work
KT42C1	KT2442 derivative strain, *phaC1* deletional mutant	De Eugenio *et al*., (2010a)
KT42C1ZC2	KT2442 derivative, *phaC1, phaZ, phaC2* deletional mutant	This work
KT42C1ZC2F	KT42C1ZC2 derivative strain, *phaF* deletional mutant	This work
KT42C1ZC2F-BG	KT42C1ZC2F derivative strain containing *bioF-gfp*	This work
KT42F	KT2442 derivative strain, *phaF* deletional mutant	Galan *et al*., (2011)

Bacterial strains		
Pseudomonas putida(continued)		
KT42F-BG	KT42F derivative strain containing *bioF-gfp*	This work
KT42F-GC	KT42F derivative strain containing *gfp-cphaF*	Galan *et al.*, (2011)
KT42-GC	KT2442 derivative strain containing *gfp-cphaF*	Galan *et al.*, (2011)
KT42I	KT2442 derivative strain, *phaI* deletional mutant	This work
KT42I-BG	KT42I derivative strain containing *bioF-gfp*	This work
KT42I-BGF	KT42I-BG derivative strain containing *phaF*	This work
KT42I-F	KT42I derivative strain containing *phaF*	This work
KT42I-GC	KT42I derivative strain containing *gfp-cphaF*	Galan *et al.*, (2011)

Bacterial strains used for adhesion and antimicrobial study	**Origin/Characteristics**
Bacillus subtilis subsp. *subtilis*	CECT 39
Escherichia coli	CECT 516
Mycobacterium smegmatis^{T}	CECT 3020
Pseudomonas aeruginosa PAO1	CECT 4122
Salmonella enterica subsp. *enterica*^{T}	CECT 722
Stapylococcus aureus 61115	A. Vindel, ISCIII/MRSA
Stapylococcus aureus 61268	A. Vindel, ISCIII/MRSA
Stapylococcus aureus 61314	A. Vindel, ISCIII/MRSA
Stapylococcus aureus subsp. *aureus*^{T}	CECT 86
Stapylococcus aureus Xen29	Caliper LS, Inc.
Stapylococcus epidermidis^{T}	CECT 232
Streptococcus dysgalactiae subsp. *equisimilis*	CECT 926
Streptococcus pyogenes	CECT 985

Plasmids		
pAmilux	Amp^R , *lux*; plasmid carring *Photorhabdus luminescens luxCDABE* (*lux*) gene cluster	Mesak *et al*., (2009)
pAmiluxBLAZ	pAmilux derivative carring *lux* gene cluster under control of *blaZ* gene promoter	Provided by Prof. Lasa
pAmiluxSPA	pAmilux derivative carring *lux* gene cluster under control of *spa* gene promoter	Provided by Prof. Lasa
pCNB5	Km^R, Amp^R, pUTminiTn*5*, *lacI*^{q}*::Ptrc*	De Lorenzo *et al*., (1993)
pCNB5-*bioF-gfp-clytag*	pCNB5 derivate containing *bioF-gfp-clytag*	This work
pCNB5-*gfp-cterm*	pCNB5 derivate containing *gfp-cterm*	This work
pGEM-T	Amp^R, cloning vector	Invitrogen^{TM}
pPF61	Tc^R, pJMT6, *lacI*^{q}*::Ptrc::phaF*	Prieto *et al.*, (1999)
pKNGFdel	pKNG101 derivate containing fragments upstream and downstream *phaF* gene	Galan *et al.*, (2011)
pGreenTIR	Amp^R , *ori*pMB1; plasmid harbouring GFP cassette	Miller *et al*., (1997)
pUC18Not-*gfp*	pUC18Not derivate containing GFP casstet	This work
pK18*mobsacB*	Km^R, ColE *ori*V, Mob^+, *lac*Zα, *sacB*; vector for allelic exchange homologous recombination mutagenesis	Schäfer *et al*., (1994)
pK18*mobsacB-c1zc2*	Vector used for *phaC1ZC2* deletion	Escapa *et al*., (2013)
pKI18*mobsacB*	pK18*mobsacB* derivate containing fragments upstream and downstream *phaI* gene	This work
pKNG101	Sm^R, *ori*R6K, *sacB*; vector for allelic exchange homologous recombination mutagenesis	Kaniga *et al*., (1991)
pMAB20	pVLT31 derivative containing *pF-bioF*	Biomedal S.L.
pMAB20-*gfp-lytag*	pMAB20 derivate harboring *gfp-lytag*	Biomedal S.L.
pRK600	Cm^R, ColE1 *ori*V RK2 Mob^+ Tra^+; donor of transfer functions	Kessler *et al*., (1992)
pUC18Not	Am^R, *lac*Zα. Identical to pUC18 but with NotI-polylinker of pUC18-NotI as MCS	Herrero *et al*., (1990)
pUC18Not-*gfp-cterm*	pUC18Not derivate containing GFP-C-term	This work
pVLT31	Tc^R, expression vector bearing *lacI*^{q}*::Ptac*	De Lorenzo *et al*., (1993)

Oligonucleotide primers
F5mutI GCGGATCCCCGGTCAGCTTCTCGATCTG (*BamHI*)
F3mutI CGGAATTGGAGAGCAGGATGGCTGGC (*EcoRI*)
X5mutI CGGAATTCATGGAGGCTGGGCTTGAG (*EcoRI*)
X3mutI TCCCCCGGGAGATCACCTGTGCTGGCC (*SmaI*)
D5mutF CGGGATCCCAACGAACTCGGCATCAGC (*BamHI*)
I3mutF TCCCCCGGGCTGGACACGCTTGGCGAGG (*SmaI*)
D3mutF CGGAATTCCAACACTACATCTCCAGCAG (*EcoRI*)
I5mutF CGGAATTCGCCAGCCATCCTGCTCTCC (*EcoRI*)
GFP-F GGGAATTCTGATTAACTTTATAAGGAGGAAAAACAT (*EcoRI*)
GFP-RBamHI CGGGATCCTTTGTATAGTTCATCCATGCCAT (*BamHI*)
C-termF (GFP) CGGGATCCTCGCGCGCTGCAGCAAC (*BamHI*)
C-termR (GFP) GCCAAGCTTCAGATCAGGGTACCGGTGCC (*HindIII*)
FR1-C1ZC2-5` GCTCTAGAGATCCAGATCCAGATCGACGCGGC (*XbaI*)
FR1-C1ZC2-3` CGGGATCCCATCTACGACGCTCCGTTGTCC (*BamHI*)

[T] type strain; CECT, Colección Española de Cultivos Tipo; ISCIII, Instituto de Slud Carlos III; MRSA, methicillin-resistant *S. aureus* (clinical isolate); Underlined sequence means the restriction site for restriction enzymes shown in brackets.

For optimal PHA production, a pre-culture of the *P. putida* strains was cultivated overnight in LB medium, washed and inoculated at 0.3 OD_{600} in 0.1 N M63, a nitrogen-limited minimal medium (13.6 g of KH_2PO_4/L, 0.2 g of $(NH_4)2SO_4$/L, 0.5 mg of $FeSO_4 \cdot 7H_2O$/L, adjusted to pH 7.0 with KOH) at 30 °C and 250 rpm as previously described (Moldes *et al*., 2004). This medium was supplemented with 1 mM $MgSO_4$ and a solution of trace elements (composition 1 000 × 2.78 g of $FeSO_4 \cdot 7H_2O$/L, 1.98 g of $MnCl_2 \cdot 4H_2O$/L, 2.81 g of $CoSO_4 \cdot 7H_2O$/L, 1.47 g of $CaCl_2 \cdot 2H_2O$/L, 0.17 g of $CuCl_2 \cdot 2H_2O$/L, 0.29 g of $ZnSO_4 \cdot 7H_2O$/L). Sodium octanoate 15 mM was used as carbon source. Growth was monitored with a Shimadzu UV-260 spectrophotometer at OD_{600}.

For analyzing: (i) biofilm formation; (ii) bacterial adhesion properties on PHACOS and PHO; (iii) antibacterial activity of PHACOS and PHO and (iv) minimal inhibitory concentration (MIC) of their fatty acid precursors and derived dimers/trimers, bacteria

were transferred from a stock frozen at -80 °C with 15% of glycerol, to a screw-capped test tubes with Nutrient Agar slant culture medium (Nutrient Broth DifcoTM (ref 234000, Becton, Dickinson and Company, France) supplemented with 1.5% agar) and incubated at 37 °C for 16-24 h to pre-culture all bacterial strains. Afterwards, bacteria were transferred onto fresh slant culture medium and incubate at 37 °C for 16-20 h.

Bacterial test inoculum for adhesion experiments and antibacterial activity testing were prepared by resuspending bacteria pre-cultured on slant medium in 2 mL of 1/500 diluted Nutrient Broth (NB), to serve as cell suspension according to the protocol described in ISO 22196:2011 "Measurement of antibacterial activity on plastics and other non-porous surfaces". Bacterial concentration was estimated via colony forming units counting (CFU) in the suspension by plating 10-fold serial dilutions in phosphate-buffered physiological saline, 10 mM, pH 7.2 (PBS) on LB agar plates (Sambrook and Rusell, 2001). CFU were counted after 24 h incubation at 37 °C.

For the assays corresponding to bacterial capacity to form biofilms on polymer surfaces, cells pre-cultured on slant medium were transferred and grown with aeration in trypticase soy broth (TSB) supplemented with 0.3% glucose and 0.4% yeast extract (enriched TSB or e-TSB) for 20 h at 37 °C. Bacterial concentration was estimated spectrophotometrically at OD_{600}.

For MIC determination, test inoculums were prepared by resuspending bacteria pre-cultured on slant medium in 2 mL of Muller-Hinton broth II (MHB II, Becton Dickinson). Bacterial concentration was estimated spectrophotometrically at OD_{600}.

Luminescent derivates of *Staphylococcus aureus*^{T} were used for *in vivo* real-time monitoring of implant infection were. Namely, two strains harbourig *lux* operon inserted in antibiotic selection plasmid *S. aureus* (pAmiBLAZ) and *S. aureus* (pAmiSPA), and *S. aureus* Xen29 carrying bioluminescent construct in a chromosome (Table 4). All bacterial strains were pre-cultured in trypticase soy agar plates (TSA) and incubated at 37 °C for 24 h. The appropriate selection antibiotics, chloramphenicol (10 µg/mL) or kanamycin (200 µg/mL) were added when needed. TSB was used as the growth medium to culture the bacterial pathogens.

2. Molecular biology techniques

Standard molecular biology techniques were performed as previously described (Sambrook and Russell, 2001). PCR products were purified with the High Pure plasmid isolation kit (Roche Applied Science). DNA fragments were purified with Gene-Clean Turbo (Q-BIO-gene). Genomic DNA from *P. putida* KT2442 was isolated with the Genomic Prep Cells and Tissue DNA Isolation kit (Amersham Biosciences). All cloned inserts and DNA fragments were confirmed by DNA sequencing with fluorescently labeled dideoxynucleotide terminators and AmpliTaq FS DNA polymerase (Applied Biosystems Inc.) in an ABI Prism 377 automated DNA sequencer (Applied Biosystems Inc.). Transformation of *E. coli* cells was carried out using the RbCl method (Sambrook and Rusell, 2001). All oligonucleotides used for PCR amplification are listed in Table 4.

3. Construction of different genetically manipulated *P. putida* KT2442 and *S. aureus*^{T} strains

3.1. Construction of PhaF and PhaI null mutants of *P. putida* KT2442

The *phaF* gene was deleted by marker exchange as described previously using the mobilizable suicide plasmid pKNG101 (Kaniga *et al.*, 1991). The deletion of *phaF* gene was engineered with the DNA fragments DmutF and ImutF of 575 bp and 402 bp respectively, generated by PCR using the primer pairs D5mutF and D3mutF for DmutF, and I5mutF and I3mutF for ImutF. These two fragments were digested with the appropriate restriction enzymes and ligated using T4 ligase resulting in a single 977 bp fragment carrying a deletion of the *phaF* gene which was cloned into the unique *Bam*HI and *Sma*I sites of pKNG101 to yield pKNGFdel. Plasmid pKNGFdel was used to deliver the *phaF* mutation to the host chromosome via homologous recombination. Biparental mating was performed following protocols described by De Lorenzo and

Timmis (1994), using *E. coli* SM10λ*pir* (pKNGFdel) as donor strain and *P. putida* KT2442 as recipient strain. For conjugation, 100 µL of overnight cultures of donor and recipient strains were mixed in 5 mL of 10 mM $MgSO_4$ and collected on a Millipore filter which was subsequently placed on an LB agar plate and incubated overnight at 30 °C. After incubation, the cells were resuspended in 5 mL of 10 mM $MgSO_4$ and plated on M63 selective plates supplemented with 5% sucrose as described previously (Kaniga *et al*., 1991). Transconjugants (Suc^R, Sm^S) were isolated. The second crossover event was confirmed by PCR using primers D5mutF and I3mutF. The resultant mutant strain was denoted KT42F.

P. putida KT42I, *phaI* gene deleted strain, was constructed by disruption of *phaI* gene using plasmid pK18*mobsacB* (Schäfer *et al*., 1994). The 481 bp and 339 bp fragments upstream and downstream *phaI* gene were PCR-amplified with F5mutI and F3mutI primers (for FmutI fragment) and X5mutI and X3mutI primers (for XmutI fragment). Total DNA of *P. putida* KT2442 strain was used as template. The resulting fragments were digested with the appropriate restriction enzymes and ligated using T4 ligase resulting in a single 820 bp fragment carrying a deletion of the *phaI* gene which was cloned into the unique *BamHI* and *SmaI* sites of pK18*mobsacB* to yield pKI18*mobsacB*. Plasmid pKI18*mobsacB* was used to deliver the *phaI* mutation to the host chromosome via homologous recombination. Triparental mating was performed following protocols described by Herrero *et al*. (1990), using *E. coli* DH10B (pKI18*mobsacB*) as donor strain, *E. coli* HB101 (pRK600) as helper strain and *P. putida* KT2442 as recipient strain. Successful gene disrupted strains were selected in M63 0.1N plates supplemented with 0.1% citrate, 5% sucrose and kanamycin and confirmed by DNA sequencing and SDS-PAGE analysis. The second crossover was confirmed by PCR amplification using F5mutI and X3mutI primer. Similarly, *P. putida* KT42C1ZC2 strain was constructed using the plasmid pK18*mobsacB-c1zc2* (Table 4). The second crossover was confirmed by PCR amplification using FR1-C1ZC2-5` and FR1-C1ZC2-3` primer.

3.2. *P. putida* KT42C1ZC2 PhaF null mutant strain construction

To construct *P. putida* KT42C1ZC2F strain, the *phaF* gene was inactivated by marker exchange using the mobilizable suicide plasmid pKNGFdel as previously described (Galan *et al*., 2011). Briefly, biparental filter-mating technique was performed (De Lorenzo and Timmis, 1994) using *E. coli* SM10λ*pir* (pKNGFdel) as donor strain and *P. putida* KT42C1ZC2 as recipient strain. Transconjugants (Suc^R, Sm^S) were isolated. The second crossover event was confirmed by PCR using primers D5mutF and I3mutF.

3.3. Complementation of *P. putida* KT42F, *P. putida* KT42I and *P. putida* KT42I-BG strains

Plasmid pPF61, harbouring the *phaF* gene from *P. putida* GPo1 under the control of the *Ptrc* promoter (Prieto *et al.*, 1999) was introduced into *P. putida* KT42F, *P. putida* KT42I and *P. putida* KT42I-BG chromosome by triparental mating. The resulting strains named KT42F-F, KT42I-F and KT42I-BGF, respectively were cultivated in PHA production medium in the presence of 5 mM (isopropyl-1-thio-β-D-galactopyranoside) IPTG as described (Prieto *et al.*, 1999).

3.4. Construction of *P. putida* strains producing GFP and PhaF C- terminal domain fusion protein

The *gfp-cphaF* fusion was obtained by amplification of two DNA fragments. GFP cassette was amplified from plasmid pGreenTIR (Miller and Lindow, 1997) with GFP-F and GFP-RBamHI oligonucleotides (Table 4). After digestion with the corresponding restriction endonucleases, the GFP cassette was cloned into pUC18Not plasmid yelding pUC18Not-*gfp*. DNA sequence of *phaF* coding C-terminal domain was PCR amplified from genomic DNA of *P. putida* KT2442 using C-termF (GFP) and C-termR (GFP) oligonucleotides. Obtained PCR product was digested and cloned into pGEM-T

plasmid. The fragment obtained after digestion with *HindIII* and *BamHI* was cloned into pUC18Not*gfp* plasmid. *E. coli* strain DH10B was transformed with the resulting hybrid plasmid pUC18Not-*gfp-cterm*. Construction was confirmed by sequencing using an ABI Prism 3730 DNA Sequencer. The *gfp-cterm* fusion was cloned from pUC18Not-*gfp-cterm* plasmid into pCNB5 vector as *NotI* fragment. Constructed plasmid pCNB5-*gfp-cterm* was introduced into the *P. putida* KT2442 and *P. putida* KT42F chromosomes by triparental mating yielding KT42-GC and KT42F-GC, respectively. Conjugates were isolated after plating on M63 0.1N selective plates supplemented with 0.2% citrate and kanamycin. Afterwards, colonies were picked to LB plate with and without IPTG. Selection of fluorescent green colonies was done from LB plate supplemented with IPTG by fluorescent magnifying lamp.

3.5. Insertion of BioF (N-terminal of PhaF protein) and GFP fusion as a monocopy into the chromosome of *P. putida* strains

To study localization of BioF *in vivo*, the mobile cassette carrying the *bioF-gfp* fusions were inserted as a monocopy into the chromosome of different *P. putida* strains via mini-Tn*5* transposons. A 1730 bp DNA *NotI*/*NotI* fragment containing *Ptac*:: *bioF-gfp-clytag* was obtained after digestion from pMAB20-*gfp-clytag* plasmid, kindly provided by Biomedal S.L. Plasmid pCNB5 was used as cloning vector where *bioF-gfp* was inserted as *NotI* fragment to yield pCNB5-*bioF-gfp* allowing to drive the expression of the fusion under the control of *lacI*^{q}*-Ptrc* regulatory system. *E. coli* CC118λ*pir* cells were transformed and positive clones were selected in LB plates supplemented with kanamycin. Resulting construction (pCNB5-*bioF-gfp*) was transferred into *P. putida* KT2442, *P. putida* KT42F, *P. putida* KT42I, *P. putida* KT42C1ZC2 and *P. putida* KT42C1ZC2F by triparental mating technique to give rise to *P. putida* KT42-BG, *P. putida* KT42F-BG, *P. putida* KT42I-BG, *P. putida* KT42C1ZC2-BG and *P. putida* KT42C1ZC2F-BG respectively (Figure 17A). Transconjugants were selected on 0.1N M63 plates supplemented with 0.2% citrate, kanamycin, 0.1 mM IPTG and confirmed by SDS-PAGE and Western blot analysis as previously described (Moldes *et al*., 2004). Western blot analysis was performed with the ECL Western Blotting Detection Kit

(Amersham Biosciences) according to the protocol described by the manufacturer. Rabbit polyclonal antiserum against PhaI and BioF was generated as previously described (Moldes *et al*., 2004). Colonies were picked to LB plate with and without IPTG. Selection of fluorescent green colonies was done from LB plate supplemented with IPTG by fluorescent magnifying lamp.

3.6. Construction of *S. aureus*^{T} luminescent strains

Bioluminescent *S. aureus*^{T} strains were generated by transforming parental strain with a promoterless-*lux* cloning vector, pAmilux (Mesak *et al*., 2009) carring modified *Photorhabdus luminescens luxCDABE* (*lux*) gene cluster (Table 4). These vectors (pAmiBLAZ and pAmiSPA) were constructed and kindly provided by the group of Prof. Iñigo Lasa (Instituto de Agrobiotecnología, CSIC, UPNA, Gobierno de Navarra). Briefly, to construct the vectors, promoters of *S. aureus* genes *blaZ* (β-lactamase) and *spa* (protein A) were inserted into pAmilux plasmid to yield pAmiBLAZ or pAmiSPA, respectively. Transformants were selected on TSA plates supplemented with chloramphenicol (10 µg/mL). Successful transformation was confirmed by bioluminescent colonies screening using an IVIS Lumina bioimaging system (Xenogen).

4. Flow cytometry

Cells were harvested and washed twice with distilled water and resuspended in water to a final OD_{600} of 0.2 for staining with Nile Red. A Nile Red stock solution was made by dissolving the dye to a concentration of 1 mg/mL in dimethyl sulfoxide (DMSO). Three microliters stock solution was added to 1 mL of cell suspension. The mixture was incubated in the dark for 15 min and analyzed by flow cytometry (flow cytometer Coulter EPICS XL). *P. putida* KT42C1 minus strain (a *phaC1* mutant which produces <1% CDW PHA) (De Eugenio *et al*., 2010a; Table 4) was used as negative control. A calibration curve for the quantification of the PHA content using flow

cytometry was made comparing the fluorescence intensity and PHA content analyzed by gas chromatography throughout the growth curve in *P. putida* KT2442 (data not shown). The relation between both parameters was fitted to the equation y= 30.874 Ln(x) + 38.11 with a R^2=0.9984. This equation has been used to translate the cytometry fluorescence intensity data into PHA values.

5. Transmission electron microscopy

Cells were harvested, washed twice in PBS, and fixed in 5% (w/v) glutaraldehyde in the same solution. Afterwards, cells were suspended in 2.5% (w/v) OsO_4 for 1 h, gradually dehydrated in ethanol (30, 50, 70, 90, and 100% (v/v); 30 min each) and propylene oxide (1 h), embedded in Epon 812 resin. Ultrathin sections (thickness 70 nm) were cut with a microtome using a Diatome diamond knife. The sections were picked up with 400 mesh cupper grids coated with a layer of carbon and subsequently observed in a Jeol-1230 electron microscope (JeolLtd., Akishima, Japan).

To determine the size of PHA granules from the micrographs, 50 cells of the wild-type and of the mutant were selected, in which the PHA granule diameter was measured. We analyzed 100 granules of the wild-type and 100 of the *phaF* mutant strain. Only granules with sharp boundaries were selected. The number of PHA granules per cell was determined only from cells which were fully visible in the electron micrographs.

6. *In vivo* localization of the C- and N-terminal domain of PhaF by fluorescence microscopy

P. putida KT42-GC and KT42F-GC strains were cultivated overnight in LB medium. Then, cells were washed and inoculated at 0.3 OD_{600} in 0.1 N M63. Cultures were induced with 2 mM IPTG in the exponential phase of growth (0.6 OD_{600}) to induce the production of the GFP-CPhaF fusion protein. Staining for nucleoids was performed by incubation with 2 µg/mL (4´,6-diamidino-2-phenylindole, DAPI) for 15 min while the PHA granules were visualized after staining with 1 µg/mL Nile Red for 15 min in dark. Then cells were fixed with 4% paraformaldehyde at room temperature for 1 h, washed tree times with PBS and visualised by confocal microscopy Laser Confocal espectral (CLSM) Leica TCS SP2-AOBS.

P. putida KT42-BG, *P. putida* KT42F-BG, *P. putida* KT42I-BG, *P. putida* KT42I-BGF, *P. putida* KT42C1ZC2-BG and *P. putida* KT42C1ZC2F-BG living cells producing BioF-GFP fusion protein were visualized with a Zeiss Axioplan Universal epifluorescence microscope operated for incident-light fluorescence and contrasting techniques of bright field and phase contrast. Cells cultivated in LB medium or in PHA producing conditions were induced with 2 mM IPTG in the exponential phase of growth for the production of the BioF-GFP fusion protein and observed after 8 h of incubation. Micrographs were recorded with digital camera Leica DFC350FX.

For detailed examination of BioF-GFP fusion protein, nucleoid and granules co-localization, *P. putida* KT42I-BGF strain was cultivated overnight in LB medium. Once washed, cells were inoculated at 0.3 OD_{600} in 0.1 N M63. Cultures were induced with 2 mM IPTG in the exponential phase of growth for the production of the BioF-GFP fusion protein. Nucleoid and PHA granules staining and cell fixing was performed as previously described (see above). Afterwards, cells were visualised by confocal microscopy Laser Confocal espectral (CLSM) Leica TCS SP2-AOBS.

7. PHA quantification and analysis of monomer composition

PHA monomer composition and cellular PHA content were determined by gas chromatography-mass spectrometry (GC-MS) following previously described protocol (De Eugenio *et al*., 2010a). Briefly, samples were subjected to methanolysis in the presence of 15% (w/v) sulfuric acid, and resulting methyl esters of monomers were analyzed by injecting 1 µL of sample into Perkin Elmer AutoSystem gas chromatograph equipped with SPB1 Supelco capillary column (25 m x 0.25 mm inner diameter x 0.22 µm) and ionization detector. Biomass was calculated as previously described (De Eugenio *et al*., 2010a).

An additional, quantification of the PHA content was performed by Flow cytometry (flow cytometer Coulter EPICS XL). Analysis was done as described before (see section 4; Galan *et al*., 2011).

To determine PHA monomer composition, GC-MS and nuclear magnetic resonance (NMR) analysis were carried out as previously described (Escapa *et al*., 2011).

8. Protein quantification

Content of BioF-GFP fusion protein was quantified by flow cytometry, fluorometry and software package QuantityOne protein for protein quantification in SDS-PAGE protein gels.

For BioF-GFP fluorescence quantification by flow cytometry, 1 mL of cells grown in PHA producing conditions was harvested after 8 h of incubation, washed twice with distilled water and resuspended in water to a final OD_{600} of 0.2. *P. putida* KT42C1 strain (De Eugenio *et al*., 2010a) was used as negative control.

Furthermore, an additional quantification of BioF-GFP fluorescence was performed by fluorometry, allowing the comparison of fluorescence of GFP in whole

cells and isolated granules carrying GFP. *P. putida* strains were cultivated in PHA producing conditions. When OD_{600} reached 0.6 the culture was induced with 0.1 mM IPTG. After 8 h of incubation, 1 mL of cultures were harvested, washed twice with distilled water and resuspended in water to a final OD_{600} of 0.2 for fluorometry analysis of whole cells. The rest of the culture was used for granule isolation. After harvesting, cells were resuspended in 15 mM Tris-HCl pH 8, and disrupted by twofold passage through a French press (1 000 lb/in^2). The extracts were centrifuged 30 min at 10 000 × g, and the pellet fraction was dissolved in 5 mL of 15 mM Tris-HCl pH 8. Granule isolation was done by centrifugation (12 000 x g for 30 min) onto 55% glycerol (Merrick and Doudoroff, 1964) of total crude extract kept at 4 °C during the entire process. After extraction, granules containing PHA-immobilized GFP protein were resuspended in 15 mM Tris-HCl pH 8 to a final OD_{600} of 0.2 and analyzed by fluorimetry OD_{498} (excitation)/OD_{509} (emission).

For BioF-GFP quantification by QuantityOne, isolated granules proteins were separated in 12.5% SDS-polyacrylamide gels and stained with Coomassie brilliant blue G-250 following previously described protocol (Sambrook and Russell, 2001). Protein content calculation in examined *P. putida* strains was carried out by densitometric scanning using Gel Doc XR and analyzed using Quantity One software (version 4.6 basic) (Bio-Rad, Hercules, CA) and calibrating with broad-range molecular mass markers from Bio-Rad.

9. Polymer preparation, disk fabrication and endotoxin analysis

All mcl-PHA applied in this study were prepared as previously reported (Escapa *et al*., 2011) and kindly provided by Biópolis S.L. The monomer content of PHACOS was 29.7% of non-functionalized monomers 3HA (17.5% of OH-C8, 10.3% of OH-C10, and 1.9% of OH-C6 monomers) and 70.3% of functionalized monomers (46.4% of OH-6ATH and 23.9% of OH-4ATB monomers). The poly([*R*]-3-hydroxyoctanoate-*co*-[*R*]-3-hydroxyhexanoate) hereandafter PHO, consisted of 8.5% OH-C6 and 91.5% OH-C8. An

optimized downstream processing was applied to eliminate endotoxins as previously described (Furrera *et al*., 2007). Briefly, 1 g of PHA was dissolved in 100 mL of chloroform at 40 °C under vigorous stirring, the suspension was pressure filtered and the polymer was precipitated by addition of non-solvent methanol. Finally, the polymer was dried under vacuum at 40 °C for 48 h. This procedure was repeated two times to obtain mcl-PHA with endotoxin units (EU) ≤20 EU/g, in compliance with the endotoxin requirements for biomedical applications. The endotoxin content was measured using *Limulus* amebocyte lysate (LAL)-test (Pyrogent Plus Single Test Kit, 0.125 EU/mL, Lonza) according to the protocol described elsewhere (Furrera *et al*., 2007). Each analysis was carried out at least twice. The values of PHACOS and PHO endotoxicity were always <12 EU/g and <15 EU/g, respectively.

For disk fabrication, poly(ethylene terephthalate) (PET) disks were coated with PHACOS or PHO by solvent-casting method: polymeric materials dissolved in chloroform (2% w/v) were applied over sterile, endotoxin-free PET disks (6 mm diameter) kindly supplied by ACCIONA (Barcelona, Spain) in a dust-free atmosphere. The coatings were allowed to dry for 72 h at room temperature and the resulting PHACOS-coated disks (PHACOS disks), PHO-coated disks (PHO disks) and control PET disks were sterilized with ethylene oxide at 40 °C.

10. Mcl-PHA micro- and nano-particles preparation

The preparation of microparticles was carried out by the emulsion technique previously described (Reyes-Ortega *et al*., 2013) and modified as follows: 1 mL water was first emulsified during the addition of 10 mL of PHA polymer solution in dicloromethane (1% w/v). The resulting water-in-oil emulsion was sonicated for 8 min and thereafter mixed under vigourous stirring with a 2% polyvinylalcohol (PVA, M_w: 31 000-50 000 Da, 87-89% hydrolyzed, Sigma) aqueous solution. PVA was used as a surfactant to avoid microparticle agglomeration. Moreover, the inversion of emulsion was achieved. Suspension was vigourous stirred in dust-free atmosphere at room

temperature overnight to evaporate dichlormethane. Afterwards, three washing cycles with deionized water followed by centrifugation (12 000 rpm for 20 min at 25 °C) were applied to remove the PVA. The values of particle size and standard deviation were determined with an accuracy of 0.04 µm using a Beckman Coulter LS230. The morphology and the size of microparticles was analyzed by environmental scanning electron microscopy (ESEM) using a Philips XL 30 ESEM apparatus at an accelerating voltage of 15 keV. It was equipped with a field emission Hitachi SU800 apparatus. The samples were prepared by deposition of the corresponding microparticle suspension (0.01 mg/mL) over glass disks (13 mm diameter and 1 mm thickness), and the solvent (H_2O) was evaporated at room temperature for 24 h. All the samples were sputter-coated with chrome prior to examination by ESEM. Comercialy available polystyrene microparticles (5µm, 79633-5ML-F, Sigma-Aldrich) were used as control.

PHA nanoparticles were prepared as previouslu described (Schirmer and Jendossek, 1994). Briefly, polymer dissolved in chloroform (10 volumes) was added slowly with stirring to cold water (1 volume). Organic solvent was removed using rotary evaporator and susequently polymer/water emulsion (PHA latex) was obtained. The values of PHA particle size and standard deviation were determined with an accuracy of 0.04 µm using a Beckman Coulter LS230.

11. Biofilm formation on mcl-PHA

The ability of bacteria to form biofilm *in vitro* on PHACOS, PHO and PET disks was examined by ESEM, crystal violet assay and CFU counting. By means of those assays we studied the capacity of PHACOS disks to prevent bacterial biofilm formation on its surface in comparison to the other materials. *S. aureus*^{T} and *P. aeruginosa* CECT 4122 were used as model strains able to form biofilm on diverse materials.

The same optimal conditions as previously described for pneumococcal biofilm formation (Moscoso *et al*., 2006) were used to induce the production of biofilms by all examined strains. Briefly, biofilm formation was carried out (in triplicate) as follows:

sterile endotoxin-free PHO, PHACOS or control PET disks were placed in 24-flat bottom multiwell plates (Falcon, Becton Dickinson) and each well was inoculated with 1 mL of a 1:100 dilution (in TSB) of a saturated culture previously grown in e-TSB (see section 1). Plates were incubated under static conditions for 16 h at 37 °C and bacterial growth was determined by measuring the optical density at 595 nm (OD_{595}) using a plate reader (microplate absorbance reader 2020; Anthos Labtec Instruments GmbH).

For ESEM examination, following the incubation samples were washed three times with distilled water and fixed with 2.5% glutaraldehyde for 2 h at room temperature. The dried samples were mounted on aluminum stumps and sputter-coated with chrome before examination ESEM apparatus (Philips XL 30) at an accelerating voltage of 15 keV.

Formed biofilm was quantified by crystal violet assay according to previously described protocol (Moscoso *et al*., 2006). Briefly, after the staining with 0.5% crystal violet and rinsing to remove non adherent bacteria, biofilm was mechanically removed from the disks using disposable steril micropipette tip, solubilized in 95% ethanol (200 µL per well) and the absorbance was determined at OD_{595} using an Anthos 2020 microplate absorbance reader (Anthos Labtec Instruments).

For CFU counting of bacteria present in the biofilm, pre-incubated disks were washed with distilled water to remove non adhered bacteria. Biofilm, without staining in this case, was mechanically removed from the disk using disposable steril micropipette tip, subsequently 10-fold dilutions were made in PBS and plated on LB plates. CFU were determined after 24 h incubation at 37 °C.

12. Bacterial adhesion to polymers

The number of bacteria ahered to the biopolymer surfaces was determined using two methods: (i) bacteria adhesion to polymer microparticles and (ii) bacteria adhesion to polymer films. Adhesion to microparticles was monitored by radioactively labelling of bacteria, while adhesion to polymer films was determined by ESEM. Moreover, the number of viable cells was determined.

12.1. Adhesion of radioactively labeled bacteria to microparticles

For enumeration of cells attached to microparticles bacterial strains (*S. aureus*^{T}, *S. epidermidis*^{T}, *P. aeruginosa, Salmonella enterica*^{T}) were radioactively labeled. Following overnight pre-cultivation in LB medium, cells were washed with PBS and inoculated at OD_{600} 0.1 in MHB II containing Glucose, D-[^{14}C(U)] (NEC042X250UC, PerkinElmer, USA), with specific activity 250-360 mCi/mmol. Glucose, D-[^{14}C(U)] was added at concentration of 20 μCi/mL of cell culture and incubated for 24 h at 37 °C. As a control, cells were grown in MHB II supplemented with non labeled (cold) glucose. Following the incubation, counts per minute (cpm) were recorded and cell concentration was determined spectrophotometrically to define the yield of radioactive labeling. Repeated experiments gave consistently high count rates in the order of 100 000 cpm in 1 mL of cell culture (≈10^8 CFU/mL).

For attachment assay, 1 mL of previously prepared microparticles (see section 10) was mixed with radioactively labeled bacteria to reach final concentration of 1 mg/mL of microparticles and 10^8 CFU/mL of bacteria. Suspension was incubated 1 h at 37 °C with shaking and subsequently left 10 min to sediment for enumeration of microparticle-attached bacteria. Three washing cycles were applied to remove unattached cells. Cpm of plactonic and microparticle-attached bacteria was determined.

12.2. Bacteria adhesion to PHACOS and PHO films

The reference strains *S. aureus*^{T} and *P. aeruginosa* were used for *in vitro* adhesion experiments. Inocula were prepared by suspending pre-cultured bacteria in 2 mL of 1/500 (v/v) diluted NB. Bacterial suspensions (1-2 x 10^8 CFU/mL) were placed on PHACOS, PHO and control disks and incubated at 37 °C for 24 h.

Bacterial cells adherence on PHACOS, PHO and control disks was determined by ESEM. With this aim, disks were washed three times with PBS and fixed with 2.5% glutaraldehyde for 2 h at room temperature. The dried samples were mounted on aluminum stumps and sputter-coated with chromium before examination under an ESEM apparatus (Philips XL 30) at an accelerating voltage of 15 kV.

An additional test to determine the percentage of viable bacteria from the total number of adhered cells was performed. Bacteria were washed out from the disks and stained with the LIVE/DEAD BacLight bacterial viability kit L-13152 (Invitrogen-Molecular Probes) following the manufacturer's instructions. Samples were visualized with a Zeiss Axioplan Universal epifluorescence microscope operated for incident-light fluorescence and contrasting techniques of bright field and phase contrast. Micrographs were recorded with a digital camera Leica DFC350FX.

13. Measurement of mcl-PHA antimicrobial activity

Antibacterial activity was determined according to the ISO 22196:2011 protocol "Measurement of antibacterial activity on plastics and other non-porous surfaces", with minor modifications. Bacterial strains used in this study are listed in Table 4. Each disk was placed into a separate sterile Petri dish with the test surface uppermost and wet filter paper beneath to maintain a relative humidity ≥90%. Test inoculums (6.2-25.0 x 10^3 CFU/cm^2) prepared in 1/500 diluted NB were placed onto the analyzed surfaces without cover film and incubated at 37 °C for 24 h. Each material was tested in triplicate. Two set of controls were used: (i) non-coated PET disks for determination

of bacterial viability and (ii) PHO disks to analyze the effect of non functionalized PHA on bacterial viability. The controls and PHACOS disks were analyzed at 0 h and 24 h. After incubation, disks were washed with 1 mL of PBS. The number of colonies recovered from PET disks at 0 h was used to determine the recovery rate of the bacteria from the disks under investigation. Antibacterial activity was calculated as the R value. R = 0 means that the logarithm of number of viable cells in the sample disk after 24 h is identical to that of control disk at the same time point, whereas R = 1 means 10-fold less viable cells recovered from sample disk after 24 h than from the control disk.

An additional test was performed to determine the activity of PHACOS against higher cell density conditions up to 1×10^{10} cells/cm^2. Bacterial viability was determined on PHACOS and PHO disks according to ISO 22196:2011 following the protocol stated before. Each disk was inoculated with correspondent *S. aureus*^{T} suspension in 1/500 diluted NB, starting with suspensions of 1×10^4 cells/cm^2 to 1×10^{10} cells/cm^2. Following the incubation, disks were washed with 1 mL of PBS. CFU were determined by plating 10-fold serial dilutions on LB plates and incubation at 37 °C for 24 h.

14. Determination of Minimal Inhibitory Concentration (MIC)

The minimal inhibitory concentration (MIC) of polymer precursors 6-acetythiohexanoic acid (545554, Sigma-Aldrich), octanoic acid (C5038, Sigma-Aldrich) and hexanoic acid (P9767, Sigma-Aldrich) was calculated by microdilution assay according to CLSI (Clinical and Laboratory Standards Institute) standard procedure. Activity of compounds was tested on *S. aureus*^{T} strain. To determine the antibacterial activity of PHACOS hydrolyzate, two reaction mix containing 3.4 mg/mL of PHACOS latex in 0.2 M Tris-HCl (pH 8), and a control containing 3.0 mg/mL of PHO latex in 0.2 M Tris-HCl (pH 8) (see section 10) were separately subjected to enzimatic hydrolysis with mcl-PHA extracellular depolymerase PhaZGK13, from *Pseudomonas fluorescens* GK13

(0.2 mg per assay) (Martinez *et al*., 2012). Following 1 h incubation at 37 °C, supernatants of each reaction mix were centrifuged and filtrated (0.2 µm pore size). The degradation products were identified and quantified by HPLC mass spectrometry (HPLC-MS).

Stock solution of each compound was prepared in PBS with an initial concentration of 60 mM. Afterwards, serial dilutions were made in MHB II to determine MIC values. Briefly, the sterile 96-well round bottom clear polystyrene plates (Cultek S.L.U., Spain) were prepared by dispensing 100 µL of appropriate dilution of tested compound in culture broth per well. The *S. aureus*^{T} inoculum in MHB II was added to each well, providing a final concentration of 5 x 10^5 CFU/mL. A positive control (containing inoculum without tested compound) and negative control (containing tested compound without inoculum) were included in each microplate. MIC was defined as the lowest concentration of tested substance that inhibited visible growth of test bacteria.

15. *In vitro* biocompatibility

15.1. Cell cultures

The toxic effect of the analyzed polymers was evaluated using two type of cells, murine RAW 264.7 macrophages (ECACC, Sigma, P11) and BALB 3T3 fibroblasts (ATCC, CCL-163, P12), while inflammatory activity was monitored only on RAW 264.7 and effects on cell proliferation only on BALB 3T3. Cells were cultured in Dulbecco´s modified Eagle´s medium (DMEM) enriched with HEPES for BALB 3T3 cells and 110 mg/L of sodium pyruvate for RAW 264.7 cells and supplemented with 10% fetal bovine serum (FBS), 100 units/mL penicillin, 100 µg/mL streptomycin and 200 mM L-glutamine (complete medium). A humidified atmosphere at 37 °C with 5% CO_2 and 95% of air was used for cell culture growth and maintenance.

15.2. MTT assay

The *in vitro* effects of products released from the polymers on cellular viability was assessed by the 3-(4,5-dimethylthiazol-2-yl)-2,5-diphenyltetrazolium bromide (MTT) assay (Mosmann, 1983). PHO, PHACOS and control PET disks were immersed in 5 mL of FBS-free DMEM each and placed on a roller mixer at 37 °C. The medium was removed at different time points (1, 2 and 7 days) and replaced with fresh medium. All the extracts were obtained under sterile conditions. RAW 264.7 cells were seeded at a density of 2 x 10^5 cells/mL in complete medium, while BALB 3T3 cells at a density of 1 x 10^5 cells/mL, plated in a sterile 96-well culture plate and grown to confluence. The culture medium was replaced with the corresponding extract and incubated at 37 °C in humidified air with 5% CO_2 for 24 h. Afterwards, cell viability was determined by adding MTT (0.5 mg/mL in PBS) and incubated for 4 h at 37 °C. Excess medium and MTT reagent were withdrawn and dimethylsulfoxide was added to solubilize the formazan crystals formed in viable cells. The absorbance was measured at OD_{570} (test wavelength) and OD_{630} (reference wavelength) using a microplate reader (Biotek SYNERGY-HT). The cell viability (CV) was calculated from equation:

$$CV\ (\%) = 100 \times (OD_S - OD_B)/OD_C$$

where OD_S, OD_B and OD_C are the optical density of formazan production for the sample, blank (DMEM without cells) and control respectively.

15.3. Griess assay

The inflammatory activity of polymers was investigated using nitric oxide inhibitory assay performed according to the method of Wang *et al*. (2008). Briefly, RAW 264.7 cells were seeded in 96-well plates at a density of 2 x 10^5 cells/mL and incubated at 37 °C for 24 h. After incubation, the corresponding extracts were added. Control wells received lipopolysaccharide (LPS) (1 mg/mL–1) and cells were incubated for 24 h. The nitrite concentration was determined by the Griess reaction (Schmidt and Kelm, 1996). Aliquots (100 µL) of the supernatant from RAW 264.7 cells were reacted with 100 µL of Griess reagent (1:1 mixture of 0.1% *N*-(1-naphthyl) ethylenediamine in

water and 1% sulphanilamide in 5% phosphoric acid) in a 96 well plate and the OD_{548} was recorded using a Biotek SYNERGY-HT reader. The nitrite concentration was calculated from a calibration curve previously obtained using known $NaNO_2$ concentrations. Data were expressed as percentage of NO production.

15.4. Cell proliferation assay

Alamar Blue assay (AB) was performed to monitore cell metabolic activity. BALB 3T3 cells were seeded at a density of 8 x 10^4 cell/mL over the disks placed in 24-well culture and grown for 24 h. To each specimen 1 mL of Alamar Blue dye (10% Alamar Blue solution in phenol red free DMEM medium) was added and after 4 h of incubation 100 µL from each test sample was transferred to a 96-well plate to determine OD_{530} (excitation) and OD_{590} (emission). Then, to continue monitoring of cell growth disks were washed twice with PBS and 1 mL of culture medium was added. The procedure was repeated at defined time points (1, 5 and 10 days).

15.5. Cell morphology

For determination of cell adhesion and morphology, PHO, PHACOS and control PET disks were placed in a 24-well tissue-culture plate. BALB 3T3 cell suspension was added at a density of 8 x 10^4 cells/mL per well in 1 mL of respective culture medium and allowed to attach at 37 °C. Cell morphology and adhesion was monitored by ESEM. Samples were collected at different time points (1, 2 and 7 days), washed with PBS to remove unattached cells and immobilized with 2.5% glutaraldehyde in distilled water for 1 h at room temperature. The dried samples were mounted on aluminum stumps and sputter-coated with chrome before examination.

16. *In vivo* responses and anti-bacterial effects

16.1. Preparation of hydro-indocyanine green (H-ICG)

Hydro-indocyanine green (H-ICG) was synthesized from ICG (Acros Organics) by reduction with sodium borohydride as previously described (Kundu *et al*., 2009). Briefly, 2 mg of dye was dissolved in 4 mL of methanol and reduced with 2-3 mg of sodium borohydride (Aldrich). Solvent was removed by stirring reaction mix for 5 min under reduced pressure. The dye was nitrogen capped and stored overnight at -20 °C. For bioimaging, the resulting solid was dissolved in sterile water to final concentration of 1 mg/mL and further filtered to remove solid precipitates.

16.2. Sample preparation, implantation and bioimaging

In vivo inflammation was examined using biomaterial disks incubated for 30 min at 37 °C with *S. aureus*^{T} suspension in 1/500 diluted NB (1×10^4 cells/cm^2) under static conditions. After incubation disks were placed and keept in sterile containers until implantation.

To real-time monitore *in vivo* implant-associated infection, biomaterial disks were pre-colonized with *S. aureus* luminescent strains. Bioluminescent derivative strains were tested following different protocol than stated for non luminescent strain to obtain highest expression of *lux* genes. Bacterial strains were cultivated overnight in TSB with aeration at 37 °C. The cultures were diluted with fresh TSB to OD_{595} 0.1 and incubated for 3-4 h to reach exponencial growth phase (OD_{595} 0.7). Afterwards, bacterial test inoculums were prepared in 2 mL of 1/500 diluted NB, to serve as cell suspension. Bacterial concentration was estimated spectrophotometrically at OD_{595}. Bacterial suspensions (1×10^4 to 1×10^{10} cells/cm^2) were placed on previously prepared sterile endotoxin-free PHO and PET disks. Each concentration was examined

in triplicate. For *in vivo* assay, following 30 min incubation under static conditions at 37 °C disks were placed and keept in sterile containers until implantation.

National Institutes of Health guidelines for the care and use of laboratory animals (NIH Publication #85-23 Rev. 1985) were observed. All surgical procedures were approved by the Institutional Animal Care and Use Committee at the Georgia Institute of Technology. Sterile, endotoxin-free disks (6 mm diameter) were implanted subcutaneously in the back of 6-8 weeks old male BALB/c mice (Jackson Laboratories) anesthetized by isofluorane. A single 1 cm incision was made on the dorsum proximal to the spine, and a subcutaneous pocket laterally spanning the dorsum was created. Sterile disks (two per subject on either side of the spine) were implanted, and the incision was closed using sterile wound clips. Mice undergoing the same surgical procedure but receiving no biomaterial implants were used as sham controls to account for surgery-associated trauma/inflammation, whereas some mice received dye injection but no surgery, dye-only control (see below). The same procedure was followed for implants incubated with bacteria.

For bioimaging of ROS linked with biomaterial-associated inflammation (Selvam *et al*., 2011), 30 µL of H-ICG (1 mg/mL in sterile water) was injected near the vicinity of the implant at 1, 4, 7 and 14 days post-surgery/implantation. Thirty minutes later, the animal was anesthetized and the whole body of the animal was scanned in an IVIS Lumina® bioimaging system (Xenogen). Biofluorescence was integrated using Living Image®software Version 3.1 (Xenogen).

Furthermore, bacterial infection was *in vivo* real-time monitored. For the measurement of bioluminescence of subcutaneously implanted disks pre-colonized with bioluminescent *S. aureus* strains, mice were anesthetized with isofluorane and imaged with a CCD camera (IVIS Lumina® bioimaging system, Xenogen) directly following implantation and 1, 4, 7 days post-implantation/surgery. Total counts from the metabolically active *S. aureus* were collected during a 2 min exposure using the IVIS Imaging System and Living Image software (Xenogen Corporation). Bioluminescent images were displayed using a pseudocolor scale (blue representing the least-intense light and red representing the most-intense light) that was overlaid on a gray-scale

image to generate a two-dimensional picture of the distribution of bioluminescent bacteria in the animal. To account for the background luminescence, one uninfected mouse was imaged along with the infected animals. The total counts from a region were quantified using the Living Image software package (Xenogen Corporation), and the data are presented as total counts contained within each region. Moreover, infection induced inflammation was determined. ROS was bioimaged 7 days post-surgery/implantation. Bioimaging was performed as previously described (see above). Intensity of inflammation was correlated with CFU used to induce infection.

16.3. Implant analysis

Mice were sacrificed at specific time points (7 and 14 days post-implantation) and the disks were carefully explanted with the intact surrounding tissue to avoid disrupting the cell-material interface. For immunohistochemical staining, explants were embedded in optimal cutting temperature compound (OCT, Tissue-Tek) and cryosectioned at 10 µm. Fresh-frozen cryostat sections were incubated in 100 µM hydro-Cy5 (H-Cy5, Sigma) for 45 min at 37 °C to stain for intracellular ROS. Following incubations in H-Cy5, sections were fixed with 4% paraformaldehyde and were stained with primary rat monoclonal antibodies (Abcam) against the macrophage marker (CD68) or neutrophil marker (NIMP-R14). AlexaFluor 488-conjugated goat anti-mouse specific antibody (Invitrogen) was used as a secondary antibody. Moreover, *S. aureus* was vizualized in bacteria pre-colonized samples using primary rat monoclonal antibodies (Abcam) against *S. aureus*. The sections were mounted with antifade mounting media containing DAPI (Vector Labs) and imaged under a Nikon C1 imaging system. Five-six fields per sample were acquired and ImageJ software was used to count the fluorescent-labeled cells. For CFU counting, each explant was placed in glass tube containing 1 mL of PBS and sonicated for 10 min in ultrasonic bath to remove adhered bacteria. Afterwards, two more sonicating cycles were applied (5 min and 30 s) interspersed with 30 s of vortexing. Serial dilutions were plated on LB agar plates and CFU were determined after 24 h incubation at 37 °C.

17. Gravimetric assay

The kinetics of polymers weight loss was studied by immersing disks (6 mm diameter and 1 mm thickness) in PBS at 37 °C. The weight of the damped disks was monitored after different intervals of immersion time (1, 7, 14, 30 and 60 days). The remaining PBS was removed (drying) and the disks were weighed on balance (Sartorius). The percent of weight loss was calculated from the initial dry mass of the disks and the mass of the damped disks after certain immersion time.

18. Statistical analysis

Statistical analysis was performed by two-way ANOVA using Tukey post-hoc test with $P \leq 0.05$ considered significant. For longitudinal ROS bioimaging studies, a two-way repeated measures ANOVA was used to account for the variance within subjects. Pair-wise comparisons were performed using Bonferroni post-hoc test with $P \leq 0.05$ considered significant.

IV. Results

Herein we describe two different strategies for polymer functionalization and thereby added-value PHA obtainment for industrial and biomedical applications. The first strategy consists of bacterial *in vivo* production of tailor-made functionalized nano-beads where proteins attached to the natural PHA granule have been engineered to display fusion proteins of interest. The second strategy relays on the functionalization of the polymer itself by using metabolic engineering approach to design bacterial strains able to produce new non-natural polyesters carrying functionalized groups in the side chain. In the previous work, a strain of *P. putida* able to accumulate PHACOS was constructed (Escapa *et al*., 2011). Herein, we analyzed novel properties of PHACOS both *in vitro* and *in vivo*.

1. Bacterial production of tailor made functionalized nano-beads

PHA granules represent a useful tool for immobilization of recombinant protein due to their unique structure (Figure 3). Using the advantage of the presence of natural proteins (GAPs) on the granule surface we designed functionalized PHA nano-beads. Phasins are one of the most abundant proteins attached to the PHA granule. Therefore, they were chosen as tags for anchoring recombinant proteins to bacterial PHA granules. Moreover, we investigated their physiological function trying to describe the key factors that drive the *in vivo* immobilization of the tag/recombinant proteins to PHA granules. The N-terminal half of *P. putida* phasin PhaF was used as a peptide tag to anchor the protein to bacterial PHA granules. This system provides a useful tool for *in vivo* immobilization of active proteins to a biodegradable support.

1.1. The role of PhaF in the PHA machinery

In the previous work of our research group phasins have been employed as a component of BioF system to immobilize proteins onto PHA granules (see Introduction section 4). However, their physiological role in mcl-PHA machinery is not completely understood. To improve existing model and maximize recombinant protein yield we have investigated PhaF and PhaI phasins involvement in cell physiological processes. Moreover, by swapping different phasin domains we intent to optimize the *in vivo* attachment of recombinant proteins to mcl-PHA granules and achieve the most favorable conditions for their immobilization.

1.1.1. PhaF affects heterogeneity of the cell population concerning the PHA production

Previously obtained results showed that the total PHA content in *P. putida* GPo1 PhaF mutant strain was considerably reduced in comparison to that of wild-type strain, when the PHA content was studied in cell dividing continuous culture (Prieto *et al.*, 1999). Based on this observation, we focus our interest on studying the PHA production not only at stationary phase, but throughout the growth curve and thereby analyze PhaF dependent variation of PHA content in all fermentation stages. With this aim, the *phaF* gene of the prototype PHA producer strain *P. putida* KT2442 was deleted using pKNGFdel suicide vector. The PHA production abilities of the resulting *P. putida* KT42F strain was compared to that of the wild-type bacterium when cultured in optimal PHA production conditions. To monitor the PHA content at each stage of the growth curve, a fast and accurate method for analysis of PHA content by flow cytometry was adapted for *Pseudomonas* strains. Fluorescence intensity of Nile red stained granules recorded by flow cytometer was correlated with data of PHA content obtained by gas chromatography. The relation between those parameters was further used to translate the cytometry fluorescence intensity data into PHA values.

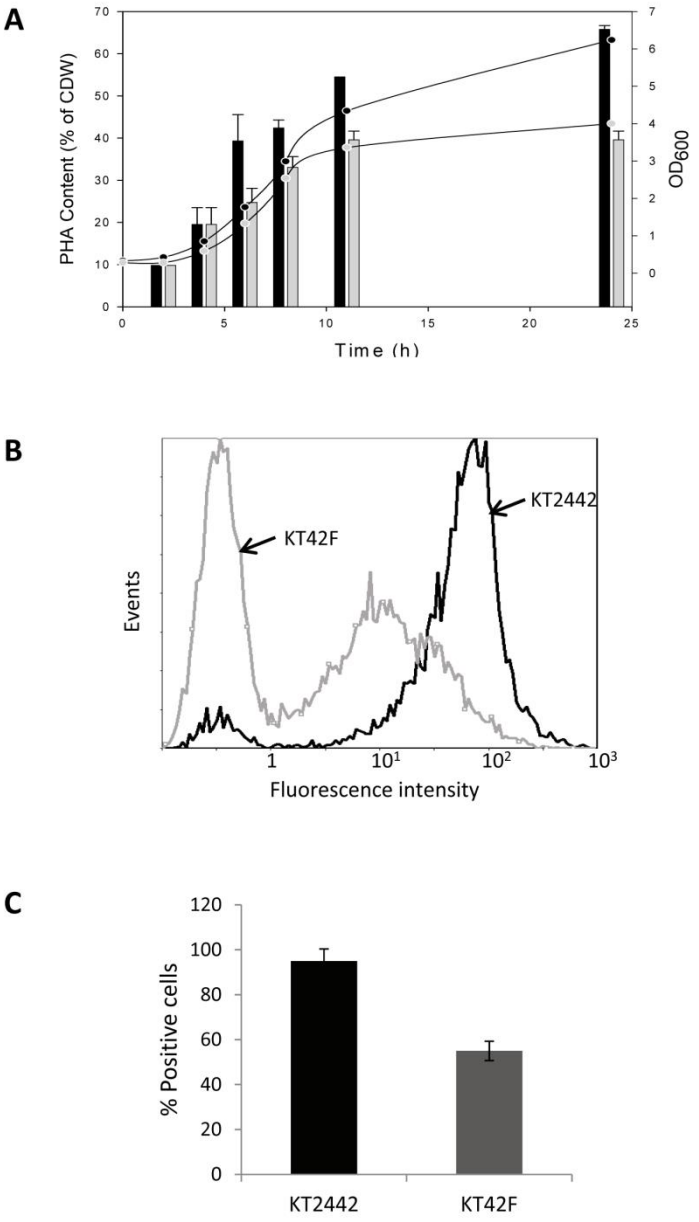

Figure 11. Study of cell population heterogeneity in terms of PHA production by flow cytometer. A, Quantification of PHA content (bars) and OD_{600} (circles) of *P. putida* KT2442 (black bars and black circles) and KT42F (gray bars and gray circles) strains throughout the growth curve; B, Example of a flow cytometer histogram of the *P. putida* KT2442 (black plot) and the *P. putida* KT42F (gray plot) strains grown in PHA production medium during 7 h; C, Percentage of PHA positive cells KT2442 (black column) and KT42F (gray column).

Cells from *P. putida* KT2442 and its *phaF* disrupted mutant strain KT42F were harvested from the culture at different growth times. Figure 11A shows that at the early exponential phase of growth (2 h and 4 h), wild-type and mutant strain harboured similar PHA content, around 10% and 20% of cell dry weight (CDW), respectively. After 6 h of growth the total PHA content detected in the wild-type strain KT2442 was slightly higher than that of the mutant strain KT42F. This difference showed increasing pattern over the growth curve, being maximal (1.5-fold) after 24 h (Figure 11A). Obtained result demonstrates that PhaF is not essential for the synthesis of PHA in *P. putida* KT2442, but contributes to optimize the synthesis and accumulation of PHA.

Besides, these flow cytometry analyses allowed us to relate the total PHA content of the cell population *versus* the PHA content of individual cells (heterogeneity of the population). Figure 11B shows an example of a histogram of KT42F and wild-type cells after 7 h of growing. A major overlay corresponding to positive fluorescent cells was detected in the wild-type cells (Figure 11B), demonstrating a homogeneous population regarding the PHA granules content. Interestingly, two main overlays showing different fluorescence intensities (Figure 11B), were detected in the KT42F sample. In this case, only 55% of cell population displayed positive PHA content while the rest of the cells were negative, implying the absence of PHA granules (Figure 11C). These results revealed the presence of at least two different cell populations in terms of PHA content in the KT42F cultures suggesting a role of PhaF in PHA granules partition during cell division.

1.1.2. Impact of PhaF mutation on granule location and segregation during cell division

To monitor the presence of the PHA granules during cell division at early growth phase and the influence of PhaF protein presence or absence on the PHA content, samples from wild-type and KT42F mutant strains were taken at different growth times for TEM analysis (Figure 12 and 13).

Interestingly, cells at time zero (LB grown cells used to inoculate the cultures) contained a few and small granules of PHA which constitute less than 1% of the CDW (Figure 12 and 13). In perfect correlation with the PHA content (Figure 11A), the size and number of the PHA granules in the wild-type cells increased progressively during the growth curve being maximal at 24 h (Figure 14). Most of the cells contained 5-6 granules of diameter about 500 nm (Figure 14). The number and average size of the granules in the KT42F mutant were lower when compared to those of the wild-type strain (Figure 14). This confirmed the results obtain by flow cytometry, thereby proving a remarkable heterogeneity of the total KT42F population in terms of PHA content and the presence of PHA empty cells when PhaF protein is not produced.

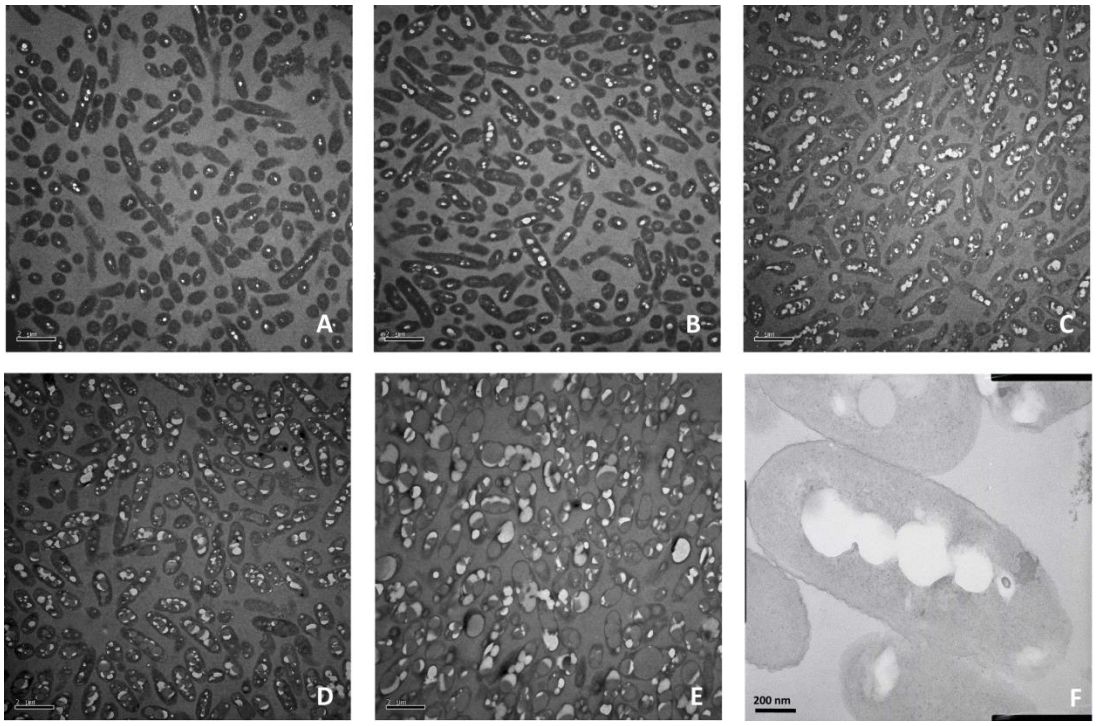

Figure 12. TEM images of *P. putida* KT2442 growth curve in PHA production medium. A-E, Samples taken 0, 2, 4, 6 and 24 h after the inoculation (Panels A, B, C, D and E, respectively) and processed as described in Material and methods (see section 4); F, Detail of the granule distribution of a single cell from a 4 h culture in PHA production medium.

TEM studies provided additional information regarding granule distribution in the cell. Throughout first 4 h of growth, granules were detected at the center of the cross section of the majority of wild-type cells, *i.e.*, located running lengthwise the cell,

forming a characteristic needle array (Figure 12B, C, F). This distribution was less evident when the accumulation of PHA was close to the 50% CDW after 6 h of growth (Figure 12D, E). In contrast, the granules in the KT42F mutant strain were agglomerated in one of the cell poles (Figure 13B, C, F) at the early growth stages (2 h and 4 h).

In agreement with the results observed by flow cytometry (Figure 11), the PHA content of the mutant was similar to that of the wild-type strain at the earliest stages of growth (Figure 13B, C, F).

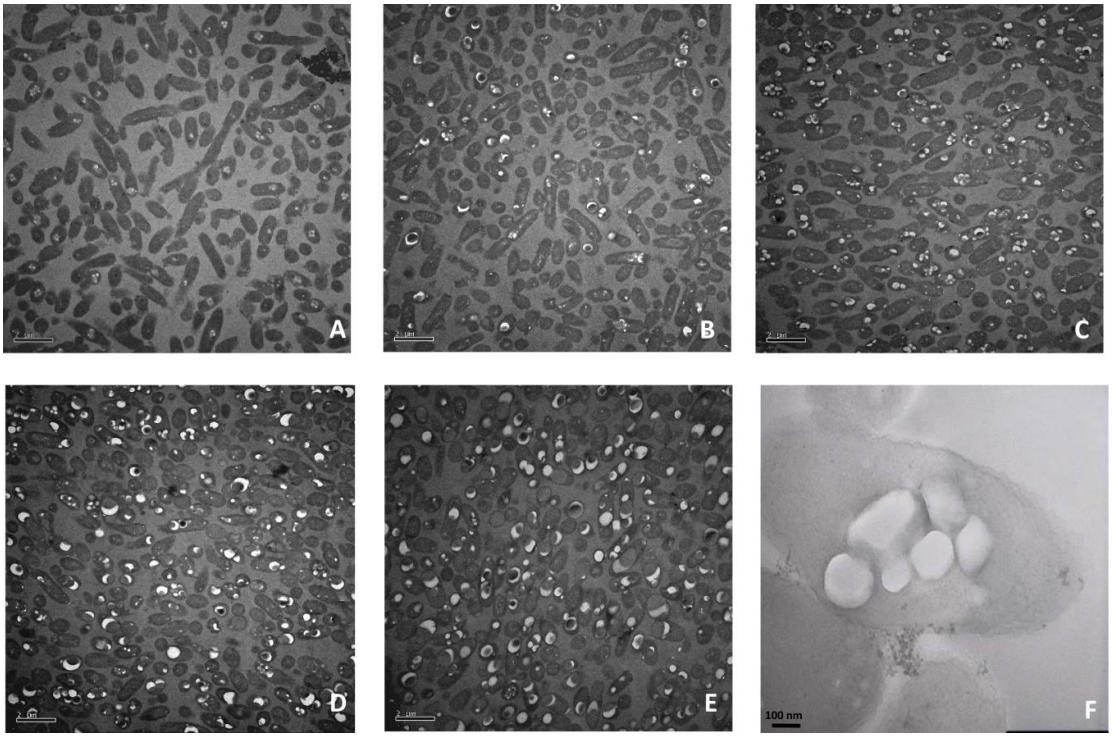

Figure 13. TEM images of *P. putida* KT42F growth curve in PHA production medium. A-E, Samples taken 0, 2, 4, 6 and 24 h after the inoculation (Panels A, B, C, D and E, respectively); F, Detail of the granule distribution of a single cell from a 4 h culture in PHA production medium.

Moreover, at 24 h of growing 34% of mutant cells did not contain PHA granules generating two markedly different cell populations, *i.e.*, with and without PHA (Figure 11B, 13E). While wild-type strain distributed the previously formed PHA granules among the daughter cells keeping the needle array structure, the PHA granules in the PhaF mutant strain remained agglomerated in one of the daughter cells (Figure 15). It

is worth noting that granules did not coalesce in a single big granule, as reported for other microorganism lacking phasins (Wieczorek *et al*., 1995), very likely due to the presence of the other phasin PhaI (see below).

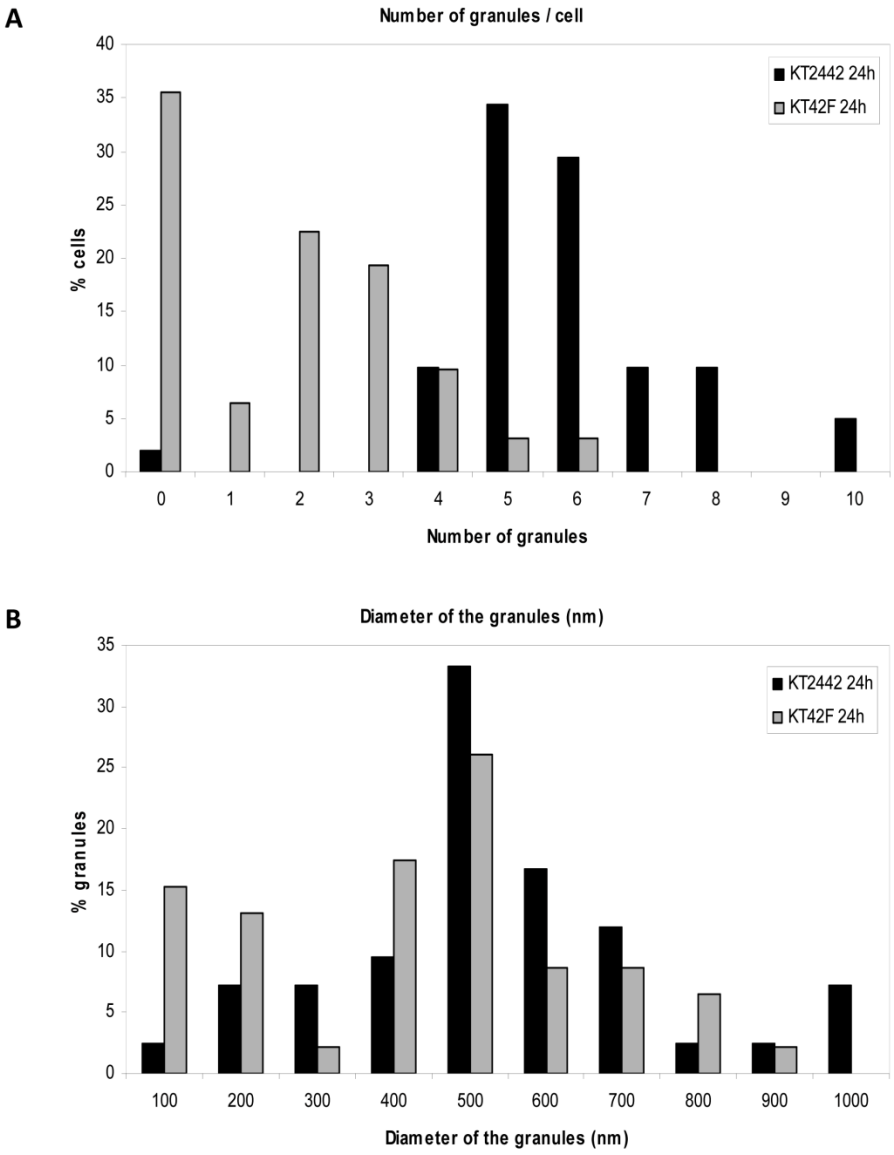

Figure 14. Determination of granule size and number in KT2442 and KT42F strains of *P. putida* by TEM images analysis. A, The granule number distributions in KT2442 (black bars) and KT42F (gray bars); B, Granule size distributions in KT2442 (black bars) and KT42F (gray bars).

Additionally, *P. putida* KT42F cells were complemented using pPF61 plasmid that harbours the *phaF* gene under the control of the *Ptrc* promoter (Prieto *et al.*, 1999). This allowed *in trans* production of PhaF from *P. putida* GPo1 and gave rise to *P. putida* KT42F-F strain (Figure 15). It was observed that the presence of PhaF ensures the segregation of the PHA granules during the cell division. In addition, obtained results provide evidence for the reduction of the total PHA content at 24 h in the mutant strain (Figure 11) by a dilution effect as a consequence of the presence of PHA empty cells.

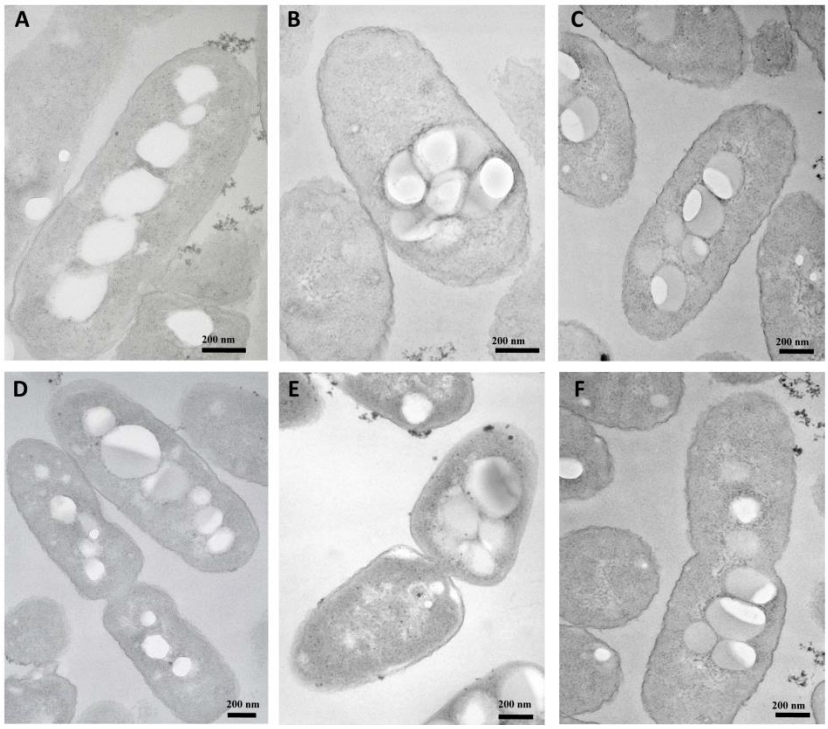

Figure 15. Analysis of the *P. putida* KT42F complementation and PHA segregation by TEM. A-C, Samples taken after 4 h growth in PHA production medium. Detail of the PHA granule distribution of KT2442 (A), KT42F (B) and the complemented strain KT42F-F (C); D-F, Segregation of PHA granules during cell division in KT2442 (D), KT42F (E) and KT42F-F (F).

1.1.3. DNA binding abilities of PhaF protein

The involvement of PhaF in the *pha* transcriptional regulatory system was first demonstrated in *P. putida* GPo1 (Prieto *et al.*, 1999). Disruption of the *phaF* gene in *P. putida* GPo1 strain led to an increased expression rate of *phaC1* gene, suggesting that PhaF acts as a negative regulator of the *pha* cluster in this strain. This function was ascribed to its C-terminal half due to its similarity with histone-like proteins. However, there was no evidence pointing to direct binding of PhaF to the *pha* promoter regions. Later, the binding of PhaF protein to DNA was proven to be non-specific, *i.e.*, independent of the recognition of a specific operator DNA sequence. Moreover, it was shown by spectroscopical techniques that PhaF binds DNA *in vitro* through its C-terminal domain in a non-specific manner (Galan *et al*., 2011; Maestro *et al*., 2013).

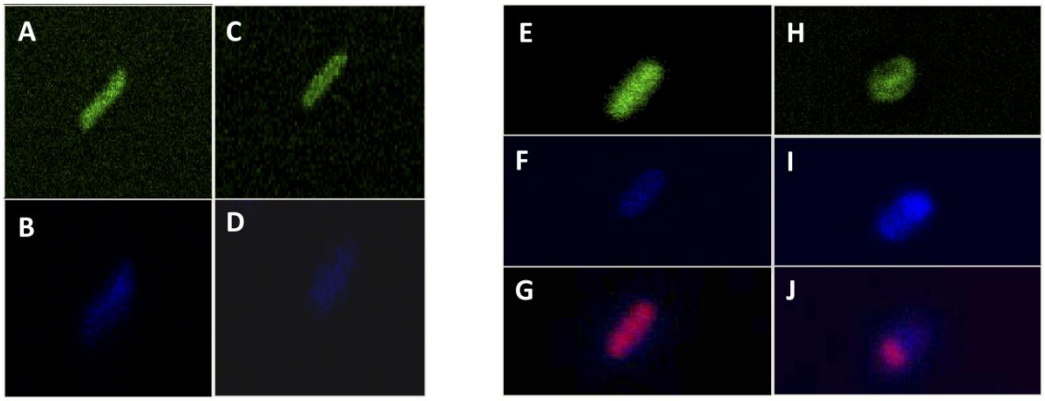

Figure 16. *In vivo* localization of GFP-CPhaF fusion protein in KT42-GC (A, B, E-G) and KT42F-GC (C, D, H-J) *P. putida* strains by confocal microscopy. A, Localization of GFP-CPhaF fusion protein (in green) in KT42-GC strain cultured in LB medium (non PHA producing conditions); B, Localization of nucleoid (in blue) in KT42-GC strain cultured in LB medium; C, Localization of GFP-CPhaF fusion protein (in green) in KT42F-GC strain cultured in LB medium; D, Localization of nucleoid (in blue) in KT42F-GC strain cultured in LB medium; E, Localization of GFP-CPhaF fusion protein (in green) in KT42-GC strain cultured in PHA producing conditions; F, Nucleoid (in blue) in KT42-GC strain cultured in PHA producing conditions; G, PHA granules (in red) in KT42-GC strain cultured in PHA producing conditions; H, Localization of GFP-CPhaF fusion protein (in green) in KT42F-GC strain cultured in PHA producing conditions; I, Nucleoid (in blue) in KT42F-GC strain cultured in PHA producing conditions; J, PHA granules (in red) in KT42F-GC strain cultured in PHA producing conditions.

To confirm these findings *in vivo*, we constructed a fusion protein between the reporter green fluorescent protein (GFP) and the DNA binding domain of PhaF protein (C-PhaF). This *gfp-cphaF* construction was introduced into the *P. putida* KT2442 and *P. putida* KT42F chromosomes using pCNB5 plasmid, pUTmini-Tn*5* vector that carries minitransposon allowing insertion of heterologus DNA fragment in the chromosome of the strain of interest. This allowed the construction of GFP-CPhaF producing strains, KT42-GC and KT42F-GC respectively. *In vivo* localization of the GFP-CPhaF fusion protein was analysed by confocal microscopy (Figure 16). Cells were stained with two different dyes to analyse localization of: (i) PHA granules (Nile Red-stained); (ii) nucleoid (DAPI-stained) and (iii) GFP-CPhaF protein. Our results confirm the co-localization of GFP-CPhaF fusion protein and nucleoid in wild-type and PhaF minus cells, independently of the presence or absence of the PHA granules. Furthermore, PHA granules produced in the wild-type cells that contained native PhaF protein, co-localized with the nucleoid and GFP reporter. However, PHA granules produced in the KT42F mutant strain were located independently of the nucleoid and GFP reporter. These results prove the involvment of PhaF in the intracellular localization of the PHA granule and its role as nucleoid-binding protein.

1.2. The function of PhaI in the PHA metabolism

As mentioned earlier, *P. putida* KT2442 harbours two phasins, PhaF and PhaI. Those phasins belong to the same operon (Figure 4) and share considerable sequence similarity (Prieto *et al*., 1999). Since we spotted the key role of PhaF, we analyzed the physiological role of the other *P. putida* phasin protein PhaI. The effect of its absence on granule formation and localization as well as its possible coordinated activity with PhaF was tested.

1.2.1. The outcome of PhaI phasin deficiency considering PHA granule accumulation/formation

Previously we showed that lack of PhaF phasin, involved in PHA granules localization and balanced distribution during cell division induce considerable reduction of total PHA content due to the defect in granule segregation, and consequently presence of population heterogeneity. Those findings demonstrated a new role for phasins within the PHA apparatus that could be critical for cell survival under stress conditions. Based on this observation, we laid stress on studying the influence of phasins on PHA accumulation, comparing the PHA production abilities of different phasin mutant strains to that of the wild-type bacterium. With this aim, *P. putida* KT2442 strain was genetically manipulated to generate disruption mutations of the respective phasin genes designing *P. putida* KT42F that lacks *phaF* (see section 1.1.3), *P. putida* KT42I-F that lacks *phaI* and *P. putida* KT42I that lacks both *phaF* and *phaI* phasing genes (Figure 17A). By Western blot analysis we demonstrate that wild-type and *phaF* mutant strain produce PhaI, while strains KT42I-F and KT42I do not (Figure 17B). It is worth to remark that the presence of low dosage of PhaF in KT42I-F is due to the complementation of KT42I strain with *lacI*^{q}*::Ptrc::phaF* monocopy expression system. Thus the production of PhaF is driven by the addition of IPTG. Furthermore, we show that wild-type strain produce higher quantity (7.5 fold) of PhaF when compared to KT42I-F strain, whereas KT42F and KT42I do not produce PhaF, last very likely due to a polar mutation in the *phaIF* operon (Figure 17B).

For PHA content analysis by GC-MS, cells were cultured in optimal PHA production conditions and harvested after 24 h of growth. Wild-type strain showed PHA content of 63% of cell dry weight (CDW), while mutant strain lacking PhaF, PhaI and both phasins produced less amount of PHA, 33%, 21% and 7% respectively (Table 5). These results demonstrate that when *P. putida* strain lacks both phasins, PHA production dramatically decreases, suggesting that PhaF and PhaI phasins work in harmony and are essential for the optimal PHA synthesis and accumulation.

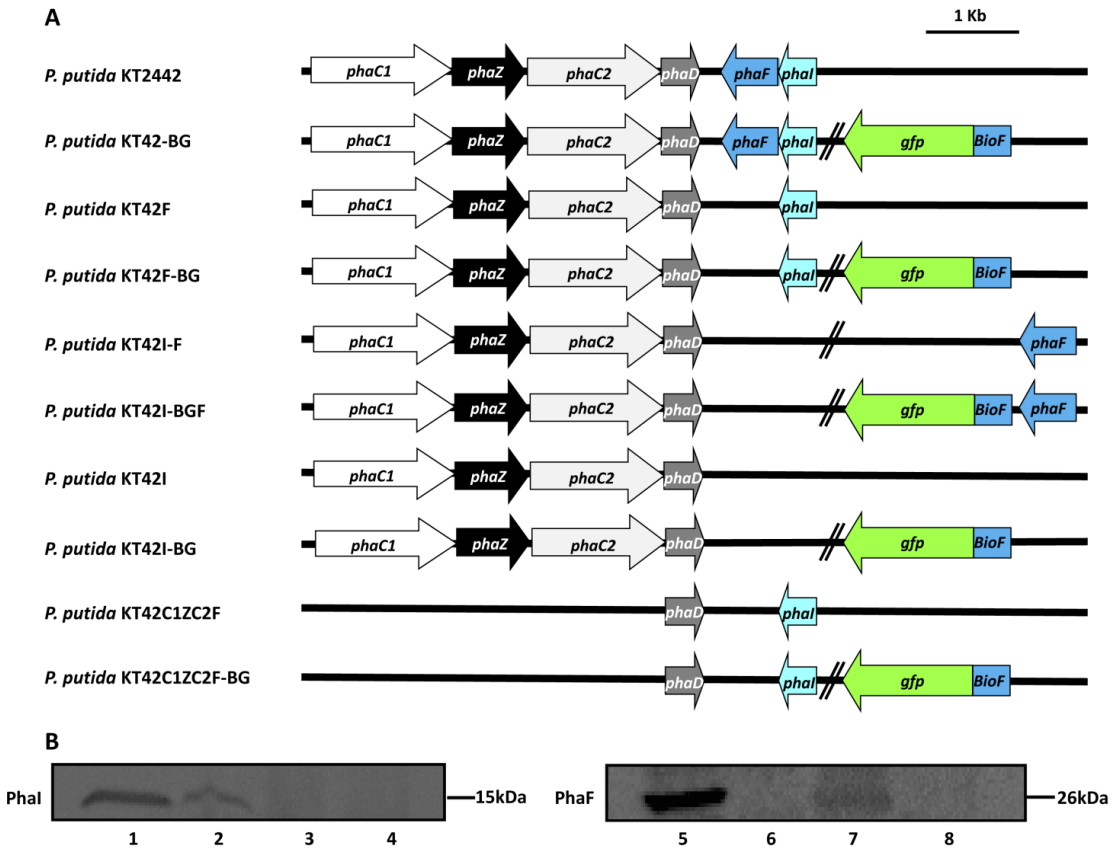

Figure 17. Comparative representation of *pha* gene cluster organization of different *P. putida* strains and Western blot analysis. A, Scheme of constructed *P. putida* KT2442 mutant strains. Arrows indicate different genes involved in PHA metabolism (for details see Figure 4), their relative size and transcriptional direction. Different mutant strains were constructed KT42F, KT42I-F, KT42I, KT42C1ZC2F lacking *phaF*, *phaI,* both *phaF* and *phaI* and *phaC1*, *phaZ, phaC2*, *phaF* respectively. *bioF* was fused with *gfp* (bi-colour arrow, blue and green) and randomly (marked with two parallel lines) inserted in the chromosome of each strain, wild-type and mutant strains on *pha* cluster giving rise to KT42-BG, KT42F-BG, KT42I-BGF, KT42I-BG and KT42C1ZC2F-BG; B, Western blot analysis of phasin synthesis in different *P. putida* strains applying antibody against PhaI (left) and BioF tag (right). Lines 1, 5: KT2442; lines 2, 6: KT42F; lines 3, 7: KT42I-F; lines 4, 8: KT42I.

Table 5. Quantification of PHA content by GC-MS and protein quantification by Quantity One analysis

P. putida strain	PHA %	Biomass (g/L)	Protein mg/g biomass	Protein mg/L culture	Protein mg/g PHA
KT2442	63.27±1.42	1.40±0.11	_	_	_
KT42F	33.36±1.19	0.65±0.18	_	_	_
KT42I-F	20.75±1.35	0.62±0.22	_	_	_
KT42I	7.44±0.39	0.58±0.17	_	_	_
KT42-BG	53.51±3.22	1.14±0.10	1.46±0.36	1.49±0.37	2.92±0.53
KT42F-BG	33.85±1.88	0.80±0.06	4.06±0.66	3.53±0.57	11.38±0.65
KT42I-BG	19.62±1.02	0.69±0.07	4.16±0.35	2.62±0.47	20.17±0.73
KT42I-BGF	42.10±1.28	1.00±0.23	9.73±0.42	10.31±0.49	22.42±0.85

1.2.2. BioF tag or its fusion derivatives can replace PhaI in *P. putida* in terms of PHA production

Because PhaI and N-terminal domain of PhaF (BioF) show high structural similarity and their 3D models predict a possible interaction between proteins through the oligomerization linker (Maestro *et al*., 2013), we investigated the possibility of PhaI functional replacement by BioF. To monitor the influence of BioF on PHA content, *bioF-gfp* was stably integrated into the chromosome of *P. putida* phasin mutant strains. *P. putida* KT2442-BG, KT42F-BG, KT42I-BGF and KT42I-BG cells (Table 4; Figure 17A) were cultured in optimal PHA producing conditions for 24 h and their PHA content was analyzed by GC-MS. Interestingly, *P. putida* KT42I-BGF and KT42I-BG showed an increase in PHA content being, 42% and 20% of CDW respectively, when compared to their correspondent strains that did not produce BioF-GFP (Table 5). However, we did not observe significant difference in PHA accumulation in KT42F-BG strain when compared to KT42F strain, showing PHA content of 34% and 33% of CDW, respectively. These results were confirmed by flow cytometry analysis, where fluorescence of Nile

red stained PHA granules was recorded for the determination of PHA cell content. In perfect correlation with GC-MS results, no significant difference was observed between KT2442 and KT42-BG. Similarly, the result obtained for PhaF phasin mutant (KT42F) and KT42F-BG strain showed no difference between these two strains in PHA content (data not shown). However, PhaI mutant harboring BioF-GFP fusion protein recovered PHA production to the level of PhaF mutant, while KT42I-BGF strain showed PHA content similar to that of wild-type. Taking into account the results presented above we definitively conclude that BioF tag or its fusion derivatives can replace the role of PhaI phasin in *P. putida* strain in terms of PHA content.

1.2.3. The effect of PhaI absence on population homogeneity

Since, a deletion of *phaF* resulted in a defected granule segregation and population heterogeneity in terms of PHA granules content (see section 1.1.), we interrogated the required imposition of phasin domains to reconstruct a uniform granule distribution and optimal PHA production.

By flow cytometry analyses, we were able not only to determine the PHA content but to relate this parameter to the cell population, this is, the PHA content of individual cells (heterogeneity of the population). Figure 18A and C show a major overlay corresponding to positive fluorescent cells in the wild-type cells indicating a homogeneous population regarding the PHA granules content. Two main overlays showing different fluorescence intensities were detected in the KT42I, KT42I-BG and KT42F samples (Figure 18A). In the case of KT42I, KT42I-BG and KT42F strains, only 24%, 51% and 45% of cell population displayed positive PHA content while the rest of the cells were PHA granule free (Figure 18A). This indicates the occurrence of two different cell populations in terms of PHA content and confirms the role of PhaF C-terminal domain in granule distribution. Interestingly, population heterogeneity was not spotted for KT42I-BGF strain (80% positive cells) as shown in Figure 18B and C, suggesting that PhaI phasin can be replaced by BioF domain, and that the presence of PhaF at low dosage (Figure 17B) is sufficient to control granules segregation during cell division.

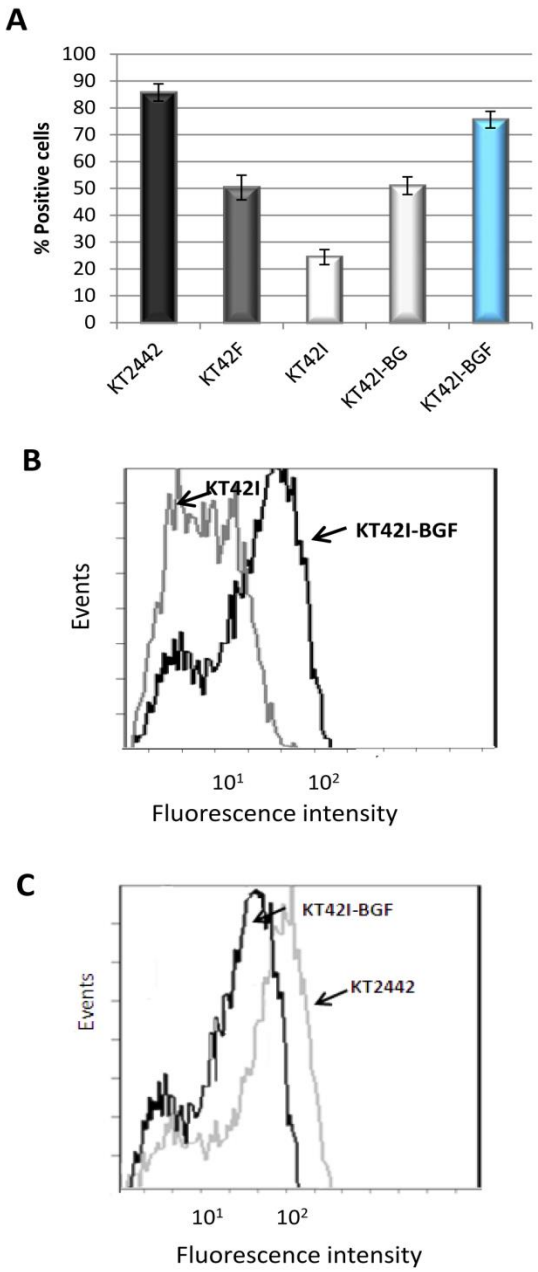

Figure 18. Study of cell population heterogeneity in terms of PHA production by flow cytometer. A, Percentage of PHA positive cells KT2442 (black bar), KT42F (dark grey bar), KT42I white bar, KT42I-BG light grey bar and KT42I-BGF (blue bar); B, Example of a flow cytometer histogram of the *P. putida* KT42I and *P. putida* KT42I-BGF strains grown in PHA producing conditions; C, Example of a flow cytometer histogram of the *P. putida* KT2442 and *P. putida* KT42I-BGF strains grown in PHA producing conditions.

Flow cytometry assay confirmed that lack of wild-type phasins affects PHA production and influence granule segregation, and that BioF can replace those roles of PhaI. To analyze *in vivo* granule segregation and BioF fusion localization, we monitored GFP reporter fused to BioF (see Materials and methods section 3.5). The strains KT42-BG, KT42F-BG, KT42I-BGF, KT42I-BG (Table 5; Figure 17A) producing BioF-GFP have been used to analyse the *in vivo* localization of the BioF-GFP fusion protein by epifluorescent microscopy. These experiments were performed as well with the strain KT42C1ZC2F-BG, unable to accumulate PHA since it lacks both synthase genes, *phaC1* and *phaC2*. As reported for the wild-type strain (see section 1.1; Figure 15), KT42-BG strain contained more than one granule located running lengthwise the cell, forming a characteristic needle array and during cell division equally distributed between daughter cells. PhaF and double PhaF and PhaI phasins mutant strains expressing BioF-GFP fusion (KT42F-BG, KT42I-BG) contained usually one or agglomerated pool of granules located in one of the cell poles (Figure 19B, C).

However, PhaI phasin mutant strain complemented with *phaF* and expressing *biof-gfp* fusion (KT42I-BGF) showed similar phenotype to that of wild-type strain in terms of granule segregation and number (Figure 19D, H). Additionally, diverse functions of BioF and the C-terminal module of PhaF were confirmed by comparative *in vivo* monitoring of BioF-GFP and GFP-CPhaF (Figure 19); BioF-GFP fusion protein co-localize with PHA granules in wild-type and phasin minus strain grown in PHA producing conditions, whereas the PhaF C-terminal domain interacts with nucleoid independently on the strain and growth conditions (Figure 19G). By monitoring BioF-GFP fusion protein in KT42C1ZC2F-BG strain, not capable of producing PHA, we investigated the localization of BioF module in the absence of PHA granules (Figure 19E, F). In fact, in the absence of PHA granules, BioF domains interact, likely through leucine-zipper motif, forming small cytoplasmatic inclusions that are accumulated mainly in the vicinity of the membrane at the cell poles.

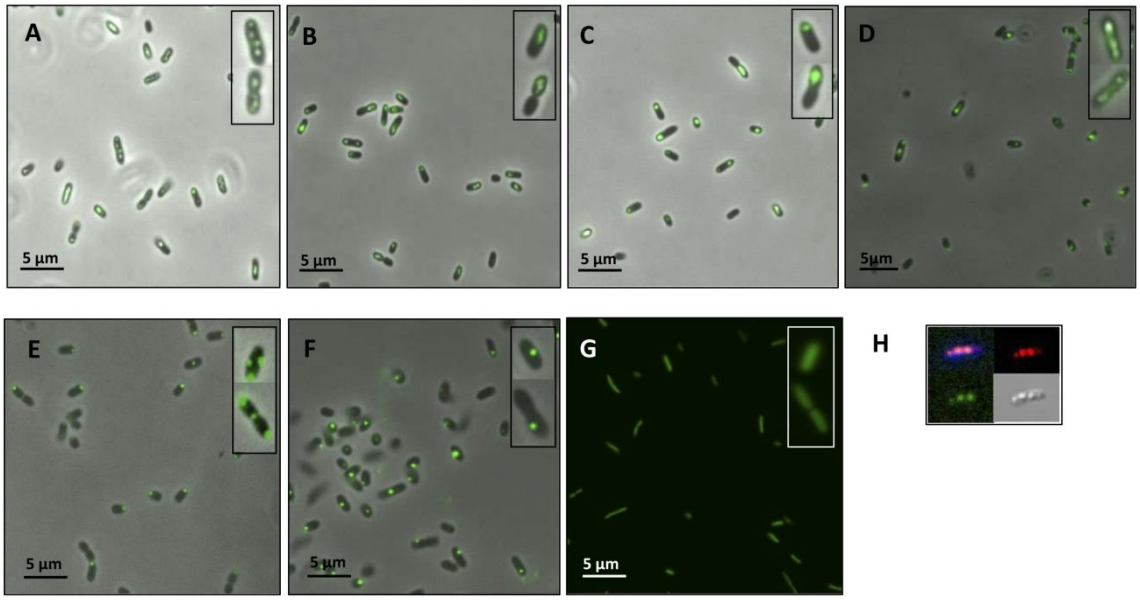

Figure 19. *In vivo* localization of BioF-GFP (A-F; H) and GFP-CPhaF (G) fusion protein in *P. putida*. Epifluorescence analysis of A, KT42-BG; B, KT42F-BG; C, KT42I-BG; D, KT42I-BGF and E, KT42C1ZC2F-BG in PHA producing condition; F, Shows KT42C1ZC2F-BG strain cultured in LB medium (non PHA producing conditions); G, Shows *in vivo* localization of GFP-CPhaF fusion protein in KT42I-GC in PHA producing conditions; H, Represents detailed confocal microscopy analysis of BioF-GFP protein localization within KT42I-BGF cells demonstrating granules (in red), nucleoid (in blue) and BioF-GFP protein (in green).

To analyse in detail the recovery of wild-type phenotype of KT42I-BGF strain and the localization of the granules, the cells were stained with two different dyes and visualized by confocal microscopy (Figure 19H). With this aim, we monitored *in vivo* localization of: (i) PHA granules (Nile Red-stained); (ii) nucleoid (DAPI-stained) and (iii) BioF-GFP protein. Obtained results confirm the co-localization of the fusion protein BioF-GFP and PHA granules in KT42I-BGF cells. Furthermore, we confirm that the presence of PhaF ensures the segregation of the PHA granules during the cell division. Moreover, when whole protein PhaF is produced together with BioF tag the strain recovers wild-type phenotype accumulating more than one granule and showing granule distribution similar to that of wild-type strain.

1.2.4. The influence of phasins on BioF protein recruitment on the surface of PHA granule

Based on the results presented above, we focused our interest in encountering most favourable host for the BioF system concerning expression or not of the natural *phaF* and *phaI* phasins to achieve the best BioF fusion protein yield. We monitored the biomass and PHA production, as well as the concentration of fusion protein attached to the granules in the presence/absence of phasins in the *P. putida* strains to establish the optimal conditions for *in vivo* immobilization of BioF fusion proteins,.

The amount of BioF-GFP protein was found to be higher in phasin mutant strains according to the results obtained by SDS-PAGE analysis (Figure 20). Additionally, in all tested conditions BioF-GFP fusion protein was mainly associated with the granules (Figure 19, 21). To quantify the difference in fusion protein content in the presence and the absence of phasins, Gel Doc Quantity One analysis were conducted on the base of SDS-PAGE acrylamide gels. Relative content of BioF-GFP fusion protein in phasin mutant strains was 4-folds higher than the concentration of fusion protein accumulated by wild-type strain. The best immobilized protein yield was obtained when PhaF phasin and BioF tag were expressed simultaneously, giving BioF-GFP concentration of 9.73 mg/g of biomass in *P. putida* KT42I-BGF strain. Furthermore, BioF-GFP concentration found in wild-type strain was 6.6-fold lower when compared to KT42I-BGF strain as shown in Table 5.

The influence of different pattern of phasin expression on BioF-GFP concentration was monitored by flow cytometry. In perfect correlation with the results obtained by Quantity One the lowest BioF-GFP concentration was observed in KT42-BG strain. KT42F-BG and KT42I-BG showed similar levels of BioF-GFP protein, that were about 4-fold higher when compared to that of KT42-BG strain, while the best protein yield was obtained in KT42I-BGF strain (Figure 22).

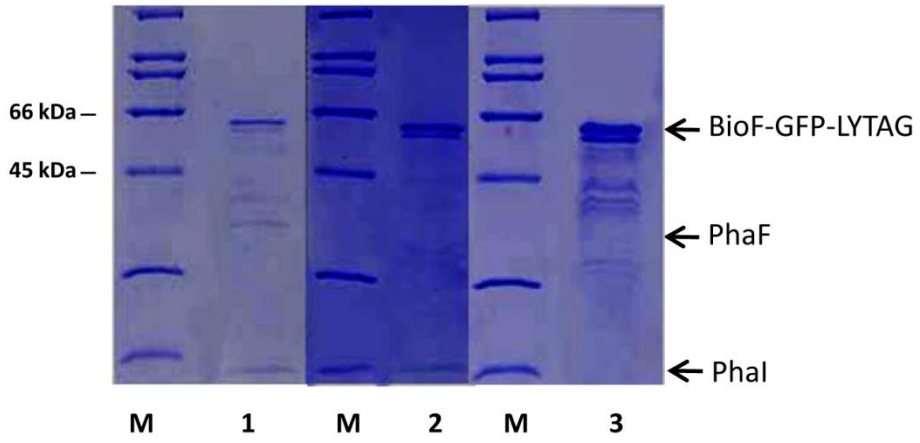

Figure 20. Comparative SDS-PAGE analysis of BioF::GFP fusion protein production and granule association depending on phasin presence/absence in *P. putida* strains. Line 1, *P. putida* KT42-BG granules; Line 2, *P. putida* KT42F-BG granules; Line 3, *P. putida* KT42I-BG granules; M, Molecular weight markers (BioRad, Prestained SDS-PAGE Broad Range Standard). BioF-GFP fusion protein, PhaF and PhaI are marked with the arrows.

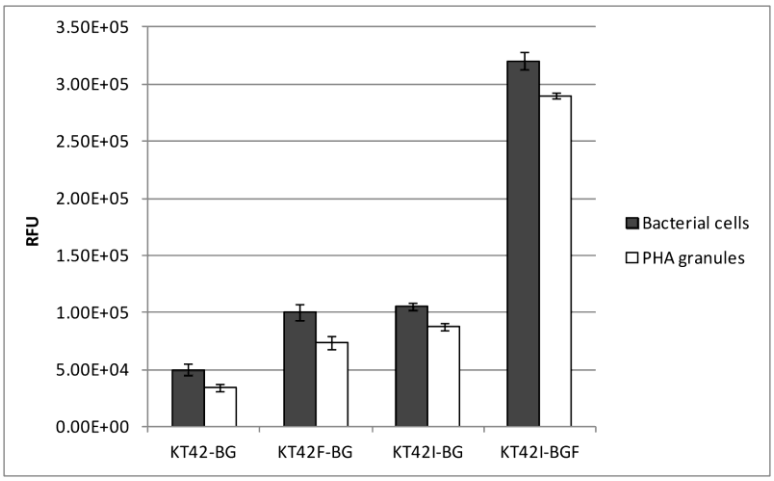

Figure 21. Fluorymetry comparative analysis of green fluorescence level of *P. putida* cells and PHA granules. From left to right KT42-BG, KT42F-BG, KT42I-BG and KT42I-BGF cells harbouring BioF-GFP fusion protein (gray bars) and isolated PHA granules (white bars) of correspondent strains carrying BioF-GFP fusion anchored to the granule surface. RFU, relative fluorescence unit.

The concentration of BioF-GFP in the cells was compared with the concentration of BioF-GFP immobilized to the granules by fluorometry analysis. Similar concentration of fusion protein was found in the cells and in the isolated granules (Figure 21). Those results are in agreement with the data obtained by SDS-PAGE analysis that showed that majority of the BioF-GFP protein was immobilized on PHA granules surface (Figure 20). In addition, fluorometry results verified the results of flow cytometry for BioF-GFP quantification in different *P. putida* strains.

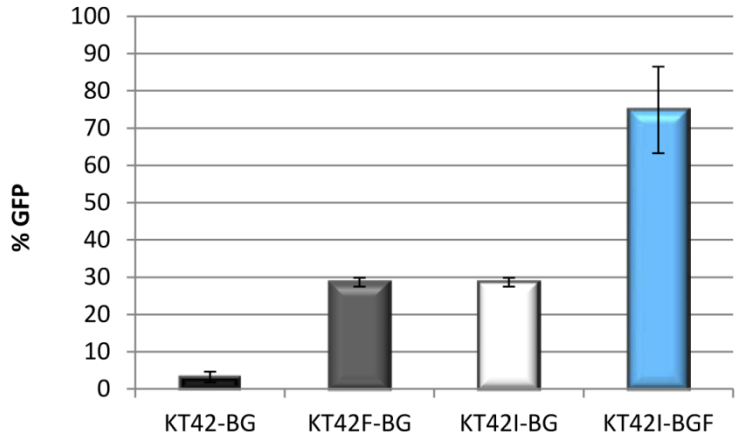

Figure 22. Relative quantification of fusion protein production in *P. putida* cells by flow cytometry. KT42-BG (black bar), KT42F-BG (gray bar), KT42I-BG (white bar) and KT42I-BGF (blue bar).

2. Mcl-PHA side chain functionalization

Previously, our research team established the optimal conditions for thioester group incorporation in side chain of mcl-PHA and PHACOS production. In spite of existence of numerous reported side chain functionalized mcl-PHA, this was the first published data on thioester group incorporation. Herein we investigate PHACOS antibacterial activity, as well as its advantages in terms of bacterial adhesion and biocompatibility over non functionalized PHO for biomedical application.

2.1. PHACOS prevents *Staphylococcus aureus* biofilm formation

It is known that the quality of bacterial biofilm on mcl-PHA, varies depending on both bacterial strain and material purity that supports biofilm formation (Mauclaire *et al*., 2010). Herein, the ability of *S. aureus*^{T} and *P. aeruginosa* (Table 4) to form biofilms on PHACOS and PHO surfaces was examined by ESEM, crystal violet assay and CFU counting.

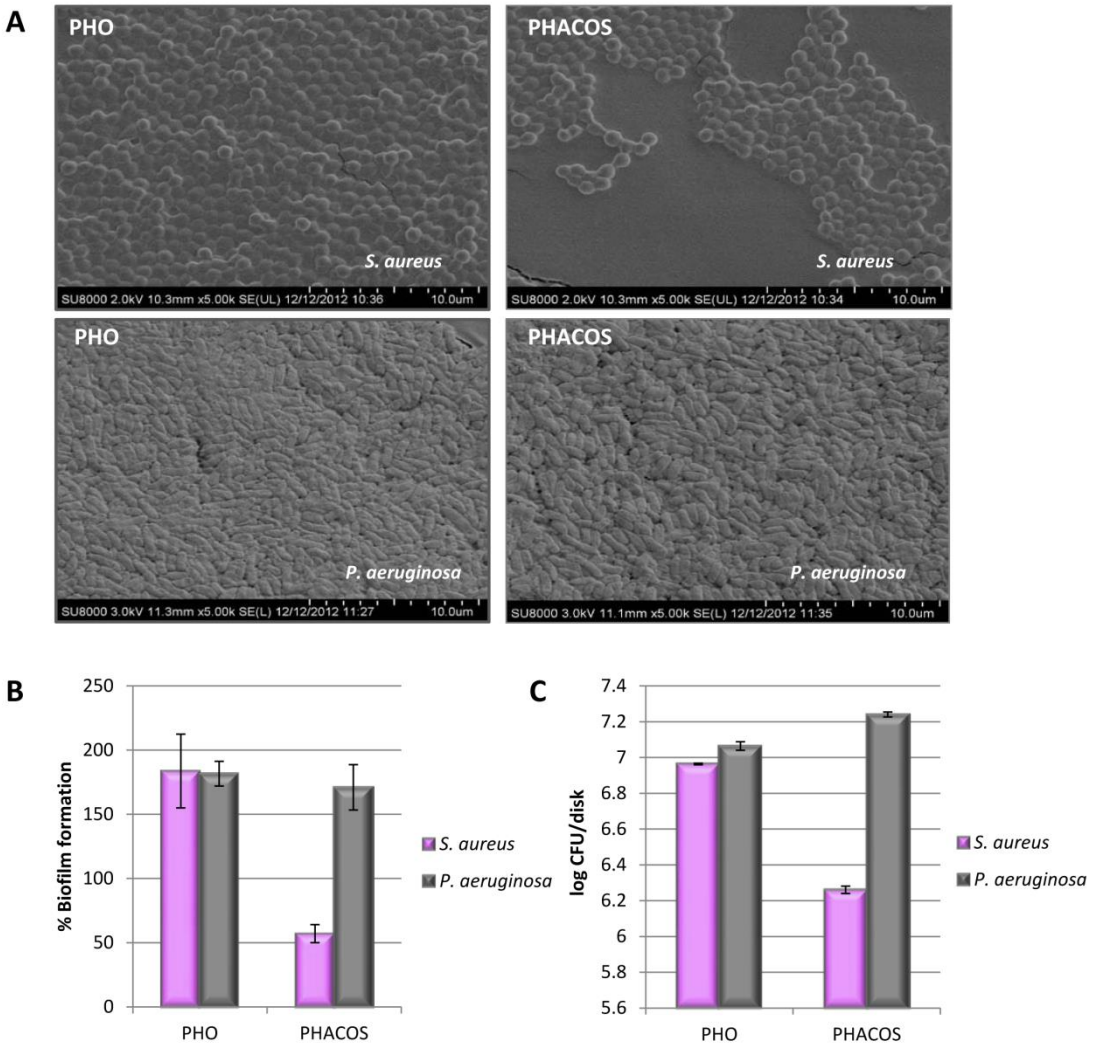

Figure 23. Study of PHACOS and PHO disks capacity to inhibit bacterial biofilm formation. A, ESEM of *S. aureus* and *P. aeruginosa*; B, Crystal violet staining assay to quantify formed biofilm where the value of capacity of biofim formation on PET disks is considered 100%; C, CFU counting of deatached cells that were forming biofilm.

ESEM observation suggested less biofilm formed by *S. aureus*^{T} than *P. aeruginosa* on PHACOS, while the biofilms formed on PHO were similar. However, adhered cells were always observed in both polymers (Figure 23A). *S. aureus*^{T} formed 3-fold less biofilm than *P. aeruginosa* on PHACOS, whereas the biofilm formed on PHO was similar in case of both strains, as shown by crystal violet staining (Figure 23B). Moreover, CFU counting confirmed these results, showing that the *S. aureus*^{T} biofilm on PHACOS contained 10% of the bacteria found in *P. aeruginosa* biofilm (Figure 23C). Additionally, PHACOS had significantly less *S. aureus*^{T} counts than PHO.

2.2. *S. aureus*^{T} adheres equally to PHACOS and PHO

To determine whether the differences in biofilm formation on PHACOS resulted from differences in the initial bacterial attachment, the number of bacteria adhered to polymer surfaces was analyzed. With that aim, mcl-PHA microparticles were prepared by water-in-oil-in-water emulsion/solvent evaporation technique (Reyes-Ortega *et al*., 2013) and used to evaluate *S. aureus*^{T} and *P. aeruginosa* surface adhesion (see Materials and methods section 10 for details).

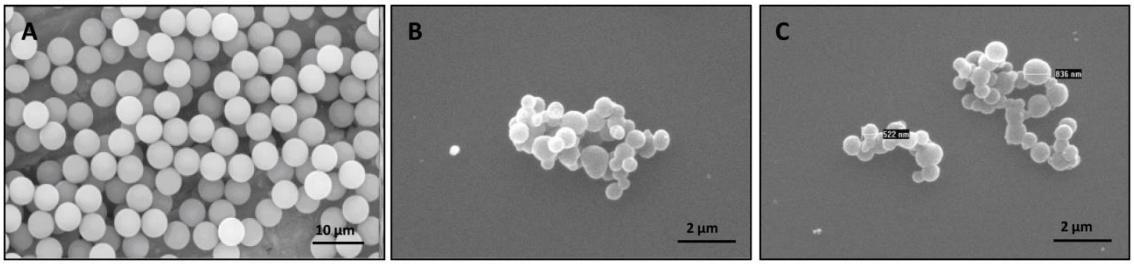

Figure 24. Microparticles morphology and size examination by ESEM. A, Polystyrene microparticles; B, PHB microparticles; C, PHO microparticles.

The average size of mcl-PHA particle was 4 µm determined by Coulter. However, ESEM analysis of particle morphology showed their agglomeration tendency (Figure 24). Commercially available polystyrene 5 µm particles were used as positive control. Cells were radioactively labelled and the quantitative determination of particle-bound

bacteria was performed by cpm monitoring. To radioactively label the cells, bacteria were cultured in MHB II medium supplemented with glucose, D-[^{14}C(U)] (20 µCi/mL of cell culture). The adhesion assay was performed by incubating the suspension of microparticles and bacterial cells. Direct examination of the adhesion of bacteria to solid particles is usually complicated, as both viable counting and optical methods have very limited applicability (Fleminger and Shabati, 1995). Instead, adhesion of cells to such particles is usually determined by monitoring the disappearance of bacteria from the supernatant. Although convenient, this method is not very accurate, especially when the percentage of adsorbed bacteria is low or when the cells and/or particles tend to form aggregates that coprecipitate with the solid particles. In contrast, radioactive labeling of bacteria provides a rapid and sensitive way to monitor their adhesion on solid particles. Moreover, this method could offer the possiblity of automation that may allow recording of an immense number of interactions and the possibility to simultaneously record effects on both particle adhering and planktonic bacteria. Lower number of *S. aureus*^{T} then *P. aeruginosa* adhered to PHO microparticles was spotted. While 13% of assayed *P. aeruginosa* cells were attached to PHO microparticles, in case of *S. aureus*^{T} only 4.1% of assayed cells were particle-bound (Table 6). To discard the possibility of particle aggregation influence on bacterial adhesion, we used different approach investigating the rate of bacterial adhesion to mcl-PHA films.

Table 6. Monitoring of bacterial adhesion to microparicles

Bacterial strain	%PHO particle-bound bacteria	Bound CFU/ mg PHO	%Polystyrene particle-bound bacteria	Bound CFU/mg polystyrene
P. aeruginosa	13 ± 0.3	1.3 x 10^6	1.6 ± 0.1	0.6 x 10^6
S. epidermidis^{T}	4.2 ± 0.3	0.4 x 10^6	3.1 ± 0.3	0.3 x 10^6
S. typhimurium	3.6 ± 0.2	0. 3 x 10^6	35.7 ± 0.6	3.6 x 10^6
S. aureus^{T}	4.1 ± 0.5	0.4 x 10^6	32.6 ± 0.3	3.3 x 10^6

Subsequently, bacterial adhesion to mcl-PHA films was monitored by ESEM. To that end, PET (6 mm) disks were coated with PHO and PHACOS by solvent-casting method. Non coated PET disks were used as a control. In these experiments, bacteria were suspended in a 1/500 diluted NB medium and deposited on the PHACOS and PHO surfaces during 24 h. The lack of nutrients in the diluted suspension impedes biofilm formation, but allows testing the adhesion step of biofilm formation. Although there were no differences in adhesion of *S. aureus*^{T} to PHO and PHACOS the number of *S. aureus*^{T} adhered cells was lower than that of *P. aeruginosa* on both surfaces (PHO and PHACOS) (data not shown). Thus, the process of bacterial surface adhesion was not affected by the polymer chemical structure in this case; even so biofilm development of *S. aureus*^{T} on PHACOS was altered.

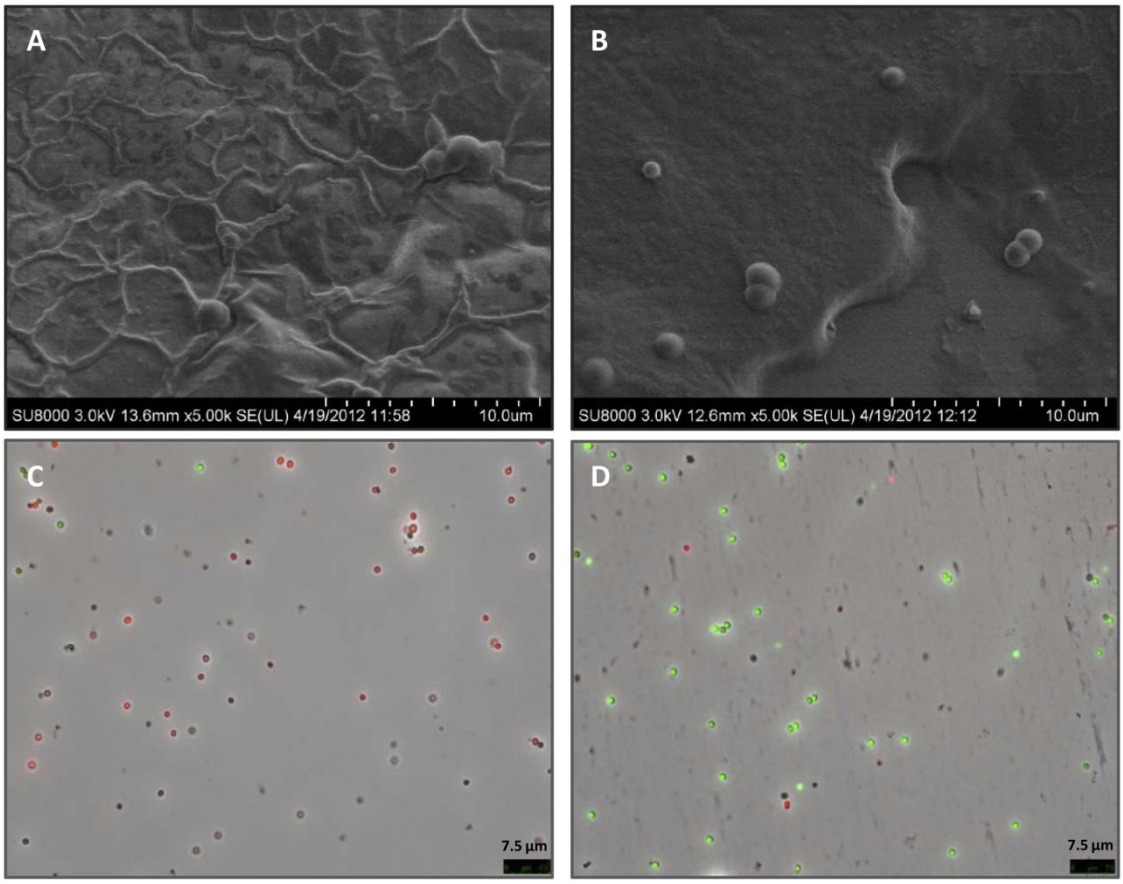

Figure 25. Measurement of antiadherent (A, B) and antibacterial activity (C, D) of PHACOS and PHO surfaces against *S.aureus*. A,B ESEM of PHACOS (A) and PHO (B); C,D Fluorescent Microscopy using Bacterial Viability test (LIVE/DEAD *Bac*Light^{TM}, Invitrogen) of *S. aureus*^{T} that was in contact with PHACOS (C) and PHO (D).

Therefore, we next examined whether PHACOS has impact on bacterial viability. To do so, PHACOS and PHO adhered cells were washed out from polymer surfaces and tested by LIVE/DEAD BacLightTM kit (Figure 25C, D). Interestingly, the percentage of viable *S. aureus*^{T} cells incubated on PHACOS was greatly decreased (20%) in comparison to those on PHO (83%). As shown in Figure 25C, most of *S. aureus*^{T} cells were not viable (red stained) after the contact with PHACOS, whereas bacteria on PHO were mostly viable (green stained) (Figure 25D). This suggests that PHACOS possess anti-staphylococcal activity.

2.3. PHACOS shows antibacterial activity against methicillin-resistant (MRSA) *S. aureus* strains

We further analyzed the antibacterial activity of PHACOS following ISO 22196:2011 standard protocol by characterizing the effectiveness of this potential antibacterial agent. In this assay we compared the viability of nine Gram-positive and two Gram-negative pathogen strains (Table 4) after contacting the PHACOS surface (see Material and methods section 13 for details). Susceptibility to PHACOS was evident only in some Gram-positive bacteria. Moreover, the antimicrobial activity of PHACOS was apparently restricted to *S. aureus* strains, including MRSA clinical isolates showing R value of ≈1.03 (Figure 26).

To calculate the maximal antimicrobial activity of PHACOS in terms of cell/cm^2, we analyzed the effectiveness of PHACOS in the presence of a range of bacterial concentrations (10^4 to 10^{10} cells/cm^2). It was observed that PHACOS is not effective against high bacterial concentration, when inoculums exceed 10^6 cells/cm^2. This result suggested that direct contact between bacteria and the polymer is a prerequisite for PHACOS antimicrobial activity.

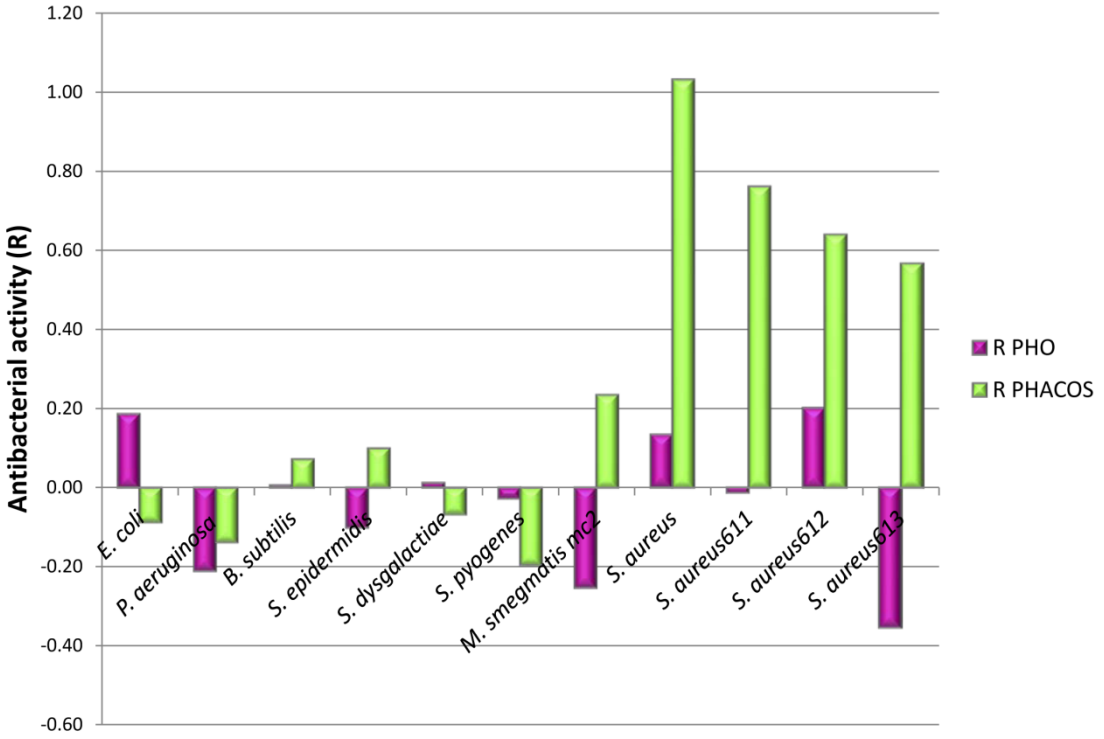

Figure 26. Measurement of antibacterial activity of polymer (PHACOS and PHO) surfaces according to ISO 22196:2007 standard protocol, where R = 1 means 10-fold less viable cells recovered from sample disk after 24 h when compared to that of control disk. According to ISO 22196:2007 when the stated conditions are satisfied, the test is deemed valid and R value is recorded to the first decimal place after rounding the second decimal place down.

2.4. Antimicrobial activity of PHACOS lies on thioester group

To examine whether the antimicrobial activity of PHACOS was due to the presence of thioester groups in the side chain of polymer, the antimicrobial activity of some fatty acids with structures similar to PHACOS monomers (octanoic, hexanoic and 6-acetylthiohexanoic acids) as well as of dimers/trimer was studied against *S. aureus*^{T} following microdilution CLSI (Clinical and Laboratory Standards Institute) standard protocol. To obtain the mix of dimers/trimers, PHO and PHACOS were subjected to enzymatic hydrolysis with PhaZGK13, *Pseudomonas fluorescens* GK13 extracellular mcl-PHA depolymerase as describes elsewhere (Martinez *et al*., 2012). The reaction products were identified and quantified by HPLC-MS. PHACOS hydrolyzate was

composed of 63% trimers (three monomers of OH-6ATH fused) and 30% of trimers containing mix of OH-C8 and OH-6ATH monomers. The rest (7%) was a mix of all monomers and dimers. The PHO hydrolyzate contained 66% of dimers (two OH-C8 monomers fused) and 26% of trimers (three OH-C8 monomers fused) and the rest was a mix of all OH-C8 and OH-C6 monomers and dimers.

Inhibitory effect of thioester group of polymer precursors and dimers/trimers suspension on bacterial growth was determined by monitoring MIC values. MIC of 6-acetylthiohexanoic acid (40 μM) was 15-fold lower than that of hexanoic acid (0.7 mM). Moreover, octanoic acid was less harmful to staphylococci (MIC = 3 mM) in comparison to hexanoic acid (data not shown). MIC of PHACOS derived hydroxycarboxylic acid suspension (composed of 7% dimers and 63% trimers) showed the same value as 6-acetylthiohexanoic acid (40 μM). These results taken together suggest that thioester group and possibly, also the chain length play a relevant role on the microbicidal activity of PHACOS.

2.5. Examination of possible toxic effect of mcl-PHA on mammalian cells

The viability and metabolic functions of mammalian cells in culture were measured using the MTT assay. This test is dependent on the intact activity of a mitochondrial enzyme, succinate dehydrogenase that may be impaired after exposure of cells to toxic species. No detectable mitochondrial damage was found for any of the tested surfaces. Cellular viability (CV) of macrophages in presence of extracts prepared from the polymers was around 100%, indicating the absence of their cytotoxic effect (Figure 27A, B). Similary, no changes in metabolic activity were detected among PET, PHO and PHACOS for fibroblasts (Figure 27C). Therefore, all tested polymers presented cytocompatibility levels equivalent to the PET control.

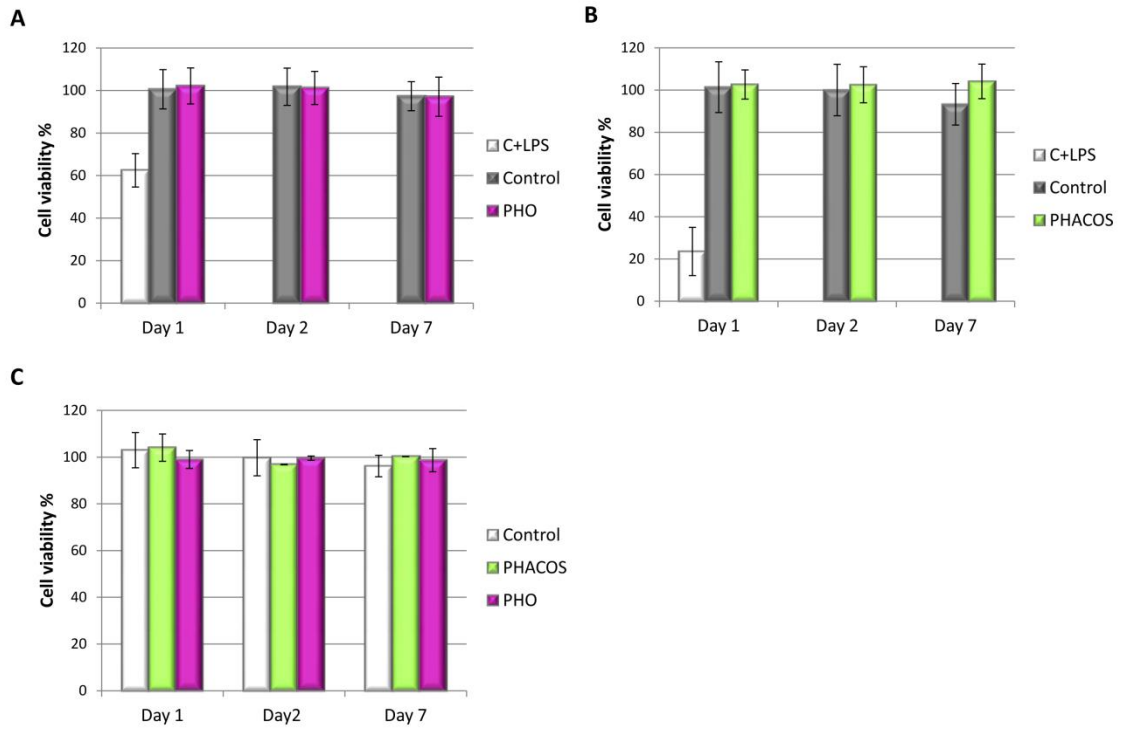

Figure 27. *In vitro* determination of PHACOS and PHO cytotoxicity by MTT assay. A,B Viability test performed on RAW 264.7 macrophages where as negative control extracts incubated with PET disks were used and as a positive control cells were treated with LPS to monitor the decrease in cell viability; C, MTT assay on BALB 3T3 fibroblasts where as a control extracts incubated with PET disks were used.

To measure the inflammatory activity of tested polymers, a nitric oxide (NO) inhibitory assay was employed. NO is a mediator and regulator in many pathological reactions, especially in acute inflammatory responses (Wang *et al*., 2008c). Pro-inflammatory agents, such as LPS, can significantly increase NO production in macrophages through activation of inducible nitric oxide synthase (iNOS) (Kojima *et al*., 2000). LPS-stimulated RAW 264.7 cells were used as a reference to evaluate the NO production of extracts coming from the polymeric samples. No significant differences in NO activity was measured for extracts from PHO and PHACOS (less than 10 mM NO) compared to the PET control, even thought the LPS positive control produced robust increase in NO activity (Figure 28A).

Cell methabolic activity and proliferation was monitored using Alamar Blue (AB) assay. AB is a redox indicator that changes colour with the chemical reduction of the culture medium, occurring as the result of cells growth and proliferation. This reagent can be withdrawn and replaced with fresh medium, for monitoring cell proliferation. It is soluble, stable in culture media and nontoxic for cells (Nakayama *et al*., 1997). The results of the assay demonstrated similar cell metabolic activity between PHACOS and control (Figure 28B). However, lower metabolic activity as well as lower adhesion rates and proliferation were observed on PHO compared to PHACOS and control samples. Figure 28B demonstrates twofold higher adhesion of cells on PHACOS then on PHO during first 10 days, possibly due to greater roughness of PHACOS as it is known that the cell behaviour depends on surface roughness and surface free energy (Wise *et al*., 1998).

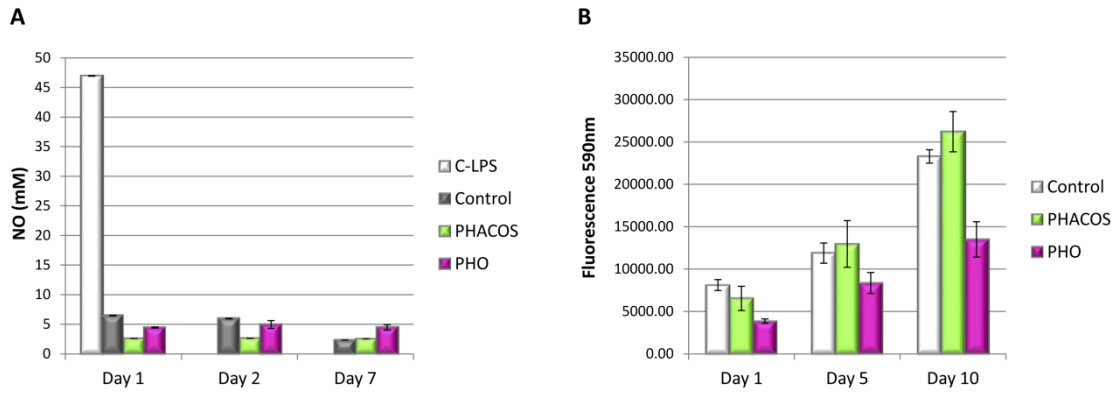

Figure 28. Determination of PHACOS and PHO *in vitro* immunocompatibility by Griess (A) and Alamar blue assays (B). A, Griess test for determination of PHACOS and PHO inflammatory effect on RAW 264.7 macrophages as a measurement of NO production in cells treated with lipopolysacharide-positive control (white bars), extracts incubated with PET-negative control (grey bars), extracts incubated with PHACOS (green bars) and extracts incubated with PHO (purple bars); B, Alamar blue assay for determination of BALB 3T3 fibroblasts *in vitro* proliferation on PHACOS (green bars) and PHO surfaces (purple bars), where white bars represent PET control.

Finally, we examined weather PHACOS promotes mammalian cell adhesion using ESEM. These studies provided additional information about fibroblasts adhesion, morphology and growth when being in direct contact with materials. PHACOS

supported equivalent levels of cell activity whereas on PHO cell activity was reduced, although fibroblasts showed no evidences of morphological alterations. Besides, poor cell adhesion was observed on PHO surfaces during first two days, the morphology and growth of fibroblasts was apparently normal after 7 day of incubation.

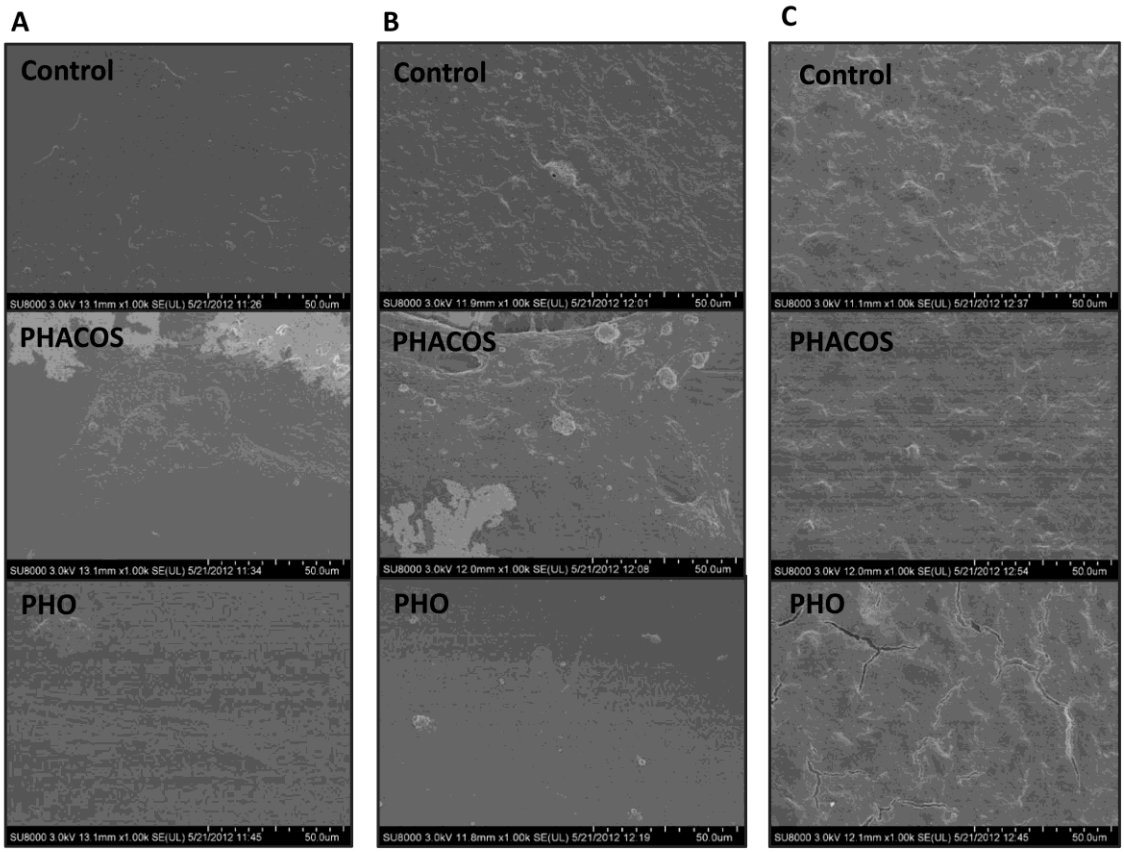

Figure 29. ESEM study of BALB 3T3 fibroblasts morphology and *in vitro* adhesion to PHACOS and PHO. A, Cell adhesion after 1 day incubation on PET, PHACOS and PHO disk (from top to bottom); B, Cell adhesion after 2 days incubation on PET, PHACOS and PHO disk (from top to bottom); C, Cell adhesion after 7 days incubation on PET, PHACOS and PHO disk (from top to bottom).

3. *In vivo* study of PHACOS antibacterial properties against *S. aureus*

The use of H-ICG to evaluate the production of reactive oxygen species (ROS) linked to implant-associated inflammation has recently been established (Selvam *et al*., 2011). The H-ICG was synthesized from commercially available ICG dye via a one-step reduction with sodium borohydride. This dye possess excellent stability to auto-oxidation, tunable emission wavelengths, and importantly, high selectivity and specificity as well as nanomolar sensitivity to ROS. In addition, it is small a molecule that can diffuse from the injection site or vascular bed into the tissue and cells directly associated with the implanted device. These attributes render H-ICG ideal probe for detecting implant-associated inflammation. Of note, ICG is a FDA-approved fluorophore that has found wide use as a noninvasive imaging agent. PET is used in many biomedical devices including sutures, vascular grafts, sewing cuffs for heart valves, and components for percutaneous access devices. Therefore, sterile, endotoxin-free PET disks (6 mm diameter), and PHO and PHACOS coated PET disks were implanted subcutaneously in the back of 6-8 weeks old male BALB/c mice (Jackson Laboratories) anesthetized by isofluorane. A single 1-cm incision was made on the dorsum proximal to the spine, and a subcutaneous pocket laterally spanning the dorsum was created. Sterile disks (two per subject on either side of the spine) were implanted, and the incision was closed using sterile wound clips.

To monitor extracellular ROS associated with inflammatory responses to subcutaneously implanted biomaterials in mice a single local injection of H-ICG dye was applied at the vicinity of the surgery site/implant of anesthetized mice at defined time points. Animals were imaged 30 min after injection via an IVIS fluorescence imaging system. To account for surgery-associated trauma/inflammation, mice undergoing the same surgical procedure, but receiving no PET implants were used as sham controls, whereas some mice received dye injection but no surgery, dye-only control. As expected, mice receiving biomaterial implants exhibited increases in fluorescence signal over time that were higher than the dye-only control (Figure 30, 31). Notably, no significant differences in fluorescence signals were observed among

sterile PHACOS and PHO implants and the sham control during 14 days experiment. This result indicated minimal inflammation associated with tested polymers.

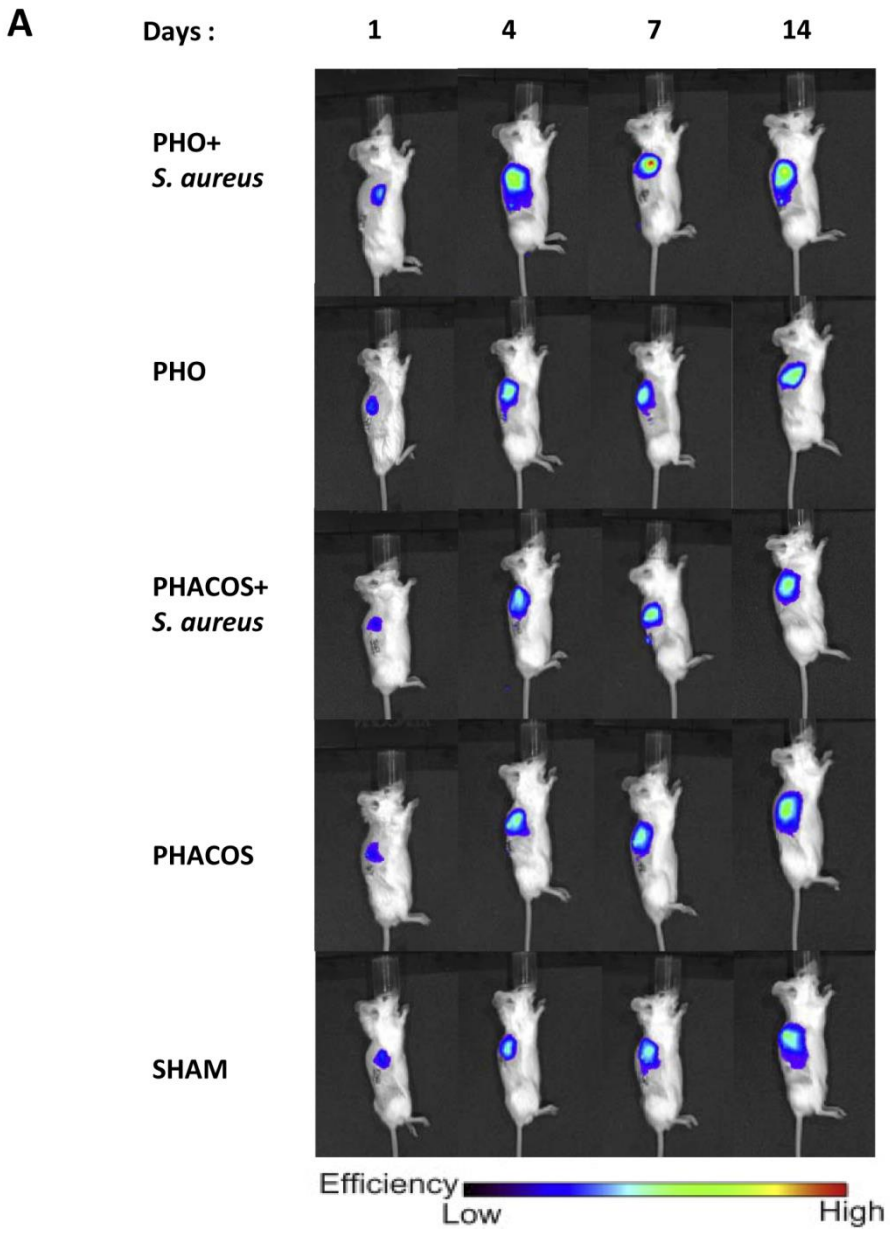

Figure 30. *In vivo* biocompatibility ROS imaging of PHACOS and PHO implant associated inflammation after subcutaneous administration of H-ICG. Bioimaging data of animal scanned in an IVIS® imaging system.

We also examined whether PHACOS exhibits antimicrobial properties *in vivo*. With that aim, six animal groups were monitored: (i) dye-only control group (shaved mice, no surgical procedure); (ii) sham group (mice undergoing surgical procedure, but not receiving implant); (iii) mice receiving sterile PHO disk; (iv) mice receiving sterile PHACOS implant; (v) mice receiving PHO implant pre-colonized with *S. aureus*^{T} and (vi) mice receiving PHACOS implant pre-colonized with *S. aureus*^{T}. After a short incubation with *S. aureus*^{T}, biomaterial disks (PHACOS and PHO) were implanted subcutaneously as described above. Implant-associated inflammation was monitored for 14 days.

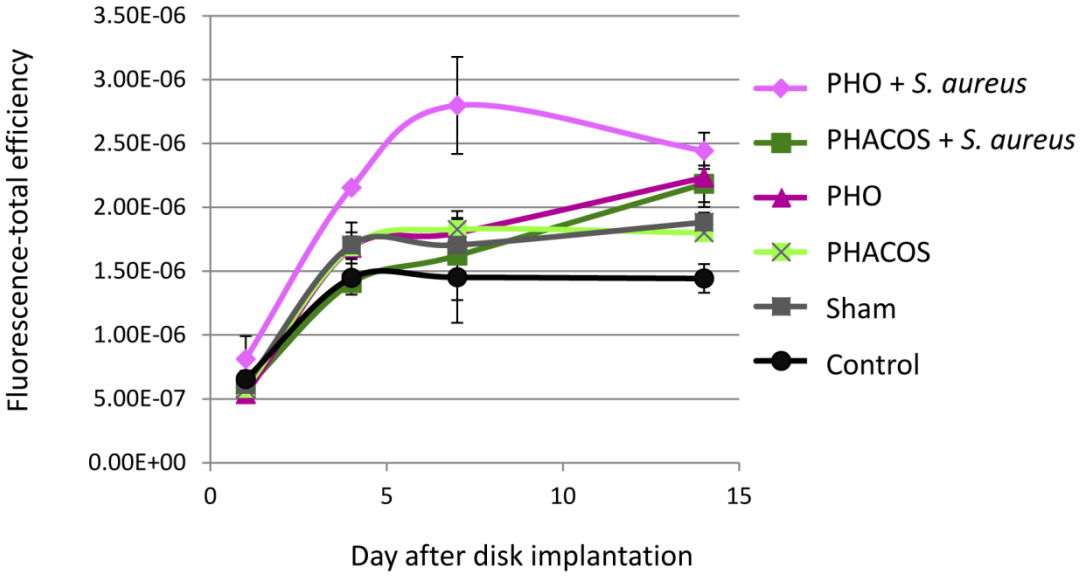

Figure 31. *In vivo* biocompatibility ROS imaging of PHACOS and PHO implant associated inflamation after subcutaneous administration of H-ICG. Quantification of ROS fluorescence data from mice with PHACOS and PHO implants incubated with *S. aureus* and sterile PHACOS and PHO implants.

Significantly higher ROS signals were observed for PHO disks incubated with bacteria compared to sterile PHO disks (Figure 30, 31). These increased levels reflect the elevated inflammatory response associated with the infected implant. Remarkably, PHACOS disks incubated with bacteria exhibited significantly lower ROS signal compared to bacteria-incubated PHO, and the ROS levels for bacteria-incubated PHACOS were not different from the levels for sterile PHACOS implants. Taken together, these results demonstrate that PHACOS effectively controls biomaterial-

associated infections by *S. aureus* in an *in vivo* model of device-related infection. At 14 day post-implantation, inflammation to bacteria-incubated PHO and PHACOS disks have become similar, most likely due to the fact that animals were able to eliminate 10^3 CFU/cm^2 (see above; Figure 41).

Subsequently, mice were sacrificed and the disks were retrieved along with intact implant-associated tissues to avoid disrupting the cell-material interface. Explants were embedded in optimal cutting temperature compound (OCT,Tissue-Tek), freezed and cryosectioned at 10 µm. Using immunohistochemistry, we analyzed macrophage (CD68+, green) and neutrophil (NIMP-R14+, green) recruitment to the implant. Firstly, fresh-frozen cryostat sections were treated with hydro-Cy5 (H-Cy5) for intracellular ROS staining, after which the sections were incubated with antibodyes against macrophages (CD68, green) (Figure 32A) or neutrophils (NIMP-R14, green) (Figure 32B). Additionally, total cell number (DAPI stained, blue) was compared with the number of inflammatory cells (Figure 32).

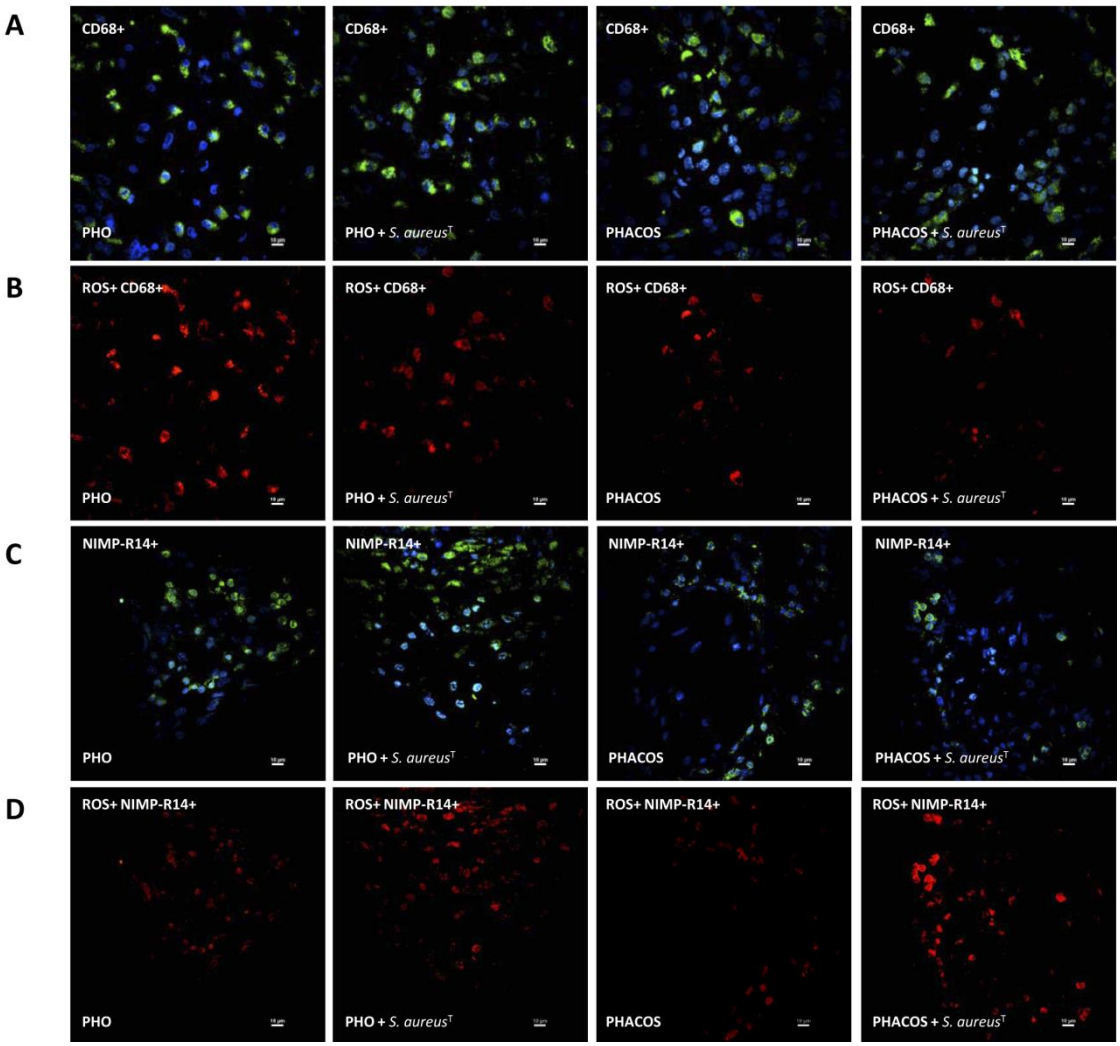

Figure 32. Immunohistochemical staining for macrophages (A,B) and neutrophils (C,D) in implant-associated inflammation and intracellular ROS in 14-day implants. A, Representative images of macrophages (CD68+, green) and nuclei (DAPI, blue) co-localization in sterile PHO, *S. aureus*^{T} pre-colonized PHO, sterile PHACOS, *S. aureus*^{T} pre-colonized PHACOS implants (from left to right); B, Intracellular ROS (H-Cy5+, red) co-localizing with macrophages in sterile PHO, *S. aureus*^{T} pre-colonized PHO, sterile PHACOS, *S. aureus*^{T} pre-colonized PHACOS implants (from left to right); C, Neutrophils (NIMP-R14+, green) and nuclei (DAPI, blue) co-localization in sterile PHO, *S. aureus*^{T} pre-colonized PHO, sterile PHACOS, *S. aureus*^{T} pre-colonized PHACOS implants (from left to right); D, Intracellular ROS (H-Cy5+, red) co-localizing with neutrophils in sterile PHO, *S. aureus*^{T} pre-colonized PHO, sterile PHACOS, *S. aureus*^{T} pre-colonized PHACOS implants (from left to right).

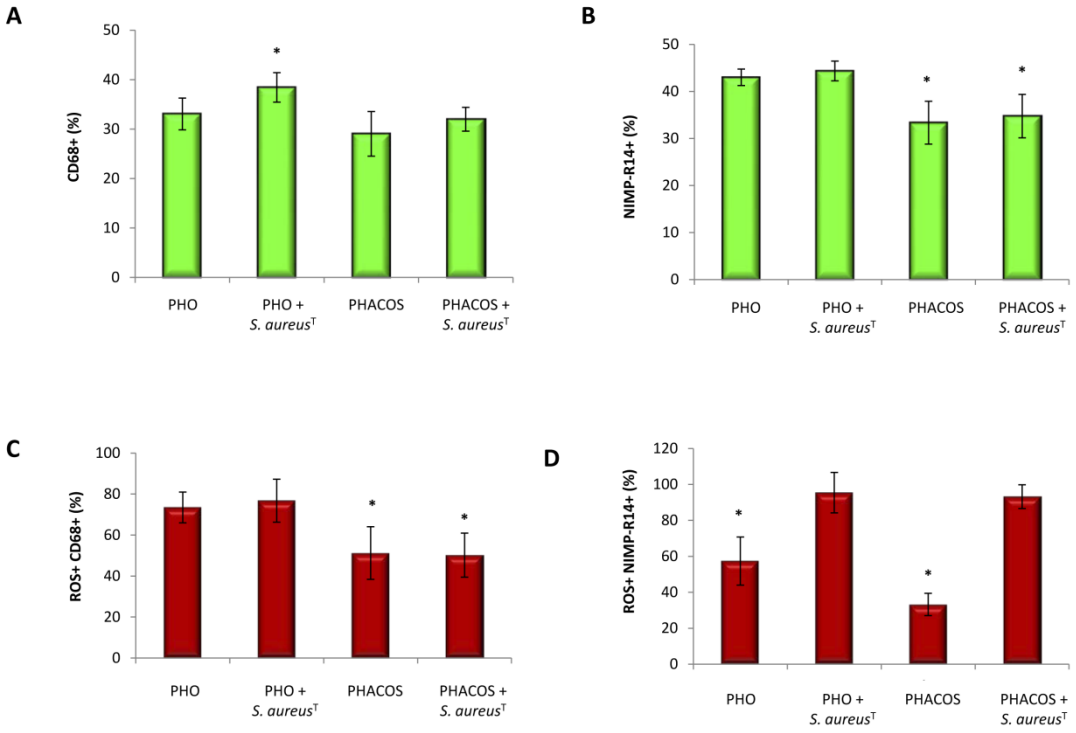

Figure 33. Immunohistochemical staining for macrophages and neutrophils in implant-associated inflammation. A, Quantification of CD68+ macrophages; B, Quantification of NIMP-R14 neutrophils; C, Quantification of ROS+ cells stained positive for CD68+; D, Quantification of ROS+ cells stained positive for NIMP-R14+.

Higher recruitment of inflammatory cells was found to the vicinity of the sterile PHO implants (76% of total cell number) compared with sterile PHACOS implants (62% of total cell number) at 14 days post-implantation. Moreover, when the implants were pre-colonized with *S. aureus*^{T}, the influx of inflammatory cells was higher in the vicinity of the PHO implant (82% of total cell number) than around PHACOS implant (65% of total cell number) as shown in Figures 32 and 33. It is worth noting that there was a statistically significant difference ($P < 0.05$) between macrophage recruitment to *S. aureus*^{T} pre-colonized PHO (38% macrophages) and *S. aureus*^{T} pre-colonized PHACOS (31% macrophages) implant (for details see Materials and methods section 16). Remarkably, there was no statistically significant difference ($P = 0.05$) in macrophage recruitment between *S. aureus*^{T} pre-colonized PHACOS (31% macrophages) and sterile PHACOS implants (29% macrophages). Moreover, significant differences ($P < 0.05$) in

neutrophil recruitment to sterile PHO (43% neutrophils) and sterile PHACOS (33% neutrophils) implants, as well as between *S. aureus*^{T} pre-colonized PHO (44% neutrophils) and *S. aureus*^{T} pre-colonized PHACOS implants (34% neutrophils) were observed. Taken together, obtained results indicate mild inflammatory response to sterile PHACOS implant and its antimicrobial effectiveness *in vivo*.

In addition, we co-stained for intracellular ROS activity using hydro-Cy5 (H-Cy5) as previously described (Lin *et al*., 2009). Importantly, co-staining analysis for inflammatory cell markers and ROS activity demonstrated that neutrophils and macrophages are primarily responsible for the ROS activity associated with the implant (Figure 33). As expected, neutrophils are mainly responsible for ROS activity, when the implants are pre-colonized with *S. aureus*^{T}.

3.1. *In vitro* degradation of mcl-PHAs

In vitro degradation of PHO and PHACOS polymers was analyzed using gravimetry assay. The polymers were incubated in PBS and weighed dry during 32 days. According to the obtained results no significant mass change was observed (Table 7). Consequently, applying this method we could not detect any sign of polymer degradation. In addition, degradation of polymers was examined by RMN. However, variations between control polymer (polymer that was not incubated in PBS) and polymer incubated in PBS were not observed (data not shown).

Table 7. *In vitro* monitoring of PHACOS and PHO degradation

Incubation period	PHO (mg)	PHACOS (mg)
6 h	0.0281±0.0014	0.0388±0.0020
24 h	0.0281±0.0021	0.0383±0.0011
7 days	0.0283±0.0016	0.0395±0.0014
15 days	0.0281±0.0018	0.0391±0.0012
32 days	0.0280±0.0014	0.0385±0.0016

4. Real-time non invasive *in vivo* monitoring of mcl-PHA implant associated infection

On time detection and appropriate treatment of implant associated infection is of great importance, taking into account that each year from 150 million implanted intravascular devices in the United States (Mermel *et al*., 2009), 250 000 result in bloodstream infections (O'Grady *et al*., 2011). *S. aureus* is one of the most common pathogens associated with these cases. Herein we describe a strategy for non invasive real-time monitoring of bacterial mcl-PHA implant infection using bioluminescent *S. aureus* strains. Furthermore, we develop a new method for detecting early stages of bacterial infection and quantification of pathogen number correlating infection and the intensity of infection induced inflammatory response. To that end, the sensitivity of H-ICG imaging probes was tested in terms of its accuracy of detection of increasing inflammation induced using higher bacterial inoculums to pre-colonize implants.

4.1. *In vivo* tracking of bioluminescent *S. aureus* on PHO implants

To assess the feasibility of using bioluminescence as a quantitative indicator of bacterial number, *in vivo* studies using mice animal model were performed. Bioluminescent counts were correlated with the number of viable bacteria used to pre-colonize PHO disks (see Material and methods section 16 for details). PHO disks were inoculated with one of three different bioluminescent *S. aureus* strains, which contained *lux* genes in: (i) an antibiotic selection plasmid (pAmiSPA or pAmiBLAZ) and (ii) the bacterial chromosome (Xen29). The total bioluminescent counts from the infected sites were quantified by Living Image software during 7 days.

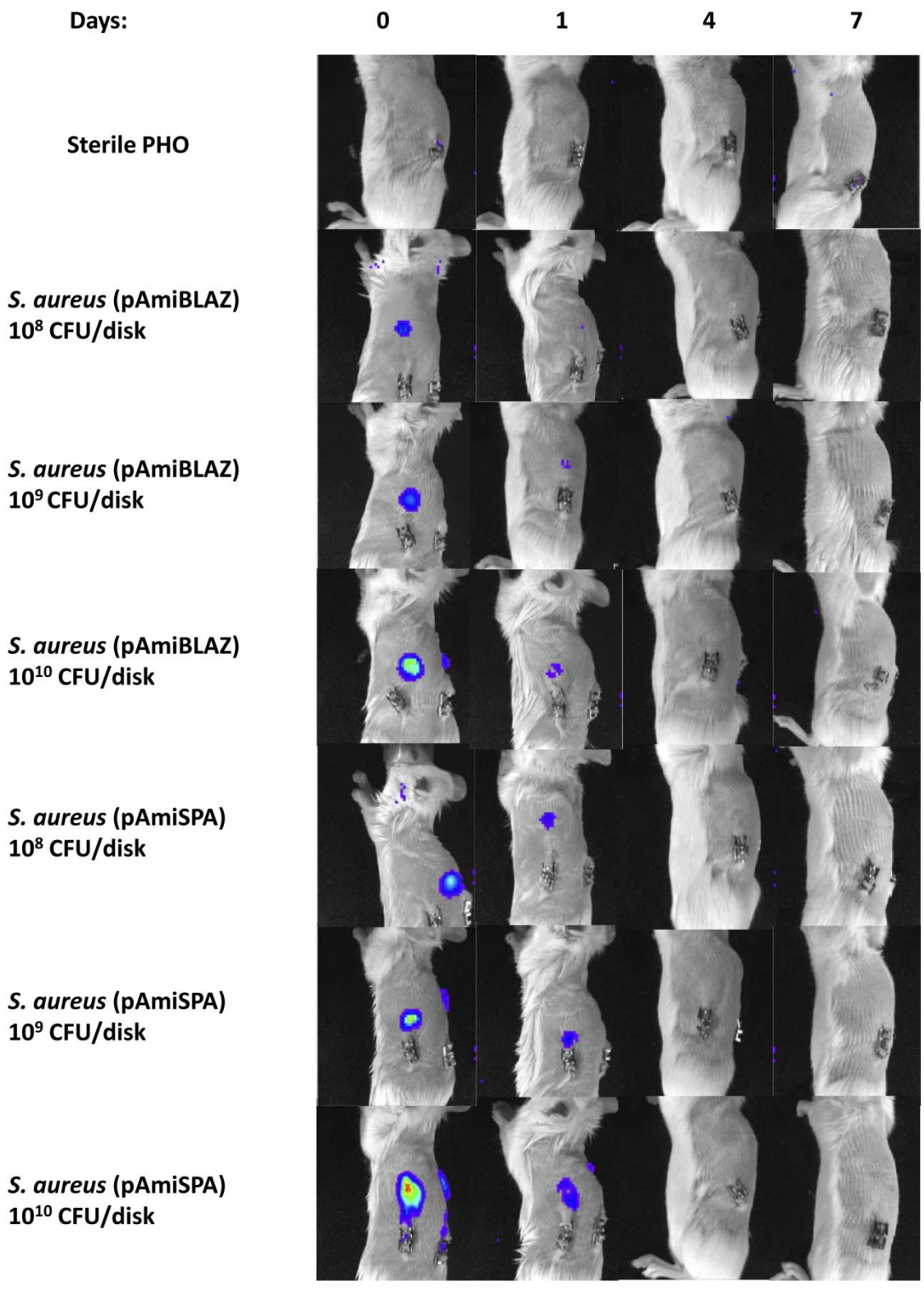

Figure 34. *In vivo* imaging of PHO implant associated infection by using *S. aureus* luminescent strains. Bioimaging data of animal scanned in an IVIS® imaging system.

Bioluminescent signal of *S. aureus* (pAmiSPA) and *S. aureus* (pAmiBLAZ) strains was only detected when the disks were pre-colonized with high bacterial inoculums (10^9-10^{10} CFU/disk), while bioluminescence of lower inocula was unmeasurable. The two inocula 10^9 and 10^{10} CFU/disk of both strains showed concentration-dependant increment in bioluminescent signals (Figure 34) and peaked 1 h post-implantation. Over next 4 days post-implantation bioluminescent signal decreased and by day 7 could not be detected (Figure 34), most likely due to the decreased metabolic activity of bacterial population. Moreover, it was observed that during exponential phase of bacterial growth, the bioluminescence output was proportional to the bacterial biomass. However, once the cultures reached stationary phase, the bioluminescence no longer correlated with the number of cells (data not shown).

In addition, we tested other bacterial strain *S. aureus* Xen29 having *lux* operon stably integrated in the chromosome that allowed non invasive monitoring of the progression of infection in the experimental model using lower bacterial inoculums (10^5-10^6 CFU/disk). Following the implantation, bioluminescence of bacteria pre-colonized disks increased exponentially over 24 h and peaked on day 1 post-implantation (approximately 2.6 x 10^4 total counts/disk for bacterial inoculum 10^6 CFU/disk and 1.2 x 10^4 total counts/disk for bacterial inoculum 10^5 CFU/disk) as demonstrated in Figure 35. However, on day 4 bioluminescent signal decreased significantly (1 x 10^4 total counts/disk for inoculum 10^6 CFU/disk), still being higher than the one observed on day 4 for 10^{10} CFU/disk *S. aureus* (pAmiSPA) (6 x 10^3 total counts/disk) (Figure 34, 35). By day 7, bioluminescence could not be detected in any of the tested strains. The number of CFU recovered from disks was counted following the 7-day imaging. It was observed that independently on the bacterial inoculums used to pre-colonize implants, mice were able to eliminate 10^3 CFU (see below; Figure 38).

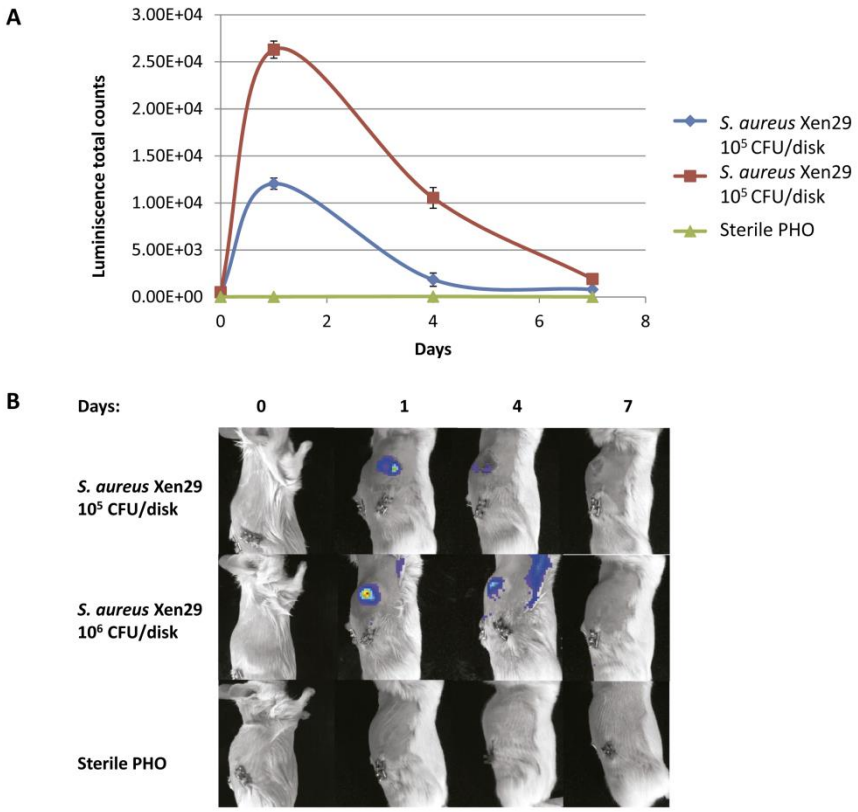

Figure 35. *In vivo* imaging of PHO implant associated infection using *S. aureus* Xen29 luminescent strain. A, Monitoring of luminiscent signal of *S. aureus* Xen29 in PHO implants pre-colonized with different bacterial inocula; B, Bioimaging data of animal scanned in an IVIS® imaging system.

4.2. Precise monitoring of biomaterial-associated inflammation by fluorescence imaging

The inflammation is a key determinant of the infection presence. Thus, potential difference in the intensity of inflammation induced by infection with different bacterial inoculums was evaluated. Inflammation levels associated with disks pre-colonized with different *S. aureus* (pAmiSPA) and *S. aureus* (pAmiBLAZ) inoculums were recorded on day 7 post-implantation using H-ICG sensor (Figure 36).

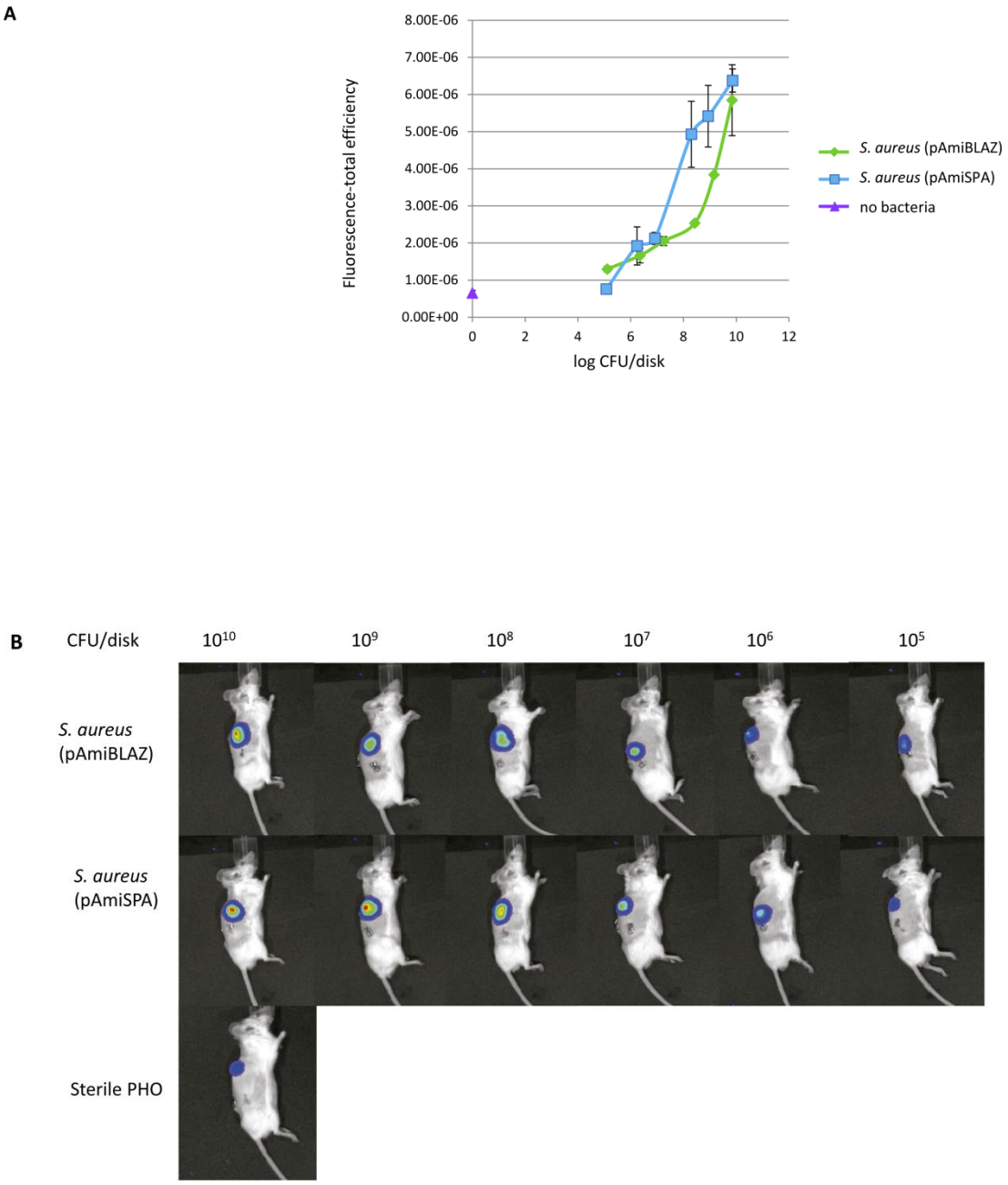

Figure 36. *In vivo* ROS imaging of implant associated inflammation using H-ICG NIFR sensor 7 days post-implantation of PHO implants pre-colonized with *S. aureus* (pAmiSPA) and *S. aureus* (pAmiBLAZ). A, Green line, inflammation provoked by implant pre-colonized with different CFU of *S. aureus* (pAmiBLAZ); blue line, inflammation provoked by implant pre-colonized with different CFU of *S. aureus* (pAmiSPA); purple, inflammation provoked by steril PHO implant; B, Bioimaging data of animal scanned in an IVIS® imaging system.

Fluorescent signal was found to closely correlate with bacterial inoculums. Therefore, we conclude that this sensors posses enough sensitivity to detect difference in inflammation induced by different bacterial inoculums.

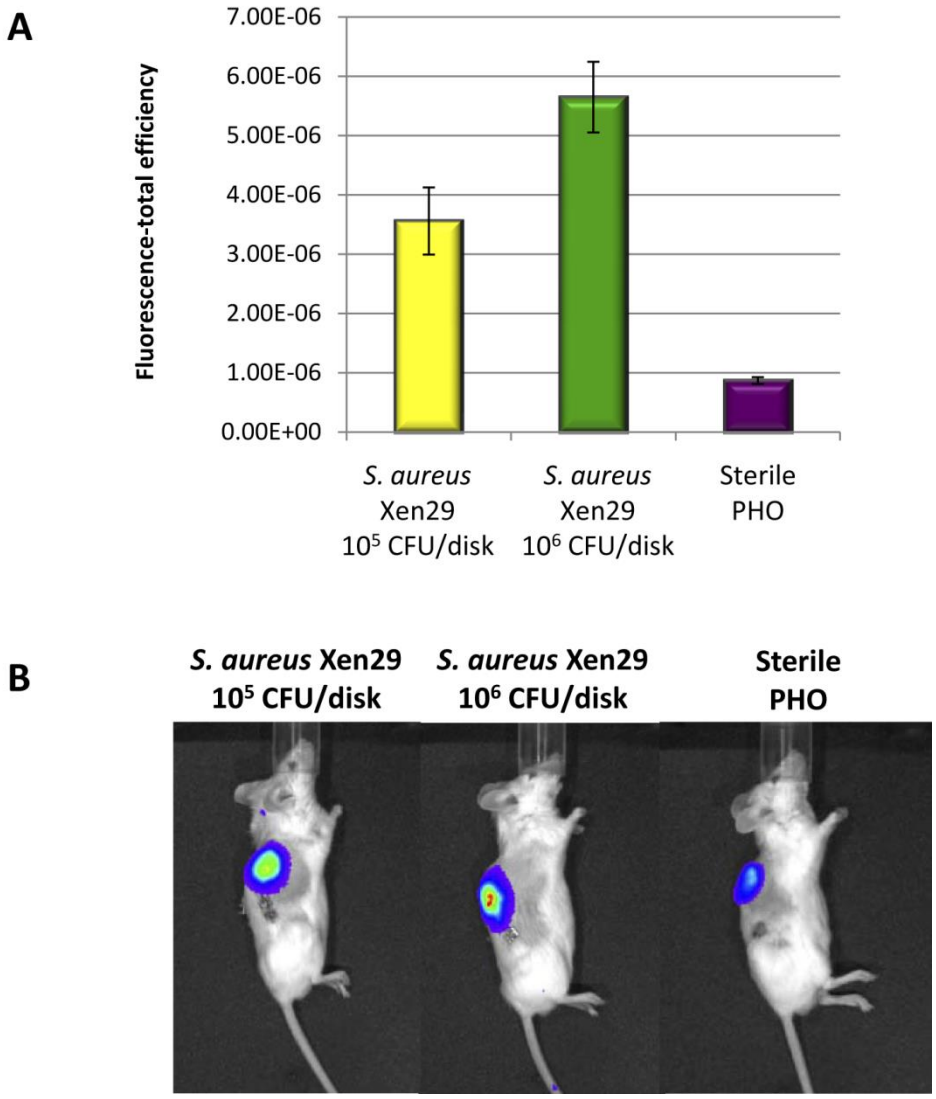

Figure 37. *In vivo* ROS imaging of PHO implant associated inflammation using H-ICG NIFR sensor after implant infection with *S. aureus* Xen29. A, Quantification of ROS fluorescence data from mice with PHO implants incubated with *S. aureus* Xen29 and sterile PHO implants; B, Bioimaging data of animal scanned in an IVIS® imaging system.

Additionaly, we monitored inflammation induced by infection provoked by implantation of PHO disks pre-colonized with *S. aureus* Xen29 (10^5 and 10^6 CFU/disk). In perfect correlation with results obtained for *S. aureus* (pAmiSPA) and *S. aureus*

(pAmiBLAZ), it was demonstrated that when implant is infected with higher *S. aureus* Xen29 inoculum, stronger inflammation is induced (Figure 37).

Following imaging, mice were sacrificed and the disks were retrieved along with implant-associated tissues. The CFU recovered from explanted disks were analyzed. We observed that the starting density of bacterial inoculums did not influence mice ability to eliminate bacteria. In all examinated cases the reduction of bacterial number was aproximately 10^3 CFU (Figure 38). Although, we demonstrated that *S. aureus* strains are able to form biofilm *in vitro* on both surfaces, PET and PHO (see section 2.1; Figure 23), this experiment provide evidence that using this *in vivo* infection model, stable infection could not be achieved.

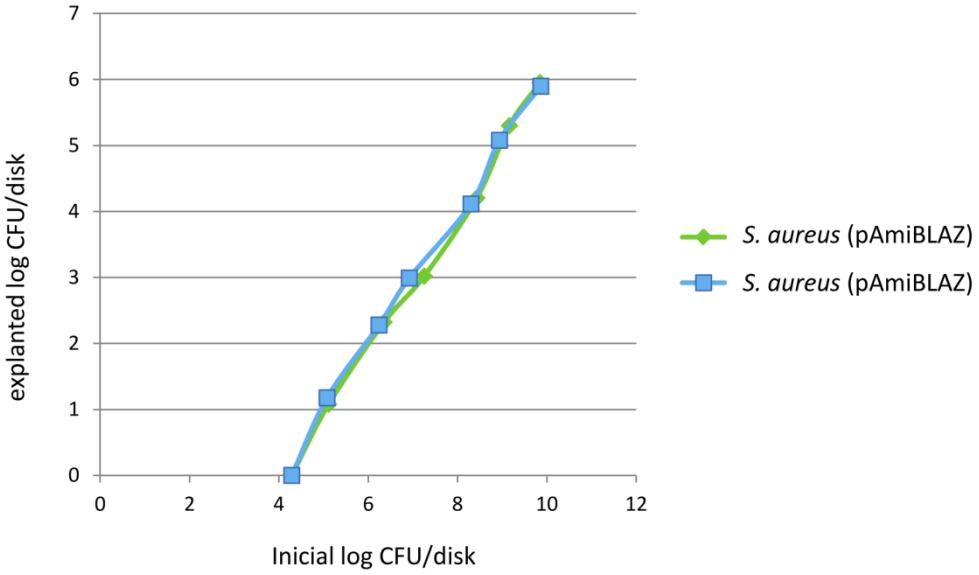

Figure 38. Infection stability analysis. Comparison of inicial CFU and CFU after PHO disk explantation. Green line, *S. aureus* (pAmiBLAZ) strain; blue line, *S. aureus* (pAmiSPA).

By means of immunohistochemistry, we analyzed macrophage (CD68) and neutrophil (NIMP-R14) recruitment to the implant at day 7 post-implantation (Figure 39). It was observed that as bacterial inoculums used to pre-colonize PHO implants was higher, the influx of inflammatory cells was higher being 76% for sterile implant and growing exponentially to 100% for implant pre-colonized with 10^7 CFU/disk (Figure 39). Moreover, the number of both macrophages and neutrophils was increasing in the

vincinity of PHO implant with the increasing number of *S. aureus* Xen29 cells used to pre-colonize implants.

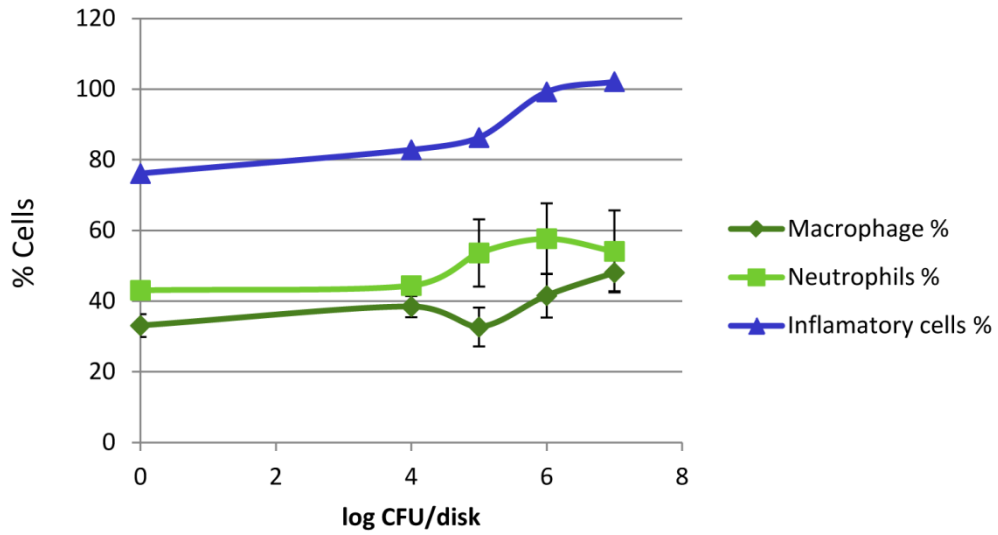

Figure 39. Immunohistochemical staining for macrophages and neutrophils in implant-associated inflammation. Quantification of CD68+, NIMP-R14 and total number of inflammatory cells stained with DAPI.

Apart for inflammatory cell staining, samples were stained for bacteria as well using the same protocol. *S. aureus* immunohistochemical assays can be of great value, particularly for cases where rapid and accurate diagnostics is required. Grape-like clustering of *S. aureus* common to *Staphylococcus* species was spotted in all analyzed samples (Figure 40). Bacterial cells were observed only in the vicinity on contaminated implants, thus showing the pattern of localized infection (data not shown).

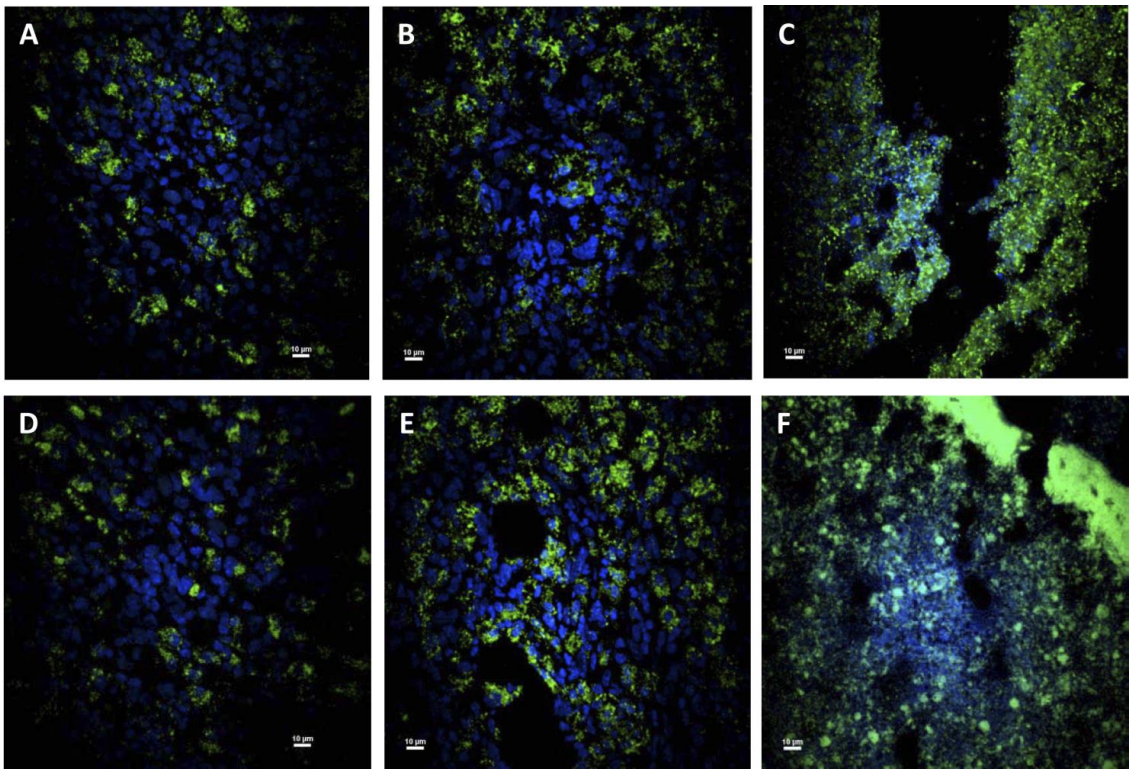

Figure 40. Immunohistochemical staining for *S. aureus* (pAmiBLAZ) (A-C) and *S. aureus* (pAmiSPA) (D-E) in PHO implant associated infection. A,D 10^8 CFU/implant; B,E 10^9 CFU/implant; C,F 10^{10} CFU/implant. *S. aureus* shown in green, mice cells surrounfing implant in blue.

The initial signs of implant surrounding tissue damage became visible with increasing number of bacteria used to pre-colonize disks. Necrosis was evident when inoculums of 10^{10} CFU/disk were used to pre-colonize implants. DAPI stained nuclei lost sharp borders and finally were completely destroyed (Figure 40). This phenomenon was observed only in the near vicinity of contaminated implant, whereas the cells of tissue located farther from the implant did not show signs of cell death (data not shown).

V. Discussion

Microbial polyesters play an important role in the development of second generation biomaterials, especially for biomedical applications. Various modification techniques were developed in this work to improve biopolymer properties. Herein, we describe different strategies focused on designing new PHA by introducing specific modifications that confer novel properties to the polymer (Figure 41).

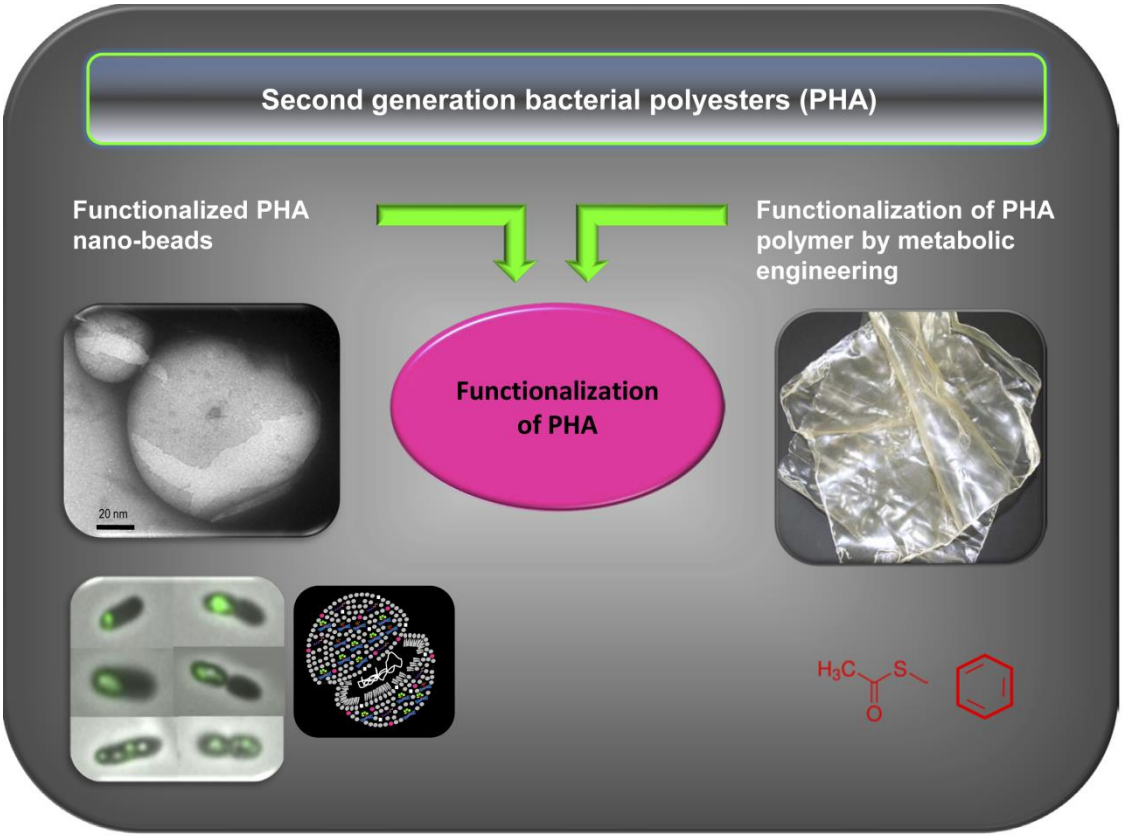

Figure 41. Strategies for added-value PHA production. Two different approaches were applied, *in vivo* functionalization of PHA nano-beads using phasins for recombinant protein anchoring to the PHA granule and metabolic engineering to modify the PHA chemical structure incorporating functional group in the side chain of the polymer.

1. *In vivo* functionalization of PHA nano-beads

One of the chosen approaches consists of *in vivo* bacterial production of tailor-made functionalized nano-beads, where proteins attached to the natural PHA granule have been engineered to display fusion proteins of interest (Figure 41). To refine the system, we tried to solve the puzzle of how functionally diverse, or even a multifunctional set of phasins, should be combined to generate an optimal yield of *in vivo* protein immobilization onto granule surface in a coherent cell phenotype of *P. putida* KT2442. The modules of *P. putida* phasin proteins were proved to perform different functions, supported by their particular structure, distributed in separate domains (Figure 5).

1.1. Nucleoid-associated PhaF phasin drives intracellular location and segregation of polyhydroxyalkanoate granules in *Pseudomonas putida* KT2442

Two models of PHB granule formation have been described in bacteria, the micelle model and the budding model, both accounting for the stabilized location of the synthase and phasin on the granule surface (revised in Grage *et al*., 2009). Nevertheless, the role of phasins in granules formation is still unknown (Rehm, 2006). In the micelle model, a self-assembly process is initiated resulting in the formation of insoluble cytoplasmic inclusions with a phospholipid monolayer containing covalently attached polyester synthases at the surface. In the budding model, the hydrophobic synthase binds to the inner face of the plasma membrane, and buds from this membrane, leading to a granule surface covered with a lipid monolayer and phasins. However, TEM studies of granule formation and degradation in *C. necator* H16 revealed dark-stained elements ringed by small granules at early stages of PHB production. These structures named “mediation elements” were located near the center of cells or along a longitudinal strip in the cell center (Tian *et al*., 2005). These results were at odds with the micelle and membrane budding models, but led to an alternative model for granule formation, in which granules are localized and the new

"mediation elements" function as scaffolds for the granule initiation sites. The fate of granules during cell division, that is, whether they are equally distributed between daughter cells, is not known (Tian *et al*., 2005).

We have explored the physiological role of the PhaF and PhaI phasins from the prototype microorganism *P. putida* KT2442. One of the peculiarities of the PhaF phasin is its modular organization in a PHA granule binding domain (located at the N-terminus) and an AKP-rich domain (located at the C-terminus) (Figure 5). In fact, we had previously demonstrated the ability of PhaF from *P. putida* GPo1 to bind PHA granule (phasin-like activity), and as a transcriptional regulator, suggesting putative DNA binding activity (Prieto *et al.,* 1999; Moldes *et al.,* 2004). This C-terminal domain from the PhaF protein with a DNA-binding histone-like function is unique among phasins. In this respect, the phasins identified from *C. necator* H16 (PhaP1, PhaP2, PhaP3 and PhaP4) display an alanine-rich C-terminal region showing a very high isoelectric point (Neumann *et al.*, 2008). Nevertheless, further investigations are needed to exclude that this positive charge might participate in the interaction with mediation elements or that the latter might simply be the nucleoid of the cell.

This work demonstrates that PhaF plays a crucial role in granule localization and distribution, since the lack of this protein unbalances granule segregation during cell division (see Annex 2, Figure 13). A similar system of needle array localization of organelles inside prokaryotic cells has been observed for the intracellular magnetosomes from *Magnetospirilum gryphiswaldense* (Komeili *et al.*, 2006). They are assembled in a regular chain in order to achieve the maximum magnetic moment, against the physical tendency of magnetosome agglomeration. In the aforementioned system, the protein responsible for magnetosome alignment is MamJ which has a high content of acidic amino acids and a repeated domain structure that appears to interact with a linear cytoskeleton-like structure composed of MamK (actin-like protein). This directs the assembly and localization of the prokaryotic organelles (Scheffel *et al.*, 2006). *P. putida* KT2442 (Nelson *et al.*, 2002) posses members of all cytoskeletal systems described in bacteria (revised in Gitai *et al.*, 2005 and Gerdes *et al*., 2010) like the tubulin homologous FtsZ (annotated as PP1342 in the chromosome); ParAB (PP_0001-2) and MinCDE (PP_1732-34) systems, where ParA and MinD are similar

variant P loop ATPases, which form cytoskeletal-like filaments on DNA and membranes, respectively, to solve different problems (DNA segregation and septum placement) by analogous molecular mechanisms; Actin homologue MreB (PP_0934), similar to the actin-like protein MamK, which forms a helix essential for maintenance of cell shape, and has recently been hypothesized to act as a scaffold for transporting proteins to different locations throughout the bacterial cell (Kimberly *et al.*, 2010). Our work demonstrated PhaF to be a central player in the machinery, controlling PHA granule segregation and localization in the cell. Moreover, whether or not *P. putida* KT2442 cytoeskeletal proteins facilitate the needle array structure, by direct or indirect interaction with PhaF, is still an open question and currently the precise mechanisms by which PHA granules are positioned by PhaF are unknown. Since PhaF shows a unique ability to bind at least two ligands (the PHA granules and the nucleoid) our work supports the idea that the PhaF function localizing and segregating the PHA granules implies a new mechanisms, whish is different to that described for magnetosomes (MamK/MamJ) or DNA segregation in bacteria (ParA-like mechanism). Given the unspecific DNA binding abilities of the C-terminal part of PhaF (see Annex 2), we cannot discount the possibility that bacterial chromosome may play a role as granule carrier during the division process. In this respect, previous studies have determined the cellular position of different chromosomal sites, demonstrating that they were positioned along the long axis of the cell in a linearly ordered fashion from the origin to the terminus (Teleman *et al.*, 1998; Niki *et al.*, 2000; Viollier *et al.*, 2004).

The unspecific PhaF-DNA interaction validates the classification of this phasin as a histone-like protein and raises further questions about the physiological roles of PhaF in *P. putida*. Eukaryotic H1 histones are also called linker histones because they are chromatin-associated proteins that bind to the nucleosome exterior and dramatically stabilize the highly condensed states of chromatin fibers (Zlatanova *et al.*, 2000). In eukaryotic organisms, there is evidence that linker histones are also involved in transcriptional regulation by determining the accessibility of nucleosomal DNA to the transcriptional machinery (Zlatanova *et al.*, 2000). Furthermore, it has been demonstrated that histones of the H1 family provide the DNA compaction required by

the changing physiological needs of the cell during the different cell cycle stages (Kasinsky *et al.*, 2001).

Examples of bi-functional proteins containing the AKP-rich domain are found in eukaryotic organisms, such as *Drosophila melanogaster* ribosomal proteins L22 and L23a (Koyama *et al.*, 1999), and in the prokaryotic organisms *Pseudomonas aeruginosa* AlgP (Deretic and Konyecsni, 1990) and *Stenotrophomonas* sp. putative DnaK suppressor. It is also worth mentioning the translation factor IF-2 in Actinobacteria, which contains an AKP-rich region in its N-terminal domain involved in translation initiation and ribosome binding (Caserta *et al.*, 2006). Also, the Hc1 and Hc2 proteins from *Chlamydia trachomatis* play a role in chromosome condensation, regulating the stage specific differentiation during the life cycle (Kaul *et al.*, 1996). Moreover, BpH1 and BpH2 proteins from *Bordetella pertussis,* are known to condense DNA, protect it from digestion with DNaseI *in vitro* and could be involved in transcriptional regulation (Goyard, 1996).

1.2. Swapping phasin modules to optimize the *in vivo* immobilization of proteins to mcl-PHA granules in *P. putida*

As previously mentioned, PhaF phasin is composed of N- and C-terminal domains (see above). These two structuraly and functionally different modules are linked via a leucine zipper motif, also present in PhaI phasin. The leucine zipper motif is tought to be a protein-protein interface. Moreover, it has been hypothesized that many of the biological properties of phasin proteins depend on multimerization via this coiled-coil region, which provides a highly specific, physiologically relevant protein-protein interaction (Maestro *et al*., 2013).

The function of PhaI phasin, and its possibile substitution by PhaF phasin or BioF tag have been investigated in this study. We illustrate the utility of the PhaF/PhaI structure redundancy, being autonomous modular units working in harmony. Both C- and N-terminal PhaF phasin modules are revealed to be essential for optimal PHA biosynthesis and accumulation in *P. putida* KT2442. When one of the modules is

missing, PHA production decreases. Moreover, when a strain lacks both phasins, the PHA production falls to 7% of CDW, suggesting their cooperative functioning. However, BioF tag or its fusion derivatives can replace PhaI role in *P. putida* in terms of PHA production. Nevertheless, the phenotype of the phasin mutant strains lacking C-terminal domain of PhaF differs to that of the wild-type strain in terms of granule distribution, showing population heterogeneity. PhaF N- and C-terminal domains were tracked *in vivo* by monitoring their fusions with the GFP reporter. As expected, GFP-CPhaF co-localized with nucleoid, independently of the host strain and the presence or absence of PHA granules, whereas N-terminal co-localized with PHA granules in all analyzed *P. putida* strains. Moreover, in the absence of PHA granules, BioF forms intracellular inclusions, mainly at the cell poles (Figure 19E, F), which could be explained by the existence of the short leucine zipper involved in protein oligomerization, as predicted in the structural, three-dimensional model. The phenotype of the wild-type strain is recovered in the KT42I-BGF strain, which produces BioF-GFP fusion and PhaF at low dosage (Figure 17B, 18B, 19H), definitively demonstrating the essential role of the C-terminal domain of PhaF protein in granule segregation and the swappable nature of PhaI and BioF PHA binding modules.

It was previously demonstrated that phasin binding prevents unspecific attachment of other proteins, unrelated to the PHA metabolism, to the granules surface, and limits the space for recombinant proteins to anchore (Neumann *et al*., 2008). We confirm that the absence of a natural PhaI phasin favors binding of the fusion protein to the granule surface. In the absence of wild-type phasins, a higher number of recombinant tagged protein molecules anchored to the granule surface (Table 5). This could be explained by the lack of space on the surface of wild-type PHA granules coated with PhaI/PhaF N-terminal phasin modules. In fact, the protein immobilization per gram of PHA in both strains KT42I-BG and KT42I-BGF were, similarly, more than 6-folds higher than that of the wild-type strain. However, PHA production in KT42I-BG strain (19.6%) is 2-fold lower when compared to that obtained in KT42I-BGF (42.1%). Moreover, the low dosage of PhaF protein produced in the strain KT42I-BGF ensures granule distribution among the cell population, yielding a total production of 10 mg of PHA immobilized protein per liter of culture and 9.73 mg of

protein per gram of CDW. To date, this protein concentration has been reported only when *E. coli* was used as host strain for recombinant protein production anchored to PHB granules. In this respect, we have also identified the key phasin factors for optimal PHA production in *P. putida*. We have addressed the minimum amount of complete phasin proteins necessary to achieve adequate PHA production and subsequently a higher yield of immobilized recombinant protein. In wild-type *B. megaterium*, GAPs represent close to 2% of the total mass of a standard granule (Griebel *et al*., 1968), which is in perfect agreement with the maximum BioF fusion concentration reported in this work: 2.2% of recombinant protein per PHA content.

Tagged proteins were co-produced with PHB granules in the *E. coli* cells. Multiple phasins (2-3 repeats) were used and several proteins (maltose binding protein (MBP), β-galactosidase (LacZ), chloramphenicol acetyltransferase (CAT)) were successfully purified with yields of 3.17-7.96 mg of protein/g CDW (Banki *et al*., 2005). Althought *E. coli* can produce high PHB content (Chen, 2009) and consequently, high recombinant protein yield, advantages of using *P. putida* as host strain should not be overlooked (Poblete-Castro *et al*., 2012a). Indeed, we are gaining a great understanding of model mcl-PHA producer strains such as *P. puitda* KT2440, through systems biology ("omics" data, genome-scale metabolic models, etc.) (Poblete-Castro *et al*., 2012a; Poblete-Castro *et al*., 2012b; Poblete-Castro *et al*., 2013; Follonier *et al*., 2013; Nogales *et al*., 2008; Escapa *et al*., 2012). Moreover, powerful genetic tools based on synthetic biology (Silva-Rocha *et al*., 2013) support bottom-up approaches and can be used to design *P. putida* strains that generate added-value bioproducts, such as active mcl-PHA based nano-beads. Its great value as an autolytic specialized strain for mcl-PHA production has also been demonstrated (Martinez *et al*., 2011). Due to its broad metabolic versatility and genetic plasticity, which allow a variety of renewable carbon sources to be used for PHA production, *P. putida* is one of the most prominent candidates for protein production. Our work presents novel information on phasin physiological function, thus providing important insights into the critical factors that should be targeted to improve existing models. Moreover, this work defines the need for designing an *in vitro* mcl-PHA immobilization system where PhaI or BioF would be the only tag required for anchoring the recombinant protein to mcl-PHA nano-beads.

2. PHACOS, a functionalized bacterial polyester with bactericidal activity against methicillin-resistant *Staphylococcus aureus* (MRSA)

The second strategy for polymer functionalization and acquisition of added-value PHA is based on the use of metabolic engineering. This approach was used to design bacterial strains capable of producing non-natural polyesters carrying functionalized groups at the side chain (Figure 41). The synthesized polymer is characterized by different chemical structure and subsequently new features. Investigation of those novel polymer properties provided an overview of its possible applications.

Currently bacterial infections are a major cause of morbidity and mortality worldwide, and many infections can be attributed to *Staphylococcus* species (Kiedrowski and Horswill, 2011). The acute pathogenic properties of *S. aureus* (DeLeo and Chambers, 2009) as well as its ability to cause chronic infections and persist on medical implants or host tissues are recognized as significant health threat (Darouiche, 2004). In fact, the ability of *S. aureus* to form biofilms has been linked to the persistence of chronic infections (Kiedrowski and Horswill, 2011). Methicillin-resistant *S. aureus* (MRSA) refers to any strain of *S. aureus* that has developed resistance to beta-lactam antibiotics, which include penicillins (methicillin, dicloxacillin, nafcillin, oxacillin, etc.) and cephalosporins (Grundmann *et al*., 2006). MRSA are especially troublesome in hospitals, prisons, schools and nursing homes, where patients with open wounds, invasive devices, and/or weakened immune systems are at greater risk of infection (Klein *et al*., 2009).

Tremendous efforts have been made to develop compounds that not only show high efficacy, but are also less susceptible to the development of resistance in bacteria. The high incidence and rapid emergence of antibiotic resistance in various Gram-positive cocci makes these pathogens a major health hazard. *S. aureus* is Gram-positive bacteria and a common human pathogen, which most commonly colonize the anterior nares. The rest of the respiratory tract, open wounds, intravenous catheters, and the urinary tract are also potential sites for infection. *S. aureus* causes diverse diseases, ranging from minor skin and soft tissue infections to life-threatening systemic

infections, including endocarditis and sepsis (Raygada and Levine, 2009). It has been estimated that biofilms are associated with 65% of nosocomial infections (Mah and O'Toole, 2001). In addition, it was reported that during 1999-2006 the percentage of methicillin-resistant *S. aureus* infections increased >90%, or ≈10% a year, in outpatients admitted to US hospitals (Klein *et al*., 2009). The development of newer, stronger antibiotics that can overcome these acquired resistances still represents a scientific challenge, thereby new modes of antimicrobial action are required.

Antimicrobial polymers have emerged as a promising candidate for further development as antimicrobial agents with decreased potential for resistance development (Kuroda and Caputo, 2013). They have been classified as a group of biocides that has become increasingly important as an alternative to existing biocides and, in some cases, even antibiotics (Siedenbiedel and Tiller, 2012). Antimicrobial surfaces that prevent biofilm growth are considered an effective strategy to inhibit the spread of microbial infections (Siedenbiedel and Tiller, 2012). Such surfaces either repel microbes, so they cannot attach to the surface, or kill microbes in the vicinity (Siedenbiedel and Tiller, 2012). Antimicrobial polymers have been known since 1965, when Cornell and Dunraruma described polymers and copolymers prepared from 2-methacryloxytroponones that kill bacteria (Cornell and Dunraruma, 1965). In the past decade, the number of FDA-approved disinfecting polymers has significantly increased, which indicates the need for alternatives to antibiotics and environmentally critical disinfectants (Siedenbiedel and Tiller, 2012).

Recently, our research team produced PHACOS, a new second generation polymer family containing thioester groups in the side chain (Figure 8). This functionalized bacterial polyester was obtained by applying 6-ATH as precursor and decanoic acid as co-substrate in a co-feeding strategy for *P. putida* strains (Escapa *et al*., 2011). We have explored the possibility of applying PHACOS to biomedical devices. One of the peculiarities of this naturally produced bacterial polyester is the presence of thioester groups in the polymer side chain. In fact, we have shown that thioester groups play a crucial role in polymer activity against *S. aureus*. In this respect, we demonstrate the unique property of this *P. putida* biopolyester to be active against other bacterial species (see Annex 1). Nevertheless, further modification of this second generation

polymer for fine tuning of its activity and specific applications could easily be achieved using functionalized side chains to incorporate different active molecules. In addition, we observed a clear decrease in *S. aureus* biofilm development on PHACOS.

Many commonly used antimicrobial agents active against planktonic pathogens have minimal or no effect on biofilm-embedded pathogens (Agarwal *et al*., 2005; Giacometti *et al*., 2005). Interfering with the biofilm may release device-colonizing organisms and, therefore, increase the efficacy of antimicrobial agents. Thus, there is a pressing need to explore novel approaches that utilize compounds with a dual ability to disrupt the biofilm and eliminate pathogens.

Biofilm formation on biomaterials can generally be divided into two main stages: (i) bacterial adhesion, which depends on surface properties of both substrates and cells, and (ii) increase in biofilm mass, which depends on initial attachment and specific growth rate of attached cells. It was previously demonstrated that biofilm formation on PHA surfaces varies depending on both bacterial strain and quality of material supporting biofilm formation. For instance, *E. coli* attaches better to mcl-PHA coatings than *S. aureus* (Mauclaire *et al*., 2010). In addition, elimination of impurities in the biopolyester coating drastically limits biofilm formation (Mauclaire *et al*., 2010). Significant correlation was observed between bacterial attachment and roughness for *S. aureus*, a bacterium which is known to be sensitive to surface irregularities (Harris and Richards, 2006). Although PHACOS shows higher roughness than PHO, no increase in attachment of *S. aureus* cells to PHACOS was observed (Figure 25A, B). Moreover, *S. aureus* biofilm formation was lower on PHACOS when compared to PHO (Figure 23). Interestingly, investigating the previously mentioned phenomenon, we discovered the antimicrobial properties of PHACOS (Figure 26).

The potential of pathogenic biofilm to develop on mcl-PHA has been evaluated, but findings did not indicate antibacterial activity of unmodified PHA or mixed with other compounds for that purpose (Mauclaire *et al*., 2010). Furthermore, PHA was not observed to posses antiadherent properties against bacteria.

However, some 3HA, monomers derived from PHA, have been shown bactericidal to a number of Gram-negative and Gram-positive bacteria (Bergsson *et al*., 1998;

Bergsson *et al*., 1999; Bergsson *et al*., 2001; Bergsson *et al*., 2002). For instance, antibacterial activity of [*R*]-3-hydroxy-n-phenylalkanoic acid against *Listeria monocytogenes* was reported (Sandoval *et al*., 2005). Moreover, data provided by Ruth *et al*. demonstrate the antibacterial activity of aliphatic 3HA against not only *Listeria* species, but other bacterial strains such as *S. aureus* (Ruth *et al*., 2007). However, the antibacterial efficiency of the previously mentioned compounds is low, showing very high MIC values (1-5 mM).

The effect of fatty acids and monoglycerides on Gram-positive cocci was investigated (Bergsson *et al*., 2001). In contrast to monocaprin, capric, lauric and palmitoleic acids showing bactericidal activity against streptococci and staphylococci, the other tested compounds (caprylic acid, myristic acid, oleic acid, monocaprylin, monolaurin, monomyristin, monopalmitolein and monoolein) had only a minor effect on *S. aureus* viability. Furthermore, the compounds with bactericidal activity proved to be useful for protection against or treatment of infections caused by Gram-positive cocci where rapid killing of the bacteria is required (Bergsson *et al*., 2001).

The bioactivity of different doses of short-chain, medium-chain and long-chain fatty acids against Gram-positive oral bacteria *Streptococcus mutans*, *Streptococcus gordonii* and *Streptococcus sanguis* have also been studied (Huang *et al*., 2010). It was demonstrated that short-chain fatty acids C2-C5 exhibit minimal antimicrobial activity for this range of bacteria (estimated by the inhibitory concentration at 80%, IC80), while among the medium-chain fatty acids, IC80 decreased in a line with increasing fatty acid lenght. The IC80 values for octanoic acid were in the 2.5 mM to <0.1 mM range, whereas IC80 values for hexanoic acid were 2.5-0.6 mM, both strain dependent (Huang *et al*., 2010). Similarly, our study confirmed MIC values of octanoic and hexanoic acid for *S. aureus*, 3 mM and 0.75 mM, respectively, while 6-acetylthiohexanoic acid, showed a much lower MIC value (40 µM), and was more effective against *S. aureus*.

There is notable specificity in the action of fatty acids and monoglycerides against various bacteria. The difference between the activity profiles of lipids for streptococci and *S. aureus* could possibly be explained by differences in cross-linkage of

peptidoglycan polymers in the bacterial cell wall. Also, the peptidoglycan of *S. aureus* is interspersed with molecules of ribitol-teichoic acid, which is relatively specific for this bacterium (Sherris, 1990). A further study of reasons underlying the difference in activity profiles of lipids against various bacteria would be of interest.

Novel approaches for the development of antimicrobial polymers are an important area of research and many reports have been published referring to the synthesis of macromolecules that are inherently antimicrobial (biocidal polymers). These are usually positively charged macromolecules that interact with microbial cells that generally carry a negative net charge on the surface due to their membrane proteins, teichoic acids of Gram-positive bacteria, and negatively charged phospholipids on the outer membrane of Gram-negative bacteria (Siedenbiedel and Tiller, 2012). Cationic polymers have been the main focus of studies (Waschinski and Tiller, 2005), including those containing ammonium (Kenawy *et al*., 1998), phosphonium salts (Popa *et al*., 2003), pyridinium salts (Tashiro, 2001; Worley and Sun, 1996), polyguanidines and polybiguanidines (Albert *et al*., 2003), polylysine (Hancock and Chapple, 1999), polystyrenes (Gelman *et al*., 2004) and polyoxazolines (Waschinski *et al*., 2004). Antimicrobial peptides also represent a large group of natural compounds with a broad spectrum of antimicrobial activity (Zasloff, 2002). Polymeric biocides are another class of antimicrobial polymers, consisting of bioactive repeating units (*i.e.*, the polymers are just multiple interconnected biocides, which act similarly to the monomers). Often, the polymerization of biocidal monomers does not lead to active antimicrobial polymers, either because the polymers are water-insoluble, or the biocidal functions do not reach their target. Finally there are biocide-releasing polymers, which do not act through the actual polymeric component, instead the latter function as carriers for biocides, which are transferred to the target microbial cells. Such polymers are usually the most active systems, as they can release their biocides close to the cell in high local concentrations (Siedenbiedel and Tiller, 2012). These subjects have attracted the attention of many researchers, and significant improvement has been made in the understanding of essential physiochemical properties and mode of action. Conversely, there are still a number of antibacterial polymers whose exact working principles are unknown.

After our major finding regarding the antibacterial activity of PHACOS (see Annex 1), we have focused on investigating its possible mechanism(s) of action. This study suggests that PHACOS acts as a contact active surface and could therefore be considered a biocidal polymer. However, taking into account the notable antibacterial activity of 6-ATH and PHACOS-derived dimers/trimers we cannot discard the possibility that this compound may be the real polymeric biocide, as the polymerization of active monomeric units leads to antimicrobial polymer. As *in vitro* polymer degradation and monomer release have not been detected (Table 7), PHACOS cannot be classified as biocide-releasing polymers. Another property that needs further investigation is the specificity of PHACOS antimicrobial action against *S. aureus*.

Several antibacterial polymers are known to be selective against *S. aureus* over other species. Cationic polymers including polynorbornenes (Lienkamp *et al*., 2008), oligolysins (Epand *et al*., 2009), and chitosan (Raafat *et al*., 2008) all show selective activity against *S. aureus* over *E. coli*. Although the chemical structures of these polymers are quite different from each other, their cationic functionality appears to be in common, which may be the key determinant in their activity against *S. aureus*. Recently, Gibney *et al*. demonstrated that commercially available unmodified polyethyleneimines (PEIs) with branched structures (M_r = 500-12 000) are also antimicrobial with greater activity against *S. aureus* over *E. coli* (Gibney *et al*., 2012).

Although there are examples of polymers with selective activity against *S. aureus*, the precise mechanism(s) by which PHACOS decreases biofilm formation and kills bacteria is still a matter of debate. N-acetylcysteine NAC, an antioxidant with disulfide bond disruptive properties, has been shown not only to reduce adhesion but also to detach bacterial cells adhered to surfaces and to inhibit bacterial growth *in vitro* (Olofsson *et al*., 2003; Perez-Giraldo *et al*., 1997). NAC inhibits *S. aureus* growth at a concentration of 2.5 mg/mL and has bactericidal properties at a concentration of 5 mg/mL (Hernandez *et al*, 2009). The similarity between NAC and PHACOS lies in the -SH group. Although PHACOS does not contain a free -SH group, it is possibile that the functionalized thioesther side chain breaks and gives rise to a free -SH group. The recent review of Timofeeva *et al*. thoroughly discusses the influence of relevant parameters, such as molecular weight, type and degree of alkylation, and distribution

of charge on the bactericidal action of antimicrobial polymers (Timofeeva and Kleshcheva, 2011). Therefore, there are many factors that should be investigated to unravel PHACOS mode of action.

As previously stated, apart from the desirable antimicrobial properties, high biocompatibility is essential for implants to be accepted by mammals. Several factors determine whether an object is biocompatible: shape, surface porosity, chemistry of the material, and the environment (tissue) where it is incorporated (Zinn *et al*., 2001). In this respect, PHA have the potential to become an important material for medical applications. Tests have shown that PHB is biocompatible, which is not surprising when considering the fact that [*R*]-3-hydroxybutyric acid is a normal constituent of blood at concentrations between 0.3 and 1.3 mM (Wiggam *et al*., 1997) and is also found in the cell envelope of eukaryotes (Reusch, 2000). As mentioned in the Introduction (see section 6), many successful studies using various animal models have clearly demonstrated that PHA (represented by PHB, PHB-*co*-HV, P4HB, PHO and PHB-*co*-HHx) possess the biodegradability, biocompatibility and thermoprocessibility for implant applications (Chen and Wu, 2005). Application of PHO has mainly focused on heart-valve manufacture due to its mechanical and thermophysical properties. Although the biomedical applications of PHO and other mcl-PHA have recently been reviewed (Hazer *et al*., 2012), this dissertation provides the first report of studies into the *in vivo* biocompatibility and antimicrobial action of PHACOS (Figure 30, 31).

3. Real-time monitoring of bacterial infection *in vivo*: Development of bioluminescent *Staplylococcal* foreign-body mouse infection model

Device-related staphylococcal infections are a growing healthcare problem (Zimmerli *et al*., 2004; Darouiche, 2004), accounting for more than 50% of the 2 million annual hospital-acquired infections associated with indwelling devices and implants in the United States (Darouiche, 2004). *S. aureus* is one of the most common pathogens associated with these cases. Bacterial colonization and biofilm development can be prelude to both systemic infection and malfunction of the device. An additional confounding problem is an increasing incidence of multidrug-resistant *Staphylococcus aureus* (MRSA). Frequently, the affected devices must be removed to fully eliminate the infection. Removal of these devices has serious implications (Costerton *et al*., 1999; Mermel *et al*., 2001). In order to combat biofilm-associated infections, novel biomaterials and non-invasive *in vivo* screening approaches are essential for prevention and timely treatment of bacterial infections.

Together with the design of new materials and antimicrobial coatings, there is a need for the development of *in vivo* research techniques, which allow for non-invasive and accurate monitoring of infection and inflammation *in vivo* over prolonged time periods. Optical imaging of bacterial infections *in vivo* using engineered bioluminescent bacterial strains enables accurate assessment of the disease process. Bioluminescent bacterial pathogens, expressing a luciferase-based reporter system, emit visible light, which can be monitored longitudinally and nondestructively in the same animal throughout the duration of a study. It allows strategy refinement, thus reducing the number of animals used in a study and experimental cost. Such an approach provides better understanding and control of biofilm formation on PHA implants *in vivo*.

Biomaterial-related infections tend to show marked acute inflammation and might be essential for the diagnosis of ongoing infection. Therefore, to visualize infectious foci in their early phases, when morphologic changes are not yet apparent, H-ICG imaging probes were used, which allowed real-time fluorescence imaging and ROS detection around the vicinity of an implant (Selvam *et al*., 2011). In addition,

fluorescence imaging is an excellent non-invasive method of whole-body scanning, which can determine the extent of the infectious or inflammatory disease throughout the body, especially in clinically challenging cases involving trauma, infection, and compromised tissue beds.

Herein, we describe a new strategy for *in vivo* non-invasive real-time monitoring of a PHO implant-associated infection and inflammation combining two strategies: (i) monitoring bacterial infection using bioluminescent *S. aureus* strains; (ii) fluorescence imaging of ROS using H-ICG. This allowed the design of a new method to detect early stages of bacterial infection. Moreover, monitoring the inflammatory response of the host to the infected implant provides a rapid, quantitative measure of *in vivo* biofilm development. To that end, the sensitivity of the H-ICG imaging probe was tested in correlation with increasing CFU counts.

The implantation procedure triggers a response to injury, and mechanisms are activated to produce healing. The degree to which the homeostatic mechanisms are perturbed, and the extent of pathophysiological responses and their resolution are measures of the host's reactions to the biomaterial, and they may ultimately determine its biocompatibility and thus its success or failure as a device/prosthesis (Anderson, 2001). Inflammation, wound healing, and foreign-body responses are generally considered as parts of the tissue or cellular host responses to injury. From the biomaterials perspective, placement of a biomaterial in the *in vivo* environment involves injection, insertion, or surgical implantation; all of which injure the tissue. An additional perplexing problem is occurrence of implant-associated infections. Matrix proteins that immediately coat the device upon implantation (François *et al*., 1998; Francois *et al*., 2000) promote *S. aureus* adhesion, as this bacterium harbours numerous cell wall-bound surface proteins that contain binding domains for matrix proteins (Foster and Höök, 1998). A seldom considered explanation for staphylococci implant infections regards the low inoculums to establish infection. Moreover, some infections, such as post-arthroplasty related, are associated with nonspecific signs, which subsequently lead to chronic infections with catastrophic complications (Del Pozo and Patel, 2009). Early detection of those infections and timely treatment thereof

is great importance. Besides, there is compiling need for new sensitive diagnostic techniques development.

Conventional methodologies for monitoring pathogens *in vivo* are cumbersome and include biological assessment regimens. By means of bioluminescent non-invasive imaging, we were able to detect and real-time monitor bacterial infection. Using genetically engineered bioluminescent *S. aureus* strains, we monitored implant-related infection throughout the study (Figure 36, 37). However, we observed that when the implant was pre-colonized with low bacterial inocula, the bioluminescent signal could not be detected. Furthermore, bioluminescent signals were only detectable up to day 4, after which the signals decreased to background levels, indicating that when bacteria leave the exponential phase and enter stationary growth phase, bioluminescence decreases (Figure 36, 37). The same trend was observed by Kadurugamuwa *et al*., who explained that limitation of oxygen and/or substrate could be the possible cause, since the reduced expression of bioluminescence within the biofilm could be restored by replacement of the culture medium with fresh medium every 12 h (Kadurugamuwa *et al*., 2003).

Besides, it was demonstrated that implant surface chemistry is an important factor that contributes to bacterial adhesion and biofilm development. The ability of bacteria to adhere and rapidly form a biofilm on the device surface is crucial for the infection to develop. This is because in implant-associated infections, granulocytes are mainly confronted by biofilm but not by planktonic bacteria. Biomaterials play an important role in improving disease treatment and health care (Langer and Tirrell, 2004). Therefore, there is a need for development of new biomaterials that could prevent bacterial adhesion and biofilm development and simultaneously promote tissue regeneration. Mauclaire *et al*. provided an evaluation for the potential of pathogenic biofilm development on mcl-PHA (Mauclaire *et al*., 2010), even so by comparing bacterial adherence *in vitro* and *in vivo*, it was observed that *in vitro* differences in *S. epidermidis* adherence to titanium and stainless steel could not be detected in an *in vivo* animal model (Ha *et al*., 2005). No differences in infection rates were observed when titanium and stainless steel implants were challenged with

staphylococci (Ha *et al*., 2005). Therefore, *in vitro* studies of bacterial adhesion do not necessarily reflect the outcome of *in vivo* studies.

Herein, we have described a method for *in vivo* monitoring of the progression of bacterial infection on poly(3-hydroxyoctanoate-*co*-hydroxyhexanoate), as classe of polyhydroxyalkanoates, which are biomaterials with promising properties for biomedical applications (Chen, 2009). We studied inflammatory response and tissue regeneration when PHO disks were implanted subcutaneously in the backs of mice. Statistically significant differences in inflammatory response to the PHO implant and control group was not observed (Figure 40). In perfect correlation with previously reported data, we demonstrate *in vivo* biocompatibility of PHO implants and good tissue integration.

Moreover, we investigated the recruitment of immune cell and ROS response when infected polymer disks were implanted. Innate or nonspecific host defense mechanisms are required for rapid and efficacious elimination of microorganisms causing implant-associated infection (Zimmerli *et al*., 1982; Zimmerli *et al*., 1984; Vaudaux *et al*., 2000; Finlay and Cossart, 1997). However, they are difficult to detect by means of marginal laboratory and radiographic evidence (Zimmerli *et al*., 2004). In this work we have described the use of non-invasive fluorescent imaging for implant-associated inflammation monitoring. We observed that the intensity of inflammation is dependent on the number of bacteria used to pre-colonize the implant. The higher the initial bacterial inoculums, the stronger inflammation detected. Applying H-ICG-based fluorescence imaging of ROS, we were able to detect the infection accurately, even when the bacterial bioluminescencence could not be detected (Figure 38-40). Moreover, the recruitment of immune cells increased in line with increasing bacterial inocula, representing nearly 100% of the total cell number in the implant vincinity when inocula of 10^8 CFU/disk were applied (Figure 42).

The diagnosis of infection in early stages remains a challenging problem, as there is no single diagnostic approach with absolute sensitivity and specificity. Accurate diagnosis often requires the combination of tests and a strong clinical warning signs. Serologic tests (measurements of white blood-cell count, erythrocyte sedimentation

rate, and C-reactive protein level) represent the first-line of investigation and generally provide good sensitivity but lower specificity. Non-invasive imaging is a promising tool for early-stage infection diagnostics and may also be used to further support other assays for more precise diagnosis of infection.

VI. Conclusions

1. A new and unexpected role of *P. putida* PhaF phasin involved in the balanced distribution of PHA reserve granules between daughter cells during cell division has been described. This new role for phasins within the PHA apparatus could be critical for cell survival under stress conditions.
2. PHA granule and DNA binding modules of PhaF protein are separately functional and therefore suitable to construct fusion proteins.
3. The key factors involved in *in vivo* immobilization of recombinant proteins onto PHA granules using the previously designed BioF system to anchor fusion proteins on the PHA granules were determined. We illustrated the swappable nature of PHA binding modules (PhaI and BioF tag) and the fact both functional modules (PHA and DNA binding modules) are required for optimal PHA granule formation and segregation.
4. Optimal conditions were achieved to provide the highest yield of recombinant protein immobilized *in vivo* onto PHA granules. A particular combination of phasin module synthesis leading to optimal PHA production and granule distribution among cells has been defined.
5. We have described new and unexpected properties of PHACOS, a second-generation biopolymer, showing antibacterial activity specifically against *S. aureus* including MRSA clinical isolates, and able to hinder *S. aureus* biofilm formation.
6. Antibacterial activity of PHACOS has been ascribed to the functionalized side chain containing thioester groups. These findings suggest the possible mode of action of PHACOS as contact active surface, and pose new questions about the unknown antibacterial mechanism linked to this biomaterial.
7. The use of PHACOS for implants has been shown by demonstrating its biocompatibility and antimicrobial properties *in vivo*.
8. A non-invasive method for *in vivo* real-time monitoring of mcl-PHA implant associated inflammation has been developed using H-ICG sensor.
9. A strategy has been designed for *in vivo* monitoring of mcl-PHA implant infection using bioluminescent strains.
10. The possibility of applying H-ICG sensor to monitore of infection-derived inflammation has been described.

VII. References

Abraham GA, Gallardo A, San Roman J, Olivera ER, Jodra R, García B, Miñambres B, García JL, Luengo JM. (2001). Microbial synthesis of poly(β-hydroxyalkanoates) bearing phenyl groups from *Pseudomonas putida*: chemical structure and characterization. *Biomacromolecules*. 2:562–7.

Agarwal G, Kapil A, Kabra SK, Das BK, Dwivedi SN. (2005). *In vitro* efficacy of ciprofloxacin and gentamicin against a biofilm of *Pseudomonas aeruginosa* and its free-living forms. *Natl Med J India*. 18:184–6.

Albert M, Feiertag P, Hayn G, Saf R, Honig H. (2003). Structure−Activity Relationships of OligoguanidinesInfluence of Counterion, Diamine, and Average Molecular Weight on Biocidal Activities. *Biomacromolecules*. 4:1811–7.

Anderson AJ, Haywood GW, Dawes EA. (1990). Biosynthesis and composition of bacterial poly(hydroxyalkanoates). *Int. J. Biol. Macromol.* 12:102–5.

Anderson J.M. (2001). Biological responses to materials. *Annu Rev Mater Res*. 31:81–110.

Andújar M, Aponte MA, Díaz E, Schröder E. (1997). Polyesters produced by *Pseudomonas oleovorans* containing cyclohexyl groups. *Macromolecules.* 30:1611–15.

Aróstegui SM, Aponte MA, Díaz E, Schröder E. (1999). Bacterial polyesters produced by *Pseudomonas oleovorans* containing nitrophenyl groups. *Macromolecules.* 32:2889–95.

Ashby RD, Foglia TA. (1998.) Poly(hydroxyalkanoate) biosynthesis from triglyceride substrates. *Applied Microbiology and Biotechnology*. 49:431–7.

Babinot J, Renard E, Langlois V. (2010). Preparation of Clickable Poly(3-hydroxyalkanoate) (PHA): Application to Poly(ethylene glycol) (PEG) Graft Copolymers Synthesis. *Macromol Rapid Commun*. 31:619–24.

Babu GN, Christopher SS, Copley BC, Overstreet TS. (1993). Radiation curable polyolefin pressure sensitive adhesive No 5209971, 199.

Bäckström BT, Brockelbank JA, Rehm BHA. (2007). Recombinant *Escherichia coli* produces tailor-made biopolyester granules for applications in fluorescence activated cell sorting: functional display of the mouse interleukin-2 and myelin oligodendrocyte glycoprotein. *BMC Biotechnol*. 7:3 doi:10.1186/1472-6750-7-3.

Banki MR, Gerngross TU, Wood DW. (2005). Novel and economical purification of recombinant proteins: intein-mediated protein purification using *in vivo* polyhydroxybutyrate (PHB) matrix association. *Protein Science*. 14:1387–95.

Baptis JN, Ziegler JB. (1965). Method of making adsorbable surgical sutures from poly beta hydroxyl acids. US Patent No 3,225,766.

Baptist JN. (1965). US Patent No 3225766, 1965.

Bassas M, Diaz J, Rodríguez E, Espuny MJ, Prieto MJ, Manresa A. (2008a). Microscopic examination *in vivo* and *in vitro* of natural and cross-linked polyunsaturated mclPHA. *Applied Microbiology and Biotechnology*. 78:587–96.

Bassas M, Marques AM, Manresa A. (2008b). Study of the crosslinking reaction (natural and UV induced) in polyunsaturated PHA from linseed oil. *Biochemical Engineering Journal*. 40:275–83.

Bear MM, Leboucher-Durand MA, Langlois V, Lenz RW, Goodwin S, Guérin P. (1997). Bacterial poly-3-hydroxyalkenoates with epoxy groups in the side chains. *Reactive and Functional Polymers.* 34:65–77.

Behrend D, Lootz D, Schmitz KP, Schywalsky M, Labahn D, Hartwig S, Schaldach M, Unverdorben M, Vallbracht C, Langer F. (1998). PHB as bioresorbable material for intravasculat stents. *Am. J. Cardio, Tenth Annual Symposium Transcatheter Cardiovascular Therapeutics Abstract TCT-8*, 4S.

Benjamini Y, Hochberg Y. (1995). Controlling the false discovery rate: a practical and powerful approach to multiple testing. *J R Stat Soc B.* 57:289–300.

Bergsson G, Arnfinnsson J, Karlsson SM, Steingrímsson O, Thormar H. (1998). *In vitro* inactivation of *Chlamydia trachomatis* by fatty acids and monoglycerides. *Antimicrob Agents Chemother*. 42:2290–4.

Bergsson G, Arnfinnsson J, Steingrimsson O, Thormar H. (2001). Killing of Gram-positive cocci by fatty acids and monoglycerides. *APMIS.* 109:670–8.

Bergsson G, Steingrímsson O, Thormar H. (1999). *In vitro* susceptibilities of *Neisseria gonorrhoeae* to fatty acids and monoglycerides. *Antimicrob Agents Chemother*. 43:2790–2.

Bergsson G, Steingrímsson O, Thormar H. (2002). Bactericidal effects of fatty acids and monoglycerides on *Helicobacter pylori*. *Int J Antimicrob Agents*. 20:258–62.

Bian YZ, Wang Y, Aibaidoula G, Chen GQ, Wu Q. (2009). Evaluation of poly(3-hydroxybutyrate-co-3-hydroxyhexanoate) conduits for peripheral nerve regeneration. *Biomaterials*. 30:217–25.

Black J. (2006). Biological Performance of Materials. ISBN 0-8493-3959-6.

Bowald SF, Johansson EG. (1990). A novel surgical material. European patent application. No 0 349505A2.

Bowald SF, Johansson-Rudel G. (1997). A novel surgical material. European patent application. No 0 754467AI.

Brandl H, Bachofen R, Mayer J, Wintermantel E. (1995). Degradation and applications of polyhydroxyalkanoates. *Can. J. Microbiol.* 41:143–53.

Brandl H, Gross RA, Lenz RW, Fuller RC. (1990). Plastics from bacteria and for bacteria: poly(beta-hydroxyalkanoates) as natural, biocompatible, and biodegradable polyesters, *Adv. Biochem. Eng. Biotechnol.* 41:77–93.

Bridges AW, Garcia JA. (2008). Anti-inflammatory polymeric coatings for implantable biomaterials and devices. *Journal of Diabetes Science and Technology.* 2:984–94.

Bustin M, Catez F, Jae-Hwan L. (2005). The dynamics of histone H1 function in chromatin. *Mol Cell* 17:617–20.

Byrom D. (1987). Polymer synthesis by microorganisms: technology and economies, *Trends Biotechnol.* 5:246–50.

Caserta E, Tomsic J, Spurio R, La Teana A, Pon CL, Gualerzi CO. (2006). Translation initiation factor IF2 interacts with the 30S ribosomal subunit via two separate binding sites. *J Mol Biol.* 362:787–99.

Chaput C, Yahaia L`H, Selmani A, Rivard C-H. (1995). Natural poly(hydroxybutyrate-hydroxy-valerate) polymers as degradable materials. *Mat. Res. Soc. Symp. Proc.* 385:49–54.

Chen GQ, Patel MK. (2012). Plastics derived from biological sources: present and future: a technical and environmental review. *Chem Rev*. 112:2082–99.

Chen GQ, Wu Q. (2005). The application of polyxydroxyalkanoates as tissue engineering materials. *Biomat.* 26:6565–78.

Chen GQ, Zhang G Park SJ, Lee SY. (2001). Industrial production of Poly(hydroxybutirate-co-hydroxyhexanoate). *Appl Microbiol Biotechnol*. 57:50–5.

Chen GQ. (2009). A microbial polyhydroxyalkanoates (PHA) based bio- and materials industry. *Chem. Soc. Rev.* 38:2434–46.

Cheng S, Chen GQ, Leski M, Zou B, Wang Y, Wu Q. (2006). The effect of D,L-beta-hydroxybutyric acid on cell death and proliferation in L929 cells. *Biomaterials*. 27:3758–65.

Cheng S, Wu Q, Yang F, Xu M, Leski M, Chen GQ. (2005). Influence of DL-beta-hydroxybutyric acid on cell proliferation and calcium influx. *Biomacromolecules*. 6:593–7.

Choi MH, Yoon SC. (1994). Polyester biosynthesis characteristics of *Pseudomonas citronellolis* grown on various carbon sources, including 3-methyl-branched substrates. *Applied and Environmental Microbiology*. 60:3245–54.

Chung A, Liu Q, Ouyang SP, Wu Q, Chen GQ. (2009). Microbial production of 3-hydroxydodecanoic acid by *pha* operon and *fadBA* knockout mutant of *Pseudomonas putida* KT2442 harboring *tesB* gene. *Applied Microbiology and Biotechnology*. 83:513–19.

CLSI. Methods for dilution antimicrobial susceptibility tests for bacteria that grow aerobically, document M07-A8. Clinical and Laboratory Standards Institute, Wayne, PA.7 2008.

Cool SM, Kenny B, Wu A, Nurcombe V, Trau M, Cassady AI, Grøndahl L. (2008). Poly(3-hydroxybutyrate-*co*-3-hydroxyvalerate) composite biomaterials for bone tissue regeneration: *in vitro* performance assessed by osteoblast proliferation, osteoclast adhesion and resorption, and macrophage proinflammatory response. *J. Biomed. Mater. Res. A.* 82:599–610.

Cornell RJ, Donaruma LG. (1965). 2-Methacryloxytroponones. Intermediates for Synthesis of Biologically Active Polymers. *J. Med. Chem*., 8, 388–90.

Costerton JW, Stewart PS, Greenberg EP. (1999). Bacterial biofilms: a common cause of persistent infections. *Science.*284:1318–22.

Curley JM, Hazer B, Lenz RW, Fuller RC. (1996a). Production of poly(3-hydroxyalkanoates) containing aromatic substituents by *Pseudomonas oleovorans*. *Macromolecules.* 29:1762–66.

Curley JM, Lenz RW, Fuller RC. (1996b). Sequential production of two different polyesters in the inclusion bodies of *Pseudomonas oleovorans*. *International Journal of Biological Macromolecules.* 19:29–34.

Cuskey SM, Wolff JA, Phibbs PV, Olsen RH. (1985). Cloning of genes specifying carbohydrate catabolism in *Pseudomonas aeruginosa* and *Pseudomonas putida*. *Journal of Bacteriology.* 162:865–71.

Darouiche RO. (2004). Treatment of infections associated with surgical implants. N. *Engl. J. Med.* 350:1422–9.

De Eugenio LI, Escapa IF, Morales V, Dinjaski N, Galán B, García JL, Prieto MA. (2010a). The turnover of medium-chain length polyhydroxyalkanoates in *Pseudomonas putida* KT2442 and the fundamental role of PhaZ depolymerase for the metabolic balance. *Environ Microbiol.* 12:207–21.

De Eugenio LI, Galán B, Escapa IF, Maestro B, Sanz JM, García JL, Prieto MA. (2010b). The PhaD regulator controls the simultaneous expression of the *pha* genes involved in polyhydroxyalkanoate metabolism and turnover in *Pseudomonas putida* KT2442. *Environ Microbiol.* 12:1591–603.

De Eugenio LI, García P, Luengo JM, Sanz JM, Román JS, García JL, Prieto MA. (2007). Biochemical evidence that *phaZ* gene encodes a specific intracellular medium chain length polyhydroxyalkanoate depolymerase in *Pseudomonas putida* KT2442: characterization of a paradigmatic enzyme. *J. Biol. Chem*. 282:4951–62.

De Eugenio LI. (2009). Estudio bioquímico, genético y fisiológico de la degradación intracelular de polihidroxialcanoatos en *Pseudomonas putida*: Aplicaciones biotecnológicas. PhD Thesis. In: Departamento de Bioquimica y Biologia Molecular. Madrid: Universidad Complutense de Madrid (UCM). http://digital.csic.es/bitstream/10261/41822/1/Eugenio-Laura-de.pdf

De Koning GJM, van Bilsen HMM, Lemstra PJ, Hazenberg W, Witholt B, Preusting H, van der Galiën JG, Schirmer A, Jendrossek D. (1994). A biodegradable rubber by crosslinking poly(hydroxyalkanoate) from *Pseudomonas oleovorans*. *Polymer*. 35:2090–7.

De Lorenzo V, Eltis L, Kessler B, Timmis KN. (1993). Analysis of *Pseudomonas* gene products using *lacI^q/Ptrp-lac* plasmids and transposons that confer conditional phenotypes. *Gene*. 123:17–24.

De Lorenzo V, Timmis K. (1994). Analysis and construction of stable phenotypes in gram-negative bacteria with Tn5- and Tn10-derived minitransposons. *Methods in Enzymol.* 235:386–405.

Del Pozo JL, Patel R. (2009). Clinical practice. Infection associated with prosthetic joints. *N Engl J Med*. 361:787–94.

DeLeo FR, Chambers HF. (2009). Reemergence of antibiotic-resistant *Staphylococcus aureus* in the genomics era. *J. Clin. Invest*. 119:2464–74.

Deretic V, Hibler NS, Holt SC. (1992). Immunocytochemical analysis of AlgP (H_p1), a histonelike element participating in control of mucoidy in *Pseudomonas aeruginosa*. *J Bacteriol.* 174:824–31.

Deretic V, Konyecsni WM. (1990). A prokaryotic regulatory factor with a histone H1-like carboxy-terminal domain: clonal variation of repeats within *algP*, a gene involved in regulation of mucoid in *Pseudomonas aeruginosa*. *J Bacterio.l* 172:5544–54.

Doi Y, Abe C. (1990). Biosynthesis and characterization of a new bacterial copolyester of 3-hydroxyalkanoates and 3-hydroxy-omega-chloroalkanoates. *Macromolecules.* 23:3705–7.

Dong Y, Li P, Chen CB, Wang ZH, Ma P, Chen GQ. (2010). The improvement of fibroblast growth on hydrophobic biopolyesters by coating with polyhydroxyalkanoate granule binding protein PhaP fused with cell adhesion motif RGD. *Biomaterials*. 31:8921–30.

Duvernoy O, Malm T, Ramstrom J, Bowald SF. (1995). A biodegradable patch used as pericardial substitute after cardiac surgery: 6- and 24-month evaluation with CT. *Thorac. Cardiovasc. Surg*. 43:271–4.

Elbahloul Y, Steinbüchel A. (2009). Large-scale production of poly(3-hydroxyoctanoic acid) by *Pseudomonas putida* GPo1 and a simplified downstream process. *Appl Environ Microbiol.* 75:643–51.

Epand RF, Sarig H, Mor A, Epand RM. (2009). Cell-wall interactions and the selective bacteriostatic activity of a miniature oligo-acyl-lysyl. *Biophys J*. 97:2250–7.

Escapa IF, del Cerro C, García JL, Prieto MA. (2013). The role of GlpR repressor in *Pseudomonas putida* KT2440 growth and PHA production from glycerol. *Environ Microbiol.* 15:93–110.

Escapa IF, García JL, Bühler B, Blank LM, Prieto MA. (2012). The polyhydroxyalkanoate metabolism controls carbon and energy spillage in *Pseudomonas putida*. *Environ Microbiol*. 14:1049–63.

Escapa IF, Morales V, Martino VP, Pollet E, Avérous L, García JL, Prieto MA. (2011). Disruption of β-oxidation pathway in *Pseudomonas putida* KT2442 to produce new functionalized PHAs with thioester groups. *Appl. Microbiol. Biotechnol.* 89:1583–98.

Ewering C, Lutke-Eversloh T, Luftmann H, Steinbüchel A. (2002). Identification of novel sulfur-containing bacterial polyesters: biosynthesis of poly (3-hydroxy-S-propyl-ω-thioalkanoates) containing thioether linkages in the side chains. *Microbial Cell Factories*. 148:1397–406.

Fasman, G.D. (ed.). (1976). Handbook of biochemistry and molecular biology.Section A. Proteins, 3rd ed., vol. III. CRC Press, Inc., Cleveland, Ohio.

FDA U.S. Department of Health and Human Services, F.D.A. Guidance for Industry, 1997, Rockville, p.54.

FDA. Guideline on validation of the Limulus amebocyte lysate test as an end-product endotoxin test for human an animal parenteral drugs, biological products, and medical devices. In: U.S. Department of Health and Human Services FaDA, editor. Rockville, MD1987. http://www.gmpua.com/Validation/Method/LAL/FDAGuidelineForTheValidationA.pdf.

Fiedler S, Steinbüchel A, Rehm BHA. (2000). PhaG-mediated synthesis of poly (3-hydroxyalkanoates) consisting of medium-chain-length constituents from nonrelated carbon sources in recombinant *Pseudomonas fragi*. *Applied and Environmental Microbiology.* 66:2117–24.

Finlay BB, Cossart P. (1997). Exploitation of mammalian host cell functions by bacterial pathogens. *Science*. 276:718–25.

Fleminger G, Shabtai Y. (1995). Direct and Rapid Analysis of the Adhesion of Bacteria to Solid Surfaces: Interaction of Fluorescently Labeled Rhodococcus Strain GIN-1 (NCIMB 40340) Cells with Titanium-Rich Particles. *Appl Environ Microbiol*. 61:4357–61.

Follonier S, Escapa IF, Fonseca PM, Henes B, Panke S, Zinn M, Prieto MA. (2013). New insights on the reorganization of gene transcription in *Pseudomonas putida* KT2440 at elevated pressure. *Microb. Cell Fact*., 12:30. doi: 10.1186/1475-2859-12-30.

Foster TJ, Höök M. (1998). Surface protein adhesins of *Staphylococcus aureus*. *Trends Microbiol*. 6:484–8.

Francois P, Schrenzel J, Stoerman-Chopard C, Favre H, Herrmann M, Foster TJ, Lew DP, Vaudaux P. (2000). Identification of plasma proteins adsorbed on hemodialysis tubing that promote *Staphylococcus aureus* adhesion. *J Lab Clin Med*. 135:32–42.

François P, Vaudaux P, Lew PD. (1998). Role of plasma and extracellular matrix proteins in the physiopathology of foreign body infections. *Ann Vasc Surg*. 12:34–40.

Fritzsche K, Lenz RW, Fuller RC. (1990a). An unusual bacterial polyester with a phenyl pendant group. *Die Makromolekulare Chemie*. 191:1957–65.

Fritzsche K, Lenz RW, Fuller RC. (1990b). Bacterial polyesters containing branched poly (β-hydroxyalkanoate) units. *International Journal of Biological Macromolecules.* 12:92–101.

Fritzsche K, Lenz RW, Fuller RC. (1990c). Production of unsaturated polyesters by *Pseudomonas oleovorans*. *International Journal of Biological Macromolecules*. 12:85–91.

Furrera P, Panke S, Zinn M. (2007). Efficient recovery of low endotoxin medium-chain-length poly([*R*]-3-hydroxyalkanoate) from bacterial biomass*. Journal of Microbiological Methods*. 69:206–13.

Galán B, Dinjaski N, Maestro B, De Eugenio LI, Escapa IF, Sanz JM, García JL, Prieto MA. (2011). Nucleoid-associated PhaF phasin drives intracellular location and segregation of polyhydroxyalkanoate granules in *Pseudomonas putida* KT2442. *Mol. Microbiol.* 79:402–18.

García B, Olivera ER, Miñambres B, Fernández-Valverde M, Cañedo LM, Prieto MA, García JL, Martínez M, Luengo J. (1999). Novel biodegradable aromatic plastics from a bacterial source. *Journal of Biological Chemistry.* 274:29228–41.

Garrido L. (1999). Nondestructive evaluation of biodegradable porous matrices for tissue engineering. In: Methods in Molecular Medicine, Vol.18:Tissue engineering Methods and Protocols. Totowa, New Yersey: Humana Press. pp. 35–45.

Gelman MA, Weisblum B, Lynn DM, Gellman SH. (2004). Biocidal activity of polystyrenes that are cationic by virtue of protonation. *Org Lett.* 6:557–60.

Gerdes K, Howard M, Szardenings F. (2010). Pushing and pulling in prokaryotic DNA segregation. *Cell.* 141:927–42.

Giacometti A, Cirioni O, Ghiselli R, Orlando F, Mocchegiani F, Silvestri C, Licci A, De Fusco M, Provinciali M, Saba V, Scalise G. (2005). Comparative efficacies of quinupristin–dalfopristin, linezolid, vancomycin, and ciprofloxacin in treatment, using the antibiotic-lock technique, of experimental catheterrelated infection due to Staphylococcus aureus. *Antimicrob Agents Chemother.* 49:4042–5.

Gibney K, Sovadinova I, Lopez AI, Urban M, Ridgway Z, Caputo GA, Kuroda K. (2012). Poly(ethylene imine)s as antimicrobial agents with selective activity. *Macromol Biosci*. 12:1279–89.

Gitai Z, Thanbichler M, Shapiro L. (2005). The choreographed dynamics of bacterial chromosomes. *Trends Microbiol.* 13:221–8.

Gogolewski S, Jovanovic M, Perren SM, Dillon JG, Hughes MK. (1993). Tissue response and in vivo degradation of selected polyhydroxyacids: polylactides (PLA), poly(3-hydroxybutyrate) (PHB), and poly(3-hydroxybutyrate-*co*-3-hydroxyvalerate) (PHB/VA). *J Biomed Mater Res*. 27:1135–48.

Gómez JGC, Méndez BS, Nikel PI, Pettinari MJ, Prieto MA, Silva LF. (2012). Making green polymers even greener: towards sustainable production of polyhydroxyalkanoates from agroindustrial by-products. In: Advances in Applied Biotechnology, InTech doi: 10.5772/31847.

Goyard S. (1996). Identification of BpH2, a novel histone H1 homolog in *Bordetella pertussis*. *J Bacteriol.* 178:3066–71.

Grage K, Jahns AC, Parlane N, Palanisamy R, Rasiah IA, Atwood JA, Rehm BH. (2009). Bacterial polyhydroxyalkanoate granules: biogenesis, structure, and potential use as nano-/micro-beads in biotechnological and biomedical applications. *Biomacromolecules.* 13:660–9.

Griebel R, Smith Z, Merrick JM. (1968). Metabolism of poly-beta-hydroxybutyrate. I. Purification, composition, and properties of native poly-beta-hydroxybutyrate granules from *Bacillus megaterium*. *Biochemistry*. 7:3676–81.

Gross RA, Kim O-Y, Rutherford DR, Newmark RA. (1996). Cyanophenoxy-containing microbial polyesters: Structural analysis, thermal properties, second harmonic generation and *in-vivo* biodegradability. *Polymer international*. 39:205–13.

Grundmann H, Aires-de-Sousa M, Boyce J, Tiemersma E. (2006). Emergence and resurgence of meticillin-resistant *Staphylococcus aureus* as a public-health threat. *Lancet.* 368:874–85.

Ha KY, Chung YG, Ryoo SJ. (2005). Adherence and biofilm formation of *Staphylococcus epidermidis* and *Mycobacterium tuberculosis* on various spinal implants. *Spine (Phila Pa 1976)*. 30:38–43.

Hancock REW, Chapple DS. (1999). Peptide antibiotics. *Antimicrob Agents Chemother.* 43:1317–23.

Harris LG, Richards RG. (2006). Staphylococci and implant surfaces: a review. *Injury*. 37 Suppl 2:S3–14.

Hasirci V, Gürsel I, Türsein F, Yigitel G, Korkusuz F, Alaeddinoglu G. (1998). Microbial polyhydroxyalkanoatea as biodegradable drug release materials. In: Biomedical Science and Technology. Plenum Press. pp. 183–7.

Hazari A, Johansson-Rudén G, Junemo-Bostrom K, Ljungberg C, Terenghi G, Green C, Wiberg M. (1999). A new resorbable wrap-around implant as an alternative nerve repair technique. *J Hand Surg Br*. 24:291–5.

Hazer B, Steinbüchel A. (2007). Increased diversification of polyhydroxyalkanoates by modification reactions for industrial and medical applications. *Applied Microbiology and Biotechnology.* 74:1–12.

Hazer BD, Hazer B. (2011). The effect of gold clusters on the autoxidation of PHU-co-PHO and tissue response. *J. Polym Res*. 18:251–262.

Hazer DB, Hazer B, Kaymaz F. (2009). Synthesis of microbial elastomers based on soybean oily acids. Biocompatibility studies. *Biomed Mater*. 4:035011 doi:10.1088/1748-6041/4/3/035011.

Hazer DB, Kılıçay E, Hazer B. (2012). Poly(3-hydroxyalkanoate)s: Diversification and biomedical applications A state of the art review. *Materials Science and Engineering C.* 32:637–47.

He W, Tian W, Zhang G, Chen GQ, Zhang Z. (1998). Production of novel polyhydroxyalkanoates by *Pseudomonas stutzeri* 1317 from glucose and soybean oil. *FEMS Microbiology Letters.* 169:45–9.

Hernandez MD, Mansouri MD, Aslam S, Zeluff B, Darouiche RO. (2009). Efficacy of combination of N-acetylcysteine, gentamicin, and amphotericin B for prevention of microbial colonization of ventricular assist devices. *Infect Control Hosp Epidemiol*. 30:190–2.

Herrero M, de Lorenzo V, Timmis KN. (1990). Transposon vectors containing non-antibiotic resistance selection markers for cloning and stable chromosomal insertion of foreign genes in gram-negative bacteria. *J. Bacteriol*. 172:6557–67.

Honma T, Inamura T, Kenmoku T, Kobayashi S, Yano T. (2004). Biosynthesis of novel poly (3-hydroxyalkanoates) containing benzoyl groups. *Journal of Environmental Biotechnology*. 4:49–55.

Huang CB, George BJ, Ebersole L. (2010). Antimicrobial activity of n-6, n-7 and n-9 fatty acids and their esters for oral microorganisms. *Archives of Oral Biology.* 55:555–60.

Huijberts GN, Eggink G, de Waard P, Huisman GW, Witholt B. (1992). *Pseudomonas putida* KT2442 cultivated on glucose accumulates poly(3-hydroxyalkanoates)

consisting of saturated and unsaturated monomers. *Appl Environ Microbiol.* 58:536–44.

Huisman GW, Wonink E, Meima R, Kazemier B, Terpstra P, Witholt B. (1991). Metabolism of poly(3-hydroxyalkanoates) (PHAs) by *Pseudomonas oleovorans*. Identification and sequences of genes and function of encoded proteins in the synthesis and degradation of PHA. *J.Biol.Chem*. 266:2191–98.

Imamura T, Kenmoku T, Honma T, Kobayashi S, Yano T. (2001). Direct biosynthesis of poly (3-hydroxyalkanoates) bearing epoxide groups. *International Journal of Biological Macromolecules.* 29:295–301.

ISO 22196:2011. Plastics - Measurement of antibacterial activity on plastics surfaces. http://www.iso.org/iso/catalogue_detail.htm?csnumber=54431.

Jendrossek D, Handrick R. (2002). Microbial degradation of polyhydroxyalkanoates. *Annu Rev Microbiol*. 56:403–32.

Jendrossek D, Schirmer A, Schlegel HG. (1996). Biodegradation of polyhydroxyalkanoic acids. *Appl Microbiol Biotechnol*. 46:451–63.

Jendrossek D. (2009). Polyhydroxyalkanoate granules are complex subcellular organelles (carbonosomes). *J Bacteriol*. 191:3195–202.

Ji Y, Li XT, Chen GQ. (2008). Interactions between a poly (3-hydroxybutyrate-*co*-3-hydroxyvalerate-*co*-3-hydroxyhexanoate) terpolyester and human keratinocytes. *Biomaterials.* 29:3807–17.

Johnson WCJr. (1988). Secondary structure of proteins through circular dichroism spectroscopy. *Annu Rev Biophys Biophys Chem.* 17:145–66.

Jones NL, Cooper JJ, Waters RD, Williams DF. (2000). Resorption profile and biological response of calcium phosphate filled PLLA and PHB7V in: Synthetic Bioabsorbable Polymers for Implants (Agrawal, C.M., Parr J.E., Lin S.T. eds) Scranton:ASTM 69–82.

Jones RD, Price JC, Stuedemann JA, Bowen JM. (1994). *In vitro* and *in vivo* release of metoclopramide from a subdermal diffusion matrix with potential in preventing fescue toxicosis in cattle. *J. Controlled Release* 30:35–44.

Jung K, Hany R, Rentsch D, Storni T, Egli T, Witholt B. (2000). Characterization of new bacterial copolyesters containing 3-hydroxyoxoalkanoates and acetoxy-3-hydroxyalkanoates. *Macromolecules*. 33:8571–5.

Kadurugamuwa JL, Sin L, Albert E, Yu J, Francis K, DeBoer M, Rubin M, Bellinger-Kawahara C, Parr Jr TR Jr, Contag PR. (2003). Direct continuous method for monitoring biofilm infection in a mouse model. *Infect Immun*. 71:882–90.

Kai Z, Ying D, Guo-Qiang C. (2003). Effects of surface morphology on the biocompatibility of polyhydroxyalkanoates. *Biochemical Engineering Journal*. 16:115–23.

Kalia VC, Chauhan A, Bhattacharyya G, Rashmi. (2003). Genomic databases yield novel bioplastic producers. *Nat Biotechnol*. 21:845–6.

Kaniga K, Delor I, Cornelis GR. (1991). A wide-host-range suicide vector for improving reverse genetics in gram-negative bacteria: inactivation of the *blaA* gene of *Yersinia enterocolitica*. *Gene.* 109:137–41.

Kashiwaya Y, Takeshima T, Mori N, Nakashima K, Clarke K, Veech RL. (2000). D-beta-hydroxybutyrate protects neurons in models of Alzheimer's and Parkinson's disease. *Proc Natl Acad Sci U S A*. 97:5440–4.

Kasinsky H, Lewis J, Dacks J, Ausio J. (2001). Origin of H1 linker histones. *FASEB J.* 15:34–42.

Kassab ACh, Piskin E, Bilgic S, Denkbas EB, Xu K. (1999). Embolization with polyhydroxybutyrate (PHB) microspheres: *In vivo* studies. *J. Bioact. Compat. Polym*. 14:291–303.

Kato J, Tapan M, Chakrabarty AM. (1990). AlgR3, a protein resembling eukaryotic histone H1, regulates alginate synthesis in *Pseudomonas aeruginosa*. *Proc Natl Acad Sci USA.* 87:2887–91.

Kaul R, Allen M, Bradbur EM, Wenman WM. (1996). Sequence specific binding of chlamydial histone H1-like protein. *Nucleic Acid Res.* 24:2981–9.

Kenar H, Kose GT, Hasirci V. (2010). Design of a 3D aligned myocardial tissue construct from biodegradable polyesters. *J Mater Sci Mater Med*. 21:989–97.

Kenawy ER, Abdel-Hay FI, el-Raheem A, el-Shanshoury R, el-Newehy MH. (1998). Biologically active polymers: synthesis and antimicrobial activity of modified glycidyl methacrylate polymers having a quaternary ammonium and phosphonium groups. *J Controlled Release.* 50:145–52.

Kenmoku T, Sugawa E, Yano T, Imamura T. (2002). Polyhydroxyalkanoate with (methylsulfanyl) phenoxy structure in side chain. EP1275727 B1. Priority date: 10.07.2002

Kessler B, de Lorenzo V, Timmis KN. (1992). A general system to integrate *lacZ* fusions into the chromosomes of gram-negative eubacteria: regulation of the *Pm* promoter of the TOL plasmid studied with all controlling elements in monocopy. *Mol Gen Genet*. 233:293–301.

Kiedrowski MR, Horswill AR. (2011). New approaches for treating staphylococcal biofilm infections. *Annals of the New York Academy of Sciences*. 1241:104–21.

Kim DY, Jung SB, Choi GG, Kim YB, Rhee YH. (2001). Biosynthesis of polyhydroxyalkanoate copolyester containing cyclohexyl groups by *Pseudomonas oleovorans*. *International Journal of Biological Macromolecules.* 29:145–50.

Kim DY, Kim HW, Chung MG, Rhee YH. (2007). Biosynthesis, modification, and biodegradation of bacterial medium-chain-length polyhydroxyalkanoates. *Journal of Microbiology.* 45:87–97.

Kim DY, Kim YB, Rhee YH. (1998). Bacterial poly (3-hydroxyalkanoates) bearing carbon-carbon triple bonds. *Macromolecules.* 31:4760–3.

Kim DY, Kim YB, Rhee YH. (2000). Evaluation of various carbon substrates for the biosynthesis of polyhydroxyalkanoates bearing functional groups by *Pseudomonas putida*. *International Journal of Biological Macromolecules*. 28:23–9.

Kim DY, Nam JS, Young HR, Kim YB. (2003). Biosynthesis of novel poly(3-hydroxyalkanoates) containing alkoxy groups by *Pseudomonas oleovorans*. *Journal of Microbiology and Biotechnology*. 13:632–5.

Kim HW, Chung CW, Kim SS, Kim YB, Rhee YH. (2002). Preparation and cell compatibility of acrylamide-grafted poly(3-hydroxyoctanoate). *International Journal of Biological Macromolecules.* 30:129–35.

Kim O, Gross RA, Hammar WJ, Newmark RA. (1996a). Microbial synthesis of poly (β-hydroxyalkanoates) containing fluorinated side-chain substituents. *Macromolecules.* 29:4572–81.

Kim O, Gross RA, Rutherford DR. (1995a). Bioengineering of poly(β-hydroxyalkanoates) for advanced material applications: incorporation of cyano and nitrophenoxy side chain substituents. *Canadian Journal of Microbiology.* 41:32–43.

Kim YB, Kim DY, Rhee YH. (1999). PHAs produced by *Pseudomonas putida* and *Pseudomonas oleovorans* grown with n-alkanoic acids containing aromatic groups. *Macromolecules.* 32:6058–64.

Kim YB, Kim Y, Rhee YH, Han SH, Heo GS, Kim JS. (1996b). Poly-3-hydroxyalkanoates produced from *Pseudomonas oleovorans* grown with ω-phenoxyalkanoates. *Macromolecules.* 29:3432–5.

Kim YB, Lenz RW, Fuller RC. (1991). Preparation and characterization of poly(beta-hydroxyalkanoates) obtained from *Pseudomonas oleovorans* grown with mixtures of 5-phenylvaleric acid and n-alkanoic acids. *Macromolecules.* 24:5256–60.

Kim YB, Lenz RW, Fuller RC. (1992). Poly (β-hydroxyalkanoate) copolymers containing brominated repeating units produced by *Pseudomonas oleovorans*. *Macromolecules.* 25:1852–7.

Kim YB, Lenz RW, Fuller RC. (1995b). Poly-3-Hydroxyalkanoates containing unsaturated repeating units produced by *Pseudomonas oleovorans*. *Journal of Polymer Science Part A: Polymer Chemistry*. 33:1367–74.

Kim YB, Lenz RW. (2001). Polyesters from microorganisms. *Adv Biochem Eng Biotechnol*. 71:51–79.

Kimberly NC, Gitai Z. (2010). Surface association and the MreB cytoskeleton regulate pilus production, localization and function in *Pseudomonas aeruginosa*. *Mol Microbiol.* 76:1411–26.

Klein E, Smith DL, Laxminarayan R. (2009). Community-associated methicillin-resistant *Staphylococcus aureus* in outpatients, United States, 1999-2006. *Emerg Infect Dis.* 15:1925–30.

Kojima M, Morisaki T, Izuhara K, Uchiyama A, Matsunari Y, Katano M, Tanaka M. (2000). Lipopolysaccharide increases cyclo-oxygenase-2 expression in a colon carcinoma cell line through nuclear factor-kB activation. *Oncogene.* 19:1225–31.

Komeili A, Li Z, Newman DK, Jensen GJ. (2006). Magnetosomes are cell membrane invaginations organized by the actin-like protein MamK. *Science*. 311:242–5.

Korkusuz F, Korkusuz P, Ekşioğlu F, Gürsel I, Hasirci V. (2001). *In vivo* response to biodegradable controlled antibiotic release systems. *J Biomed Mater Res*. 55:217–28.

Köse GK, Korkusuz F, Ozkul A, Soysal Y, Ozdemir T, Yildiz C, Hasirici V. (2005). Tissue engineered cartilage on collagen and PHBV matrices. *Biomaterials*. 26:5187–97.

Koyama Y, Katagiri S, Hanai S, Uchida K, Miwa M. (1999). Poly (ADP-ribose) polymerase interacts with novel ribosomal proteins, L22 and L23a, with a unique histone-like amino-terminal extensions. *Gene.* 226:339–45.

Kundu K, Knight SF, Willett N, Lee S, Taylor WR, Murthy N. (2009). Hydrocyanines: a class of fluorescent sensors that can image reactive oxygen species in cell culture, tissue, and *in vivo*. *Angew Chem Int Ed Engl*. 48:299–303.

Kuroda K, Caputo GA. (2013). Antimicrobial polymers as synthetic mimics of host-defense peptides. *WIREs Nanomed Nanobiotechnol*. 5:49–66.

Lageveen RG, Huisman GW, Preusting H, Ketelaar P, Eggink G, Witholt B. (1988). Formation of polyesters by *Pseudomonas oleovorans*: effect of substrates on formation and composition of poly-(*R*)-3-hydroxyalkanoates and poly-(*R*)-3-hydroxyalkenoates. *Applied and Environmental Microbiology.* 54:2924–32.

Langer R, Tirrell DA. (2004). Designing materials for biology and medicine. *Nature*. 428:487–92.

Lee SJ, Park JP, Park TJ, Lee SY, Lee S, Park JK. (2005). Selective immobilization of fusion proteins on poly(hydroxyalkanoate) microbeads. *Anal Chem*. 77:5755–9.

Lee SY, Choi JI, Han K, Song JY. (1999). Removal of endotoxin during purification of poly(3-hydroxybutyrate) from gram-negative bacteria. *Appl. Environ. Microbiol*. 65:2762–4.

Lee SY. (1996). Bacterial polyhydroxyalkanoates. *Biotechnol. Bioeng.* 49:1–14.

Leenstra TS, Maltha JC, Kujpers-Jagtman AM. (1995). Biodegradation of non-porous films after submucoperiosteal implantation on the plate of Baegle dogs*. J. Mater. Sci. Mater. Med.* 6:445–450.

Lemoigne M. (1926). Produits de deshydration et de polymerisation de l'acide b-oxybutyric, *Bull. Soc. Chem. Biol.* 8:770–82.

Lenz RW, Kim YB, Fuller RC. (1992). Production of unusual bacterial polyesters by *Pseudomonas oleovorans* through cometabolism. *FEMS Microbiol Lett.* 103:207–14.

Lewis JG, Rehm BHJ. (2009). ZZ polyester beads: an efficient and simple method for purifying IgG from mouse hybridoma supernatants. *Immunol. Methods*. 346:71–4.

Lienkamp K, Madkour AE, Musante A, Nelson CF, Nusslein K, Tew GN. (2008). Antimicrobial polymers prepared by ROMP with unprecedented selectivity: a molecular construction kit approach. *J Am Chem Soc*. 130:9836–43.

Lin PW, Myers LE, Ray L, Song SC, Nasr TR, Berardinelli AJ, Kundu K, Murthy N, Hansen JM, Neish AS. (2009). *Lactobacillus rhamnosus* blocks inflammatory signaling *in vivo* via reactive oxygen species generation. *Free Radic Biol Med*. 47:1205–11.

Löbler M, Sass M, Michel P, Hopt UT, Kunze C, Schmitz KP. (2002). Differential gene expression after implantation of biomaterials into rat gastrointestione. J*. Mater. Sci. Med.* 10:797–9.

Luengo JM, García B, Sandoval A, Naharro G, Olivera ER. (2003). Bioplastics from microorganisms. *Curr Opin Microbiol*. 6:251–60.

Luklinska ZB, Schluckwerder H. (2003). *In vivo* response to HA-polyhydroxybutyrate/polyhydroxyvalerate composite. *J Microsc*. 211:121–9.

Lütke-Eversloh T, Fischer A, Remminghorst U, Kawada J, Marchessault RH, Bögershausen A, Kalwei M, Eckert H, Reichelt R, Liu S-J, Steinbüchel A. (2002). Biosynthesis of novel thermoplastic polythioesters by engineered *Escherichia coli*. *Nat Mater.* 1:236–40.

Lütke-Eversloh T, Steinbüchel A. (2004). Microbial polythioesters. *Macromol Biosci.* 4:166–74.

Madison LL, Huisman GW. (1999). Metabolic engineering of poly (3-hydroxyalkanoates): from DNA to plastic. *Microbio Mol Biol Rev.* 63:21–53.

Maestro B, Galán B, Alfonso C, Rivas G, Prieto MA, Sanz JM. (2013). A new family of intrinsically disordered proteins: structural characterization of the major phasin PhaF from *Pseudomonas putida* KT2440. *PLoS One*. 8(2):e56904. doi:10.1371/journal.pone.0056904.

Mah TF, O'Toole GA. (2001). Mechanisms of biofilm resistance to antimicrobial agents. *Trends Microbiol*. 9:34–9.

Malm T, Bowald SF, Bylock A, Busch C, Saldeen T. (1994). Enlargement of the right ventricular outflow tract and the pulmonary artery with a new biodegradable patch in transannular position. *Eur Surg. Res*. 26:298–308.

Malm T, Bowald SF, Karacagil S, Bylock A, Busch C. (1992). A new biodegradable patch for closure of arterial septal defect. *Scand. J. Thor. Cardiovasl. Surg*. 26:9–14.

Marois Y, Zhang Z, Vert M, Beaulieu L, Lenz RW, Guidoin R. (1999a). *In vivo* biocompatibility and degradation studies of polyhydroxyoctanoate in the rat: a new sealant for the polyester arterial prosthesis. *Tissue Eng*. 5:369–86.

Marois Y, Zhang Z, Vert M, Deng X, Lenz R, Guidoin R. (1999b). Hydrolytic and enzymatic incubation of polyhydroxyoctanoate (PHO): a short-term *in vitro* study of a degradable bacterial polyester. *J Biomater Sci Polym Ed*. 10:483–99.

Martin DP. Peoples, OP, Williams SF. (2000). Nutritional and therapeutic uses of 3-hydroxy-alkanoate oligomers. PCT Patent Application No WO 00/04895.

Martínez V, García P, García JL, Prieto MA. (2011). Controlled autolysis facilitates the polyhydroxyalkanoate recovery in *Pseudomonas putida* KT2440. *Microbial Biotechnology.* 4:533–47.

Martínez V, de la Peña F, García-Hidalgo J, de la Mata I, García JL, Prieto MA. (2012). Identification and biochemical evidence of a medium-chain-length polyhydroxyalkanoate depolymerase in the *Bdellovibrio bacteriovorus* predatory hydrolytic arsenal. *Appl Environ Microbiol.* 78:6017–26.

Massieu L, Haces ML, Montiel T, Hernández-Fonseca K. (2003). Acetoacetate protects hippocampal neurons against glutamate-mediated neuronal damage during glycolysis inhibition. *Neuroscience*. 120:365–78.

Mauclaire L, Brombacher E, Bünger JD, Zinn M. (2010). Factors controlling bacterial attachment and biofilm formation on medium-chain-length polyhydroxyalkanoates (mcl-PHAs). *Colloids and Surfaces B: Biointerfaces*. 76:104–11.

McCool GJ, Cannon MC. (1999). Polyhydroxyalkanoate inclusion body-associated proteins and coding region in *Bacillus megaterium*. *J Bacteriol.* 181:585–92.

Medvedkin VN, Permyakov EA, Klimenko LV, Mitin YV, Matsushima N, Nakayama S, Kretsinger RH. (1995). Interactions of (Ala*Ala*Lys*Pro)n and (Lys*Lys*Ser*Pro)n with DNA. Proposed coiled-coil structure of AlgR3 and AlgP from *Pseudomonas aeruginosa*. *Protein Eng.* 8:63-70.

Mei N., Zhou P., Pan L. F., Chen G., Wu C. G., Chen X., Shao Z. Z. and Chen G. Q. (2006). Biocompatibility of poly (3-hydroxybutyrate-*co*-3- hydroxyhexanoate) modified by silk fibroin. *Journal of Materials Science: Materials in Medicine*. 17:749–58.

Mermel LA, Allon M, Bouza E, Craven DE, Flynn P, O'Grady NP, Raad II, Rijnders BJ, Sherertz RJ, Warren DK. (2009). Clinical practice guidelines for the diagnosis and management of intravascular catheter-related infection: 2009 Update by the Infectious Diseases Society of America. *Clin Infect Dis*. 49:1–45.

Mermel LA, Farr BM, Sherertz RJ, Raad II, O'Grady N, Harris JS, Craven DE. (2001). Guidelines for the management of intravascular catheter-related infections. *Infect Control Hosp Epidemiol*. 22:222–42.

Merrick JM, Doudoroff M. (1964). Depolymerization of poly-beta-hydroxybutyrate by intracellular enzyme system. *J Bacteriol*. 88:60–71.

Mesak LR, Yim G, Davies J. (2009). Improved lux reporters for use in *Staphylococcus aureus*. *Plasmid*. 61:182–7.

Miller WG, Lindow SE. (1997). An improved GFP cloning cassette designed for prokaryotic transcriptional fusions. *Gene.* 191:149–53.

Mochizuki M, Hirami M. (1997). Structural Effects on the Biodegradation of Aliphatic Polyesters. *Polym. Adv. Techno*l. 8:203–9.

Moldes C, Farinós GP, De Eugenio LI, García P, García JL, Ortego F, Hernández-Crespo P, Castañera P, Prieto MA. (2006). New tool for spreading proteins to the environment: Cry1Ab toxin immobilized to bioplastics. *Appl. Microbiol. Biotechnol.* 72:88–93.

Moldes C, García P, García JL, Prieto MA. (2004). *In vivo* immobilization of fusion proteins on bioplastics by the novel tag BioF. *Appl Environ Microbiol.* 70:3205–12.

Mosahebi A, Fuller P, Wiberg M, Terenghi G. (2002). Effect of allogeneic Schwann cell transplantation on peripheral nerve regeneration. *Exp Neurol*. 173:213–23.

Moscoso M, García E, López R. (2006). Biofilm formation by *Streptococcus pneumoniae*: role of choline, extracellular DNA, and capsular polysaccharide in microbial accretion. *Bacterio*l. 188:7785–95.

Mosmann T. (1983). Rapid colorimetric assay for cellular growth and survival: application to proliferation and cytotoxicity assays. *Journal of Immunological Methods*. 65:55–63.

Nakayama GR, Caton MC, Nova MP, Parandoosh Z. (1997). Assessment of the Alamar Blue assay for cellular growth and viability *in vitro*. *J Immunol Methods*. 204:205–8.

National Research Council. Guide for the care and use of laboratory animals. Committee on Care and Use of Laboratory Animals of the Institute of Laboratory Animal Resources, Commission on Life Sciences. In: United States Department of Health and Human Services PHS, National Institutes of Health, editor. Bethesda, MD: National Research Council; 1985. p. NIH Publication No. 85-23.

Navikov LV, Novikova LN, Mosahebi A, Wiberg M, Terenghi G, Kellerth J-Q. (2002). A novel biodegradable implant for neuronal rescue and regeneration after spinal cord injury. *Biomaterials*. 23:3369–76.

Nelson KE, Weinel C, Paulsen IT, Dodson RJ, Hilbert H, Martins dos Santos VA, Fouts DE, Gill SR, Pop M, Holmes M, Brinkac L, Beanan M, DeBoy RT, Daugherty S, Kolonay J, Madupu R, Nelson W, White O, Peterson J, Khouri H, Hance I, Chris Lee P, Holtzapple E, Scanlan D, Tran K, Moazzez A, Utterback T, Rizzo M, Lee K, Kosack D, Moestl D, Wedler H, Lauber J, Stjepandic D, Hoheisel J, Straetz M, Heim S, Kiewitz C, Eisen JA, Timmis KN, Düsterhöft A, Tümmler B, Fraser CM. (2002). Complete genome sequence and comparative analysis of the metabolically versatile *Pseudomonas putida* KT2440. *Environ Microbiol.* 4:799–808.

Neumann L, Spinozzi F, Sinibaldi R, Rustichelli F, Pötter M, Steinbüchel A. (2008). Binding of the major phasin, PhaP1, from *Ralstonia eutropha* H16 to poly(3-hydroxybutyrate) granules. *J Bacteriol.* 190:2911–9.

Niki H, Yamaichi Y, Hiraga S. (2000). Dynamic organization of chromosomal DNA in *Escherichia coli*. *Genes Dev.* 14:212–23.

Noda I. (1996). Biodegradable copolymers and plastic articles comprising biodegradable copolymers of 3-hydroxyhexanoate. The Procter & Gamble. No US5502116 A.

Nogales J, Palsson BØ, Thiele I. (2008). A genome-scale metabolic reconstruction of *Pseudomonas putida* KT2440: iJN746 as a cell factory. *BMC Syst. Biol*., 2:79. doi: 10.1186/1752-0509-2-79.

O'Grady NP, Alexander M, Burns LA, Dellinger EP, Garland J, Heard SO, Lipsett PA, Masur H, Mermel LA, Pearson ML, Raad II, Randolph AG, Rupp ME, Saint S. (2011). Guidelines for the prevention of intravascular catheter-related infections. *Am J Infect Control*. 39:S1–34.

Olivera ER, Carnicero D, Garcia B, Miñambres B, Moreno MA, Cañedo L, Dirusso CC, Naharro G, Luengo JM. (2001b). Two different pathways are involved in the beta-oxidation of n-alkanoic and n-phenylalkanoic acids in *Pseudomonas putida* U: genetic studies and biotechnological applications. *Mol. Microbiol*. 39:863–74.

Olivera ER, Carnicero D, Jodra R, Miñambres B, García B, Abraham GA, Gallardo A, Román JS, García JL, Naharro G, Luengo JM. (2001a). Genetically engineered *Pseudomonas*: a factory of new bioplastics with broad applications. *Environ Microbiol.* 3:612–18.

Olofsson AC, Hermansson M, Elwing H. (2003). N-acetyl-l-cysteine affects growth, extracellular polysaccharide production, and bacterial biofilm formation on solid surfaces. *Appl Environ Microbiol*. 69:4814–22.

Ouyang SP, Liu Q, Sun SY, Chen JC, Chen GQ. (2007). Genetic engineering of *Pseudomonas putida* KT2442 for biotransformation of aromatic compounds to chiral cis-diols. *J Biotechnol.* 132:246–50.

Park WH, Lenz RW, Goodwin S. (1998). Epoxidation of bacterial polyesters with unsaturated side chains. I. Production and epoxidation of polyesters from 10-undecenoic acid. *Macromolecules.* 31:1480–6.

Parlane NA, Wedlock DN, Buddle BM, Rehm, BH. (2009). Bacterial polyester inclusions engineered to display vaccine candidate antigens for use as a novel class of safe and efficient vaccine delivery agents. *Appl. Environ. Microbiol*. 75:7739–44.

Peoples OP, Sinskey AJ. (1989). Poly-beta-hydroxybutyrate biosynthesis in *Alcaligenes eutrophus* H16. Characterization of the genes encoding beta-ketothiolase and acetoacetyl-CoA reductase. *J Biol Chem.* 264:15293–7.

Perez-Giraldo C, Rodriguez-Benito A, Moran FJ, Hurtado C, Blanco MT, Gomez-Garcia AC. (1997). Influence of N-acetylcysteine on the formation of biofilm by *Staphylococcus epidermidis*. *J Antimicrob Chemother*. 39:643–6.

Peters V, Rehm BH. (2006). *In vivo* enzyme immobilization by use of engineered polyhydroxyalkanoate synthase. *Appl. Environ. Microbiol*. 72:1777–83.

Petsch D, Anspach FB. (2000). Endotoxin removal from protein solutions. *J Biotechnol*. 76:97–119.

Pieper-Fürst U, Madkour MH, Mayer F, Steinbüchel A. (1995). Identification of the region of a 14-kilodalton protein of *Rhodococcus ruber* that is responsible for the binding of this phasin to polyhydroxyalkanoic acid granules. *J Bacteriol.* 177:2513–23.

Poblete-Castro I, Becker J, Dohnt K, dos Santos VM, Wittmann C. (2012a). Industrial biotechnology of *Pseudomonas putida* and related species. *Appl. Microbiol. Biotechnol.* 93:2279–90.

Poblete-Castro I, Binger D, Rodrigues A, Becker J, Martins Dos Santos VA, Wittmann C. (2013). *In-silico*-driven metabolic engineering of *Pseudomonas putida* for enhanced production of poly-hydroxyalkanoates. *Metab. Eng*. 15:113–23.

Poblete-Castro I, Escapa IF, Jäger C, Puchalka J, Lam CM, Schomburg D, Prieto MA, Martins dos Santos VA. (2012b). The metabolic response of *Pseudomonas putida* KT2442 producing high levels of polyhydroxyalkanoate under single- and multiple-nutrient-limited growth: highlights from a multi-level omics approach. *Microb. Cell. Fact*. 11:34 doi:10.1186/1475-2859-11-34.

Pohlmann A, Fricke WF, Reinecke F, Kusian B, Liesegang H, Cramm R, Eitinger T, Ewering C, Pötter M, Schwartz E, Strittmatter A, Voss I, Gottschalk G, Steinbüchel A, Friedrich B, Bowien B. (2006). Genome sequence of the bioplastic-producing "Knallgas" bacterium *Ralstonia eutropha* H16. *Nat Biotechnol.* 24:1257–62.

Popa A, Davidescu CM, Trif R, Ilia G, Iliescu S, Dehelean G. (2003). Study of quaternary 'onium' salts grafted on polymers: antibacterial activity of quaternary phosphonium salts grafted on 'gel-type' styrene-divinylbenzene copolymers. *React Funct Polym*. 55:151–8.

Potter M, Steinbüchel A. (2005). Poly(3-hydroxybutyrate) granule-associated proteins: impacts on poly(3-hydroxybutyrate) synthesis and degradation. *Biomacromolecules.* 6:552–60.

Prieto MA, Bühler B, Jung K, Witholt B, Kessler B. (1999). PhaF, a polyhydroxyalkanoate-granule-associated protein of *Pseudomonas oleovorans* GPo1 involved in the regulatory expression system for *pha* genes. *J Bacteriol.* 181:858–68.

Prieto MA, De Eugenio LI, Galán B, Luengo JM, Witholt B. (2007). Synthesis and degradation of polyhydroxyalkanoates. In: *Pseudomonas*. Springer Netherlands, Dordrecht, pp. 397–428.

Qu XH, Wu Q, Zhang KY, Chen GQ. (2006). *In vivo* studies of PHB-co-HHx based polymers: Biodegradation and tissue reactions. *Biomaterials*. 27:3540–8.

Raafat D, von Bargen K, Haas A, Sahl H-G. (2008). Insights into the mode of action of chitosan as an antibacterial compound. *Appl Environ Microbiol*. 74:3764–73.

Raygada JL, Levine DP. (2009). Managing CA-MRSA Infections: Current and Emerging Options. *Infections in Medicine.* 26:49–58.

Rehm BH. (2006). Genetics and biochemistry of polyhydroxyalkanoate granule self-assembly: The key role of polyester synthases. *Biotechnol Lett.* 28:207–13.

Rehm BH. (2010). Bacterial polymers: biosynthesis, modifications and applications. *Nat Rev Microbiol*. 8:578–92.

Rehm BHA, Steinbüchel A. (1999). Biochemical and genetic analysis of PHA synthases and other proteins required for PHA synthesis. *Int. J. Biol. Macromol*. 25:3–19.

Ren Q, Grubelnik A, Hoerler M, Ruth K, Hartmann R, Felber H, Zinn M. (2005). Bacterial poly(hydroxyalkanoates) as a source of chiral hydroxyalkanoic acids. *Biomacromolecules*. 6:2290–8.

Reusch RN. (2000). Transmembrane ion transport by polyphosphate–poly-(*R*)-3-hydroxybutyrate complexes. *Biochem. Engl. Trans*. 65:280–95.

Reyes-Ortega F, Rodríguez G, Aguilar MR, Lord M, Whitelock J, Stenzel MH, San Román J. (2013). Encapsulation of low molecular weight heparin (bemiparin) into polymeric nanoparticles obtained from cationic block copolymers: properties and cell activity. *J. Mater. Chem*. 1:850–60.

Ritter H, Spee von AG. (1994). Bacterial production of polyesters bearing phenoxy groups in the side chains 1. Poly-3-hydroxyl-5-phenoxypentanoate-*co*-3-hydroxyl-9-phenoxynonanoate from *Pseudomonas oleovorans*. *Macromolecular Chemistry and Physics*. 195:1665–72.

Rouxhet L, Legras R, Schneider YJ. (1998). Interactions between biodegradable polymer, poly(hydroxybutyrate-hydroxyvalerate), proteins and macrophages. *Macromol. Symp*. 130:347–66.

Ruth K, de Roo G, Egli T, Ren Q. (2008). Identification of two acyl-CoA synthetases from *Pseudomonas putida* GPo1: one is located at the surface of polyhydroxyalkanoates granules. *Biomacromolecules*. 9:1652–9.

Ruth K, Grubelnik A, Hartmann R, Egli T, Zinn M, Ren Q. (2007). Efficient production of (*R*)-3-hydroxycarboxylic acids by biotechnological conversion of polyhydroxyalkanoates and their purification. *Biomacromolecules*. 8:279–86.

Ryan WJ, O'Leary ND, O'Mahony M, Dobson ADW. (2013). GacS-Dependent Regulation of Polyhydroxyalkanoate Synthesis in *Pseudomonas putida* CA-3. *Appl. Environ. Microbiol.* 79:1795–802.

Saad B, Ciradelli G, Matter S, Welti M. Uhlschmid GK, Neuenschwander P, Suter UW. (1996a). Characterization of the cell response of cultured macrophages and fibroblasts to particles of short-chain poly[(R)-3-hydroxybutyric acid]. *J Biomed Mater Res.* 30:429–9.

Saad B, Ciradelli G, Matter S, Welti M. Uhlschmid GK, Neuenschwander P, Suter UW. (1996b). Cell response of cultured macrophages, fibroblasts, and co-cultures of Kupffer cells and hepatocytes to particles of short-chain poly[β-3-hydroxybutyric acid]. *J Mater Sci.* 7:56–61.

Saad B, Ciradelli G, Matter S, Welti M. Uhlschmid GK, Neuenschwander P, Suter UW. (1996c). Interactions of osteoblasts and macrophages with biodegradable and highly porous polyesterurethane foam and its degradation products. *J Biomed Mater Res*. 32:355–66.

Saad B, Neuenschwander P, Uhlschmid GK, Suter UW. (1999). New versatile, elastomeric, degradable polymeric materials for medicine. *Intern J Biol Macromol*. 25:293–301.

Sambrook J, Russell DW. (2001). Molecular Cloning*. A Laboratory Manual*. Cold Spring Harbor, NY, USA: CSHL Press.

Sánchez RJ, Schripsema J, da Silva LF, Taciro MK, Pradella JGC, Gomez JGC. (2003). Medium-chain-length polyhydroxyalkanoic acids (PHAmcl) produced by *Pseudomonas putida* IPT 046 from renewable sources. *European Polymer Journal.* 39:1385–94.

Sandoval A, Arias-Barrau E, Bermejo F, Cañedo L, Naharro G, Olivera ER, Luengo JM. (2005). Production of 3-hydroxy-n-phenylalkanoic acids by a genetically engineered strain of *Pseudomonas putida*. *Appl. Microbiol. Biotechnol*. 67:97–105.

Schäfer A, Tauch A, Jäger W, Kalinowski J, Thierbach G. Pühler A. (1994). Small mobilizable multi-purpose cloning vectors derived from the *Escherichia coli* plasmids pK18 and pK19: selection of defined deletions in the chromosome of *Corynebacterium glutamicum*. *Gene.* 145:69–73.

Scheffel A, Gruska M, Faivre D, Linaroudis A, Plitzko JM, Schuler D. (2006). An acidic protein aligns magnetosomes along a filamentous structure in magnetotactic bacteria. *Nature.* 440:110–4.

Schirmer A, Jendrossek D. (1994). Molecular characterization of the extracellular poly(3-hydroxyoctanoic acid) [P(3HO)] depolymerase gene of *Pseudomonas fluorescens* GK13 and of its gene product. *J. Bacteriol.* 176:7065–73.

Schmidt HHW, Kelm M. (1996). Determination of nitrite and nitrate by the Griess reaction. In: Methods in Nitric Oxide Research. Chichester, UK: Wiley; pp. 491–7.

Scholz C, Fuller RC, Lenz RW. (1994b). Growth and polymer incorporation of *Pseudomonas oleovorans* on alkyl esters of heptanoic acid. *Macromolecules*. 27:2886–9.

Scholz C, Wolk S, Lenz RW, Fuller RC. (1994a). Growth and polyester production by *Pseudomonas oleovorans* on branched octanoic acid substrates. *Macromolecules* 27:6358–62.

Scholz C. (2010). Perspectives to produce positively or negatively charged polyhydroxyalkanoic acids. *Appl Microbiol Biotechnol.* 88:829–37.

Schweizer HP, Jump R, Po C. (1997). Structure and gene-polypeptide relationships of the region encoding glycerol diffusion facilitator (*glpF*) and glycerol kinase (*glpk*) of *Pseudomonas aeruginosa*. *Microbiology*. 143:1287–97.

Scopes RK. (1974). Measurement of protein by spectrophotometry at 205 nm. *Anal Biochem.* 59:277-82.

Selvam S, Kundu K, Templeman KL, Murthy N, García AJ. (2011). Minimally invasive, longitudinal monitoring of biomaterial-associated inflammation by fluorescence imaging. *Biomaterials*. 32:7785–92.

Sherris JC. (1990). Staphylococci. In: Medical Microbiology. An Introduction to Infectious Diseases. New York: Elsevier Science Publishing Co., Inc., 1990:275–89.

Shishatskaya EI, Khlusov IA, Volova TG. (2006). A hybrid PHB-hydroxyapatite composite for biomedical application: production, *in vitro* and *in vivo* investigation. *J Biomater Sci Polym Ed.* 17:481–98.

Shishatskaya EI, Voinova ON, Goreva AV, Mogilnaya OA, Volova TG. (2008). Biocompatibility of polyhydroxybutyrate microspheres: *in vitro* and *in vivo* evaluation. *J Mater Sci Mater Med.* 19:2493–502.

Shishatskaya EI, Volova TG, Puzyr AP, Mogilnaya OA, Efremov SN. (2004). Tissue response to the implantation of biodegradable polyhydroxyalkanoate sutures. *Journal of Materials Science: Materials in Medicine*. 6:719–28.

Shum-Tim D, Stock U, Hrkach J, Shinoka T, Lien J, Moses MA, Stamp A, Taylor G, Moran AM, Landis W, Langer R, Vacanti JP, Mayer JE Jr. (1999). Tissue engineering of autologous aorta using a new biodegradable polymer. *Ann Thorac Surg*. 68:2298–304.

Siedenbiedel F, Tiller JC. (2012). Antimicrobial Polymers in Solution and on Surfaces: Overview and Functional Principles. *Polymers*. 4:46–71.

Silva-Queiroz SR, Silva LF, Pradella JG, Pereira EM, Gomez JG. (2009). PHA(MCL) biosynthesis systems in *Pseudomonas aeruginosa* and *Pseudomonas putida* strains show differences on monomer specificities. *J. Biotechnol.* 143:111–8.

Silva-Rocha R, Martínez-García E, Calles B, Chavarría M, Arce-Rodríguez A, de Las Heras A, Páez-Espino AD, Durante-Rodríguez G, Kim J, Nikel PI, Platero R, de Lorenzo V. (2013). The Standard European Vector Architecture (SEVA): a coherent platform for the analysis and deployment of complex prokaryotic phenotypes. *Nucleic Acids Res*., 41:D666–75.

Smyth GK, Speed T. (2003). Normalization of cDNA microarray data. *Methods* 31:265–273.

Smyth GK. (2004). Linear models and empirical Bayes methods for assessing differential expression in microarray experiments. *Stat Appl Genet Mol Biol* 3: Article 3.

Sodian R, Hoerstrup SP, Sperling JS, Daebritz S, Martin DP, Moran AM, Kim BS, Schoen FJ, Vacanti JP, Mayer JE. (2000d). Early *in vivo* experience with tissue-engineered trileaflet heart valves. *Circulation*. 102:22–9.

Sodian R, Hoerstrup SP, Sperling JS, Daebritz SH, Martin DP, Schoen FJ, Vacanti JP, Mayer JE. (2000a). Tissue engineering of heart valves: *in vitro* experiences. *Ann Thorac Surg*. 70:140–4.

Sodian R, Hoerstrup SP, Sperling JS, Martin DP, Daebritz S, Mayer Jr JE, Vacanti JP. (2000b). Evaluation of biodegradable, threedimensional matrices for tissue engineering of heart valves. *ASAIO J.* 46:107–10.

Sodian R, Loebe M, Hein A, Martin DP, Hoerstrup SP, Potapov EV, Hausmann H, Lueth T, Hetzer R. (2002). Application of stereolithography for scaffold fabrication for tissue engineered heart valves. *ASAIO J*. 48:12–6.

Sodian R, Sperling JS, Martin DP, Egozy A, StockU, Mayer Jr JE, Vacanti JP. (2000c). Fabrication of a trileaflet heart valve scaffold from a polyhydroxyalkanoate biopolyester for use in tissue engineering. *Tissue Eng*. 6:183–8.

Sodian R, Sperling JS, Martin DP, Stock U, Mayer JE Jr, Vacanti JP. (1999). Tissue engineering of a trileaflet heart valve-early *in vitro* experiences with a combined polymer. *Tissue Eng.* 5:489–94.

Song JJ, Choi MH, Yoon SC, Huh NE. (2001). Cometabolism of (w-phenylalkanoic acids with butyric acid for efficient production of aromatic polyesters in *Pseudomonas putida* BMOl. *Journal of Microbiology and Biotechnology*. 11:435–42.

Song JJ, Yoon SC. (1996). Biosynthesis of novel aromatic copolyesters from insoluble 11-phenoxyundecanoic acid by *Pseudomonas putida* BM01. *Applied and Environmental Microbiology.* 62:536–44.

Sparks J, Scholz C. (2008). Synthesis and characterization of a cationic poly(β-hydroxyalkanoate). *Biomacromolecules.* 9:2091–6.

Steinbüchel A, Aerts K, Babel W, Follner C, Liebergesell M, Madkour MH, Mayer F, Pieper-Furst U, Pries A, Valentin HE. (1995). Considerations on the structure and

biochemistry of bacterial polyhydroxyalkanoic acid inclusions. *Can J Microbio*. 41:94–105.

Steinbüchel A, Hein S. (2001). Biochemical and molecular basis of microbial synthesis of polyhydroxyalkanoates in microorganisms. *Adv Biochem Eng Biotechnol.* 71:81–123.

Steinbuchel A, Valentin HE. (1995). Diversity of bacterial poly-hydroxyalkanoic acids, *FEMS Microbiol. Lett.* 128:219–28.

Steinbüchel A. (1991). In: Polyhydroxyalkanoic Acids, Macmillan Publishers, pp. 123–213.

Stock UA, Nagashima M, Khalil PN, Nollert GD, Herden T, Sperling JS, Moran A, Lien J, Martin DP, Schoen FJ, Vacanti JP, Mayer Jr JE. (2000). Tissue-engineered valved conduits in the pulmonary circulation. *J Thorac Cardiovasc Surg*. 119:732–40.

Sun J, Dai Z, Zhao Y, Chen GQ. (2007). *In vitro* effect of oligo-hydroxyalkanoates on the growth of mouse fibroblast cell line L929. *Biomaterials.* 28:3896–903.

Takagi Y, Hashii M, Maehara A, Yamane T. (1999). Biosynthesis of polyhydroxyalkanoate with a thiophenoxy side group obtained from *Pseudomonas putida*. *Macromolecules*. 32:8315–18.

Takagi Y, Yasuda R, Maehara A, Yamane T. (2004). Microbial synthesis and characterization of polyhydroxyalkanoates with fluorinated phenoxy side groups from *Pseudomonas putida*. *European Polymer Journal*. 40:1551–7.

Tashiro T. (2001). Antibacterial and Bacterium Adsorbing Macromolecules. *Macromol Mater Eng*. 286:63–87.

Teleman AA, Graumann PL, Lin DC, Grossman AD, Losick R. (1998). Chromosome arrangement within a bacterium. *Curr Biol.* 8:1102–9.

Tian J, Sinskey AJ, Stubbe J. (2005). Kinetic studies of polyhydroxybutyrate granule formation in *Wautersia eutropha* H16 by transmission electron microscopy. *J Bacteriol.* 187:3814–24.

Timm A, Steinbüchel A. (1992). Cloning and molecular analysis of the poly (3-hydroxyalkanoic acid) gene locus of *Pseudomonas aeruginosa* PAO1. *Eur J Biochem.* 209:15–30.

Timofeeva L, Kleshcheva N. (2011). Antimicrobial polymers: mechanism of action, factors of activity, and applications. *Appl Microbiol Biotechnol.* 89:475–492.

Tobin KM, O'Connor KE. (2005). Polyhydroxyalkanoate accumulating diversity of *Pseudomonas* species utilising aromatic hydrocarbons. *FEMS Microbiol. Lett.* 253:111–8.

Tokiwa Y, Calabia BP. (2004). Degradation of microbial polyesters. *Biotechnol Lett*. 26:1181–9.

Tortajada M, da Silva FL, Prieto MA. (2013). Secon-generation functionalized médium-chain-length polyhydroxyalkanoates: the gateway to high-value bioplastic applications. *International Microbiology*. 16:1–15.

Toy KE, Zhou H, Stephanopoulos GN. (2006). High-throughput screen for poly-3-hydroxybutyrate in *Escherichia coli* and *Synechocystis* sp. strain PCC6803. *Appl Environ Microbiol.* 72:3412–17.

Tracy MA, Ward KL, Firouzabadian L, Wang Y, Dong N, Qian R, Zhang Y. (1999). Factors affecting the degradation rate of poly(lactide-*co*-glycolide) microspheres *in vivo* and *in vitro*. *Biomaterials*. 20:1057–62.

Türesin F, Gürsel I, Hasirci V. (2001). Biodegradable polyhydroxyalkanoate implants for osteomyelitis therapy: in vitro antibiotic release. *J. Biomater. Sci. Polym. Ed.* 12:195–207.

Valentin HE, Stuart ES, Fuller RC, Lenz RW, Dennis D. (1998). Investigation of the function of proteins associated to polyhydroxyalkanoate inclusions in *Pseudomonas putida* BMO1. *J Biotechnol*. 64:145–57.

Vaudaux P, Francois P, Lew DP, Waldvogel FA. (2000). Host factors predisposing to and influencing therapy of foreign body infections. In: Infections associated with indwelling medical devices. ASM Press, Washington, D.C. pp. 1–26.

Viollier PH, Thanbichler M, McGrath PT, West L, Meewan M, McAdams HH, Shapiro L. (2004). Rapid and sequential movement of individual chromosomal loci to specific subcellular locations during bacterial DNA replication. *Proc Natl Acad Sci USA.* 101:9257–62.

Wang S-Y, Lan X-Y, Xiao J-H, Yang J-C, Kao Y-T, Chang S-T. (2008c). Antiinflammatory activity of *Lindera erythrocarpa* fruits. *Phytother Res*. 22:213–6.

Wang WY, Wu Q, Chen GQ. (2004a). Attachment, proliferation and differentiation of osteoblasts on random biopolyester poly(3-hydroxybutyrate-*co*-3-hydroxyhexanoate) scaffolds. *Biomaterials.* 25:669–75.

Wang Y, Bian YZ, Wu Q, Chen GQ. (2008b). Evaluation of three-dimensional scaffolds prepared from poly(3-hydroxybutyrate-*co*-3-hydroxyhexanoate) for growth of allogeneic chondrocytes for cartilage repair in rabbits. *Biomaterials.* 29:2858–68.

Wang YW, Mo WK, Yao HL, Wu Q, Chen JC, Chen GQ. (2004b). Biodegradation studies of poly(3-hydroxybutyrate-*co*-3-hydroxyhexanoate). *Polym Degrad Stabil.* 85:815–21.

Wang YW, Yang F, Wu Q, Cheng YC, Peter HF, Chen JC, et al. (2005). Effect of composition of poly(3-hydroxybutyrate-*co*-3-hydroxyhexanoate) on growth of fibroblast and osteoblast. *Biomaterials*. 26:755–61.

Wang Z, Wu H, Chen J, Zhang J, Yao Y, Chen GQ. (2008a). A novel self-cleaving phasin tag for purification of recombinant proteins based on hydrophobic polyhydroxyalkanoate nanoparticles. *Lab Chip*. 8:1957–62.

Waschinski CJ, Herdes V, Schueler F, Tiller JC. (2004). Influence of satellite groups on telechelic antimicrobial functions of polyoxazolines. *Macromol Biosci.*5:149–56.

Waschinski CJ, Tiller JC. (2005). Poly(oxazoline)s with telechelic antimicrobial functions. *Biomacromolecules.*6:235–43.

Wieczorek R, Pries A, Steinbüchel A, Mayer F. (1995). Analysis of a 24-kilodalton protein associated with the polyhydroxyalkanoic acid granules in *Alcaligenes eutrophus*. *J Bacteriol.* 177:2425–35.

Wiggam MI, O'Kane MJ, Harper R, Atkinson AB, Hadden DR, Trimble ER, Bell PM. (1997). Treatment of diabetic ketoacidosis using normalization of blood 3-hydroxy-butyrate concentration as the endpoint of emergency management. *Diabetes Care.* 20:1347–52.

Wiliams SF, Martin DP. (2000). Application of PHAs in Medicine and Pharmacy. In: Biopolymers: Polyesters III Applications and Commercial products. Wiley VCH Germany. pp. 91–127.

Williams SF, Martin DP, Horowitz DM, Peoples OP. (1999). PHA applications: addressing the price performance issue I. Tissue engineering. *International Journal of Biological Macromolecules.* 25:111–21.

Williams SF, Martin DP. (2001). Therapeutic uses of polymers and oligomers comprising gamma-hydroxybutyrate. PCT Patent Applications No 01/19361A1.

Williams SF, Martin DP. (2002). Applications of PHAs in medicine and pharmacy. In: Series of biopolymers in 10 volumes, vol. 4. Wiley/VCY/Verlag. pp.91-121.

Winkler FK, D'Arcy A, Hunziker W. (1990). Structure of human pancreatic lipase. *Nature*. 343:771–4.

Wise DL, Trantolo DJ, Altobelli DE, Yaszemski MJ, Gresser JD, Schwartz ER. (1998). Encyclopaedic Handbook of Biomaterials and Bioengineering, Part A: Materials. New York: Marcel Dekker. 269–304.

Witholt B, Kessler B. (1999). Perspectives of medium chain length poly(hydroxyalkanoates), a versatile set of bacterial bioplastics. *Curr Opin Biotechnol.* 10:279–85.

Worley SD, Sun G. (1996). Biocidal Polymers. *Trends Polym Sci*. 4:364–70.

Xiao XQ, Zhao Y, Chen GQ. (2007). The effect of 3-hydroxybutyrate and its derivatives on the growth of glial cells. *Biomaterials*. 28:3896–903.

Yang YH, Dudoit S, Luu P, Lin DM, Peng V, Ngai J, Speed TP. (2002). Normalization for cDNA microarray data: a robust composite method addressing single and multiple slide systematic variation. *Nucl Acids Res* 30:e15.

Yao YC, Zhan XY, Zhang J, Zou XH, Wang ZH, Xiong YC, Chen J,Chen GQ. (2008). A specific drug targeting system based on polyhydroxyalkanoate granule binding protein PhaP fused with targeted cell ligands. *Biomaterials*. 29:4823–30.

Ye C, Hu P, Ma MX, Xiang Y, Liu RG, Shang XW. (2009). PHB/PHBHHx scaffolds and human adipose-derived stem cells for cartilage tissue engineering. *Biomaterials.* 30:4401–6.

Yücel D, Kose GT, Hasirci V. (2010). Tissue engineered, guided nerve tube consisting of aligned neural stem cells and astrocytes. *Biomacromolecules.* 11:3584–91.

Yuste L, Hervas AB, Canosa I, Tobes R, Jimenez JI, Nogales J, Perez-Perez MM, Santero E, Diaz E, Ramos JL, de Lorenzo V, Rojo F. (2006). Growth phase-dependent expression of the *Pseudomonas putida* KT2440 transcriptional machinery analyzed with a genome-wide DNA microarray. *Environ Microbiol* 8:165–177.

Zasloff M. (2002). Antimicrobial peptides of multicellular organisms. *Nature*. 415:389–95.

Zimmerli W, Lew PD, Waldvogel FA. (1984). Pathogenesis of foreign body infection. Evidence for a local granulocyte defect. *J Clin Invest*. 73:1191–200.

Zimmerli W, Trampuz A, Ochsner PE. (2004). Prosthetic-joint infections. *N Engl J Med*. 351:1645–54.

Zimmerli W, Waldvogel FA, Vaudaux P, Nydegger UE. (1982). Pathogenesis of foreign body infection: description and characteristics of an animal model. *J Infect Dis*. 146:487–97.

Zinn M, Witholt B, Egli T. (2001). Occurrence, synthesis and medical application of bacterial polyhydroxyalkanoate. *Adv Drug Deliv Rev.* 53:5–21.

Zlatanova J, Caiafa P, van Holde K. (2000). Linker histone binding and displacement: versatile mechanism for transcriptional regulation. *FASEB J.* 14:1697–704.

Zou XH, Li HM, Wang S, Leski M, Yao YC, Yang XD, Huang QJ, Chen GQ. (2009). The effect of 3-hydroxybutyrate methyl ester on learning and memory in mice. *Biomaterials*. 30:1532–41.

Annex

MINISTERIO
DE INDUSTRIA, TURISMO
Y COMERCIO

Oficina Española
de Patentes y Marcas

Justificante de presentación electrónica de solicitud de patente

Este documento es un justificante de que se ha recibido una solicitud española de patente por vía electrónica, utilizando la conexión segura de la O.E.P.M. Asimismo, se le ha asignado de forma automática un número de solicitud y una fecha de recepción, conforme al artículo 14.3 del Reglamento para la ejecución de la Ley 11/1986, de 20 de marzo, de Patentes. La fecha de presentación de la solicitud de acuerdo con el art. 22 de la Ley de Patentes, le será comunicada posteriormente.

Número de solicitud:	P201330821	
Fecha de recepción:	04 junio 2013, 16:03 (CEST)	
Oficina receptora:	OEPM Madrid	
Su referencia:	ES1641.875	
Solicitante:	CONSEJO SUPERIOR DE INVESTIGACIONES CIENTÍFICAS (CSIC)	
Número de solicitantes:	1	
País:	ES	
Título:	USO DE POLIHIDROXIACILTIOALCANOATOS COMO BACTERICIDAS	
Documentos enviados:	Descripcion-1.pdf (28 p.) Reivindicaciones-1.pdf (3 p.) Dibujos-1.pdf (2 p.) Resumen-1.pdf (1 p.) OLF-ARCHIVE.zip FEERCPT-1.pdf (1 p.)	package-data.xml es-request.xml application-body.xml es-fee-sheet.xml feesheet.pdf request.pdf
Enviados por:	CN=ENTIDAD PONS CONSULTORES DE PROPIEDAD INDUSTRIAL SA - CIF A28750891 - NOMBRE PONS ARIÑO ANGEL - NIF 50534279J,OU=703015345,OU=fnmt clase 2 ca,O=FNMT,C=es	
Fecha y hora de recepción:	04 junio 2013, 16:03 (CEST)	
Codificación del envío:	CF:0E:3E:DC:DD:7C:7B:0E:BB:DF:50:BF:32:A2:B2:D2:00:5F:6A:6F	

/Madrid, Oficina Receptora/

Molecular Microbiology (2011) 79(2), 402–418 ■
doi:10.1111/j.1365-2958.2010.07450.x
First published online 16 November 2010

Nucleoid-associated PhaF phasin drives intracellular location and segregation of polyhydroxyalkanoate granules in *Pseudomonas putida* KT2442

B. Galán,[1] N. Dinjaski,[1] B. Maestro,[2] L. I. de Eugenio,[1] I. F. Escapa,[1] J. M. Sanz,[3] J. L. García[1] and M. A. Prieto[1]*

[1]*Department of Environmental Biology, Centro de Investigaciones Biológicas, CSIC, C/Ramiro de Maeztu, 9, 28040 Madrid, Spain.*
[2]*Instituto Universitario de Electroquímica, Universidad de Alicante, 03080- Alicante, Spain.*
[3]*Instituto de Biología Molecular y Celular, Universidad Miguel Hernández, 03202-Elche, Spain.*

Summary

The PhaF is a nucleoid-associated like protein of *Pseudomonas putida* KT2442 involved in the polyhydroxyalkanoate (PHA) metabolism. Its primary structure shows two modular domains; the N-terminal PHA granule-binding domain (phasin domain) and the C-terminal half containing AAKP-like tandem repeats characteristic of the histone H1 family. Although the PhaF binding to PHA granules and its role as transcriptional regulator have been previously demonstrated, the cell physiology meaning of these properties remains unknown. This work demonstrates that PhaF plays a crucial role in granule localization within the cell. TEM and flow cytometry studies of cells producing granules at early growth stage demonstrated that PhaF directs the PHA granules to the centre of the cells, forming a characteristic needle array. Our studies demonstrated the existence of two markedly different cell populations in the strain lacking PhaF protein, i.e. cells with and without PHA. Complementation studies definitively demonstrated a key role of PhaF in granule segregation during the cell division ensuring the equal distribution of granules between daughter cells. *In vitro* studies showed that PhaF binds DNA through its C-terminal domain in a non-specific manner. All these findings suggested a main role of PhaF in PHA apparatus through interactions with the segregating chromosome.

Accepted 28 October, 2010. *For correspondence. E-mail auxi@cib.csic.es; Tel. (+34) 918373112; Fax (+34) 915360432.

Introduction

Many proteins like histone H1 have the ability to bind to a variety of DNA sequences, the recognition of which depends on some general rather than specific features of the DNA molecule (Bustin *et al*., 2005). The eukaryotic histone H1 is involved in the condensation of chromatin and in blocking access to nucleosomal DNA (Zlatanova *et al*., 2000; Kasinsky *et al*., 2001). This is achieved mainly by the electrostatic neutralization of the negative charges on the linker DNA connecting adjacent nucleosomes. Consequently, these proteins show a positively charged DNA-binding region built up from four to five amino acid stretches with high content of lysine and alanine residues usually interspersed by a proline residue, resulting in a proline-kinked AK α-helix organization which is referred to as the AKP helix (Kasinsky *et al*., 2001). This motif appears to have compositional similarity to some of the histone H1-like proteins from bacteria. The best-characterized members of this group of prokaryotic proteins are probably AlgP and AlgR3 from *Pseudomonas aeruginosa* strain PAO and *P. aeruginosa* strain 8882 respectively (Deretic and Konyecsni, 1990; Kato *et al*., 1990; Deretic *et al*., 1992). These two homologous proteins are known to participate in the full transcriptional activation of the *algD* gene encoding the key biosynthetic enzyme guanosine diphospho-D-mannose dehydrogenase and contain 45 and 40 repeat units of the consensus AAKP tetrapeptide (interspersed with AAKTA pentapeptide) sequences in their C-terminal domain respectively (Medvedkin *et al*., 1995).

A prokaryotic protein containing this AKP helix region within its sequence is the PhaF phasin from *Pseudomonas* species (Timm and Steinbüchel, 1992; Valentin *et al*., 1998; Prieto *et al*., 1999; Moldes *et al*., 2004) (Fig. 1). According to primary structure analyses, PhaF is organized in two domains: (i) the highly positive charged histone like domain at C-terminal half, containing eight AAKP-like tandem repeats, and (ii) the N-terminal part that share sequence similarity with the rest of the phasin family (Prieto *et al*., 1999; Moldes *et al*., 2004). Phasins are located on the surface of the bacterial polyhydroxyalkanoate (PHA) granules, bacterial polyesters accumulated

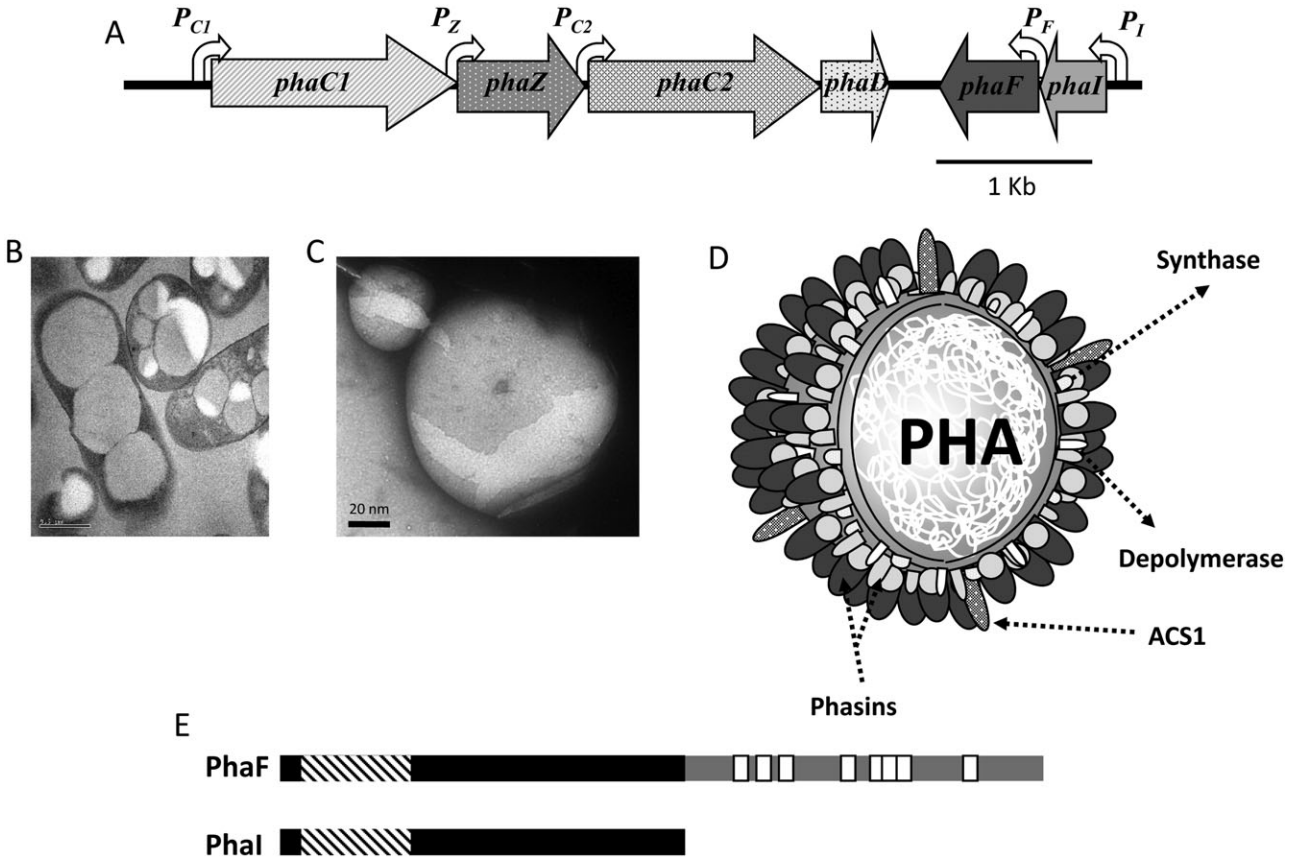

Fig. 1. *pha* gene cluster organization, granule structure and scheme of phasins domains in *P. putida* KT2442.
A. Genetic organization of *pha* cluster, in *P. putida* KT2442. The open arrows indicate the directions of gene transcription. The *phaC1* and *phaC2* genes encode two synthases and are separated by the *phaZ* gene that encodes an intracellular depolymerase. *phaD* gene encodes a transcriptional regulator. *phaF* and *phaI* genes code for phasins. Promoter regions are indicated as curved white arrows.
B. TEM image of mcl-PHA-producing cells of *P. putida* KT2442.
C. TEM image of a PHA granule from *P. putida* KT2442.
D. Model of PHA granule structure. Granules are composed of PHA coated by a monolayer of phospholipids and granule associated proteins (GAPs). The most abundant GAPs are phasins. Polymerases (or synthases), depolymerases and acyl CoA synthetase (ACS1) are also associated to the granule.
E. Domain architecture of the phasins PhaF and PhaI. The N-terminal domain of PhaF is similar to PhaI protein. Hatched and white boxes indicate the putative granule binding sites and the AAKP repeated motifs respectively.

in the cytoplasm as reserve storage granules that are believed to play a role as sink for carbon and reducing equivalents when other nutrients are limited (Madison and Huisman, 1999; Steinbüchel and Hein, 2001; Moldes *et al*., 2004; O'Leary *et al*., 2005). Phasins are thought to generate an interphase between the cytoplasm and the hydrophobic core of PHA granules, preventing them from coalescence (Steinbüchel *et al*., 1995). They also play a role in controlling the size and the number of the granules per cell (Pieper-Fürst *et al*., 1995; Wieczorek *et al*., 1995; Grage *et al*., 2009). In the case of medium-chain-length PHA (mcl-PHA) granules from pseudomonads, formed by hydroxyalkanoic acid monomers consisting of 6–14 carbon atoms, two phasins PhaF and PhaI have been identified as the major granule-associated proteins (Prieto *et al*., 1999). The PhaF N-terminal domain shows 57% of similarity to the complete amino acid sequence of the protein PhaI (Fig. 1E) and it is responsible for the granule binding (Moldes *et al*., 2004). Previous studies performed in *Pseudomonas putida* GPo1 (formerly *Pseudomonas oleovorans* GPo1) demonstrated a bi-functional role for the PhaF protein, as phasin, showing structural function linked to the N-terminal domain (Moldes *et al*., 2004), and as transcriptional regulator, a function very likely related to the histone-like C-terminal domain but not demonstrated yet (Prieto *et al*., 1999). PhaF minus mutants showed increased *pha* cluster transcription rate when cells were cultured in batch fermentation, while PHA content remained unaltered. However, in continuous culture, that is, when cell division and PHA formation occurred simultaneously, the lack of PhaF phasin affected considerably the PHA content of the cells (Prieto *et al*., 1999).

In this work a functional analysis was performed to investigate the role of phasin PhaF in the PHA metabolism, cell physiology and transcriptional regulation of the *pha* genes in the model mcl-PHA producer strain *P. putida* KT2442. Moreover, we demonstrate that PhaF binds DNA unspecifically and it plays a role in the equal distribution of PHA granules between daughter cells during cell division.

Results

PhaF affects heterogeneity of the cell population concerning the PHA production

Previous results from our laboratory showed that the total PHA content of a PhaF mutant strain of *P. putida* GPo1 was reduced considerably in comparison with that of wild-type strain when the PHA content was studied in cell dividing continuous culture (Prieto *et al*., 1999). Based on this observation, we focus our interest in studying the PHA production not only at stationary phase but throughout the growth curve to analyse PhaF-dependent variation in terms of PHA content in all fermentation stages. With this aim, the *phaF* gene of the prototype PHA producer strain *P. putida* KT2442 was deleted by using a suicide vector (see *Experimental procedures*). The PHA production abilities of the resulting strain *P. putida* KT42F was compared with that of the wild-type bacterium when cultured in optimal PHA production conditions. To monitor the PHA content at every stage of the growth curve, a fast and accurate method for analysis of PHA content by flow cytometry was adapted in this work for *Pseudomonas* strains based on a method described previously (Toy *et al*., 2006) (see *Experimental procedures* for details) (Fig. 2).

Cells from *P. putida* KT2442 and its *phaF*-disrupted mutant strain KT42F were harvested from the culture at different growth times. Figure 2A shows that at the early exponential phase of growth (2 h and 4 h), wild-type and mutant strains showed similar PHA content, around 10% and 20% of cell dry weight (CDW) respectively. After 6 h of growth the total PHA content detected in the wild-type strain KT2442 was slightly higher than that of the mutant strain KT42F. This difference increased over the growth curve, being maximal (1.5-fold) after 24 h of growing (Fig. 2A). This result demonstrates that PhaF is not essential for the synthesis of PHA in *P. putida* KT2442 but contributes to optimize the yield of PHA synthesis and accumulation.

Besides, flow cytometry analyses allow us to relate the total PHA content of the cell population versus the PHA content of individual cells (heterogeneity of the population). Figure 2B shows an example of a histogram of KT42F and wild-type cells after 7 h of growing. A major overlay corresponding to positive fluorescent cells was detected in the wild-type cells (Fig. 2B), demonstrating a homogeneous population regarding the PHA granules content. Interestingly, two main overlays showing different fluorescence intensities (Fig. 2B) were detected in the KT42F sample. In this case, only 55% of cell population displayed positive PHA content while the rest of the cells were negative, suggesting that they did not contain PHA granules (Fig. 2C). These results demonstrated the presence of at least two different cell populations in terms of PHA content in the KT42F cultures suggesting a role of PhaF in PHA granules partition during cell division.

Role of PhaF on granule location and segregation during cell division

To monitor the presence of the PHA granules during cell division at early growth phase and the influence of the PhaF protein on the PHA content, samples from wild-type and KT42F mutant strains were taken at different growth times for TEM analysis (Figs 3 and 4). Interestingly, cells at time zero, that is, LB-grown cells used to inoculate the cultures (see *Experimental procedures*), contain a few and small granules of PHA which constitute less than 1% of the CDW (Figs 3A and 4A). In perfect correlation with the PHA content (Fig. 2A), the size and number of the PHA granules in the wild-type cells increased progressively during the growth curve being maximal at 24 h of growing (Fig. 3). Most of the cells contained five to six granules of about 500 nm of diameter (Fig. 5). The number and average size of the granules in the KT42F mutant are decreased when compared with those of the wild-type strain (Fig. 5). These results confirmed those obtained by flow cytometry, which showed a remarkable heterogeneity on the total population in the KT42F culture in terms of PHA content and the presence of PHA empty cells when PhaF protein is not produced.

TEM studies also provided additional information about granule distribution in the cell, and we observed that after 2 h and 4 h of growing, granules were detected in the wild type at the centre of the cross-section of the majority of the cells, i.e. located running lengthwise the cell, forming a characteristic needle array (Fig. 3B, C and F). This distribution was less evident when the accumulation of PHA was close to the 50% CDW after 6 h of growing (Fig. 3D and E). In contrast, the granules in the KT42F mutant strain were agglomerated (Fig. 4B, C and F) at the early times (2 h and 4 h) in one of the cell poles. In agreement with the results observed by flow cytometry (Fig. 2), the PHA content of the mutant was similar to that of the wild-type strain at the earliest stages of growth (Fig. 4B, C and F). Moreover, at 24 h of growth 34% of mutant cells did not contain PHA granules generating two markedly different cell populations in the culture, i.e. with and without PHA (Figs 2B and 4E). While wild-type strain

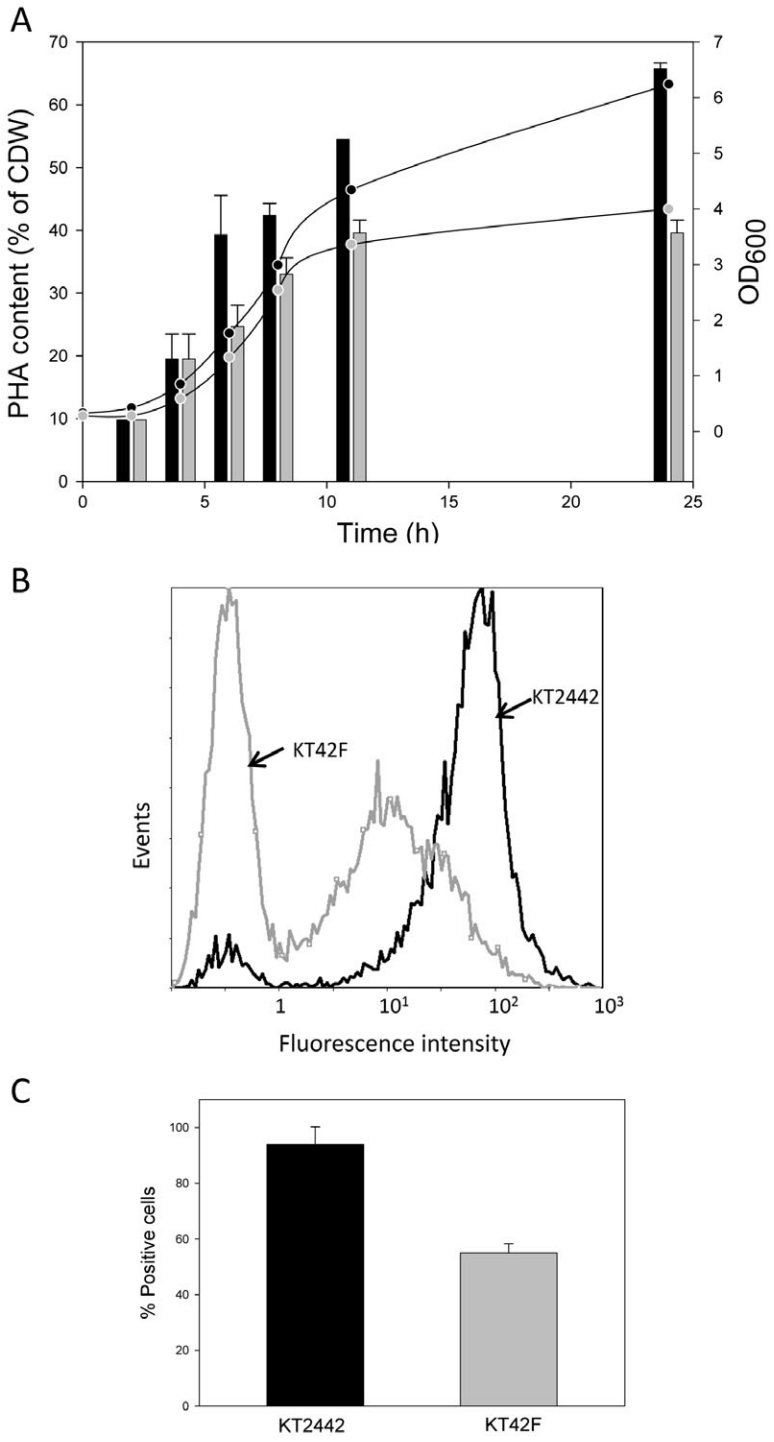

Fig. 2. Study of cell population heterogeneity in terms of PHA production by flow cytometer.
A. Quantification of PHA content (bars) and OD_{600} (circles) of *P. putida* KT2442 (black bars and black circles) and KT42F (grey bars and grey circles) strains throughout the growth curve.
B. Example of a flow cytometer histogram of the *P. putida* KT2442 (black plot) and the *P. putida* KT42F (grey plot) strains grown in PHA production medium during 7 h (see *Experimental procedures* for details).
C. Percentage of PHA-positive cells KT2442 (black column) and KT42F (grey column).

distributed the previously formed PHA granules among the daughter cells keeping the needle array structure, the PHA granules in the PhaF mutant strain remained agglomerated in one of the daughter cells (Fig. 6). It is worth noting that granules did not coalesce in a single big granule, as reported for other microorganism lacking phasins (Wieczorek *et al.*, 1995), very likely due to the presence of the other phasin PhaI (data not shown). On the other hand, *P. putida* KT42F cells were complemented by *in trans* production of PhaF from *P. putida* GPo1 giving rise to *P. putida* KT42F-F strain (see *Experimental procedures* for details) (Fig. 6). These results demonstrated that the presence of PhaF ensures the segregation of the PHA granules during the cell division. Moreover, we have

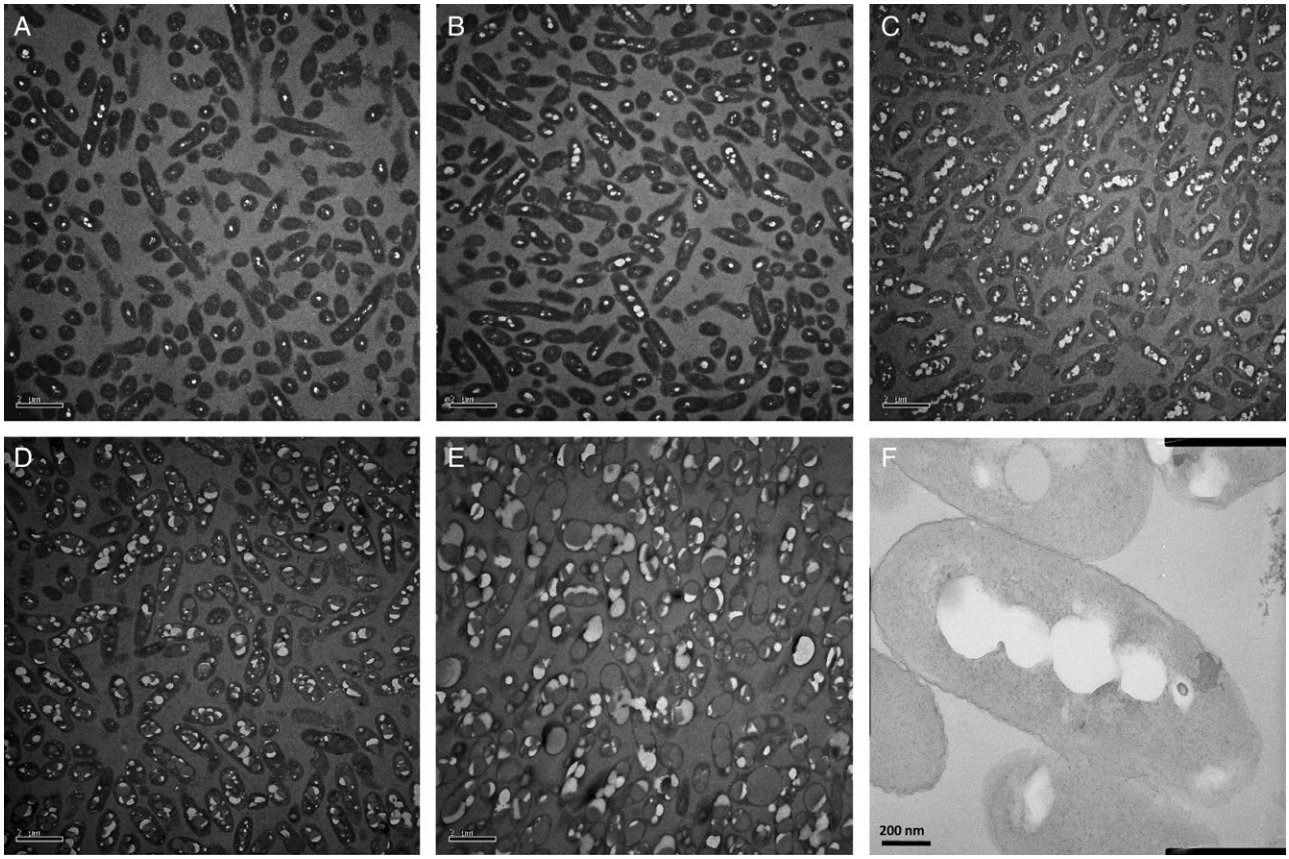

Fig. 3. TEM images of *P. putida* KT2442 cells harvested at different time points during growth in PHA production medium.
A–E. Samples were taken 0, 2, 4, 6 and 24 h after inoculating (A, B, C, D and E respectively) and processed as described in *Experimental procedures*.
F. Detail of the granule distribution of a single cell from a 4 h culture in PHA production medium.

confirmed that *P. putida* cells lacking exclusively the C-terminal half of the PhaF protein (Moldes *et al*., 2004) showed similar phenotype in terms of PHA to that of KT42F (Moldes, 2003). In addition, these results explain the reduction of the total PHA content at 24 h in the mutant strain (Fig. 2) by a dilution effect due to the presence of PHA empty cells.

DNA-binding abilities of PhaF protein and its role as transcriptional regulator

The involvement of PhaF in the *pha* transcriptional regulatory system was first demonstrated in *P. putida* GPo1 (Prieto *et al*., 1999). Disruption of the *phaF* gene led to an increased expression rate of *phaC1* gene, suggesting that PhaF acted as a negative regulator of the *pha* cluster in this strain. This function was ascribed to its C-terminal half due to the similarity observed to histone-like proteins, but there was no evidence pointing to direct binding of PhaF to the *pha* promoter regions so far.

Five different promoter regions were recently determined as part of the *pha* cluster in *P. putida* KT2442 (Fig. 1A), being P_{C1} and P_I the most active promoters of the gene cluster. P_{C1} and P_I direct the transcription of *phaC1ZC2D* and *phaIF* operons respectively (Fig. 1A) (de Eugenio *et al*., 2010a). These promoters are carbon source-dependent controlled by the PhaD regulator, which activates the transcription when fatty acids were present in the culture medium. To check whether PhaF affects the expression profile of the *pha* cluster in this model strain, the transcription rate of *phaC1, phaF* and *phaI* genes was monitored in the mutant KT42F and the wild-type strains by real-time RT-PCR. Both strains were cultured in octanoic acid or glucose as preferred or poor PHA precursors respectively (see *Experimental procedures* for details).

Transcription of *phaC1* and *phaI* genes reaches its maximum level in the wild-type strain after 8 h of culturing in the presence of octanoic acid (Fig. 7). When *phaF* was disrupted, the transcription level of *phaC1* was decreased approximately 3.5-fold respect to wild type, confirming that the lack of PhaF protein affects the transcription control of the *phaC1ZC2D* operon (Fig. 7). The expression profile of *phaI* gene was also significantly altered

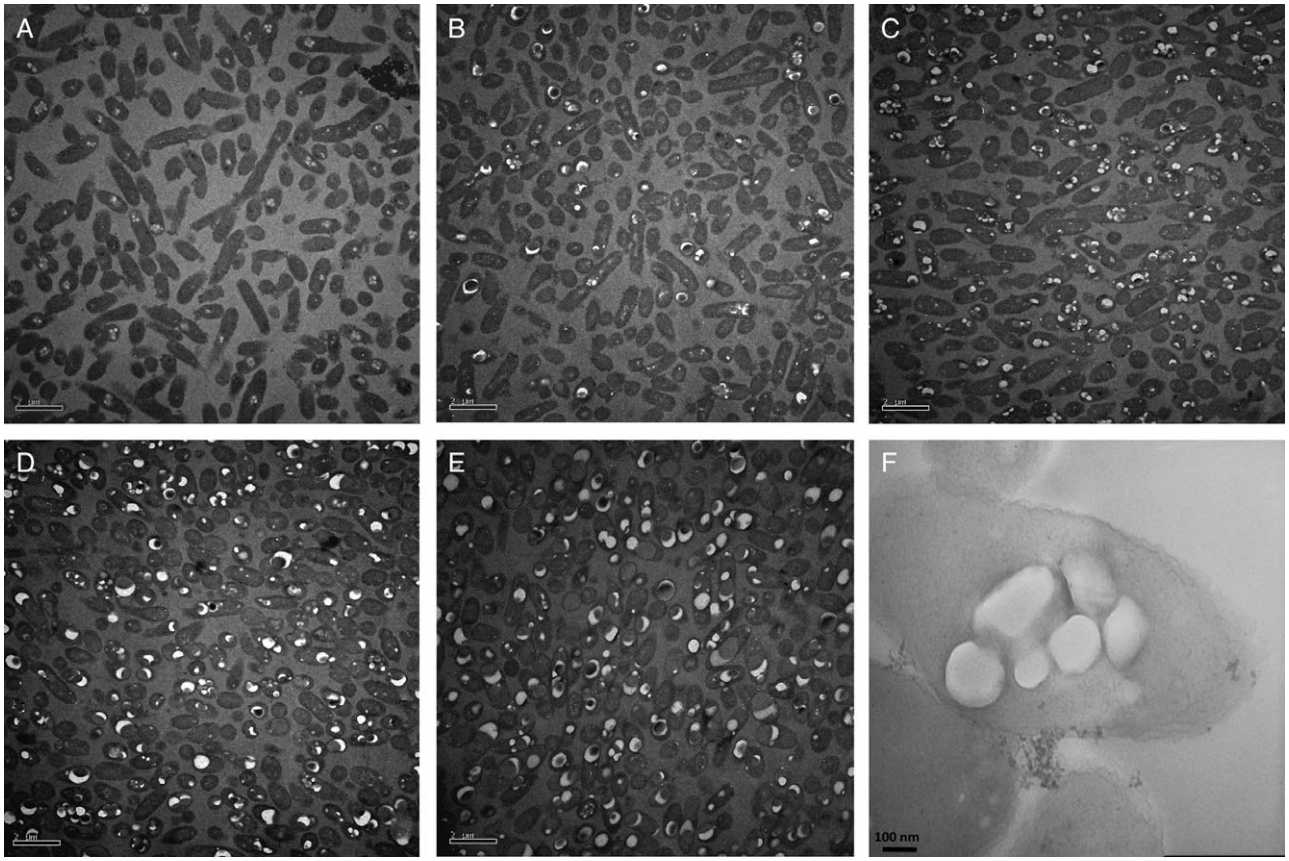

Fig. 4. TEM images of *P. putida* KT42F cells harvested at different time points during growth in PHA production medium.
A–E. Samples were taken 0, 2, 4, 6 and 24 h after the inoculum (A, B, C, D and E respectively) and processed as described in *Experimental procedures*.
F. Detail of the granule distribution of a single cell from a 4 h culture in PHA production medium.

in the mutant strain. While in the wild-type strain the maximum transcriptional level is reached in the mid-exponential phase, in the mutant strain lacking PhaF the highest transcriptional level is reached in the stationary phase (Fig. 7). The production of the PhaI phasin in the KT42F mutant strain was confirmed by SDS-PAGE analysis of the PHA granule fraction (data not shown). These results confirm that the lack of PhaF altered the transcription rate of the *pha* genes.

Taking into account the results presented above we cannot discard the possibility that PhaF, similarly to other nucleoid-associated proteins, would exert a global pleiotropic effect in other unrelated *pha* genes. The application of microarray technology has allowed us to determine the genes that are altered in the mutant strain. A total of 18 genes were significantly upregulated (2- to 9.2-fold) and 39 were downregulated (–1.9- to –27-fold) (Table S1). This result confirms that the absence of the PhaF protein affects the expression of other genes unrelated to the *pha* cluster.

The specificity of the PhaF binding to P_{C1} and P_I promoter regions was also analysed by gel retardation assays. Three different fragments were used as DNA probes: PC1 (266 bp), PI (441 bp) and PF (219 bp) covering the entire *phaC1*, *phaI* and *phaF* upstream regions respectively (Fig. 1). Purified PhaF protein was able to bind the three DNA fragments in a protein concentration-dependent manner (Fig. 8A–C). However, when 6000-fold excess amount of an unrelated DNA, such as that of salmon sperm, was added to the reaction mixture, migration of the labelled fragment was not retarded in any of the three DNA fragments tested. Similar results were obtained when unlabelled PI probe was added (Fig. 8D). These results indicated that binding of PhaF protein to DNA was not specific, i.e. it is independent of the recognition of a specific operator DNA sequence.

Binding of DNA to PhaF was also assessed by spectroscopical techniques. Near-UV circular dichroism experiments (CD) were performed with a 31-mer non-specific DNA fragment (nspDNA) that contains a sequence completely unrelated to the *pha* DNA regions. Figure 9A shows that the experimental wavelength spectrum registered for a 1:1 mixture of the whole PhaF and nspDNA differs from the theoretical sum of protein and DNA

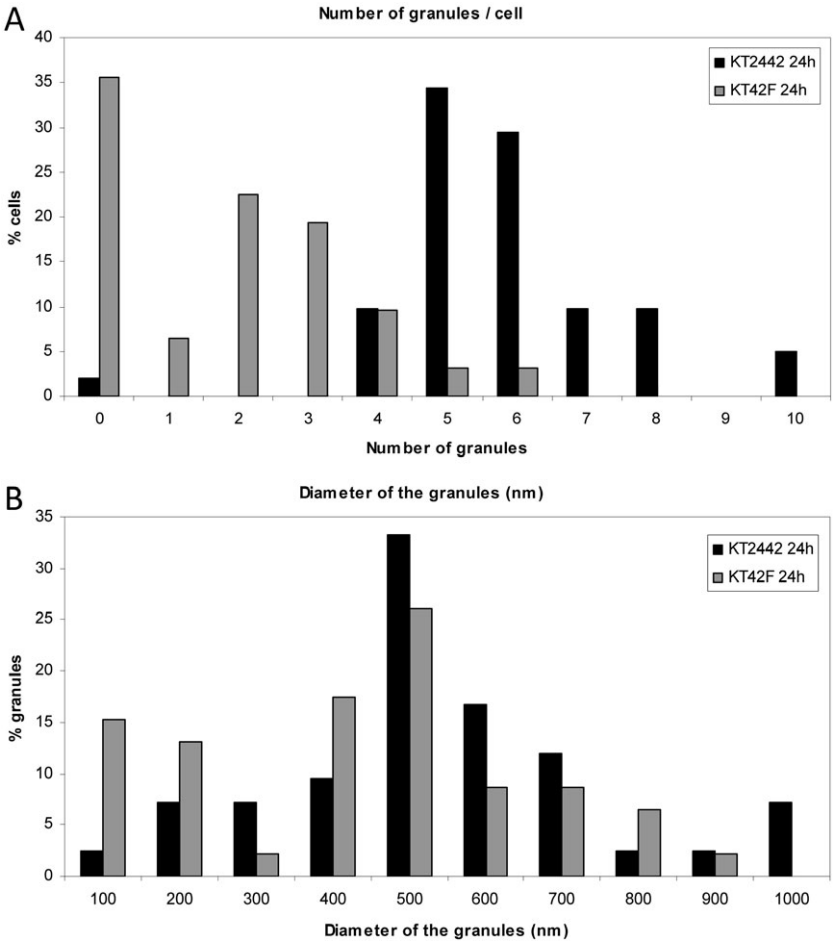

Fig. 5. Determination of granule size and number in KT2442 and KT42F strains of *P. putida*. The granule number (A) and granule size distributions (B) in KT2442 (black bars) and KT42F (grey bars) were determined by TEM images analysis as described in *Experimental procedures*.

spectra recorded separately, especially in the 260–290 nm region. This suggests the formation of a DNA–protein complex that may affect to the environment of the bases in the nucleic acid. In order to corroborate this hypothesis, the stability of the nspDNA fragment in the presence or absence of PhaF was assessed by CD-monitored thermal denaturation experiments (Fig. 9B). To exclusively check the DNA signal, we followed the ellipticity at 244 nm, a wavelength where proteins barely display an appreciable signal (Johnson, 1988). In the absence of protein, a sigmoidal transition with a melting temperature (t_m) of 54.1 ± 0.2°C was observed, whereas addition of an equimolar concentration of PhaF protein induced a significant increase in the thermal stability of the nspDNA fragment (t_m = 63.9 ± 0.2°C). To check the involvement of the PhaF C-terminal moiety in the DNA-binding properties, we expressed and purified independently this polypeptide sequence (C-PhaF) as described in *Experimental procedures*, and checked its DNA-binding capabilities by CD. Remarkably enough, the C-PhaF protein was also able to bind the nspDNA oligomer (Fig. 9), inducing a thermal stabilization of the latter comparable to that produced by full-length PhaF (t_m = 60.6 ± 0.2°C). Therefore, these results would confirm that PhaF binds *in vitro* to DNA through its C-terminal domain in a non-specific manner.

To confirm these findings *in vivo*, we have constructed a fusion protein between the reporter green fluorescent protein (GFP) and the DNA-binding domain of the protein PhaF (C-PhaF) (see *Experimental procedures*). The strains KT42-GC and KT42F-GC expressing GFP::C-PhaF fusion protein in *P. putida* KT2442 and *P. putida* KT42F, respectively, have been used to analyse the localization *in vivo* of the GFP::C-PhaF fusion protein by confocal microscopy (Fig. S1). By staining the cells with two different dyes, we have analysed the *in vivo* localization of (i) the PHA granules (Nile Red-stained), (ii) the nucleoid (DAPI-stained) and (iii) the protein GFP::C-PhaF. Our results confirm the colocalization of the fusion protein GFP::C-PhaF and nucleoid in wild-type and PhaF minus cells, independently of the presence or absence of the PHA granules. Furthermore, PHA granules produced in the wild-type cells, which contain native PhaF protein, colocalized with the nucleoid and GFP reporter. However, PHA granules produced in the KT42F mutant strain localized independently of the nucleoid and GFP reporter

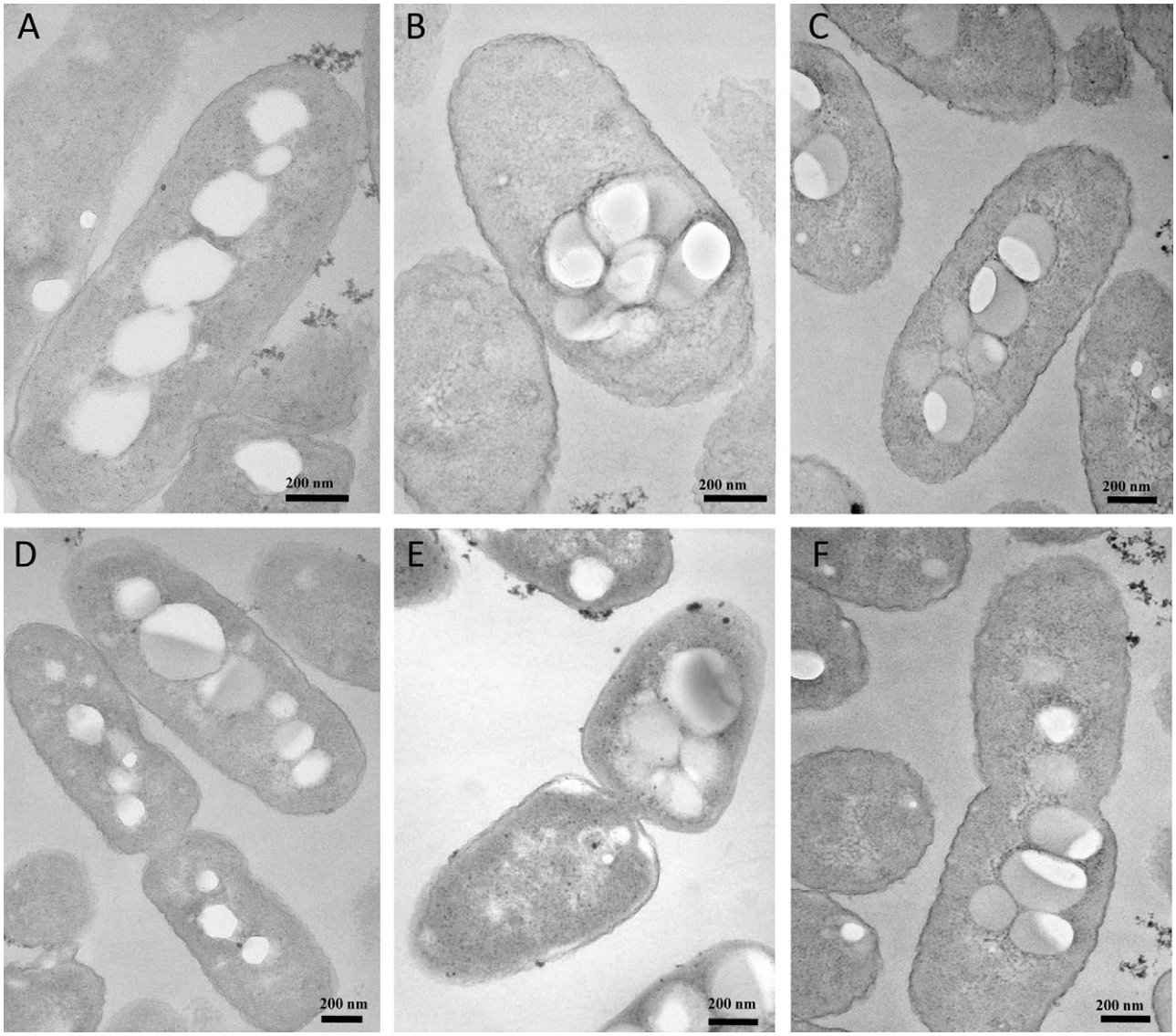

Fig. 6. Analysis of the *P. putida* KT42F complementation and PHA segregation by TEM.
A–C. Samples were taken after 4 h growth in PHA production medium. Detail of the PHA granule distribution of KT2442 (A), KT42F (B) and the complemented strain KT42F-F (C).
D–F. Segregation of PHA granules during cell division in KT2442 (D), KT42F (E) and KT42F-F (F).

system. These results provide support to the role of PhaF as nucleoid-binding protein and its function in the intracellular localization of the PHA granule.

Discussion

Phasins have been described as amphiphilic proteins which generate an interphase between the cytoplasm and the hydrophobic core of PHA granules (Steinbüchel *et al*., 1995). They are widespread among bacteria, sharing similar functions but differing in their primary structures (Grage *et al*., 2009). Generally, they consist of a hydrophobic domain which associates with the surface of the PHA granules and a hydrophilic domain which is exposed to the cytoplasm. The amphiphilic layer stabilizes the PHA granules and prevents them from coalescing (Wieczorek *et al*., 1995). Other functions proposed for phasins are: to control the number and surface of granules, to protect the host cell by contributing to coverage of the hydrophobic surface of the polymer, to prevent protein misfolding on the hydrophobic granule (Steinbüchel *et al*., 1995) or to serve as a storage source of nitrogen (McCool and Cannon, 1999). However, the role of phasins in granules formation is not understood yet (Rehm, 2006). Two models of polyhydroxybutyrate (PHB) granule formation have been described in bacteria, the micelle model and

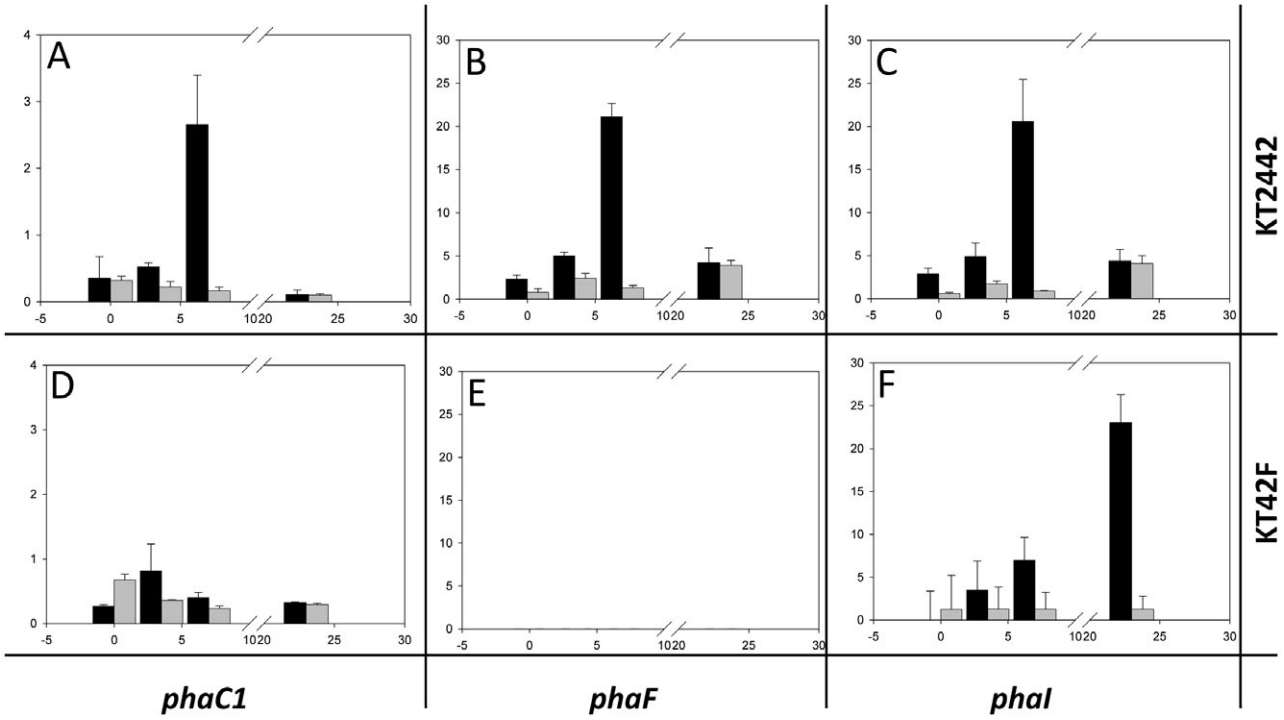

Fig. 7. Effect of the PhaF production on the expression rates of the *pha* genes. Real-time RT-PCR quantification of the *pha* genes transcription profiles throughout growth of *P. putida* KT2442 (A–C) and *P. putida* KT42F (D–F) cultured in M63 0.1 N plus 15 mM sodium octanoate (black bars) or 20 mM glucose (grey bars). An initial concentration of 5 ng of cDNA was used for quantitative RT-PCR. Error bars represent standard deviation calculated from the results of three independent experiments. *y*-axis: transcription level (cDNA ng); *x*-axis: time of culture (hours). Samples along the growth curve were taken at 0, 3.5, 7 and 23 h. The transcription of *phaC1* (A and D), *phaF* (B and E) and *phaI* (C and F) genes is depicted.

the budding model, both accounting for the stabilized location of the synthase and phasin on the surface of the granule (revised in Grage *et al*., 2009). In the micelle model, a self-assembly process is initiated resulting in the formation of insoluble cytoplasmic inclusions with a phospholipid monolayer which contains covalently attached polyester synthases at the surface. In the budding model, the hydrophobic synthase binds to the inner face of the plasma membrane and buds from this membrane, leading to a granule surface covered with a lipid monolayer and phasins. However, TEM studies of granule formation and degradation in *Cupriavidus necator* H16 (formerly *Ralstonia eutropha* H16) revealed dark-stained elements ringed by small granules at early stages of PHB production. These structures named 'mediation elements' were located near the centre of cells or along a longitudinal strip in the centre of the cells (Tian *et al*., 2005). These results were at odds with the micelle and membrane budding models, and led to an alternative model for granule formation, in which granules are localized and the new 'mediation elements' function as scaffolds for the granule initiation sites. The fate of granules during cell division, that is, whether they are equally distributed between daughter cells, is not known (Tian *et al*., 2005).

We have explored the physiological role of the nucleoid-associated phasin PhaF from the prototype microorganism *P. putida* KT2442. One of the peculiarities of this protein is its modular organization in a PHA granule-binding domain (located at the N-terminus) and an AKP-rich domain (located at the C-terminus). In fact, we had previously demonstrated the abilities of PhaF from *P. putida* GPo1 for binding to PHA granule (phasin-like activity), and as transcriptional regulator, suggesting a putative DNA-binding activity (Prieto *et al*., 1999; Moldes *et al*., 2004). This C-terminal domain from the PhaF protein with a DNA-binding function nucleoid-associated is unique among phasins. In this sense, the identified phasins from *C. necator* H16 (PhaP1, PhaP2, PhaP3 and PhaP4) display an alanine-rich C-terminal region showing a very high isoelectric point (Neumann *et al*., 2008). Nevertheless, further investigations are needed to exclude that this positive charge might participate in the interaction with the 'mediation elements' or the latter might be simply the nucleoid of the cell.

This work demonstrates that PhaF plays a crucial role in granule localization and distribution, since the lack of this protein unbalance granule segregation during cell division (Fig. 6). Similar system of localization of

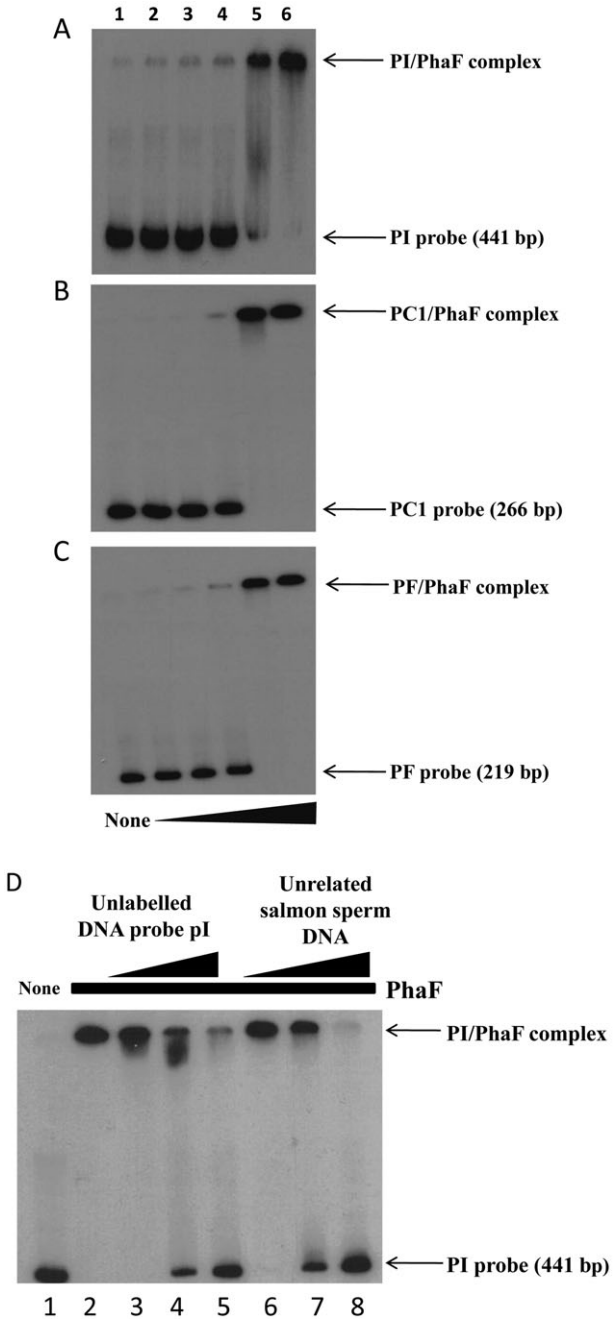

Fig. 8. Gel retardation analyses of PhaF binding to the P_I, P_{C1} and P_F promoter regions.
A–C. The DNA probes used [PI (A), PC1 (B) and PF (C)] are indicated schematically on the right of the figure. PhaF protein purification and gel retardation analyses were performed as described in *Experimental procedures*. Lanes 2–6, contained increasing concentrations (30, 50, 100, 200 and 500 nM) of PhaF protein. Lane 1 contained no protein. The DNA–PhaF complexes are indicated.
D. PhaF-binding competition analysis to P_I promoter with unlabelled DNA-specific probe (lanes 3–5) and unrelated salmon sperm DNA (lanes 6–8). Gel retardation was performed in the presence of 300 nM PhaF. Lane 1 contains no PhaF protein. Lane 2 is a control containing no unlabelled specific probe.

organelles as needle array inside prokaryotic cells has been observed for the intracellular organelles magnetosomes from *Magnetospirilum gryphiswaldense* (Komeili *et al*., 2006). They are assembled into a regular chain in order to achieve the maximum magnetic moment, against the physical tendency of magnetosome agglomeration. In this system, the protein responsible for this alignment is MamJ which has a high content of acidic amino acids and a repeated domain structure, which appears to interact with a linear cytoskeleton-like structure composed by MamK (actin-like protein) that directs the assembly and localization of the prokaryotic organelles (Scheffel *et al*., 2006). *P. putida* KT2442 (Nelson *et al*., 2002) posses members of all cytoskeletal systems described in bacteria (revised in Gitai *et al*., 2005; Gerdes *et al*., 2010) like the tubulin homologous FtsZ (annotated as PP_1342 in the chromosome); ParAB (PP_0001-2) and MinCDE (PP_1732-34) systems, where ParA and MinD are similar variant P loop ATPases that form cytoskeletal-like filaments on DNA and membranes, respectively, to solve different problems (DNA segregation and septum placement) by analogous molecular mechanisms; actin homologue MreB (PP_0934), similar to the actin-like protein MamK, which forms a helix essential for maintenance of cell shape, and it has been recently hypothesized to act as a scaffold for transporting proteins to different locations throughout the bacterial cell (Kimberly and Gitai, 2010). Our work revealed PhaF as central player in the machine to control PHA granule segregation and localization in the cell. Moreover, whether or not *P. putida* KT2442 cytoskeletal proteins facilitate the needle array structure by direct or indirect interaction with PhaF is still an open question and at this point, the precise mechanisms by which PHA granules are positioned by PhaF remains elusive. Since PhaF shows a unique ability for binding at least two ligands, the PHA granules and the nucleoid, our work provides support to consider that the PhaF function localizing and segregating the PHA granules implies new mechanisms different from that of described for magnetosomes (MamK/MamJ) or DNA segregation in bacteria (ParA-like mechanism). Taking into account the unspecific DNA-binding abilities of the C-terminal part of PhaF, we cannot discard that the bacterial chromosome could play a role as granule carrier during the division process. In this sense, previous studies have determined the cellular position of different chromosomal sites demonstrating that they were positioned along the long axis of the cell in a linearly ordered fashion from the origin to the terminus (Teleman *et al*., 1998; Niki *et al*., 2000; Viollier *et al*., 2004).

The unspecific PhaF–DNA interaction validates the classification of this phasin as nucleoid-associated protein and raises further questions about the physiological roles of PhaF in *P. putida*. Eukaryotic H1 histones are also

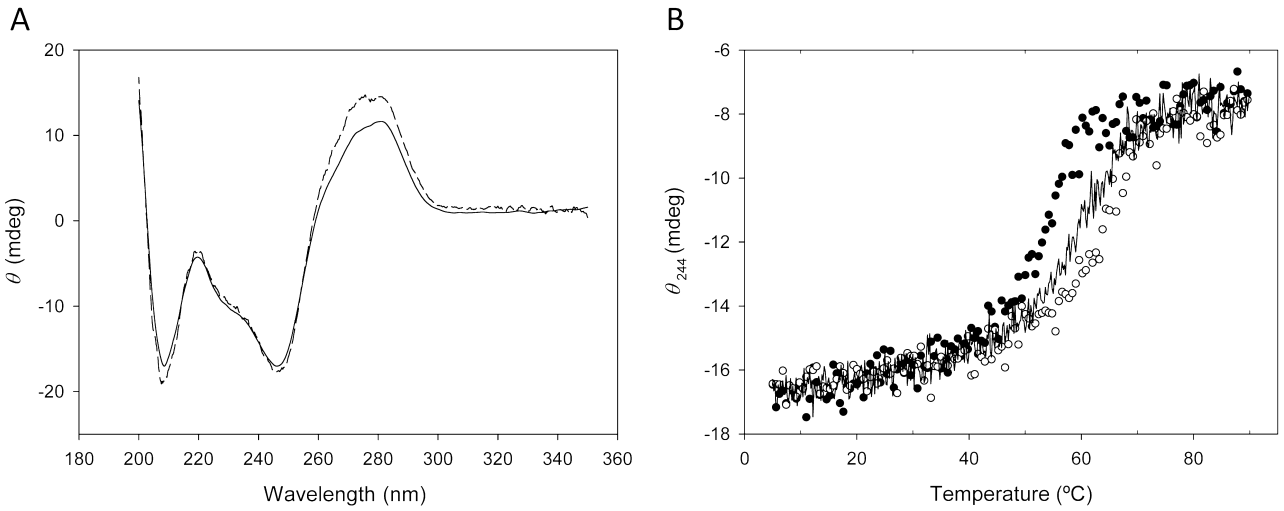

Fig. 9. Binding of PhaF and C-PhaF to DNA monitored by CD.
A. Wavelength spectra of a solution containing 9 μM PhaF and 9 μM nspDNA (solid line), and theoretical spectra obtained from the arithmetic sum of spectra recorded for 9 μM PhaF and 9 μM nspDNA separately (dashed line).
B. Thermal stability of 9 μM nspDNA (black circle), 9 μM nspDNA plus 9 μM PhaF (white circles) and 9 μM nspDNA plus 9 μM C-PhaF (solid line).

called linker histones because they are chromatin-associated proteins that bind to the exterior of nucleosomes and dramatically stabilize the highly condensed states of chromatin fibres (Zlatanova *et al*., 2000). In eukaryotic organisms, there is evidence that linker histones are also involved in transcriptional regulation by determining the accessibility of the nucleosomal DNA to the transcriptional machinery (Zlatanova *et al*., 2000). Furthermore, it has been demonstrated that histones of the H1 family provide the DNA compaction required by the changing physiological needs of the cell during the different stages of cell cycle (Kasinsky *et al*., 2001). We have undoubtedly demonstrated that the lack of PhaF protein in *P. putida* affects transcription rate of *pha* cluster. Moreover, the transcriptomic analysis carried out in the strain KT42F suggested that the expressions of other genes unrelated to PHA metabolism were also modified in this strain, but the mechanism involved in this global effect is still unclear and pleiotropic effects related to the existence of two populations in terms of PHA content cannot be excluded. Even more, PhaF might contribute to the chromosomal DNA overcondensation needed when the cells contained more than 50% of PHA of CDW in the cytoplasm.

Examples of bi-functional proteins containing the AKP-rich domain are found in eukaryotic organisms, such as the ribosomal proteins L22 and L23a of *Drosophila melanogaster* (Koyama *et al*., 1999), and in the prokaryotic organisms like AlgP from *P. aeruginosa* (Deretic and Konyecsni, 1990) and the putative DnaK suppressor from *Stenotrophomonas* sp. It is also worth to mention the cases of the translation factor IF-2 from Actinobacteria which contains an AKP-rich region in its N-terminal domain that is involved in translation initiation and binds to the ribosome by interacting with the initiator tRNA (Caserta *et al*., 2006). Also, the Hc1 and Hc2 proteins from *Chlamydia trachomatis* play a role in the chromosome condensation regulating the stage-specific differentiation during the life cycle (Kaul *et al*., 1996) and BpH1 and BpH2 proteins from *Bordetella pertussis,* which are known to condense the DNA and protect it from digestion with DNase I *in vitro*, could be involved in transcriptional regulation (Goyard, 1996).

Summing up, we have described here a new and unexpected role for the PhaF phasin of *P. putida* KT2442 involved in the balanced distribution of the PHA reserve granules between daughter cells during cell division. This ability has been ascribed to the particular composition of its C-terminal domain which mimics nucleoid-associated proteins, and confers the protein an unspecific DNA-binding capacity. Therefore, the distribution of reserve materials between the two daughter cells appears to be associated to the co-ordinated segregation of chromosomes, which might act as granule carriers through PhaF interactions. These findings lead arguments to an alternative model for PHA granule formation in bacteria, open a more complex view of the bacterial organelles segregation and transcriptional regulation related to PHA metabolism, and demonstrated a new role for phasins within the PHA apparatus that could be critical for cell survival under stress conditions.

Experimental procedures

Bacterial strains, plasmids, media and growth conditions

The *P. putida* strain KT2442, a derivative strain of the parental strain KT2440 whose complete nucleotide sequence of the genome is accessible in the data bank (Nelson *et al.*, 2002), was used throughout this study. *Escherichia coli* DH10B (Invitrogen) and *E. coli* BL21(DE3) (harbouring the T7 RNA polymerase gene under control of the *lacUV5* promoter) were used as hosts for gene cloning and overexpression respectively. Plasmid pET-29a(+) (Novagen) is an *ori*ColE1 vector that confers kanamycin resistance and allows gene cloning and expression under the control of the T7 promoter. *E. coli* cells were grown with aeration at 37°C in Luria–Bertani medium (Sambrook and Russell, 2001) containing, where appropriate, 50 μg ml^{-1} kanamycin. *P. putida* KT2442 cells were cultivated with aeration at 30°C. For optimal PHA production, a pre-culture of the *P. putida* strains was cultivated overnight in LB medium, washed and inoculated at 0.3 OD_{600} in 0.1 N M63, which is a nitrogen-limited minimal medium in the presence of 15 mM octanoic acid as carbon source (de Eugenio *et al.*, 2010b). The appropriate selection antibiotics, kanamycin (50 μg ml^{-1}), gentamicin (5 μg ml^{-1}) or rifampicin (50 μg ml^{-1}), were added when needed.

Molecular biology techniques

Standard molecular biology techniques were performed as previously described (Sambrook and Russell, 2001). PCR products were purified with the High Pure plasmid isolation kit (Roche Applied Science). DNA fragments were purified with Gene-Clean Turbo (Q-BIO-gene). Genomic DNA from *P. putida* KT2442 was isolated with the Genomic Prep Cells and Tissue DNA Isolation kit (Amersham Biosciences). All cloned inserts and DNA fragments were confirmed by DNA sequencing with fluorescently labelled dideoxynucleotide terminators and AmpliTaq FS DNA polymerase (Applied Biosystems) in an ABI Prism 377 automated DNA sequencer (Applied Biosystems). Transformation of *E. coli* cells was carried out using the RbCl method (Sambrook and Russell, 2001).

Construction of a PhaF null mutant of P. putida *KT2442*

The *phaF* gene was inactivated by marker exchange as described previously using the mobilizable suicide plasmid pKNG101 (Kaniga *et al.*, 1991). The deletion of *phaF* gene was engineered with the DNA fragments DmutF and ImutF of 575 bp and 402 bp, respectively, generated by PCR using the primer pairs D5mutF 5′-CGGGATCCCAACGAACTCGGC ATCAGC-3′ and D3MutF 5′-CGGAATTCCAACACTACATC TCCAGCAG-3′ for DmutF, and I5mutF 5′-CGGAATTCGCCA GCCATCCTGCTCTCC-3′ and I3mutF 5′-TCCCCCGGGC TGGACACGCTTGGCGAGG-3′ for ImutF. These two fragments were digested with the appropriate restriction enzymes and ligated using T4 ligase resulting in a single 977 bp fragment carrying a deletion of the *phaF* gene which was cloned into the unique BamHI and SmaI sites of pKNG101 to yield pKNGFdel. Plasmid pKNGFdel was used to deliver the *phaF* mutation to the host chromosome via homologous recombination. Biparental mating was performed following protocols described by de Lorenzo and Timmis (1994), using *E. coli* SM10λpir (pKNGFdel) as donor strain and *P. putida* KT2442 as recipient strain. For conjugation, 100 μl of overnight cultures of donor and recipient strains were mixed in 5 ml of 10 mM $MgSO_4$ and collected on a Millipore filter which was subsequently placed on an LB agar plate and incubated overnight at 30°C. After incubation, the cells were resuspended in 5 ml of 10 mM $MgSO_4$ and plated on M63 selective plates supplemented with 5% sucrose as described previously (Kaniga *et al.*, 1991). Transconjugants (Suc^R, Sm^S) were isolated. The second cross-over event was confirmed by PCR using primers D5MutF and I3MutF. The resultant mutant strain was denoted KT42F.

Flow cytometry

Cells were harvested and washed twice with distilled water and resuspended in water to a final OD_{600} of 0.2 for staining with Nile Red. A Nile Red stock solution was made by dissolving the dye to a concentration of 1 mg ml^{-1} in dimethyl sulphoxide (DMSO). Three microlitres of stock solution were added to 1 ml of cell suspension. The mixture was incubated in the dark for 15 min and analysed by flow cytometry (flow cytometer Coulter EPICS XL). *P. putida* KT42C1 minus strain (a *phaC1* mutant which produces < 1% CDW PHA) (de Eugenio *et al.*, 2010b) was used as negative control. A calibration curve for the quantification of the PHA content using flow cytometry was made comparing the fluorescence intensity and PHA content analysed by gas chromatography throughout the growth curve in *P. putida* KT2442 (data not shown). The relation between both parameters was fitted to the equation $y = 30.874\ \mathrm{Ln}(x) + 38.11$ with a $R^2 = 0.9984$. This equation has been used to translate the cytometry fluorescence intensity data into PHA values.

Complementation of P. putida *KT42F*

Plasmid pPF61, harbouring the *phaF* gene from *P. putida* GPo1 under the control of the *Ptrc* promoter (Prieto *et al.*, 1999), was introduced into *P. putida* KT42F chromosome by triparental mating. The resulting strain called KT42F-F was cultivated in PHA production medium in the presence of 5 mM isopropyl-1-thio-β-D-galactopyranoside (IPTG) as described (Prieto *et al.*, 1999).

Transmission electron microscopy

Cells were harvested, washed twice in PBS and fixed in 5% (w/v) glutaraldehyde in the same solution. Afterwards, cells were suspended in 2.5% (w/v) OsO_4 for 1 h, gradually dehydrated in ethanol [30%, 50%, 70%, 90% and 100% (v/v); 30 min each] and propylene oxide (1 h), embedded in Epon 812 resin. Ultrathin sections (thickness 70 nm) were cut with a microtome using a Diatome diamond knife. The sections were picked up with 400 mesh cupper grids coated with a layer of carbon and subsequently observed in a Jeol-1230 electron microscope (JeolLtd., Akishima, Japan).

To determine the size of PHA granules from the micrographs, 50 cells of the wild type and of the mutant were

selected, in which the PHA granule diameter was measured. We analysed 100 granules of the wild type and 100 of the mutant. Only granules with sharp boundaries were selected. The number of PHA granules per cell was determined only from cells which were fully visible in the electron micrographs.

Construction of P. putida *strains expressing a cassette consisting in a fusion gene* GFP *and C- terminal domain of PhaF*

The GFP::C-PhaF fusion was obtained by amplification of two DNA fragments. GFP cassette was amplified from plasmid pGreenTIR (Miller and Lindow, 1997) with GFP-F 5′-GGGAATTCTGATTAACTTTATAAGGAGGAAAAACAT-3′ (an engineered EcoRI restriction site is underlined) and GFP-RBamHI 5′-CGGGATCCTTTGTATAGTTCATCCATGCCAT-3′ (an engineered BamHI restriction site is underlined) oligonucleotides. After digestion with the corresponding restriction endonucleases, the GFP cassette was cloned into pUC18Not plasmid yelding pUC18NotGFP. *phaF* C-terminal domain was PCR amplified using C-termF (GFP) 5′-CGGGATCCTCGCGCGCTGCAGCAAC-3′ (an engineered BamHI restriction site is underlined) and C-termR (GFP) 5′-GCCAAGCTTCAGATCAGGGTACCGGTGCC-3′ (an engineered HindIII restriction site is underlined) oligonucleotides from genomic DNA of *P. putida* KT2442. Obtained PCR product was digested and cloned into pGEM-T plasmid. The fragment obtained after digestion with HindIII and BamHI was cloned into pUC18NotGFP plasmid. The resulting hybrid plasmid pUC18NotGFP-Cterm was transformed into *E. coli* strain DH10B. Construction was confirmed by sequencing using an ABI Prism 3730 DNA Sequencer. The GFP::C-PhaF fusion was cloned from pUC18NotGFP-Cterm plasmid into pCNB5 vector as NotI fragment. Constructed plasmid pCNB5-GFP-Cterm was introduced into the *P. putida* KT2442 and *P. putida* KT42F chromosomes by triparental mating yielding KT42-GC and KT42F-GC respectively. Conjugates were isolated after plating on M63 0.1 N selective plates supplemented with 0.2% citrate and kanamycin. Afterwards colonies were picked in LB plates and LB plates with IPTG and selected with a fluorescent magnifying lamp.

In vivo *localization of the C-terminal domain of PhaF by fluorescence microscopy*

Pseudomonas putida KT42-GC and KT42F-GC strains were cultivated overnight in LB medium. Then, cells were washed and inoculated at 0.3 OD_{600} in 0.1 N M63. Cultures were induced with 2 mM IPTG in the exponential phase of growth to induce the production of the GFP::C-PhaF fusion protein. Nucleoids staining was performed by incubation with 2 μg ml^{-1} DAPI for 15 min while the PHA granules were visualized after staining with 1 μg ml^{-1} Nile Red for 15 min. Then cells were fixed with 4% paraformaldehyde at room temperature for 1 h, washed tree times with PBS and visualized by confocal microscopy Laser Confocal espectral (CLSM) Leica TCS SP2-AOBS.

Real-time RT-PCR assay

Total RNA was extracted from *P. putida* KT2442 and *P. putida* KT42F strains. Cells were inoculated at 0.3 OD_{600} in 0.1 N M63 medium with 15 mM octanoate or 10 mM glucose as carbon sources. Cells were harvested throughout the growth curve and stored at –20°C. Pellets were thawed and cells lysed in TE buffer (10 mM Tris-HCl pH 7.5, 1 mM EDTA) containing 5 mg ml^{-1} lysozyme by a series of freeze/unfreeze cycles. RNAs were extracted using the RNeasy mini Kit (Qiagen), including a DNase I treatment according to the manufacturer's instructions, precipitated with ethanol, washed and resuspended in 40 μl of RNase-free water. The concentration and purity of the RNA samples were measured by ND1000 Spectrophotometer (Nanodrop Technologies). Synthesis of total cDNA was carried out with 20 μl of reverse transcription reactions containing 1 μg of RNA, 0.5 mM dNTPs, 200 U of SuperScript II Reverse Transcriptase (Invitrogen) and 5 μM random hexamers as primers, in the buffer recommended by the manufacturer. Samples were initially heated at 65°C for 5 min and then were incubated at 42°C for 1 h, terminated by incubation at 70°C for 15 min. The cDNA obtained was purified using Geneclean Turbo Kit (MP Biomedicals) and the concentration was determined by a ND1000 Spectrophotometer (Nanodrop Technologies). For the analysis of the transcript levels target cDNAs (5 ng) and reference samples were amplified three times in separate PCR reactions using 0.2 μM of primers C1RT5′ (5′-CTGGGCACCAGCGAAGGCG-3′) and C1RT3′ (5′-GTAATCGACAGCACCGCGTC-3′) for *phaC1,* F-RTf (5′-GTCATGTTTAGACGGAATACCCAG-3′) and F-RTr (5′-GCGGCCAACCACCAGCTTG-3′) for *phaF* and I-RTf (5′-GCACCGGTCAGCTTCTCGATC-3′) and I-RTr (5′-GGAGCGAACTTGAAGAAGCC-3′) for *phaI* by iQ5 Multicolor Real-Time PCR Detection System (Bio-Rad). Real-time PCR was performed using SYBR Green technology in an ABI Prism 7000 Sequence Detection System (Applied Biosystems). Samples were initially denatured by heating at 95°C for 4 min, followed by 30 cycles of amplification (95°C, 1 min; test annealing temperature, 65°C, 1 min; elongation and signal acquisition, 72°C, 30 s). For relative quantification of the fluorescence values, a calibration curve was made using dilution series from $5 \cdot 10^{-7}$ to 5 ng of *P. putida* KT2442 genomic DNA sample.

Hybridization and processing of DNA microarrays

RNA for microarray analyses was obtained from three independent cultures grown under identical conditions. Precultures of the *P. putida* strains were cultivated overnight in LB medium, washed, inoculated at 0.3 OD_{600} in PHA production medium and grown during 8 h.

Aliquots of 50 ml were harvested by centrifugation at 4°C and frozen at –20°C. The cell pellet was resuspended in 1 ml of TriPure Isolation Reagent (Tri Reagent LS, Molecular Research Center) and incubated at room temperature for 5 min, after which cell lysis was complete. The solution was centrifuged in a microfuge at 12 000 r.p.m. for 10 min at 4°C and the pellet was discarded. Two hundred microlitres of chloroform was added to the supernatant and the mixture was vigorously shaken for 15 s. After 15 min at room temperature, the mixture was centrifuged (12 000 r.p.m., 15 min, 4°C) and the aqueous phase was recovered. Five hundred microlitres of isopropanol was added and, after 10 min at room temperature, the sample was centrifuged at 12 000 r.p.m. for 10 min at 4°C. The pellet was washed with 70% (v/v)

ethanol, dried and resuspended in 300 µl of H_2O. DNase I (2 µl, 10 units μl^{-1}) was added and the mixture incubated at 37°C for 2 h. After extracting the sample two to three times with acid phenol, the nucleic acids were recovered by precipitation with sodium acetate and ethanol. The pellet was washed with 70% (v/v) ethanol, dried and resuspended in 100 µl of H_2O. After discarding the presence of contaminating DNA by polymerase chain reaction (PCR), the samples were purified by using RNeasy columns (Qiagen), which helped to eliminate the 5S rRNA. RNA integrity was checked with a capillary electrophoresis system (Agilent 2100 Bioanalyzer).

cDNA was obtained from RNA preparations of the control and test strains (KT2442 and KT42F respectively), fluorescently labelled with either Cy3 or Cy5, mixed, and used to hybridize the DNA microarray as reported previously (Yuste *et al*., 2006). Four microarrays corresponding to independent experiments (biological replicas) were used and statistically analysed as described before (Yuste *et al*., 2006) using the LIMMA software package (Smyth, 2004). The results for each replica (mean intensity for each spot) were normalized within each array using the lowest intensity-depend normalization method (Yang *et al*., 2002) and between arrays using the scale method (Yang *et al*., 2002). Differential expression was calculated using linear models and empirical Bayes moderated *t*-statistics (Smyth and Speed, 2003; Smyth, 2004). The probability values obtained (*P*-values) were adjusted for multiple testing to control the false discovery rate (Benjamini and Hochberg, 1995). Genes were considered differentially expressed when they fulfilled the filter parameters of expression ratio ≥ 1.9 and FDR ≤ 0.1. The replica with lowest adjusted *P*-value was chosen for each gene. Data have been deposited at http://www.ebi.ac.uk/arrayexpress/.

Gel retardation assays

For the labelling of the probes in competition gel retardation assays DNA fragments of 266, 451 and 219 bp containing the P_{C1}, P_I and P_F promoters (de Eugenio *et al*., 2010a) were amplified by PCR using 100 ng of *P. putida* KT2442 genomic DNA as template and a combination of one unlabelled primer and the second primer 5′ end-labelled with phage T4 polynucleotide kinase [γ-^{32}P]-ATP (3000 Ci $mmol^{-1}$). The primers used were PI5 (5′-CCGGAATTCGCCAGAAAATGCCTGAG AAGCTC-3′) and the labelled primer PI3 (5′-CGCGGATC CATGCTGTGTACCTCATGCTC-3′), for the PI DNA fragment containing P_I promoter, PC13 (5′-CGGGGATCCATCTACG ACGCTCCGTTGT-3′) and the labelled primer PC15 (5′-TTTGAATTCGGCCTGCGGGGTTTAGAG-3′) for the PC1 DNA fragment containing P_{C1} promoter and pF5 (5′-CCGGAATTCCCAGCTTGACGAAGTCGGTGA-3′) and the labelled primer pF3 (5′-CGCGGATCCATCCTGCTCTCCT TATGGTTTGTG-3′) for the DNA fragment PF containing P_F promoter. The reaction mixtures contained 9 µl of 20 mM Tris-HCl pH 7.5, 50 mM KCl, 500 µg ml^{-1} BSA, 1 nM DNA probe and purified PhaF in a 20 µl final volume (see below). After incubation for 5 min at room temperature, mixtures were fractionated by electrophoresis in 5% polyacrylamide gels buffered with 0.5× TBE (45 mM Tris-borate, 1 mM EDTA). The gels were dried onto Whatman 3MM paper and exposed to Hyperfilm MP (Amersham Pharmacia Biotech).

Overproduction and purification of PhaF protein

The *phaF* gene was PCR amplified from *P. putida* KT2442 genomic DNA using the oligonucleotides PhaF F (5′-GG AATTCCAT**ATG**GCTGGCAAGAAGAACACC-3′; the *phaF* start codon is indicated in boldface letter, and an engineered NdeI restriction site is underlined) and C-term BamHI (5′-CGGGATCCTCAGATCAGGGTAACCGGTGCC-3′; an engineered BamHI restriction site is underlined). The resulting 808 bp DNA fragment was ligated as a NdeI/BamHI DNA fragment into the NdeI/BamHI double-digested pET-29a(+) plasmid, giving rise to plasmid pETPhaF (6.2 kb) that express the *phaF* gene under the control of the T7*lac* promoter and the ribosome binding site from the pET-29a(+) plasmid. *E. coli* BL21(DE3) cells harbouring plasmid pETPhaF were grown until the cultures (1 l) reached 0.6 OD_{600}. Overexpression of the cloned gene was then induced during 3 h by the addition of 0.2 mM IPTG. Cells were harvested at 4°C, resuspended in 50 ml of 20 mM sodium phosphate buffer, pH 7.0 plus 100 mM NaCl, disrupted by sonication (Branson 250 instrument) and centrifuged again at 4°C (10 000 *g*).

Inclusion bodies containing denatured PhaF were redissolved in 25 ml of 8 M urea followed by centrifugation for 15 min at 4°C (10 000 *g*). PhaF refolding was achieved by drop-to-drop addition to 250 ml of 20 mM sodium phosphate buffer, pH 7.0. The sample was centrifuged for 15 min at 4°C (10 000 *g*). Ammonium sulphate was then slowly added to the supernatant to a final concentration of 1.7 M, centrifuged again at 4°C (10 000 *g*) and the supernatant was applied onto a butyl sepharose 4 Fast Flow column (GE Healthcare) (10 × 1 cm) previously equilibrated in the same buffer as the sample. Column was extensively washed with 0.75 M ammonium sulphate, and finally the PhaF protein was eluted with 20 mM sodium phosphate buffer, pH 7.0 with a yield of around 20 mg per litre of culture and a purity of more than 95% as assessed by SDS-PAGE. Protein concentration was determined spectrophotometrically using a molar absorption coefficient at 280 nm (ε_{280}) of 19 071 M cm^{-1}, calculated according to Fasman (1976). Purified samples were dialysed against 10 mM ammonium hydrogencarbonate, lyophilized and stored at −80°C in aliquots until needed.

Overproduction and purification of the C-terminal domain of PhaF (C-PhaF protein)

The *phaF* C-terminal domain was PCR amplified from *P. putida* KT2442 genomic DNA using oligonucleotides C-term NdeI (5′-GGATTCCATATGTCGCGCGCTGCAGCAA CCAAG-3′; an engineered NdeI restriction site is underlined) and C-term BamHI (see sequence above). The resulting 383 bp DNA fragment was ligated as a NdeI/BamHI DNA fragment into the NdeI/BamHI double-digested pET-29a(+) plasmid, giving rise to plasmid pETCterm (5.7 kb) that express the *phaF* C-terminal encoding domain under the control of the T7*lac* promoter and the ribosome binding site from the pET-29a(+) plasmid. *E. coli* BL21(DE3) cells harbouring plasmid pETCterm were grown at 37°C until the cultures (1 l) reached an OD_{600} of 0.6. Overexpression of the cloned gene was then induced during 3 h by the addition of 0.2 mM isopropyl-1-thio-β-D-galactopyranoside. Cells were harvested at 4°C, resuspended in 50 ml of 50 mM Tris-HCl

buffer, pH 8.8 plus 10 mM $MgCl_2$, disrupted by sonication (Branson 250 instrument), incubated with DNase I (25 μg ml^{-1}) 15 min at room temperature and centrifuged again at 4°C (10 000 *g*). The supernatant was applied onto an Econo-Pac CM cartridge 5 × 1 (Bio-Rad) previously equilibrated in the same buffer as the sample. Column was extensively washed with the same buffer as above, and then subjected to a second wash with 0.7 M Tris-HCl buffer, pH 8.8. Finally the C-PhaF protein was eluted with 0.7 M Tris-HCl buffer, pH 8.8 plus 4 M NaCl with a yield of 30 mg per litre of culture and a purity > 95% as checked by SDS-PAGE. Since C-PhaF lacks any aromatic residues and has a peculiarly charged amino acid composition that might be inadequate for usual colorimetric methods, protein concentration was determined by peptidic bond absorbance at 205 nm according to Scopes (1974).

Circular dichroism spectroscopy

Near-UV circular dichroism (CD) experiments were carried out in a Jasco J-810 spectropolarimeter equipped with a Peltier PTC-423S system. Isothermal wavelength spectra were acquired at a scan speed 50 nm min^{-1} with a response time of 2 s and averaged over at least six scans at 20°C. For DNA-binding experiments, an unspecific DNA fragment (nspDNA) was prepared from hybridization of oligonucleotides 5′-AATTCACAGTAAAACCAGATGGCTTGATTAC-3′ and its complementary strand (Invitrogen), to a final stock concentration of 0.5 mg ml^{-1}. Protein and nspDNA concentration was 9 μM and the cuvette path length was 1 cm. Raw ellipticities (θ) are expressed in milidegrees. For the CD-monitored thermal denaturation experiments, the sample was layered with mineral oil to avoid evaporation, and the heating rate was set to 60°C h^{-1}. Melting temperatures (t_m) were calculated upon fitting the thermal denaturation curves to a simple sigmoidal equation with sloping baselines, using the SIGMAPLOT 10.0 utilities (Systat Software).

Acknowledgements

We are greatly indebted to Dr Pedro Lastres and Dr Jose Yuste for helpful discussions and technical support in flow cytometry analyses. We also appreciate the technical support of M[a] Teresa Seisdedos with the fluorescence microscopy. We thank the technical works of A. Valencia and V. Morales. This work was supported by grants from the Comunidad Autónoma de Madrid (P-AMB-259-0505), the Comisión Interministerial de Ciencia y Tecnología (BIO2007-67304-C02, BIO2010-21049, CSD2007-00005) and by European Union Grants (GEN 2006-27750-C5-3-E and NMP2-CT-2007-026515).

References

Benjamini, Y., and Hochberg, Y. (1995) Controlling the false discovery rate: a practical and powerful approach to multiple testing. *J R Stat Soc B* **57:** 289–300.

Bustin, M., Catez, F., and Jae-Hwan, L. (2005) The dynamics of histone H1 function in chromatin. *Mol Cell* **17:** 617–620.

Caserta, E., Tomsic, J., Spurio, R., La Teana, A., Pon, C.L., and Gualerzi, C.O. (2006) Translation initiation factor IF2 interacts with the 30S ribosomal subunit via two separate binding sites. *J Mol Biol* **362:** 787–799.

de Eugenio, L.I., Galán, B., Escapa, I.F., Maestro, B., Sanz, J.M., García, J.L., and Prieto, M.A. (2010a) The PhaD regulator controls the simultaneous expression of the *pha* genes involved in polyhydroxyalkanoate metabolism and turnover in *Pseudomonas putida* KT2442. *Environ Microbiol* **12:** 1591–1603.

de Eugenio, L.I., Escapa, I.F., Morales, V., Dinjaski, N., Galán, B., García, J.L., and Prieto, M.A. (2010b) The turnover of medium-chain length polyhydroxyalkanoates in *Pseudomonas putida* KT2442 and the fundamental role of PhaZ depolymerase for the metabolic balance. *Environ Microbiol* **12:** 207–221.

de Lorenzo, V., and Timmis, K. (1994) Analysis and construction of stable phenotypes in gram-negative bacteria with Tn*5*- and Tn*10*-derived minitransposons. *Methods Enzymol* **235:** 386–405.

Deretic, V., and Konyecsni, W.M. (1990) A prokaryotic regulatory factor with a histone H1-like carboxy-terminal domain: clonal variation of repeats within *algP*, a gene involved in regulation of mucoid in *Pseudomonas aeruginosa*. *J Bacteriol* **172:** 5544–5554.

Deretic, V., Hibler, N.S., and Holt, S.C. (1992) Immunocytochemical analysis of AlgP (H_p1), a histonelike element participating in control of mucoidy in *Pseudomonas aeruginosa*. *J Bacteriol* **174:** 824–831.

Fasman, G.D. (ed.) (1976) *Handbook of Biochemistry and Molecular Biology. Section A. Proteins*, 3rd edn, Vol. **III**. Cleveland, OH: CRC Press.

Gerdes, K., Howard, M., and Szardenings, F. (2010) Pushing and pulling in prokaryotic DNA segregation. *Cell* **141:** 927–942.

Gitai, Z., Thanbichler, M., and Shapiro, L. (2005) The choreographed dynamics of bacterial chromosomes. *Trends Microbiol* **13:** 221–228.

Goyard, S. (1996) Identification of BpH2, a novel histone H1 homolog in *Bordetella pertussis*. *J Bacteriol* **178:** 3066–3071.

Grage, K., Jahns, A.C., Parlane, N., Palanisamy, R., Rasiah, I.A., Atwood, J.A., and Rehm, B.H. (2009) Bacterial polyhydroxyalkanoate granules: biogenesis, structure, and potential use as nano-/micro-beads in biotechnological and biomedical applications. *Biomacromolecules* **13:** 660–669.

Johnson, W.C., Jr (1988) Secondary structure of proteins through circular dichroism spectroscopy. *Annu Rev Biophys Biophys Chem* **17:** 145–166.

Kaniga, K., Delor, I., and Cornelis, G.R. (1991) A wide-host-range suicide vector for improving reverse genetics in gram-negative bacteria: inactivation of the *blaA* gene of *Yersinia enterocolitica*. *Gene* **109:** 137–141.

Kasinsky, H., Lewis, J., Dacks, J., and Ausio, J. (2001) Origin of H1 linker histones. *FASEB J* **15:** 34–42.

Kato, J., Tapan, M., and Chakrabarty, A.M. (1990) AlgR3, a protein resembling eukaryotic histone H1, regulates alginate synthesis in *Pseudomonas aeruginosa*. *Proc Natl Acad Sci USA* **87:** 2887–2891.

Kaul, R., Allen, M., Bradbury, E.M., and Wenman, W.M. (1996) Sequence specific binding of chlamydial histone H1-like protein. *Nucleic Acids Res* **24:** 2981–2989.

Kimberly, N.C., and Gitai, Z. (2010) Surface association and the MreB cytoskeleton regulate pilus production, localization and function in *Pseudomonas aeruginosa*. *Mol Microbiol* **76:** 1411–1426.

Komeili, A., Li, Z., Newman, D.K., and Jensen, G.J. (2006) Magnetosomes are cell membrane invaginations organized by the actin-like protein MamK. *Science* **311:** 242–245.

Koyama, Y., Katagiri, S., Hanai, S., Uchida, K., and Miwa, M. (1999) Poly (ADP-ribose) polymerase interacts with novel ribosomal proteins, L22 and L23a, with a unique histone-like amino-terminal extensions. *Gene* **226:** 339–345.

McCool, G.J., and Cannon, M.C. (1999) Polyhydroxyalkanoate inclusion body-associated proteins and coding region in *Bacillus megaterium*. *J Bacteriol* **181:** 585–592.

Madison, L.L., and Huisman, G.W. (1999) Metabolic engineering of poly (3-hydroxyalkanoates): from DNA to plastic. *Microbiol Mol Biol Rev* **63:** 21–53.

Medvedkin, V.N., Permyakov, E.A., Klimenko, L.V., Mitin, Y.V., Matsushima, N., Nakayama, S., and Kretsinger, R.H. (1995) Interactions of (Ala*Ala*Lys*Pro)n and (Lys*Lys*Ser*Pro)n with DNA. Proposed coiled-coil structure of AlgR3 and AlgP from *Pseudomonas aeruginosa*. *Protein Eng* **8:** 63–70.

Miller, W.G., and Lindow, S.E. (1997) An improved GFP cloning cassette designed for prokaryotic transcriptional fusions. *Gene* **191:** 149–153.

Moldes, C. (2003) Desarrollo de nuevos sistemas para la producción de proteínas de fusión por fermentación. PhD Thesis. Departamento de Microbiología II. Madrid: Universidad Complutense de Madrid (UCM).

Moldes, C., García, P., García, J.L., and Prieto, M.A. (2004) *In vivo* immobilization of fusion proteins on bioplastics by the novel tag BioF. *Appl Environ Microbiol* **70:** 3205–3012.

Nelson, K.E., Weinel, C., Paulsen, I.T., Dodson, R.J., Hilbert, H., Martins dos Santos, V.A.P., *et al*. (2002) Complete genome sequence and comparative analysis of the metabolically versatile *Pseudomonas putida* KT2440. *Environ Microbiol* **4:** 799–808.

Neumann, L., Spinozzi, F., Sinibaldi, R., Rustichelli, F., Pötter, M., and Steinbüchel, A. (2008) Binding of the major phasin, PhaP1, from *Ralstonia eutropha* H16 to poly (3-hydroxybutyrate) granules. *J Bacteriol* **190:** 2911–2919.

Niki, H., Yamaichi, Y., and Hiraga, S. (2000) Dynamic organization of chromosomal DNA in *Escherichia coli*. *Genes Dev* **14:** 212–223.

O'Leary, N.D., O'Connor, K.E., Ward, P., Goff, M., and Dobson, A.D. (2005) Genetic characterization of accumulation of polyhydroxyalkanoate from styrene in *Pseudomonas putida* CA-3. *Appl Environ Microbiol* **71:** 4380–4387.

Pieper-Fürst, U., Madkour, M.H., Mayer, F., and Steinbüchel, A. (1995) Identification of the region of a 14-kilodalton protein of *Rhodococcus ruber* that is responsible for the binding of this phasin to polyhydroxyalkanoic acid granules. *J Bacteriol* **177:** 2513–2523.

Prieto, M.A., Bühler, B., Jung, K., Witholt, B., and Kessler, B. (1999) PhaF, a polyhydroxyalkanoate-granule-associated protein of *Pseudomonas oleovorans* GPo1 involved in the regulatory expression system for *pha* genes. *J Bacteriol* **181:** 858–868.

Rehm, B.H. (2006) Genetics and biochemistry of polyhydroxyalkanoate granule self-assembly: the key role of polyester synthases. *Biotechnol Lett* **28:** 207–213.

Sambrook, J., and Russell, D.W. (2001) *Molecular Cloning. A Laboratory Manual*. Cold Spring Harbor, NY: CSHL Press.

Scheffel, A., Gruska, M., Faivre, D., Linaroudis, A., Plitzko, J.M., and Schuler, D. (2006) An acidic protein aligns magnetosomes along a filamentous structure in magnetotactic bacteria. *Nature* **440:** 110–114.

Scopes, R.K. (1974) Measurement of protein by spectrophotometry at 205 nm. *Anal Biochem* **59:** 277–282.

Smyth, G.K. (2004) Linear models and empirical Bayes methods for assessing differential expression in microarray experiments. *Stat Appl Genet Mol Biol* **3:** Article 3.

Smyth, G.K., and Speed, T. (2003) Normalization of cDNA microarray data. *Methods* **31:** 265–273.

Steinbüchel, A., and Hein, S. (2001) Biochemical and molecular basis of microbial synthesis of polyhydroxyalkanoates in microorganisms. *Adv Biochem Eng Biotechnol* **71:** 81–123.

Steinbüchel, A., Aerts, K., Babel, W., Follner, C., Liebergesell, M., Madkour, M.H., *et al*. (1995) Considerations on the structure and biochemistry of bacterial polyhydroxyalkanoic acid inclusions. *Can J Microbiol* **41:** 94–105.

Teleman, A.A., Graumann, P.L., Lin, D.C., Grossman, A.D., and Losick, R. (1998) Chromosome arrangement within a bacterium. *Curr Biol* **8:** 1102–1109.

Tian, J., Sinskey, A.J., and Stubbe, J. (2005) Kinetic studies of polyhydroxybutyrate granule formation in *Wautersia eutropha* H16 by transmission electron microscopy. *J Bacteriol* **187:** 3814–3824.

Timm, A., and Steinbüchel, A. (1992) Cloning and molecular analysis of the poly (3-hydroxyalkanoic acid) gene locus of *Pseudomonas aeruginosa* PAO1. *Eur J Biochem* **209:** 15–30.

Toy, K.E., Zhou, H., and Stephanopoulos, G.N. (2006) High-throughput screen for poly-3-hydroxybutyrate in *Escherichia coli* and *Synechocystis* sp. strain PCC6803. *Appl Environ Microbiol* **72:** 3412–3417.

Valentin, H.E., Stuart, E.S., Fuller, R.C., Lenz, R.W., and Dennis, D. (1998) Investigation of the function of proteins associated to polyhydroxyalkanoate inclusions in *Pseudomonas putida* BMO1. *J Biotechnol* **64:** 145–157.

Viollier, P.H., Thanbichler, M., McGrath, P.T., West, L., Meewan, M., McAdams, H.H., and Shapiro, L. (2004) Rapid and sequential movement of individual chromosomal loci to specific subcellular locations during bacterial DNA replication. *Proc Natl Acad Sci USA* **101:** 9257–9262.

Wieczorek, R., Pries, A., Steinbüchel, A., and Mayer, F. (1995) Analysis of a 24-kilodalton protein associated with the polyhydroxyalkanoic acid granules in *Alcaligenes eutrophus*. *J Bacteriol* **177:** 2425–2435.

Yang, Y.H., Dudoit, S., Luu, P., Lin, D.M., Peng, V., Ngai, J., and Speed, T.P. (2002) Normalization for cDNA microarray data: a robust composite method addressing single and multiple slide systematic variation. *Nucleic Acids Res* **30:** e15.

Yuste, L., Hervas, A.B., Canosa, I., Tobes, R., Jimenez, J.I., Nogales, J., *et al*. (2006) Growth phase-dependent expression of the *Pseudomonas putida* KT2440 transcriptional machinery analyzed with a genome-wide DNA microarray. *Environ Microbiol* **8:** 165–177.

Zlatanova, J., Caiafa, P., and van Holde, K. (2000) Linker histone binding and displacement: versatile mechanism for transcriptional regulation. *FASEB J* **14:** 1697–1704.

Supporting information

Additional supporting information may be found in the online version of this article.

environmental microbiology

Environmental Microbiology (2010) **12**(1), 207–221 doi:10.1111/j.1462-2920.2009.02061.x

The turnover of medium-chain-length polyhydroxyalkanoates in *Pseudomonas putida* KT2442 and the fundamental role of PhaZ depolymerase for the metabolic balance

Laura Isabel de Eugenio, Isabel F. Escapa, Valle Morales, Nina Dinjaski, Beatriz Galán, José Luis García and María A. Prieto*

Environmental Biology Research Line, Centro de Investigaciones Biológicas, CSIC, Ramiro de Maeztu, 9, 28040 Madrid, Spain.

Summary

Polyhydroxyalkanoates (PHAs) are biodegradable polymers produced by a wide range of bacteria, including Pseudomonads. These polymers are accumulated in the cytoplasm as carbon and energy storage materials when culture conditions are unbalanced and hence, they have been classically considered to act as sinks for carbon and reducing equivalents when nutrients are limited. Bacteria facing carbon excess and nutrient limitation store the extra carbon as PHAs through the PHA polymerase (PhaC). Thereafter, under starvation conditions, PHA depolymerase (PhaZ) degrades PHA and releases *R*-hydroxyalkanoic acids, which can be used as carbon and energy sources. To study the influence of a deficient PHA metabolism in the growth of *Pseudomonas putida* KT2442 we have constructed two mutant strains defective in PHA polymerase (*phaC1*)- and PHA depolymerase (*phaZ*)-coding genes respectively. By using these mutants we have demonstrated that PHAs play a fundamental role in balancing the stored carbon/biomass/number of cells as function of carbon availability, suggesting that PHA metabolism allows *P. putida* to adapt the carbon flux of hydroxyacyl-CoAs to cellular demand. Furthermore, we have established that the coordination of PHA synthesis and mobilization pathways configures a functional PHA turnover cycle in *P. putida* KT2442. Finally, a new strain able to secrete enantiomerically pure *R*-hydroxyalkanoic acids to the culture medium during cell growth has been engineering by redirecting the PHA cycle to biopolymer hydrolysis.

Received 14 May, 2009; accepted 11 August, 2009. *For correspondence. E-mail auxi@cib.csic.es; Tel. (+34) 918 373 112; Fax (+34) 915 360 432.

Introduction

Polyhydroxyalkanoates (PHAs) are bacterial polyesters accumulated in the cytoplasm as reserve storage granules, which are generally believed to play a role as sinks for carbon and reducing equivalents when other nutrients are limited (Madison and Huisman, 1999; O'Leary *et al.*, 2005; Prieto *et al.*, 2007). The most common PHA is the poly(3-hydroxybutyrate) (PHB), considered as the prototype of the short-chain-length PHAs (scl-PHAs) (Madison and Huisman, 1999), whereas medium-chain-length PHA (mcl-PHA), containing monomers from 6 to 14 carbon atoms, is less abundant and often produced by *Pseudomonas* species (Timm and Steinbüchel, 1990; Luengo *et al.*, 2003; Prieto *et al.*, 2007). The *pha* gene cluster responsible for PHA metabolism is well conserved among the mcl-PHA Pseudomonads producer strains (Huisman *et al.*, 1991; de Eugenio *et al.*, 2007; Prieto *et al.*, 2007) (Fig. 1). It is composed of (i) two synthase (or polymerase)-coding genes (*phaC1* and *phaC2*) involved in PHA synthesis; and (ii) a depolymerase coding-gene (*phaZ*) responsible for PHA mobilization (de Eugenio *et al.*, 2007) and the *phaD* gene encoding a putative transcriptional regulator (Klinke *et al.*, 2000). The *phaF* and *phaI* genes are transcribed divergently to the other *pha* genes, and encode the phasins playing regulatory and functional roles (Prieto *et al.*, 1999a; Moldes *et al.*, 2004). PhaC, PhaZ, PhaF and PhaI have been so far identified as granule-associated proteins, but very recently, a granule-associated acyl-CoA synthetase that activates the depolymerase products (3-hydroxyalkanoic acids) into the polymerase substrates (3-hydroxyacyl-CoAs thioesters) has been identified in *Pseudomonas putida* GPo1 (Ruth *et al.*, 2008) (Fig. 1).

The PhaZ from *P. putida* KT2442 ($PhaZ_{KT}$), which has been purified and biochemically characterized as the prototype of intracellular mcl-PHA depolymerases (de Eugenio *et al.*, 2007; 2008), remains permanently associated to the PHA granules during PHA-accumulation and PHA-mobilization conditions (de Eugenio *et al.*, 2007),

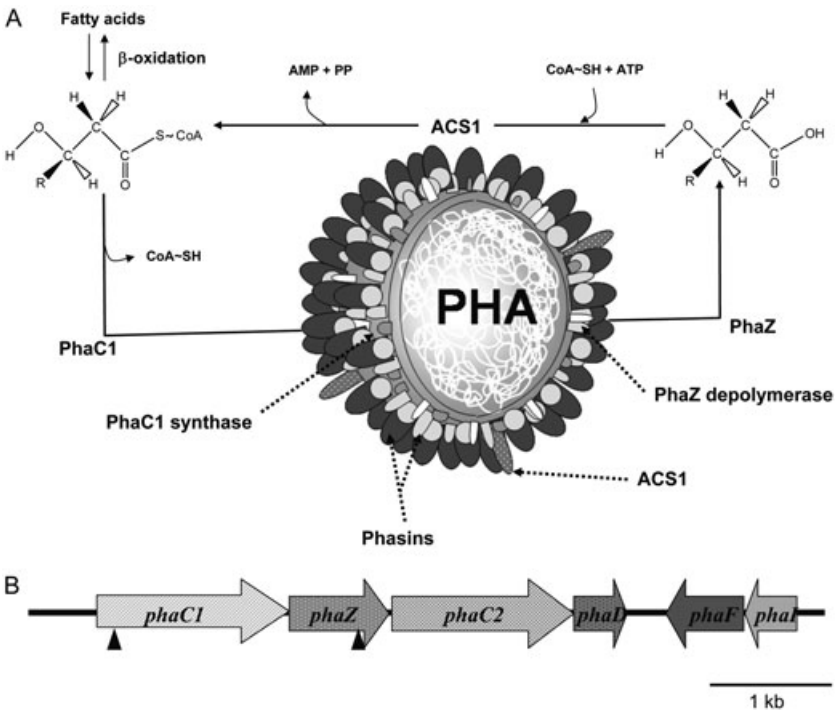

Fig. 1. PHA granule schematic representation and *pha* gene cluster in Pseudomonads.
A. Static model for PHA metabolism (adapted from Ruth *et al*., 2008). 3-Hydroxy fatty acids are released from PHA granule by PhaZ depolymerase and further activated to 3-hydroxyacyl-CoAs by ACS1 acyl synthetase. These activated monomers will be either metabolized via fatty acid degradation, or re-incorporated into PHA granule by PHA synthase (also named polymerase).
B. PHA cluster in Pseudomonads. The *phaC1* and *phaC2* genes encode two synthases and are separated by the *phaZ* gene that encodes an intracellular depolymerase. *phaD* gene encodes a transcriptional regulator. *phaF* and *phaI* genes code for phasins. Disruptions in genes *phaC1* and *phaZ* were represented as triangles. MiniTn*5* transposon and pK18*mobZ* plasmid were inserted at base 5699630 and 5701846 of KT2442 genome respectively.

but a coordinated function of PHA synthase, PHA depolymerase and acyl-CoA synthetase has not been demonstrated yet. Furthermore, the existence of $PhaZ_{KT}$ paralogues encoded in the genome of this model strain and the detection of $PhaZ_{KT}$ cross immunoreactive proteins have been also demonstrated (de Eugenio *et al*., 2007). Whether these parologous enzymes could be also involved in mcl-PHA hydrolysis, building up a more complex hydrolytic system similar to that of the model PHB producer strain *Ralstonia eutropha* H16 (York *et al*., 2001; Uchino *et al*., 2007), needs to be investigated.

In this study, we have demonstrated that mcl-PHA synthesis and mobilization in *P. putida* KT2442 is a simultaneous cyclic process where the $PhaZ_{KT}$ depolymerase plays a fundamental role. This knowledge allowed us to redirect the mcl-PHA metabolism to the production of PHA monomers.

Results

Cell viability versus PHA accumulation

It is generally accepted that bacteria accumulate PHAs in response to inorganic nutrient unbalance when they are cultured in excess carbon sources, due to the increase in the synthase substrate availability (Huisman *et al*., 1991; Madison and Huisman, 1999; Olivera *et al*., 2001; Prieto *et al*., 2007). Depending on the metabolic state of the cell, the hydroxyacyl-CoAs (HA-CoAs) will be incorporated into nascent PHA polymer chains or oxidized through the β-oxidation pathway (Fig. 1). The PHA accumulation/mobilization ability of wild-type *P. putida* KT2442 has been compared with that of synthase (KT42C1) and depolymerase (KT42Z) mutants (Table 1). The KT42C1 strain is unable to polymerize HA-CoAs, but has an intact fatty acid metabolism. It was isolated by a new counter-selection method based on the toxicity of the fluorescent dye Nile Red (see *Experimental procedures*). The lack of *phaC1* transcription in this strain has been demonstrated by RT-PCR (data not shown). To ensure that the observed effects in mutants were specifically caused by *phaZ* and *phaC1* disruptions, complementation studies were carried out (see Fig. S1). The KT2442 wild type, KT42C1 and KT42Z strains were cultured in 0.1 N M63 medium supplemented with sodium octanoate as carbon and energy sources (PHA production growth conditions) and PHA content, biomass, OD_{600} and cell viability were monitored in both cultures during the first 24 h of growth (Fig. 2). Since PHA content disturbs cells turbidimetry, the optical density cannot be used to determine the number of viable cells. Interestingly, although the final PHA content in KT2442 and KT42Z strains were similar after 24 h of growth, the PHA accumulation of KT42Z was delayed during the exponential phase (Fig. 2A and B). In this sense, mutations in the *phaC1-D* region could reduce the transcription rate of the rest of the *pha* genes due to polar mutations. However, alternatives promoters at *phaZ* and *phaC2* upstream regions ensure the transcription of the corresponding *pha* genes (L.I. de Eugenio, B. Galán, I.F. Escapa, B. Maestro,

Table 1. Strains and plasmids.

Strains/plasmid	Phenotype/relevant characteristics	Reference
P. putida		
KT2442	*P. putida* mt-2 without TOL plasmid, *hsdR*, Rf^r	Franklin *et al*. (1981)
KT42C1	KT2442 derivative strain, phaC1 insertional mutant, Km^r	This work
KT42Z	KT2442 derivative strain, *phaZ* disruptional mutant, Km^r	This work
KTLacI^q	KT2442 derivative strain, miniTn*5 lacI^q*::*Ptrc*, Km^r	This work
KTXylS	KT2442 derivative strain, miniTn*5 nahR4/P$_{sal}$→xylS2*, Km^r	This work
KTZ1	KT2442 derivative strain, miniTn*5 nahR4/P$_{sal}$→xylS2, P$_m$→phaZKT*, Km^r, Tc^r	This work
E. coli		
DH10B	F', *mcrA* Δ(*mrr hsdRMS-mcrBC*) ϕ80d*lac*ΔM15 Δ*lacX*74 *deoR recA1 araD*139 Δ(*ara-leu*)7697 *galU galK* λ *rpsL endA1 nupG*	Invitrogen
DH5α	(ϕ80*lacZ*ΔM15) *endA1 recA1 hsdR*17 (rK^- mK^-) *supE*44 Δ*lacU*169	Sambrook and Russell (2001)
CC118λpir	Δ(*ara-leu*) *araD*, Δ*lacX*74, *galE, galK, phoA*20, *thi*-1, *rpsE*, *rpoB argE* (Am), *recA1* Rf^r, Sp^r, contains λpir phage	Herrero *et al*. (1990)
MPO12	K12 derivative strain, Rf^r, *nahR::P$_{sal}$::xylS2*	Royo *et al*. (2005)
Plasmid		
pK18mob	*ori*ColE1 Mob^+ *lacZα*$^+$, Km^r used for directed insertional disruption	Schafer *et al*. (1994)
pK18mob-mutZ	pK18mob derivative containing a fragment of *phaZ* gene, Km^r	This work
pBBR1-MCS5	*ori*pBBR1 Mob^+ *lac* promoter *lacZα*$^+$, Gm^r, broad-host-range cloning and expression vector	Kovach *et al*. (1995)
pPAZ2	pBBR1MCS-5 derivative containing *phaZ* gene, Gm^r	This work
pCNB5	pUTminiTn*5*, *lacI^q::Ptrc*, Km^r, Ap^r	de Lorenzo *et al*. (1993)
pUTminiTn*5*Km1	oriR6K, oriTRP4, Km^r, Ap^r, transposon delivery vector	de Lorenzo *et al*. (1990)
pALEX1b	Cloning vector for CASCADE™ system (Biomedal), *Pm*, Ap^r	Biomedal
pPAZ6	pALEX1b derivative harbouring *phaZ* gene	This work
pUTminiTn*5*Tc	oriR6K, oriTRP4, Tc^r, Ap^r, transposon delivery plasmid	Herrero *et al*. (1990)
pUTTcZ	pUTTc derivative containing *Pm*::*phaZ* construction	This work
pCNB44S2	pUTminiTn*5*, *nahR4/Psal→xylS2*, Ap^r, Km^r	Cebolla *et al*. (2001)

J. Sanz, J.L. García and M.A. Prieto in preparation) as demonstrated for other *P. putida* strains (Sandoval *et al*., 2007). Remarkably, the mutant KT42C1 cells were considerably smaller than that of the wild-type strain (Fig. 2D). Moreover, although during the first 8 h of culture, the number of KT42C1 mutant and wild-type viable cells were similar (1×10^8 to 5×10^8 cells ml^{-1}), at the late exponential phase, the *phaC1* mutant strain increased the number of viable cells, reaching a maximum of 1.9×10^9 cells ml^{-1}; this is more than 10-fold higher than that of wild-type and KT42Z strains (Fig. 2C). Table 2 reflects all the carbon source utilization data of relevant strains, regarding PHA content, biomass, residual carbon source and the presence of 3-hydroxyalkanoic acids (HAs) in the media supernatant after 24 h of growing. Absence (KT42Z) or low content of HAs (KT2442 and KT42C1) were detected. No octanoic acid was present when KT42C1 strain medium supernatant was analysed by gas chromatography-mass spectrometry (GC-MS) (Table 2). These results excluded the carbon waste when PHA metabolism is not active even in a medium with reduced nitrogen content. It is worth to mention that the residual PHA content of KT42C1 cells is due to the low activity of PhaC2 polymerase still present in this strain (Fig. 1B). In this sense, the presence of small PHA granules has been confirmed by electronic microscopy (Fig. 2D).

Taking into account all these results, we can assume that the observed differences in biomass among these strains might be a direct consequence of the PHA content versus carbon consumption by central metabolic pathways. The complete exhaustion of octanoic acid in the KT42C1 culture correlates with the increased number of viable cells in comparison with that of the wild-type and KT42Z strains.

The lack of PHA synthesis directed the cells metabolism to consume the carbon source for increasing cell number, even in the presence of a low concentration of nitrogen and thus, we can conclude that the bacterial community is strongly influenced by PHA metabolism.

Cell viability versus PHA mobilization under carbon starvation and nitrogen extra addition

The number of viable cells in cultures of KT42C1 and KT42Z mutants and wild-type strain was monitored over 16 days of incubation to determine their ability to mobilize the accumulated PHA under carbon starvation conditions, as well as the influence of PHA content in cell viability over the time. Figure 3 shows that cell viability was constant during the first week for all the strains, maintaining the difference of an order of magnitude between KT42C1 and the other strains. At day number 7, all cultures were split up and the influence of nitrogen supplementation in cell viability was tested during 9 days. Thus, the number of viable cells was determined in culture samples supplemented with ammonium sulfate

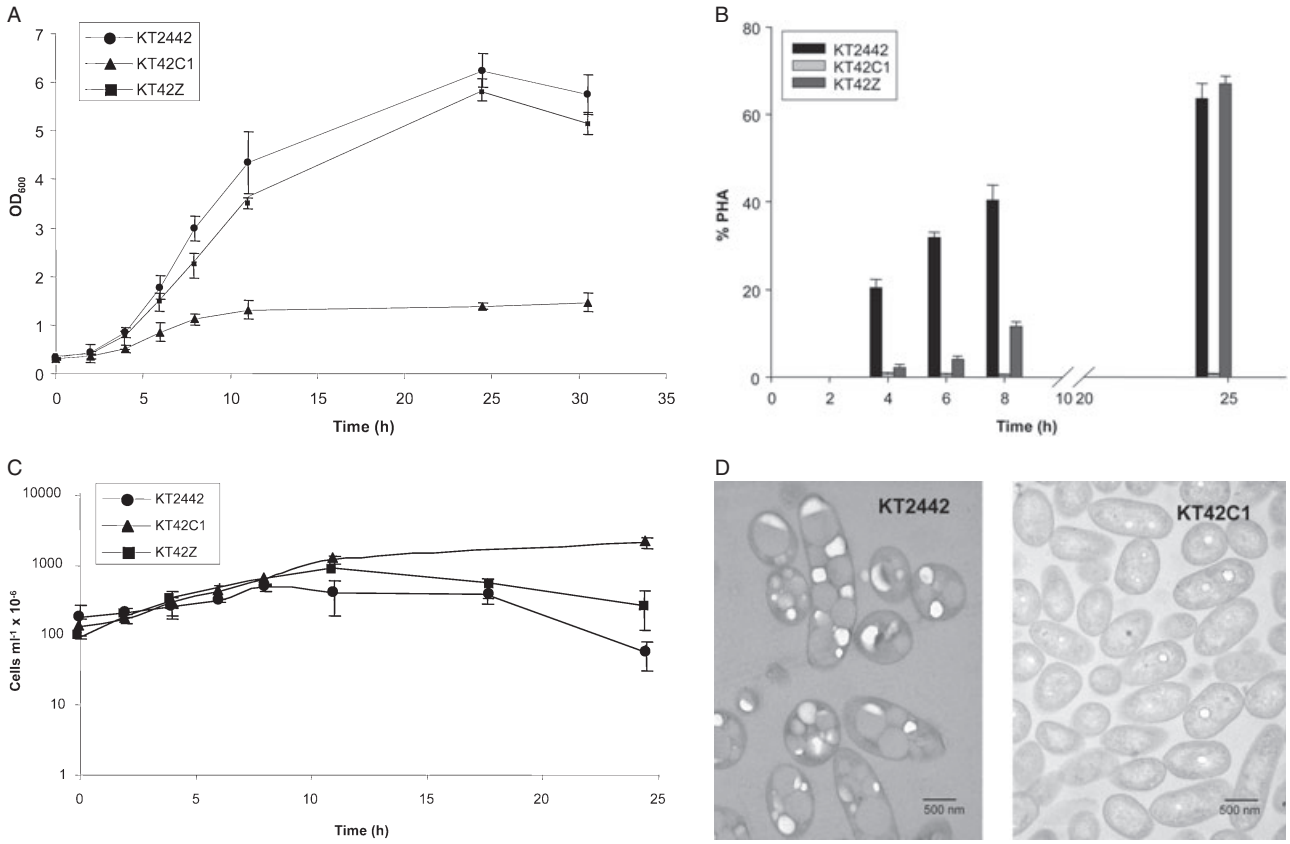

Fig. 2. Turbidimetry and PHA content versus number of viable cells in *P. putida* KT2442, KT42C1 and KT42Z cultures.
A. OD_{600} of cultures growing in 200 ml of 0.1 N M63 plus 15 mM octanoate over time. Inocula of the strains were prepared in LB medium to ensure their most similar metabolic status. Cultures were inoculated at OD_{600} of 0.3.
B. PHA content of cells growing in 0.1 N M63 plus 15 mM octanoate determined by GC.
C. Number of viable cells under PHA production conditions.
D. Electronic microscope images of KT2442 and KT42C1 strains after 24 h of growth in 0.1 N M63 plus 15 mM octanoate.
Error bars represent standard deviation found in three different experiments.

and compared with that of culture samples without nitrogen (Fig. 3). At the eighth day, PHA granules completely disappeared in KT2442 nitrogen-supplemented cells as determined by phase-contrast microscopy (data not shown). Simultaneously, the number of KT2442 cells increased to the same level of the mutant KT42C1 while that of KT42Z and KT42C1 remained unchanged. The results demonstrated that *P. putida* KT2442 is able to mobilize the stored carbon in the presence of nitrogen even in the absence of external energy sources. The cell

Table 2. HAs and PHA production, viability, residual octanoate and biomass concentrations.

P. putida strains	Intracellular PHA (% CDW)	Intracellular PHA ($g\ l^{-1}$)	Extracellular HAs ($g\ l^{-1}$)	Residual octanoate ($g\ l^{-1}$)	Biomass ($g\ l^{-1}$)	Viability (10^{-6} cells ml^{-1})
KT2442	69.89 ± 2.56	1.29 ± 0.05	0.07 ± 0.01	0.01 ± 0.004	1.85 ± 0.35	77 ± 35
KT42Z	72.33 ± 1.96	0.83 ± 0.02	nd	0.09 ± 0.01	1.14 ± 0.23	260 ± 25
KT42C1	0.50 ± 0.14	< 0.007	0.07 ± 0.006	nd	0.55 ± 0.12	1900 ± 430
KT2442 (pPAZ2)	19.08 ± 0.39	0.14 ± 0.003	0.39 ± 0.04	1.30 ± 0.06	0.76 ± 0.15	6.3 ± 1.5
KTLacI^q (pPAZ2)	46.20 ± 1.43	0.62 ± 0.02	nd	1.67 ± 0.18	1.38 ± 0.12	4.0 ± 1.5
KTLacI^q (pPAZ2) (5 mM IPTG)	24.69 ± 1.16	0.067 ± 0.003	0.24 ± 0.01	1.56 ± 0.14	0.27 ± 0.10	11.0 ± 4.5
KTZ1	64.68 ± 3.82	1.17 ± 0.07	nd	0.05 ± 0.004	1.81 ± 0.50	98 ± 29
KTZ1 (5 mM benzoate)	1.04 ± 0.01	< 0.007	0.73 ± 0.02	0.12 ± 0.003	0.60 ± 0.11	1500 ± 120

nd, not detected.

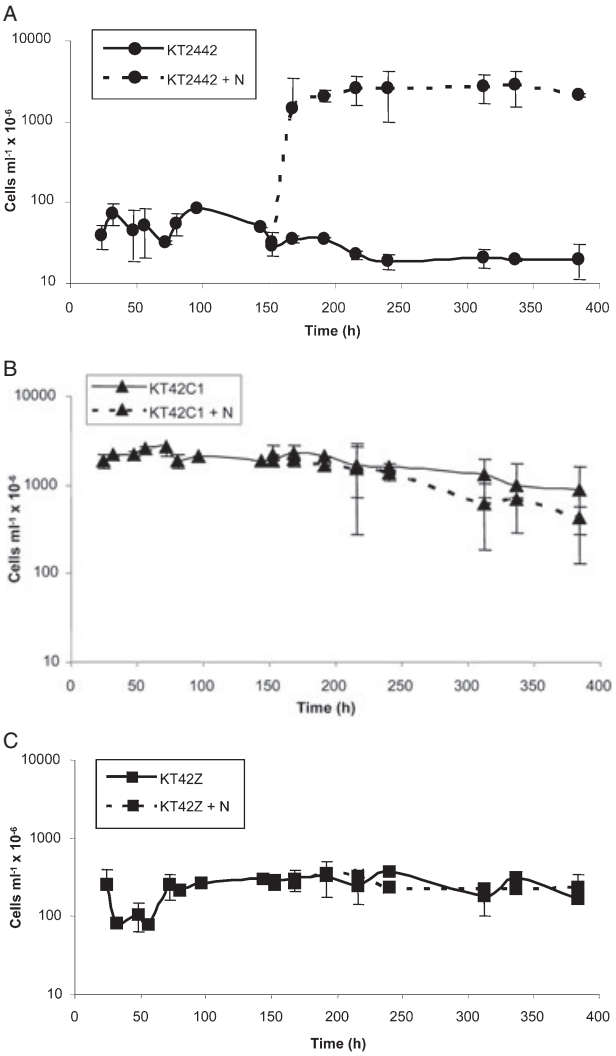

Fig. 3. Influence of nitrogen supplementation on number of viable cells in *P. putida* KT2442, KT42C1 and KT42Z cultures. Cells were grown under PHA production conditions and supplemented with 2 g l^{-1} ammonium sulfate after 1 week. Solid lines represent non-supplemented cultures. Dotted lines represent nitrogen supplemented cultures. (A) KT2442, (B) KT42C1 and (C) KT42Z cells. Error bars represent standard deviation found in three different experiments.

viability of KT42C1 cells slightly decreased after the first week of cultivation independently of the addition of extra nitrogen sources, but it kept in the same order of magnitude over 16 days of monitoring (Fig. 3). These experiments strongly suggest that the ability for PHA accumulation/mobilization in *P. putida* KT2442 makes this strain more robust to become adapted to unfavourable nutrient conditions. Moreover, the fact that addition of extra nitrogen source promotes PHA hydrolysis is in agreement with our previous finding, which demonstrated the induction of the depolymerase transcription in the presence of extra added nitrogen sources (de Eugenio *et al.*, 2007; 2008).

$PhaZ_{KT}$ depolymerase as unique functional PHA-mobilizing enzyme

The role of a $PhaZ_{KT}$-like enzyme in the mobilization of accumulated PHA has been documented previously in *P. putida* GPo1 when cells were incubated in alkaline conditions (Ren *et al.*, 2005; Wang *et al.*, 2007). The experiments shown in Fig. 3 suggest that $PhaZ_{KT}$ is the sole depolymerase of *P. putida* KT2442, because an external addition of ammonium sulfate did not increase the number of viable cells of KT42Z mutant. However, the existence of $PhaZ_{KT}$ cross immunoreactive proteins induced at PHA mobilization conditions have been also demonstrated (de Eugenio *et al.*, 2007). To exclude the implication of other hydrolases in the PHA mobilization triggered by pH conditions, we have compared in a resting cell system the PHA degradation in the wild-type strain versus the KT42Z mutant by using an extremely sensitive radioactive method previously established for the detection of PHA depolymerase activity (Fig. 4). This method is based on the use of ^{14}C-labelled PHA as depolymerase substrate and the subsequent detection of the released radioactive soluble products (de Eugenio *et al.*, 2007). To generate the labelled polyester, the wild-type strain and its KT42Z mutant were cultured for 24 h under PHA production conditions in the presence of ^{14}C-octanoic acid as PHA precursor. After centrifugation, the cells were shifted to water (pH 5.5) and different buffered solutions at pH ranging from 4 to 10.6, incubated at 30°C, and the secretion of radioactive-labelled products was monitored over the time (Fig. 4A). The highest radioactivity value was observed at alkaline conditions (50 mM glycine-NaOH buffer pH 10.6) for the wild-type strain but none radioactive metabolites was detected in the supernatant of KT42Z mutant (Fig. 4B). The absence of HAs in the supernatant of KT42Z strain was confirmed by liquid chromatography-mass spectrometry (LC-MS) analyses. These results agree with the behaviour of *P. putida* GPo1 (Ren *et al.*, 2005), and definitively demonstrate that no PHA mobilization can be achieved in KT42Z strain, suggesting that this function can be only ascribed to $PhaZ_{KT}$ in *P. putida* KT2442. A film illustrating the mobilization of PHA triggered by alkaline conditions in *P. putida* KT2442 is provided as Movie S1 in Supplementary Material. About 70% of previously accumulated PHA in the wild-type strain was mobilized to the supernatant as HAs monomers and dimers. In cells containing 1.01 g l^{-1} PHA, the HA productivity reached a maximum of 0.72 g l^{-1}. When composition of released products was analysed by LC-MS, three major peaks could be distinguished (Fig. 4C and D). Peak 1 was identified as main single charged ion *m/z* 131, corresponding to the molecular mass of the deprotonated 3-hydroxyhexanoic acid, whereas peak 2 corresponded to 3-hydroxyoctanoic acid (*m/z* 159). The deprotonated

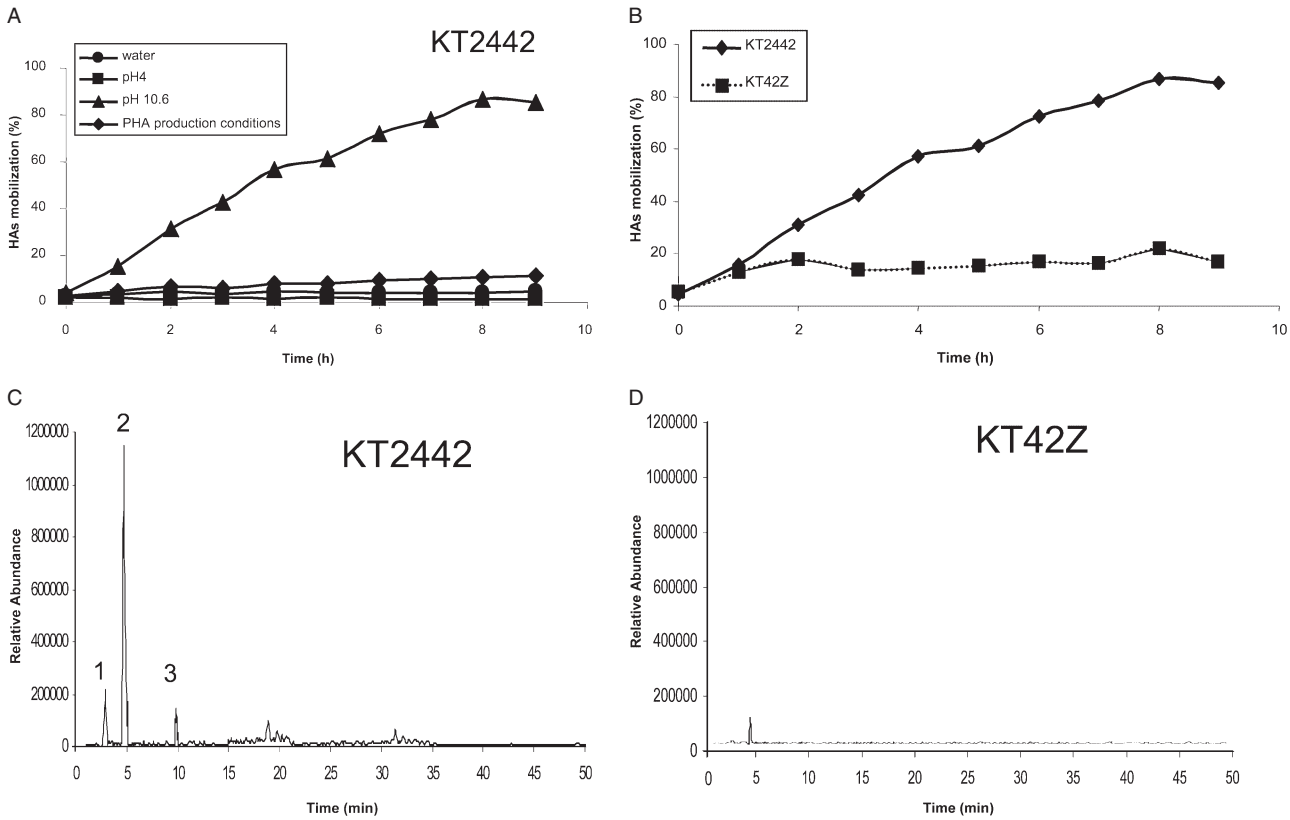

Fig. 4. pH influence on PHA mobilization in *P. putida* KT2442 and KT42Z cultures.
A and B. ^{14}C-HAs release monitored by radioactivity counting from (A) KT2442 cells suspended in various pH buffers and solutions. PHA production conditions mean incubation in M63 0.1 N plus 15 mM sodium octanoate. (B) HAs release comparison between KT2442 and KT42Z strains incubated in a buffered solution at pH 10.6.
C and D. LC-ESI-MS analysis of KT2442 (C) and KT42Z (D) supernatants incubated at Glycine-NaOH buffer 50 mM, pH 10.6.

3-hydroxyoctanoic dimer and the dimer adduct of 3-hydroxyoctanoic diester were found in peak 3 (*m/z* 301 and *m/z* 603 respectively). The three major peaks identified in wild type were absent in KT42Z supernatant.

PHA turnover directed by a functional PhaZ$_{KT}$ depolymerase

The current model for the PHB metabolism proposes the existence of continuously active PHA machinery able to accumulate or to mobilize carbon as a response to nutrient requirements and reduction power (Doi *et al.*, 1990; Uchino *et al.*, 2007). The assumption of a similar model in *P. putida* KT2442 for PHA metabolism requires the coexistence of an active depolymerase enzyme during PHA accumulation. In fact, we have demonstrated the presence of PhaZ$_{KT}$ in the PHA granules when cells are producing PHA (de Eugenio *et al.*, 2007). To support this hypothesis, the PHA accumulation/mobilization ability was tested in KT2442 and KT42Z cells exposed to starvation and excess of carbon source (Fig. 5). When cells were grown for 24 h (Fig. 5, cultures 1 and 4) or 48 h (Fig. 5, cultures 2 and 5), under PHA production conditions with octanoic acid, maximum PHA accumulation was found after 24 h of growth in both strains, with very low differences in PHA content. In agreement with the model, only 4% of HAs related to the cell dry weight (CDW) was detected in the KT2442 strain supernatant in PHA production medium (Table 2), confirming that the metabolism is directed to PHA accumulation and not to PHA mobilization. The PHA content in KT42Z mutant increased 3.5% compared with that of wild type and HAs were not detected in the supernatant (Table 2). These results might suggest that, under these growth conditions, PhaZ$_{KT}$ is inactive or very low active, and that no other depolymerase or hydrolase is able to degrade the polymer in the wild-type strain. Alternatively, it could be envisaged that PHA synthase is more active than the PHA depolymerase resulting in PHA accumulation. To discriminate between both possibilities, nonanoic acid (10 mM) was added to an existing 24 h octanoic culture [containing 60–70% poly(hydroxyoctanoate-*co*hydroxyhexanoate) (P(HO-*co*-HX))] and incubated during 24 additional hours. The results shown in Fig. 5

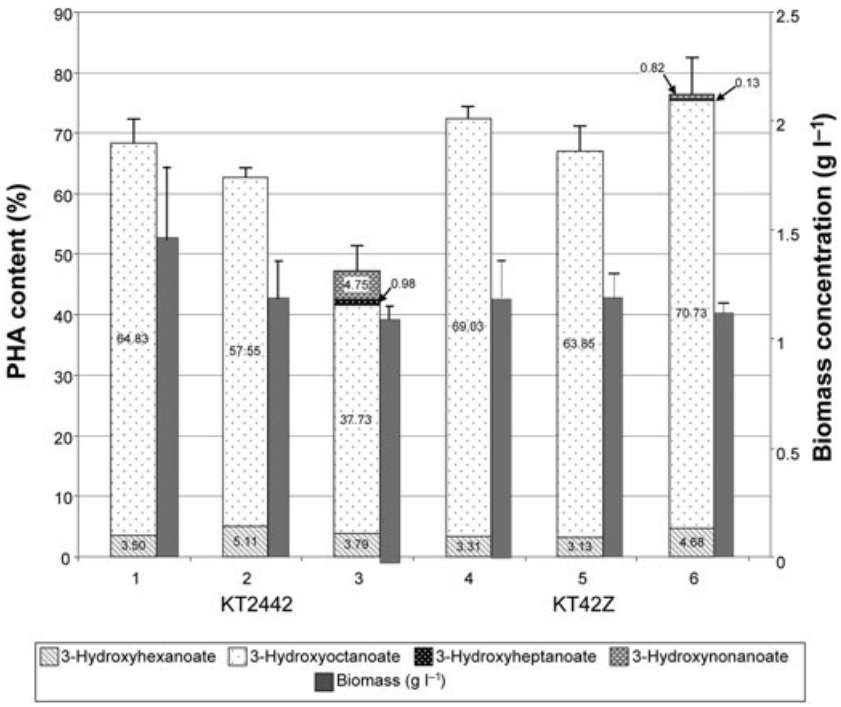

Fig. 5. Cyclic nature of PHA metabolism in *P. putida* KT2442. For PHA content and composition analysis KT2442 and KT42Z strains were cultured under different conditions for 24 or 48 h. Cultures 1 and 4 were grown in 0.1 N M63 plus 15 mM octanoate for 24 h; cultures 2 and 5 were grown in 0.1 N M63 plus 15 mM octanoate for 48 h; cultures 3 and 6 were grown in 0.1 N M63 15 mM octanoate for 24 h, supplemented with 10 mM nonanoic acid and further incubated for 24 additional hours. Numbers inside shadowed bars represent monomer ratio as percentage of CDW. Grey solid bars represent biomass concentration. Error bars represent standard deviation found in three different experiments.

demonstrate not only that $PhaZ_{KT}$ is active, but also that both PHA synthesis and hydrolysis are carried out simultaneously (Fig. 5, cultures 3 and 6). The pre-existing polymer could be distinguished from the PHA synthesized *de novo* by their monomer content/ratio, since the new one contains odd monomers like hydroxynonanoic and heptanonanoic acids (Fig. 5). The PHA polymer content and monomer composition of KT42Z mutant (Fig. 5) confirmed that $PhaZ_{KT}$ plays a crucial role in this process (Fig. 5, cultures 3 and 6). Thus, the lack of PHA depolymerase completely avoids the hydrolysis of PHA that increases from 72% of CDW at 24 h to 76% after the addition of the extra carbon source. Furthermore, the presence of odd monomers in the sediment is very low (1% of the total PHA content) indicating a reduced activity of the synthase. Biomass parameters do not change significantly after 24 h of growth, most probably due to the exhaustion of nitrogen or other inorganic nutrient in the media. Taken together, all these results definitively demonstrate the existence of PHA metabolic turnover in *P. putida* KT2442 and the crucial role played by $PhaZ_{KT}$.

Redirecting the PHA metabolism to its hydrolysis in growing cells by increasing $PhaZ_{KT}$ dosage: multicopy versus monocopy expression systems

We have demonstrated above that the lack of PHA accumulation machinery in the KT42C1 mutant strain directed the cells to completely consume the carbon and energy sources of the culture medium in order to promote cell division even when a low nitrogen concentration was supplied to the growth medium. Although PHA synthesis and hydrolysis function simultaneously in the wild-type cells, when PHA must be accumulated the synthase and depolymerase levels are precisely balanced to direct the metabolism to polymer synthesis. Then, it could be hypothesized that an extra dosage of PHA depolymerase could break this balance and redirect their PHA metabolism to the hydrolysis counterpart, even when cells were cultured under PHA production conditions. To test this hypothesis we have used the plasmid pPAZ2, which overexpresses $PhaZ_{KT}$ depolymerase. The functionality of the $PhaZ_{KT}$ depolymerase cloned in this plasmid was demonstrated by showing that an increase in the copy number of $phaZ_{KT}$ gene in a PhaZ mutant of the strain *P. putida* U resulted in a significant reduction of PHA accumulation (de Eugenio *et al*., 2007). These findings also suggested that PHA can be hydrolysed simultaneously to its synthesis during growth. In this case, we have constructed the *P. putida* KTLacI^q strain (Table 1) able to control the expression of the $phaZ_{KT}$ gene cloned in pPAZ2 by a P_{lac} promoter and the inducer IPTG (isopropyl-beta-D-thiogalactopyranoside), since this strain carries a copy of the transcriptional repressor LacI^q of *Escherichia coli* in its genome (see *Experimental procedures* for the construction). *Pseudomonas putida* KT2442 (pPAZ2) and *P. putida* KTLacI^q (pPAZ2) were cultured under PHA production conditions and samples were collected after 24 h of growth. Cells of *P. putida* KTLacI^q (pPAZ2) were also cultured in the presence of 5 mM IPTG to induce the expression of the $PhaZ_{KT}$ depolymerase. The PHA content and the composition of the culture medium of each strain were

analysed (Table 2). As expected, the PHA content in the untransformed wild-type strain was 3.5-fold higher than in the recombinant *P. putida* KT2442 (pPAZ2) which constitutively overexpresses $PhaZ_{KT}$ depolymerase. Even more, the high amount of HAs detected in the culture medium of the recombinant strain also suggests that it has increased its depolymerization capacity. This high PHA hydrolytic capacity was further confirmed when *P. putida* KTlacI^q (pPAZ2) was cultured in the presence or absence of IPTG (Table 2). In the absence of IPTG, i.e. when depolymerase extra expression is switched off, the PHA content was equally high in both *P. putida* KTLacI^q (pPAZ2) and in the wild-type strain (Table 2). Similar results were obtained in *P. putida* KT2442 carrying the control plasmid pBBR1MCS5 (data not shown). However, in the presence of IPTG, i.e. when depolymerase extra expression is switched on, the PHA content is reduced to approximately the half in *P. putida* KTLacI^q (pPAZ2) (Table 2). The amounts of HAs detected in the culture medium correlate with the PHA content, i.e. the HAs levels increases as far as the PHA content decreases when depolymerase is overexpressed. These results indicate that *phaZ* expression is perfectly controlled under P_{lac} promoter in the new recombinant strain and allowed us to demonstrate that PHA metabolic balance can be controlled and redirected to promote PHA hydrolysis and, consequently, to secrete HAs to the culture medium. Nevertheless, the growth of these recombinant strains was significantly affected by the presence of gentamicin in the growth media which causes a reduction of cell viability and biomass, and the detection of non-consumed carbon source in the culture media. To solve these problems, we studied the possibility of using a miniTn*5* expression system to control the depolymerase dosage in the recombinant strains avoiding the use of antibiotic-containing media (de Lorenzo *et al.*, 1993; Panke *et al.*, 1998; Prieto *et al.*, 1999b). Therefore, we constructed a stable and regulated expression system for $PhaZ_{KT}$ depolymerase by inserting both regulatory and expression systems into the bacterial genome using the minitransposons from Cascade™ system (Fig. S2). In this case, the overexpression of the target gene is under the control of the benzoate-dependent mutant activator XylS2 and the P_m promoter from the well-characterized *meta*-cleavage catabolic operon of the TOL plasmid of *P. putida.* Furthermore, the cascade regulatory circuit implies the control of *xylS2* expression through NahR4, the benzoate-sensitive mutant of the regulator NahR from the naphthalene degradation plasmid NAH7 (Cebolla *et al.*, 2001). First, we constructed the plasmid pPAZ6, by cloning the $phaZ_{KT}$ gene in the vector pALEX1b (Table 1, Fig. S2). For testing the overproduction of the depolymerase under the Cascade™ system, the plasmid was transferred to *E. coli* MPO12 (Table 1), which carries the *nahR-*P_{sal}*-XylS2* in its chromosome and activates P_m promoter in the presence of salicylate (Royo *et al.*, 2005) (Fig. 6). As expected, a protein band of around 32 kDa correlating with the depolymerase molecular mass was clearly detectable in these cells (Fig. 6, lane 4). The expression cassette P_m*::*$phaZ_{KT}$ from plasmid pPAZ6 was excised and cloned into the pPUTTc resulting plasmid pUTTcZ (Table 1). Then, the plasmids pUTTcZ and pCNB44S2 were transferred by conjugation into *P. putida* KT2442 resulting the recombinant KTZ1 strain, which carries into its chromosome the expression system *nahR4/*P_{sal}*::xylS2/*P_m*::*$phaZ_{KT}$ that can be induced by benzoate (Table 1). In the absence of benzoate, all parameters tested in *P. putida* KTZ1 cultures, i.e. PHA content, extracellular content of HAs, residual carbon source, biomass and viable cells, were very similar to those observed for the wild-type strain (Table 2). However, the addition of 5 mM benzoate leads to a drastic decrease in PHA content and an increase in HAs detected in the *P. putida* KTZ1 culture medium, 10-fold higher than in the wild-type strain (Table 2). The significant increase in the number of viable cells of *P. putida* KTZ1 cells with and without inducer can be explained by the ability of KT2442 and its derivative strains to mineralize benzoate (Jiménez *et al.*, 2002). In this sense, the benzoate content in the supernatant of the medium of KTZ1 varies from 0.73 g l^{-1} at time zero to 0.09 g l^{-1} after 24 h of growing, indicating that the inducer is consumed as carbon and energy source.

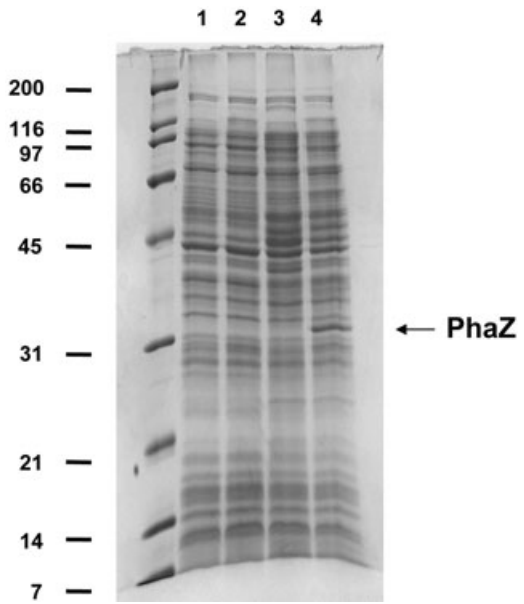

Fig. 6. PhaZ production under Cascade™ system. PhaZ expression in *E. coli* MPO12 (pPAZ6) strain. Twenty-five microlitres of each cell suspension at OD_{600} 3 was loaded. Lanes: 1, *E. coli* MPO12 before induction; 2, *E. coli* MPO12 (pPAZ6) before induction; 3, *E. coli* MPO12 after induction with 2 mM salicylate; 4, *E. coli* MPO12 (pPAZ6) after induction. Standard molecular weight markers, in kDa, are marked at the left.

Analysis of HAs released to the culture media

The chemical configuration of the HAs monomers released to the culture medium by *P. putida* KTZ1 was examined by chiral GC (Fig. 7). Whereas the racemic standard (*R,S*)-3-hydroxyoctanoate methyl ester showed two chromatographic peaks (with the retention times of 23.8 and 24.2) corresponding to the two enantiomers (Fig. 7), only one peak was detected for the samples of 3-hydroxyoctanoate methyl ester extracted from all culture media tested, indicating a high enantiomeric purity of these samples. In addition, by mixing the produced 3-hydroxyoctanoate methyl ester with the racemic standard, the area of the latter peak increased (data not shown), confirming the absolute (*R*)-configuration of all these samples. Therefore, the HAs produced in this work in a resting cell system or under PHA production conditions (Table 2) have the same configuration.

The chemical composition of the released products by *P. putida* KTZ1 cultured under PHA production conditions was also examined by LC-MS to determine the presence of dimers, trimers or higher polymers of HAs in the medium. The chromatograms revealed the presence of three major peaks (Fig. S3), where peak 1 (*m/z* 131) corresponded to the molecular mass of the deprotonated 3-hydroxyhexanoic acid and peak 2 (*m/z* 159) to 3-hydroxyoctanoic acid. Ions corresponding to *m/z* 301 and *m/z* 603 found in peak 3 highlighted the presence of the deprotonated 3-hydroxyoctanoic dimer and the dimer adduct of 3-hydroxyoctanoic diester respectively. Dimers containing 3-hydroxyhexanoic acid and polymers with higher molecular weight were not found.

Discussion

Polyhydroxyalkanoate acts as sinks for carbon and reducing equivalents when other nutrient supplies are limited (Prieto *et al*., 2007) and consequently, PHA degradation under stress conditions has been proposed as a mechanism that favours the establishment of PHA-producing bacteria in competitive environments, such as soil and rhizosphere (Madison and Huisman, 1999; Ruiz *et al*., 2001; Kadouri *et al*., 2005). Under certain circumstances, free-living bacterial cells with a higher content of PHA may survive longer than those with a lower PHA content, either because they are less susceptible to adverse factors, or because they can utilize this reserve material longer and more efficiently (Dawes and Senior, 1973; Matin *et al*., 1979). In this work, we have analysed the impact of PHA metabolism on cell viability under laboratory conditions in terms of carbon source utilization in the mcl-PHA model producer *P. putida* KT2442 strain. We have demonstrated that the ability of metabolizing PHA appears to endow the producing cells with increased endurance under carbon starvation conditions that results in an increased viable cells number. In addition, the fundamental and exclusive role of PhaZ depolymerase in PHA mobilization has been definitively demonstrated, since a mutant strain lacking the *phaZ* gene was not able to degrade the intracellular polymer.

Increased survival and respiration under starvation conditions were previously detected in PHB producer strains such as *Azospirillum brasilense* (Tal and Okon, 1985). Furthermore, *A. brasilense* mutants defective in their capability to produce PHA (*phaC*$^-$ mutant) (Kadouri *et al*., 2002) or to degrade PHA (*phaZ*$^-$ mutant) (Kadouri *et al*., 2003) survived shorter than the wild-type strain. *Pseudomonas putida* GPo1 containing PHA survived starvation better than its cognate PHA depolymerase mutant when cells were incubated under starvation conditions in natural environments, or under conditions mimicking natural settings (Ruiz *et al*., 2001). Nevertheless, the mechanisms by which the PHA metabolism favours stress alleviation in *P. putida* GPo1 are not yet fully understood, but enhanced cross-tolerance to different stress agents

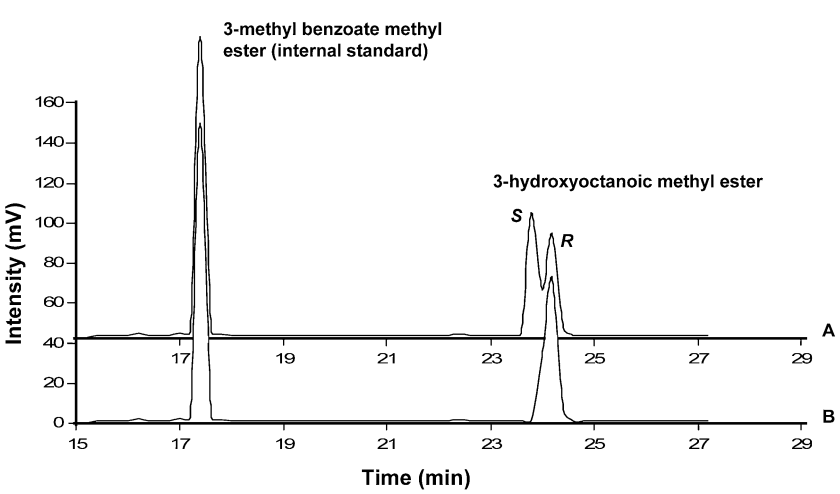

Fig. 7. Chirality of products released by PHA enzymatic hydrolysis. Chiral GC analysis of methyl esters of racemic mixtures of (A) (*R,S)*-3-OH octanoic acid and (B) (*R)*-3-OH octanoic acid identified in the *P. putida* KTZ1 supernatant after 24 h induction with benzoate 5 mM.

during PHA depolymerization has also been correlated to an increase in the concentration of RpoS, suggesting a link between PHA depolymerization and the stress tolerance (Ruiz *et al.*, 2004). Our results demonstrated that *P. putida* can support cell multiplication in the absence of an exogenous carbon source by mobilizing PHA, as previously demonstrated in the PHB producer *R. eutropha* H16 (Handrick *et al.*, 2000), and that this ability is strictly dependent on the existence of an active PhaZ depolymerase. However, under laboratory conditions growing in defined media, we have not detected survival differences among the *P. putida* KT2442 wild-type strain and PHA-metabolic defective mutants. Generally speaking, it could be presumed that bacteria control the number of community members as function of carbon/inorganic nutrient ratio. Since the lack of a fully functional PHA metabolic system avoids the ability to adapt the number of viable cells to extra source of inorganic nutrients like nitrogen (Fig. 3), this work demonstrates that the presence of the PHA synthase/depolymerase system allows *P. putida* KT2442 to adapt the carbon flux of HAs to cellular demand. In this sense, the PHA-free biomasses of *P. putida* KT2442 and KT42C1 strains were similar [22.1% and 25.7% (g biomass per g octanoate) respectively], but the rate of conversion of octanoate to biomass differed considerably when PHA contents were considered [22.2% and 74.0% (g biomass per g octanoate), for *P. putida* KT42C1 and KT2442 strains respectively]. Consequently, the increased production of metabolic intermediates in the PhaC1 mutant strain needs further investigations.

A simple view of PHA metabolism has been frequently resumed: bacteria facing carbon excess and nutrient limitation store the extra carbon substrate as PHA via PHA polymerase (PhaC). Under carbon starvation conditions, PHA depolymerase (PhaZ) degrades PHA and releases 3-hydroxycarboxylic acid monomers, which after activation to HA-CoAs, can be oxidized by the β-oxidation pathway (Fig. 1). However, a simultaneous cyclic mechanism for the biosynthesis and degradation of PHA in bacteria were early proposed in the PHB producers *Azotobacter beijerinckii* (Senior and Dawes, 1973) and *R. eutropha* (Doi *et al.*, 1990; Taidi *et al.*, 1995). In the latter strain 3-hydroxybutyryl-CoAs are released by PhaZa1 depolymerase (Kobayashi and Saito, 2003; Uchino *et al.*, 2007) in contrast with the HAs released by PhaZ $_{KT}$ enzyme (de Eugenio *et al.*, 2007). In these strains, the turnover can be explained by considering the PHA metabolism as a buffer of carbon and reducing power.

In this work we have finally demonstrated that PHA metabolism in *P. putida* KT2442 is an ongoing cycle where synthesis and degradation of the polyesters are simultaneously active to facilitate the turnover of the polymer, and the crucial role played by $PhaZ_{KT}$ depolymerase (Fig. 5). Taking into account the recent finding of an acyl-CoA synthetase (ACS1) associated with the PHA granules (Ruth *et al.*, 2008), the current model for the PHA metabolism in *P. putida* supports a coordinated activity of polymerase, depolymerase and acyl-CoA synthetase. Cells facing carbon excess and nutrient limitation directed the PHA metabolism to store the extra carbon in the form of insoluble polyesters by PHA synthase. Under carbon starvation, PHA metabolism is unbalanced to the hydrolysis pathway, and *R*-HAs monomers are excised from the polymer by the action of the PhaZ depolymerase. The released monomers are then activated to HA-CoAs by a granule associated acyl-CoA synthetase via an ATP-dependent reaction (Ruth *et al.*, 2008). These metabolites are substrates for both PHA synthase and fatty acid β-oxidation cycle and thus, depending on the metabolic state of the cell, the HA-CoAs will be either incorporated into nascent PHA polymer chains by the PHA synthase, or oxidized by the β-oxidation pathway to generate energy (Fig. 1). These results were in agreement with our previous findings, which demonstrated that the $PhaZ_{KT}$ depolymerase was produced under both PHA production and PHA mobilization growth conditions (de Eugenio *et al.*, 2007).

On the other hand, PHA has been proposed as potential source of *R*-HAs (Ren *et al.*, 2005; Ruth *et al.*, 2007). Actually, HA monomers as well as oligomers are important building blocks for biotechnological applications (Ren *et al.*, 2005; Sandoval *et al.*, 2005; Schreck and Hillmyer, 2007). The first enzymatic-based strategy developed for the production of *R*-HA monomers from mcl-PHA was described in *P. putida* GPo1 (Ren *et al.*, 2005; Ruth *et al.*, 2007; Wang *et al.*, 2007). In this approach, cells were first grown under double (carbon and nitrogen) nutrient limitation conditions in order to induce a high PHA accumulation in a continuous culture and, afterwards, re-suspended in phosphate buffer adjusted to basic environments (pH 10) as a resting cells system. These authors obtained a release of 1.05 mg ml^{-1} of HAs, in agreement with the results obtained in this work (Ruth *et al.*, 2007). Figure 4 shows that the unique enzyme responsible for the hydrolysis of the polymer in *P. putida* KT2442 under alkaline conditions is $PhaZ_{KT}$, and demonstrated that, similarly to *P. putida* GPo1, it secretes HAs monomers to the medium as a consequence of a massive PHA hydrolysis. The yield in the resting cell-production systems will be always conditioned by the PHA accumulation ability of the target strain. However, growing cell strategies for the production of enantiomeric pure HAs imply a massive PHA mobilizing system that hydrolyses PHA simultaneously to its synthesis. In this sense, different growing cell strategies have been proposed in Pseudomonads for the production of HAs (Sandoval *et al.*, 2005; Yuan *et al.*, 2008). It has been demonstrated

that overexpression of the *phaZ* gene in a PHA overproducer mutant of *P. putida* U allowed the bioconversion of different *n*-phenylalkanoic acids into a racemic mixture of the corresponding 3-hydroxyderivatives that were secreted into the culture medium with a yield of 1.92 mg ml^{-1} of HAs (Sandoval *et al.*, 2005). However, the released *(R)*-enantiomers were immediately epimerized to the *(S)*-isomers as a consequence of the genetic background of that strain, which is defective for the β-oxidation cycle (Sandoval *et al.*, 2005). Recently, it has been published that the production of the PhaZ of *Pseudomonas stutzeri* in *P. putida* KT2442, together with a putative long-chain fatty acid transport protein of *P. putida* and an acyl-CoA synthetase of *E. coli*, improved the release of HAs to 2.32 mg ml^{-1} of HAs when the cells were cultured in shake flasks (Yuan *et al.*, 2008). In this case, the chirality of the released HAs was also not determined. Therefore, our results constitute the first example of a biotechnology system able to produce pure *R*-mcl-HAs monomer by using growing cells. To direct the PHA balance to PHA hydrolysis, we have applied a tight inducible system cascade control circuit integrated into the chromosome which allows culturing the recombinant cells in the absence of antibiotics (de Lorenzo *et al.*, 1993; Cebolla *et al.*, 2001). Taking into account the great advantages of our novel *in vivo* strategy, we believe that it will pave the way for implementing a large-scale bioproduction of *R*-mcl-HAs monomers.

Experimental procedures

Bacterial strains, media and growth conditions

Bacterial strains and plasmids used in this work are described in Table 1. *Pseudomonas putida* KT2442 is a derivative strain of the parental strain KT2440 whose complete nucleotide sequence of the genome is accessible in the data bank (Nelson *et al.*, 2002). Unless otherwise stated, *E. coli* and *P. putida* strains were grown in Luria–Bertani (LB) medium (Sambrook and Russell, 2001) at 37°C and 30°C with shaking respectively. The appropriate selection antibiotics, gentamicin (10 μg ml^{-1}), chloramphenicol (34 μg ml^{-1}), kanamycin (50 μg ml^{-1}), or tetracycline (5 μg ml^{-1}), were added when needed. For P(HO-*co*-HX) production, *P. putida* strains were grown in 0.1 N M63, which is a nitrogen-limited minimal medium [13.6 g of KH_2PO_4 l^{-1}, 0.2 g of $(NH_4)_2SO_4$ l^{-1}, 0.5 mg of $FeSO_4 \cdot 7\ H_2O$ l^{-1}, adjusted to pH 7.0 with KOH], plus 2.5 g l^{-1} sodium octanoate (15 mM), for 24 h at 30°C as previously described (Moldes *et al.*, 2004). This medium was supplemented with $MgSO_4$ 1 mM and a solution of trace elements (composition 1000×: 2.78 g of $FeSO_4 \cdot 7H_2O$ l^{-1}, 1.98 g of $MnCl_2 \cdot 4H_2O$ l^{-1}, 2.81 g of $CoSO_4 \cdot 7H_2O$ l^{-1}, 1.47 g of $CaCl_2 \cdot 2H_2O$ l^{-1}, 0.17 g of $CuCl_2 \cdot 2H_2O$ l^{-1}, 0.29 g of $ZnSO_4 \cdot 7H_2O$ l^{-1}). For PHA turnover analysis, 1.6 g l^{-1} nonanoic acid (10 mM) was added to a previously 24 h growing culture of KT2442 or KT42Z strains in 0.1 N M63 medium plus 15 mM sodium octanoate. For nitrogen supplementation, a final concentration of 2 g l^{-1} $(NH_4)_2SO_4$ was added to a 7-day grown culture under PHA production conditions.

Biomass calculation

Cell densities, expressed in grams of CDW per litre, were determined gravimetrically by using tared 50 ml Falcon tubes. Forty millilitres of culture medium were centrifuged for 45 min at 3800 *g* and 4°C. Cell pellets were freeze-dried for 24 h in a lyophilizer and weighed.

Cell viability calculation

To calculate cell viability, serial dilutions from 10^{-1} to 10^{-7} were made in salt solution (0.9% NaCl). Three different spots of each dilution from 10^{-2} to 10^{-7} were plated on LB solid medium and colony-forming units (cfu) were counted. For each strain, three different experiments were carried out.

DNA manipulation and plasmid construction

DNA manipulations and other Molecular Biology techniques were essentially performed as described previously (Sambrook and Russell, 2001). Plasmid transference to the target *Pseudomonas* strains was performed by the filter-mating technique (Herrero *et al.*, 1990). DNA fragments were purified by standard procedures using Gene Clean (Bio 101, Vista, CA). Plasmid pPAZ2 was constructed as previously described (de Eugenio *et al.*, 2007). For PCR amplification, we used 2 units of AmpliTaq DNA polymerase (Perkin Elmer Life Sciences), 1 μg of DNA template, 1 μg of each deoxynucleoside triphosphate, and 2.5 mM $MgCl_2$ in the buffer recommended by the manufacturer. Conditions for amplification were chosen according to the G + C content of the corresponding oligonucleotides. *Pseudomonas putida* KT42Z strain was constructed by gene disruption of *phaZ* gene using plasmid pK18*mob* (Schafer *et al.*, 1994). An internal fragment of 335 bp of the gene was cloned in the polylinker of pK18*mob* after PCR amplification with primers PhaZMUT5′ (CCAGGATCCTCACGATTACCCCGAGCG) and PhaZMUT3′ (CCGGAATTCCAGCCAGTACCAGGGTG). The resulting construction (pK18*mob*-Z) was introduced into *P. putida* KT2442 by triparental mating and conjugants were selected in M63 0.2% citrate plus kanamycin. Disruption of *phaZ* gene was confirmed by PCR and Western blot analysis as described (de Eugenio *et al.*, 2007). *Pseudomonas putida* KT42C1 strain was constructed via disruption of *phaC1* gene by insertion of a minitransposon containing kanamycin resistance gene (Herrero *et al.*, 1990). PHA production-defective mutants were selected in plates of M63 0.1 N medium plus 2.5 g l^{-1} sodium octanoate and 0.25 mg ml^{-1} Nile Red with 100 cfu per plate. Due to the toxic effect exerted by the Nile Red, the only strains able to grow in this medium as isolated colonies were those whose PHA accumulation abilities had been impaired by disruption of genes involved in polymer metabolism. These clones were further isolated and selected by their lack of fluorescence under UV light (Spiekermann *et al.*, 1999). Mutations were identified by arbitrary PCR according to the method described by Espinosa-Urgel and

colleagues (2000), using TNSTOP (CATAAAGCTTGCTCA ATCAATCACC), TNINT (GACCTGCAGGCATGCAAGCTT CGGC), ARB1 (GGCACGCGTCGACTAGTACNNNNNNNN NNGATAT) and ARB2 (GGCACGCGTCGACTAGTAC) primers. To construct *P. putida* KTZ1 strain an 873 bp fragment was PCR-amplified from *P. putida* KT2442 genome using oligonucleotides PHAZ2 (CAGATATCAAGCTTGGC CGCAGCTGTTTCA) and PHAZ5 (GATATCGCATGCCG CAACCCTATATTTTCAG). The PCR fragment was digested with HindIII and BbuI and cloned into pALEX1b vector (Biomedal S.L.), resulting in the plasmid pPAZ6 (see also Fig. S2). This was digested with NotI and AseI and the resulting 1.9 kb fragment was purified by GeneClean and subcloned into previously NotI cut pUTTc (Herrero *et al.*, 1990), resulting in plasmid pUTTcZ, which was transferred via triparental mating to a KTXylS2 strain harbouring the regulatory module of plasmid pCNB44S2 (Cebolla *et al.*, 2001). *Pseudomonas putida* KTLacI^q was constructed by transferring the plasmid pCNB5 harbouring the LacI^q repressor in a minitransposon containing kanamycin resistance gene (de Lorenzo *et al.*, 1993).

Transmission electron microscopy

Pseudomonas putida KT2442 and *P. putida* KT42C1 cells previously grown under PHA production conditions for 24 h were harvested, washed twice in PBS and fixed in 5% (w/v) glutaraldehyde in the same solution. Afterwards, cells were included with 2.5% (w/v) OsO_4 for 1 h, gradually dehydrated in ethanol [30%, 50%, 70%, 90% and 100% (v/v); 30 min each] and propylene oxide (1 h), and embedded in Epon 812 resin. Ultrathin sections (thickness of 70 nm) were cut with a microtome using a Diatome diamond knife. The sections were picked up with 400 mesh cupper grids coated with a layer of carbon. The sections were observed in a Jeol-1230 electron microscope (Jeol, Akishima, Japan).

^{14}C-labelled 3-hydroxyalkanoic mobilization in resting cells system

Pseudomonas putida KT2442 or *P. putida* KT42Z cells were grown in ^{14}C-labelled PHA production conditions as described (de Eugenio *et al.*, 2007). After 24 h, cells were centrifuged, washed with 0.1 N M63 medium to avoid nitrogen-triggered PHA degradation, shifted to different conditions as distilled water pH 5.5, 50 mM acetate buffer pH 4 or 50 mM glycine-NaOH buffer pH 10.6 and incubated at 30°C and 250 r.p.m. Samples were taken each hour, centrifuged at 16 000 *g* for 25 min at 4°C and filtered through cellulose acetate disposable syringe filters (0.2 μ, Asahi Techno Glass). The radioactivity was determined in 100 μl aliquots of the supernatant in a scintillation counter (Beckman). PHA content was determined using GC-MS analysis as described elsewhere (Lageveen *et al.*, 1988).

3-Hydroxyalkanoic acids mobilization under PHA production conditions

Pseudomonas putida cells were inoculated into 0.1 N M63 medium containing 15 mM sodium octanoate. After 24 h, 40 ml of samples were taken, centrifuged at 3800 *g* and 4°C for 45 min and freeze-dried. HA levels in filtered supernatants and PHA content were determined using GC-MS as previously described (Lageveen *et al.*, 1988) (see below).

GC-MS analysis for PHA and HA content determinations

Polyhydroxyalkanoate monomer composition and cellular PHA content were determined by GC-MS of the methanolysed polyester. Methanolysis procedure was carried out by suspending 5–10 mg of lyophilized aliquots in 2 ml of chloroform and 2 ml of methanol containing 15% sulfuric acid and 0.5 mg ml^{-1} 3-methylbenzoic acid (internal standard) and then incubated at 100°C for 4 h. After cooling, 1 ml of demineralized water was added and the organic phase containing the resulting methyl esters of monomers was analysed by GC-MS (Lageveen *et al.*, 1988).

An Agilent (Waldbronn, Germany) series 7890A coupled with a 5975C MS detector (EI, 70 eV) and a split–splitless injector were used for analysis. An aliquot (1 μl) of organic phase was injected into the gas chromatograph at a split ratio of 1:50. Separation of compounds was achieved using an HP-5 MS capillary column (5% phenyl–95% methyl siloxane, 30 m × 0.25 mm i.d. × 0.25 mm film thickness). Helium was used as carrier gas at a flow rate of 0.9 ml min^{-1}. The injector and transfer line temperature were set at 275°C and 300°C respectively. The oven temperature programme was: initial temperature 80°C for 2 min, then from 80°C up 150°C at a rate of 5°C min^{-1} and finally up 200°C at a rate of 10°C min^{-1}. EI mass spectra were recorded in full scan mode (*m/z* 40–550).

The same sample preparation described above allowed the determination of benzoate content in samples since benzoic acid is susceptible to give rise its methyl ester form after methanolysis. Quantification of methyl-benzoate was carried out in the same chromatographic conditions as methyl esters of monomers obtained from PHA.

LC-MS analysis for identification of the products released

As preliminary step to chromatographic separation, samples were introduced to the ESI source in negative mode by direct infusion in order to optimize the MS conditions. Lyophilized aliquots (5–10 mg) were suspended in methanol and 5 μl were injected in the chromatographic system. Separation of the oligomers present in samples was carried out on a Finnigan Surveyor (Thermo Electron) pump coupled with a Finnigan LCQ Deca (Thermo Electron) ion trap mass spectrometer. The separation was performed at room temperature on a 100 × 2.1 mm (3 μm particle size) Hypersil HyPurity C18 column (Thermo Electron) at a flow rate of 100 μl min^{-1}. The mobile phase was 0.1% ammonium hydroxide in water (A) and 0.1% ammonium hydroxide in methanol (B). The following elution programme was used: at the start 95% A and 5% B; after 3 min the percentage of B was linearly increased to 95% in 7 min, then kept constant for 20 min, ramped to the original composition in 1 min, and then equilibrated for 10 min. The detection was monitored by MS-ESI spectrometry in negative mode at the conditions of source voltage

and capillary temperature that were optimized in the step of continuous infusion (3.5 kV and 200°C respectively). All spectra were recorded in full scan mode (*m/z* 50–1500).

Gas chromatography analysis of chiral hydroxy fatty acids

Samples were methanolysed as described for PHA content analysis. Separation of compounds was carried out in a Beta Dex 120 column (30 m × 0.25 mm i.d. × 0.25 mm film thickness) (Supelco, USA). Injector and detector temperature were kept at 300°C. Oven temperature was initially set at 95°C, held isothermally for 10 min and then increased at a rate of 0.5°C min^{-1} up to 120°C.

Acknowledgements

We thank P. García and E. Díaz for critical reading of the manuscript and helpful discussions. We also thank M. Arévalo from Biomedal S.L. for providing Cascade™ system (Biomedal S.L.). The technical work of A. Valencia is greatly appreciated. This work was supported by grants from the Comunidad Autónoma de Madrid (P-AMB-259-0505), the Comisión Interministerial de Ciencia y Tecnología (BIO2007-67304-C02, CSD2007-00005) and by European Union Grants (GEN 2006-27750-C5-3-E and NMP2-CT-2007-026515).

References

Cebolla, A., Sousa, C., and de Lorenzo, V. (2001) Rational design of a bacterial transcriptional cascade for amplifying gene expression capacity. *Nucleic Acids Res* **29:** 759–766.

Dawes, E., and Senior, P.J. (1973) The role and regulation of energy reserve polymers in micro-organisms. *Adv Microb Physiol* **10:** 135–266.

Doi, Y., Segawa, A., Kawaguchi, Y., and Kunioka, M. (1990) Cyclic nature of poly(3-hydroxyalkanoate) metabolism in *Alcaligenes eutrophus*. *FEMS Microbiol Lett* **55:** 165–169.

Espinosa-Urgel, M., Salido, A., and Ramos, J.L. (2000) Genetic analysis of functions involved in adhesion of *Pseudomonas putida* to seeds. *J Bacteriol* **182:** 2363–2369.

de Eugenio, L.I., García, P., Luengo, J.M., Sanz, J.M., San Román, J., García, J.L., and Prieto, M.A. (2007) Biochemical evidence that *phaZ* gene encodes a specific intracellular medium chain length polyhydroxyalkanoate depolymerase in *Pseudomonas putida* KT2442. Characterization of a paradigmatic enzyme. *J Biol Chem* **282:** 4951–4962.

de Eugenio, L.I., García, J.L., García, P., Prieto, M.A., and Sanz, J.M. (2008) Comparative analysis of the physiological and structural properties of a medium chain length polyhydroxyalkanoate depolymerase from *Pseudomonas putida* KT2442. *Eng Life Sci* **8:** 260–267.

Franklin, F.C., Bagdasarian, M., Bagdasarian, M.M., and Timmis, K.N. (1981) Molecular and functional analysis of the TOL plasmid pWWO from *Pseudomonas putida* and cloning of genes for the entire regulated aromatic ring meta cleavage pathway. *Proc Natl Acad Sci USA* **78:** 7458–7462.

Handrick, R., Reinhardt, S., and Jendrossek, D. (2000) Mobilization of poly(3-hydroxybutyrate) in *Ralstonia eutropha*. *J Bacteriol* **182:** 5916–5918.

Herrero, M., de Lorenzo, V., and Timmis, K.N. (1990) Transposon vectors containing non-antibiotic resistance selection markers for cloning and stable chromosomal insertions of foreign genes in Gram negative bacteria. *J Bacteriol* **172:** 6557–6567.

Huisman, G.W., Wonink, E., Meima, R., Kazemier, B., Terpstra, P., and Witholt, B. (1991) Metabolism of poly(3-hydroxyalkanoates) (PHAs) by *Pseudomonas oleovorans*. Identification and sequences of genes and function of the encoded proteins in the synthesis and degradation of PHA. *J Biol Chem* **266:** 2191–2198.

Jiménez, J.I., Miñambres, B., García, J.L., and Díaz, E. (2002) Genomic analysis of the aromatic catabolic pathways from *Pseudomonas putida* KT2440. *Environ Microbiol* **4:** 824–841.

Kadouri, D., Burdman, S., Jurkevitch, E., and Okon, Y. (2002) Identification and isolation of genes involved in poly(beta-hydroxybutyrate) biosynthesis in *Azospirillum brasilense* and characterization of a *phbC* mutant. *Appl Environ Microbiol* **68:** 2943–2949.

Kadouri, D., Jurkevitch, E., and Okon, Y. (2003) Poly beta-hydroxybutyrate depolymerase (PhaZ) in *Azospirillum brasilense* and characterization of a *phaZ* mutant. *Arch Microbiol* **180:** 309–318.

Kadouri, D., Jurkevitch, E., Okon, Y., and Castro-Sowinski, S. (2005) Ecological and agricultural significance of bacterial polyhydroxyalkanoates. *Crit Rev Microbiol* **31:** 55–67.

Klinke, S., de Roo, G., Witholt, B., and Kessler, B. (2000) Role of *phaD* in accumulation of medium-chain-length poly(3-hydroxyalkanoates) in *Pseudomonas oleovorans*. *Appl Environ Microbiol* **66:** 3705–3710.

Kobayashi, T., and Saito, T. (2003) Catalytic triad of intracellular poly(3-hydroxybutyrate) depolymerase (PhaZ1) in *Ralstonia eutropha* H16. *J Biosci Bioeng* **96:** 487–492.

Kovach, M.E., Elzer, P.H., Hill, D.S., Robertson, G.T., Farris, M.A., Roop, R.M., II, and Peterson, K.M. (1995) Four new derivatives of the broad-host-range cloning vector pBBR1MCS, carrying different antibiotic-resistance cassettes. *Gene* **166:** 175–176.

Lageveen, R.G., Huisman, G.W., Preusting, H., Ketelaar, P., Eggink, G., and Witholt, B. (1988) Formation of polyesters by *Pseudomonas oleovorans*. Effect of substrates on formation and composition of poly-(*R*)-3-hydroxyalkanoates and poly-(*R*)-3-hydroxyalkenoates. *Appl Environ Microbiol* **54:** 2924–2932.

de Lorenzo, V., Herrero, M., Jakubzik, U., and Timmis, K.N. (1990) Mini-Tn*5* transposon derivatives for insertion mutagenesis, promoter probing, and chromosomal insertion of cloned DNA in gram-negative eubacteria. *J Bacteriol* **172:** 6568–6572.

de Lorenzo, V., Eltis, L., Kessler, B., and Timmis, K.N. (1993) Analysis of *Pseudomonas* gene products using $lacI^q/P_{trp}$-lac plasmids and transposons that confer conditional phenotypes. *Gene (Amst)* **123:** 17–24.

Luengo, J.M., García, B., Sandoval, A., Naharro, G., and Olivera, E.R. (2003) Bioplastics from microorganisms. *Curr Opin Microbiol* **6:** 251–260.

Madison, L.L., and Huisman, G.W. (1999) Metabolic engineering of poly(3-hydroxyalkanoates): from DNA to plastic. *Microbiol Mol Biol Rev* **63:** 21–53.

Matin, A., Veldhuis, C., Stegeman, V., and Veenhuis, M. (1979) Selective advantage of a *Spirillum* sp. in a carbon-limited environment. Accumulation of poly-beta-hydroxybutyric acid and its role in starvation. *J Gen Microbiol* **112:** 349–355.

Moldes, C., García, P., García, J.L., and Prieto, M.A. (2004) *In vivo* immobilization of fusion proteins on bioplastics by the novel tag BioF. *Appl Environ Microbiol* **70:** 3205–3212.

Nelson, K.E., Weinel, C., Paulsen, I.T., Dodson, R.J., Hilbert, H., Martins dos Santos, V.A.P., *et al.* (2002) Complete genome sequence and comparative analysis of the metabolically versatile *Pseudomonas putida* KT2440. *Environ Microbiol* **4:** 799–808.

O'Leary, N.D., O'Connor, K.E., Ward, P., Goff, M., and Dobson, A.D. (2005) Genetic characterization of accumulation of polyhydroxyalkanoate from styrene in *Pseudomonas putida* CA-3. *Appl Environ Microbiol* **71:** 4380–4387.

Olivera, E.R., Carnicero, D., García, B., Minambres, B., Moreno, M.A., Cañedo, L., *et al.* (2001) Two different pathways are involved in the beta-oxidation of *n*-alkanoic and *n*-phenylalkanoic acids in *Pseudomonas putida* U: genetic studies and biotechnological applications. *Mol Microbiol* **39:** 863–874.

Panke, S., Sánchez-Romero, J.M., and de Lorenzo, V. (1998) Engineering of quasi-natural *Pseudomonas putida* strains for toluene metabolism through an ortho-cleavage degradation pathway. *Appl Environ Microbiol* **64:** 748–751.

Prieto, M.A., Buhler, B., Jung, K., Witholt, B., and Kessler, B. (1999a) PhaF, a polyhydroxyalkanoate-granule-associated protein of *Pseudomonas oleovorans* GPo1 involved in the regulatory expression system for *pha* genes. *J Bacteriol* **181:** 858–868.

Prieto, M.A., Kellerhals, M.B., Bozzato, G.B., Radnovic, D., Witholt, B., and Kessler, B. (1999b) Engineering of stable recombinant bacteria for production of chiral medium-chain-length poly-3-hydroxyalkanoates. *Appl Environ Microbiol* **65:** 3265–3271.

Prieto, M.A., de Eugenio, L.I., Galán, B., Luengo, J.M., and Witholt, B. (2007) Synthesis and degradation of polyhydroxyalkanoates. In *Pseudomonas: A Model System in Biology. Pseudomonas*, Vol. V. Ramos, J.L., and Filloux, A. (eds). Berlin, Germany: Springer, pp. 397–428.

Ren, Q., Grubelnik, A., Hoerler, M., Ruth, K., Hartmann, R., Felber, H., and Zinn, M. (2005) Bacterial poly(hydroxyalkanoates) as a source of chiral hydroxyalkanoic acids. *Biomacromolecules* **6:** 2290–2298.

Royo, J.L., Moreno-Ruiz, E., Cebolla, A., and Santero, E. (2005) Stable long-term indigo production by overexpression of dioxygenase genes using a chromosomal integrated cascade expression circuit. *J Biotechnol* **116:** 113–124.

Ruiz, J.A., López, N.I., Fernández, R.O., and Méndez, B.S. (2001) Polyhydroxyalkanoate degradation is associated with nucleotide accumulation and enhances stress resistance and survival of *Pseudomonas oleovorans* in natural water microcosms. *Appl Environ Microbiol* **67:** 225–230.

Ruiz, J., Lopez, N.I., and Mendez, B.S. (2004) *rpoS* gene expression in carbon-starved cultures of the polyhydroxyalkanoate-accumulating species *Pseudomonas oleovorans*. *Curr Microbiol* **48:** 396–400.

Ruth, K., Grubelnik, A., Hartmann, R., Egli, T., Zinn, M., and Ren, Q. (2007) Efficient production of (*R*)-3-hydroxycarboxylic acids by biotechnological conversion of polyhydroxyalkanoates and their purification. *Biomacromolecules* **8:** 279–286.

Ruth, K., de Roo, G., Egli, T., and Ren, Q. (2008) Identification of two acyl-CoA synthetases from *Pseudomonas putida* GPo1: one is located at the surface of polyhydroxyalkanoates granules. *Biomacromolecules* **9:** 1652–1659.

Sambrook, J., and Russell, D.W. (2001) *Molecular Cloning. A Laboratory Manual*. Cold Spring Harbor, NY, USA: CSHL Press.

Sandoval, A., Arias-Barrau, E., Bermejo, F., Cañedo, L., Naharro, G., Olivera, E.R., and Luengo, J.M. (2005) Production of 3-hydroxy-*n*-phenylalkanoic acids by a genetically engineered strain of *Pseudomonas putida*. *Appl Microbiol Biotechnol* **67:** 97–105.

Sandoval, A., Arias-Barrau, E., Arcos, M., Naharro, G., Olivera, E.R., and Luengo, J.M. (2007) Genetic and ultrastructural analysis of different mutants of *Pseudomonas putida* affected in the poly-3-hydroxy-*n*-alkanoate gene cluster. *Environ Microbiol* **9:** 737–751.

Schafer, A., Tauch, A., Jager, W., Kalinowski, J., Thierbach, G., and Puhler, A. (1994) Small mobilizable multi-purpose cloning vectors derived from the *Escherichia coli* plasmids pK18 and pK19: selection of defined deletions in the chromosome of *Corynebacterium glutamicum*. *Gene* **145:** 69–73.

Schreck, K.M., and Hillmyer, M.A. (2007) Block copolymers and melt blends of polylactide with Nodax microbial polyesters. preparation and mechanical properties. *J Biotechnol* **132:** 287–295.

Senior, P.J., and Dawes, E.A. (1973) The regulation of poly-beta-hydroxybutyrate metabolism in *Azotobacter beijerinckii*. *Biochem J* **134:** 225–238.

Spiekermann, P., Rehm, B.H., Kalscheuer, R., Baumeister, D., and Steinbüchel, A. (1999) A sensitive, viable-colony staining method using Nile red for direct screening of bacteria that accumulate polyhydroxyalkanoic acids and other lipid storage compounds. *Arch Microbiol* **171:** 73–80.

Taidi, B., Mansfield, D.A., and Anderson, A.J. (1995) Turnover of poly(3-hydroxybutyrate) (PHB) and its influence on the molecular mass of the polymer accumulated by *Alcaligenes eutrophus* during batch culture. *FEMS Microbiol Lett* **129:** 201–206.

Tal, S., and Okon, Y. (1985) Production of the reserve material poly-β-hydroxybutyrate and its function in *Azospirillum brasilense* Cd. *Can J Microbiol* **31:** 608–613.

Timm, A., and Steinbüchel, A. (1990) Formation of polyesters consisting of medium-chain-length 3-hydroxyalkanoic acids from gluconate by *Pseudomonas aeruginosa* and other fluorescent pseudomonads. *Appl Environ Microbiol* **56:** 3360–3367.

Uchino, K., Saito, T., Gebauer, B., and Jendrossek, D. (2007) Isolated poly(3-hydroxybutyrate) (PHB) granules are complex bacterial organelles catalyzing formation of PHB from acetyl coenzyme A (CoA) and degradation of PHB to acetyl-CoA. *J Bacteriol* **189:** 8250–8256.

Wang, L., Armbruster, W., and Jendrossek, D. (2007)

Production of medium-chain-length hydroxyalkanoic acids from *Pseudomonas putida* in pH stat. *Appl Microbiol Biotechnol* **75:** 1047–1053.

York, G.M., Junker, B.H., Stubbe, J., and Sinskey, A.J. (2001) Accumulation of the PhaP phasin of *Ralstonia eutropha* is dependent on production of polyhydroxybutyrate in cells. *J Bacteriol* **183:** 4217–4226.

Yuan, M.Q., Shi, Z.Y., Wei, X.X., Wu, Q., Chen, S.F., and Chen, G.Q. (2008) Microbial production of medium-chain-length 3-hydroxyalkanoic acids by recombinant *Pseudomonas putida* KT2442 harboring genes *fadL*, *fadD* and *phaZ*. *FEMS Microbiol Lett* **283:** 167–175.

Supporting information

Additional Supporting Information may be found in the online version of this article:

Fig. S1. Complementation of *Pseudomonas putida* KT42C1 and KT42Z strains.

Fig. S2. Schematic representation of *Pseudomonas putida* KTZ1 strain construction.

Fig. S3. LC-ESI-MS analysis of HAs and oligomers obtained from PHA enzymatic hydrolysis.

Movie S1. PHA mobilization in *Pseudomonas putida* KT2442 cells triggered by alkaline conditions. For film preparation, KT2442 cells cultured in 0.1 N M63 plus 15 mM octanoate for 23h were centrifuged, washed in salt solution and resuspended in Glycine-NaOH buffer, pH 10.6. Sealed preparations were imaged on a Leica AF6000 LX system microscope (Mannheim, Germany) in a Pecon environmental chamber kept at 30°C. The chamber stage was buffered with air maintained in a humid environment. Images were captured using a 100×1.4 NA objective lens with the Hg-arc lamp. Optical sections (exposure time $\simeq 50$ milliseconds, 1000×1000 pixels) were imaged at 5 second intervals for up to 4 hours.

Please note: Wiley-Blackwell are not responsible for the content or functionality of any supporting materials supplied by the authors. Any queries (other than missing material) should be directed to the corresponding author for the article.